International Relativistic Astrophysics PhD
IRAP Ph.D.

Massive Fast Rotating Highly Magnetized White Dwarfs: Theory and Astrophysical Applications

Thesis Advisors
Prof. Remo Ruffini
Dr. Jorge A. Rueda

Ph.D. Student
*Diego Leonardo Caceres Uribe**

*D.L.C.U. acknowledges the financial support by the International Relativistic Astrophysics (IRAP) Ph.D. program.

Academic Year 2016–2017

Contents

General introduction

The importance of magnetism in white dwarfs (WDs) was addressed several decades ago, being Ostriker and Hartwick (1968) the first addressing their importance on the structure of these kind of stars. It was understood that the effect of magnetic fields was to increase the radius of the WDs and that they cannot be arbitrarily large, otherwise the WD becomes unstable. While theoretical efforts were undertaken to understand the effect of magnetic fields on the structure and stability of WDs, on the observational field the number of magnetic WDs reported has increased significantly in the last years (Ferrario et al., 2015). As is stated in the title of this dissertation, the main purpose of this work is to address the issue of magnetism in WDs, mainly their structure and their application to some of the most enigmatic objects discovered recently in the field of astrophysics, the *Soft Gamma-ray repeaters* (SGRs) and the *Anomalous X-ray pulsars* (AXPs), objects that traditionally have been associated with a particular model, the *magnetar model*, a fact that make them being better known in literature simply as *magnetars*.

In chapter 1 I make an introduction to the motivation behind this dissertation. I explain, from a brief historical point of view, the observational discovery of pulsars. We explain also how these peculiar astrophysical objects were finally associated to the previously theoretically hypothesized Neutron Stars (NSs). NSs are very compact objects, first proposed by Landau (1932) and Baade and Zwicky (1934d), and were proposed as the result of supernova explosions of massive stars. Then I explain how the discovery of AXPs and SGRs established a new paradigm in the field of neutron stars (NSs), where it was established the idea that a new kind of pulsar has been discovered, the *magnetar*. A magnetar is a very magnetic NS, with magnetic fields of the order $\sim (10^{14} - 10^{15})$ G. The fundamental difference between a magnetar and an ordinary pulsar is the mechanism responsible for the electromagnetic wave emission: in a magnetar the magnetic field energy powers the electromagnetic wave emission while in a traditional pulsar the rotational energy is responsible for that. This difference lays on the fact that rotational energy loss of a typical NS cannot explain energetically the electromagnetic emission of AXPs/SGRs. Is at this point where we remind the existence of an alternative model to the magnetar model, first proposed by Paczynski (1990), which also intends to explain AXPs/SGRs invoking a magnetic WD instead of a magnetar. In this model the magnetic WD would be more like a traditional pulsar instead of a magnetar, i.e., the WD would behave like a rotationally powered pulsar.

The WD model is a motivation to study in the most realistic way the structure and stability of rotating WDs. Therefore, in chapter 2 I address the main points behind the structure and stability of these compact objects. I explain the main physical effects that play a role in the structure of WDs such as degeneracy pressure, Coulomb repulsion or gravitational force, and then I consider the consequences of the instabilities that are produced by different phenomena such as inverse β-decay, pycnonuclear fusion reactions or General Relativity (GR). We show the main aspects of WDs that obey the relativistic Feynman-Metropolis-Teller equation of state, both in the static (Rotondo et al., 2011a) and uniformly rotating (Boshkayev et al., 2013) cases.

We proceed in chapter 3 with the topic of magnetism in WDs. In the first part of this chapter we give attention to what observations have revealed about magnetic WDs. Observations show that the most magnetic WDs are in the range $(10^6 - 10^9)$ G. In the last years different missions have allowed to increase the number of reported magnetic WDs, which now we know make up a significant percentage of the total number of observed WDs. We show information regarding their average masses, their observed periods and we mention the main models that intend to explain their origin and evolutionary channel. From these models, of special importance is the double degenerate merger model, which also was considered by Paczynski (1990) as the most probable scenario for the origin of the pulsar-like WDs that would explain AXPs/SGRs. In the second part we deal with the recently proposed model of ultra-magnetic WDs (proposed by Das and Mukhopadhyay, 2012, 2013) as an explanation to the observation of superluminous supernovae Type Ia that would require the existence of super-Chandrasekhar WDs, typically of the order $(2.1 - 2.8)M_\odot$. In that model the way the WD can reach such masses is through the hypothetical presence of very high magnetic fields, usually as large as 10^{18} G. We therefore show this treatment ignores several microscopic effects that render unstable this ultra-magnetic WDs, whose properties resemble more the characteristics of typical NSs. We also show that other instabilities due to the breaking of spherical symmetry or the violation of the virial theorem also invalidate the conclusions obtained in that model.

In chapter 4 we address the model of highly rotating and magnetic WDs for AXPs/SGRs. We show that the WDs of this model should have magnetic fields in the range $(10^6 - 10^9)$ G, making them very similar in this aspect to the magnetic WDs observed in nature and about which we talked in the first part of chapter 3. Therefore these WDs do not have the problem of instabilities like the ultra-magnetic ($B \sim 10^{18}$ G) super-Chandrasekhar WDs proposed by Das and Mukhopadhyay (2012, 2013) to explain superluminous supernovae type Ia. We also show that these WDs are also stable against instabilities produced by the high stage of rotation. This is because the periods of AXPs/SGRs are in the range $(2 - 12)$ s, putting them close but above the lower boundary limit imposed by the mass-shedding limit, a limit that establishes a minimum rotation period (between 0.3s and 2.2s) for rotating WDs and which depends on the nuclear

composition. We then show that in all cases these WDs can thoroughly explain from the energetic point of view AXPs/SGRs. We also show that the model of uniformly rotating WDs explained in chapter 2 can give more precise information about parameters like masses, radii, moments of inertia or magnetic fields. We show that the model cannot only explain the persistent emission but also the transient emission, where starquakes happening inside the star produce glitches and outbursts that have been already confirmed by observations. After this, we also show that the information coming from observations in the optical, infrared and ultraviolet does not contradict the WD model.

In chapter 5 we talk about the emission in X-rays. In this case, as we mentioned before, the WD has to be modelled as a rotationally powered pulsar, thus, we consider the model of a traditional pulsar, showing first the general characteristics of this model and the main considerations behind it. A key point in this model is that the condition on the magnetic field for the pair production of electrons and positrons through the process $\gamma + B \rightarrow e^- + e^+$ must be satisfied, something that depends on the period of rotation and the magnetic field. This condition defines a theoretical limit called *death-line*, which determines when a compact star (WD or NS) will behave or not as an active pulsar. We show that when we consider the death-line for a WD rotating as fast as AXPs/SGRs, the WD should behave like an active pulsar, or in other words, the magnetic field and the angular velocity are high enough to ensure the pair production of electrons and positrons. When this pair production is ensured, these particles hit the surface of the compact star and the heat reradiated will be observed on earth as a blackbody spectrum. Almost all AXPs/SGRs in the range of $(2-10)$ keV emit radiation that can be decomposed in a blackbody+power-law components. The blackbody component in this range of soft X-rays is associated with this heat re-radiated by the WD surface. We therefore show that within this model the luminosity predicted agrees with the luminosity observed. We also remark that in order to have such small areas of emission for these blackbodies it is crucial to consider that in the surface of the WD we have the presence of multipoles. We then show that the pulsed fraction observed in these objects can be explained considering the different possible viewing angles. We also mention that in order to be able to see this spot on the surface of the star, we must have certain conditions on the surface that make the hot spot re-radiate efficiently the heat proportioned by the inward particle bombardment. We do this in appendix A, where we have used the heat transport and energy balance equations applied to the actual conditions of density and temperature under the polar cap of the WD.

In chapter 6 we reconsider the fact that some AXPs/SGRs could be modelled as traditional rotationally powered pulsars instead of being modelled as magnetars. For this, we explore the possibility that the electromagnetic wave emission can be explained from the rotational energy loss of NSs, but considering the full range of masses, moments of inertia and radii possible for realistic configurations of NSs. This analysis implies that the AXPs/SGRs that could be rotationally powered pulsars could be 11 out of 23. This is significant because

before this estimate was done, only 4 AXPs/SGRs were recognised as potential pulsars powered by rotation. We therefore conclude that the consideration of the full range of parameters can be significant to determine a wider range of the efficiencies of any neutron star. We also perform an analysis about the glitches and outbursts observed, considering the possibility that they could be triggered by starquakes.

Finally we give the general conclusions. We analyze the consequences of several of our analysis done throughout this document, pointing out also to applications and future work on this area.

The results of this work have been published in the following articles:

- *On the stability of ultra-magnetized white dwarfs,* Journal of the Korean Physical Society, Vol. 65, No.6, September 2014, pp. 846-849. *Dynamical Instability of White Dwarfs and Breaking of Spherical Symmetry Under the Presence of Extreme Magnetic Fields,* The Astrophysical Journal, Volume 794, Issue 1, article id. 86, 7 pp. (2014). The results of these two articles are shown in chapter 3.
- *Thermal X-ray emission from massive, fast rotating, highly magnetized white dwarfs,* Monthly Notices of the Royal Astronomical Society, Volume 465, Issue 4, p.4434-4440. The results are shown in chapter 5.
- *The rotation-powered nature of some soft gamma-ray repeaters and anomalous X-ray pulsars,* Astronomy & Astrophysics, Volume 599, id.A87, 10 pp. The results are shown in chapter 6.

Chapter 1

Anomalous X-ray pulsars and Soft Gamma-ray repeaters: A new class of pulsars

This chapter will explain the main motivation of this work. First, I will give a general introduction to pulsars, considering the main historical and theoretical aspects of this field of astrophysics, and which has gained new interest in the scientific community either in the theoretical or in the observational fields. Then I will address the implications of the discovery of the well known Anomalous X-ray pulsars and Soft Gamma-ray repeaters (AXPs/SGRs), whose observation brought a new challenge to the theoretical understanding of these objects and stimulated and renewed the interest on pulsars. Particularly, a new hypothesis was formulated, that these objects are highly magnetic neutron stars, but despite this has been the main model assumed to describe AXPs/SGRs, there have been proposed other models that try to give account of the observations, particularly, a pulsar-like white dwarf model that was proposed at the end of the 80's and beggining of 90's. This model is the main motivation of this work. At the end of this chapter, I will give some conclusions and perspectives. This chapter gives the motivation to start the next chapters, which are thought to be connected following a logic line.

In 1967 a research group using the Mullard Radio Astronomy Observatory in Cambridge made an important discovery, the first observation of what we know today as pulsars. The object, PSR 1919+21 had a periodicity of 1.3373 seconds and a pulse width of 0.04 seconds. The results of their work were published in 1968 (see, e.g., Hewish et al., 1968) and its importance was rapidly recognized when the Nobel committee decided to award Hewish, the head of the group, with the Nobel prize in Physics in 1974.

Immediately there were raised various hypotheses to explain the mechanism that produced the pulsations. Three of them were considered: radial pulsations, orbital motion and rotation. Pulsating white dwarfs were ruled out after theoretical calculations showed that the shortest period for the fundamental mode

is $\sim$ 2 s (Meltzer and Thorne, 1966; Shapiro and Teukolsky, 1986), much bigger than many observed pulsar periods. Rotating white dwarfs were excluded after calculations showed that the smallest possible period of rotation of a white dwarf (WD) is $\sim$ 1 s (Boshkayev et al., 2013; Ostriker, 1968; Shapiro and Teukolsky, 1986). And binary WDs were also ruled out because a pair in contact would have an orbital period not less than 1.7 s (Ostriker, 1968).

Regarding a neutron star (NS) as a source of the pulsation, both three possibilities were considered as were considered for a WD. Following Meltzer and Thorne (1966), stable neutron stars have central densities in the range $(2.7 \times 10^{13} - 6.0 \times 10^{15})$ g·cm^{-3}. This implies fundamental periods in the range $(8 \times 10^{-4} - 5 \times 10^{-2})$ s. This range of values is very small compared to the values measured of many pulsars that have measured periods $\sim$ 0.1 s. Hence, pulsations of neutrons stars are easily ruled out as an explanation to the observations. Then, there remain only two possibilities, orbital motion and rotation. In the case of a binary neutron star system, thorough calculations (Ostriker, 1968; Shapiro and Teukolsky, 1986) of gravitational wave emission of such a system, with a period in the range of the observed periods of pulsars $(10^{-3} - 4)$ s, show that the period of this system should decrease with time. Instead, observations show that the period of pulsations is increasing with time, something that is inconsistent with an orbital origin of the pulsations.

So, the only natural explanation that remains is that pulsations come from a rotating neutron star, a picture that then was immediately widely accepted up to these days. This idea and the remark that this rotating neutron stars should have magnetic fields $\sim 10^{12}$ G was first put forward by Gold (1968). After that, Gold (1969) showed that the rotational energy loss of the Crab pulsar was roughly the same as the energy required to power the Crab Nebula. This helped to establish the rotating neutron star model as the most plausible model that can give account of pulsar observations.

When pulsars were first observed the idea of the hypothetical existence of NSs was already advanced decades before. Baade and Zwicky (1934d) were the first to propose the idea of neutron stars, pointing out their very high density, small radius and that they would be formed in supernova explosions. Supernovae explosions had already been observed. For example, Chinese astronomers in 1054 A.D. observed the supernova explosion that created the Crab pulsar and nebula. In november 1572 Tycho Brahe observed and reported a new star or *nova* in the Cassiopeia constellation. This supernova (SN 1572) is also known as Tycho's supernova. In October 9, 1604, another new supernova (SN 1604) was observed, in that case by Johannes Kepler's student and assistant. He named it Kepler's supernova to honor his professor. In 1885 Hartwig observed a supernova in our companion galaxy Andromeda (or M31). So, these observations made Baade and Zwicky to raise their hypothesis that supernovae represent rapid transitions of ordinary stars into NSs, that this transition process would be responsible of the great amount of luminosity or energy released and observed

and that these explosions contribute to cosmic rays detected on earth (Baade and Zwicky, 1934a,b,c; Zwicky, 1938).

The idea of NSs was also elaborated independently by Oppenheimer and Volkoff (1939), who assumed matter to be composed of an ideal gas of free neutrons at high density. This work focused on the hypothesis that neutron cores in massive normal stars might be a source of stellar energy. When thermonuclear fusion became understood, the idea of NSs was generally ignored by the astronomical community, in part also because their thermal radiation would be too faint to be observed with telescopes on earth. However, many theoretical works were done to discuss the equation of state and different NS models were proposed (see, e.g., Ambartsumyan and Saakyan, 1960; Cameron, 1959; Hamada and Salpeter, 1961; Harrison et al., 1965). Rotating magnetic neutron stars were proposed as the energy source in supernovae remnants by Wheeler (1966) and Pacini (1967). The interest on NSs was further stimulated by the discovery of pulsating, compact X-ray sources (X-ray pulsars) by the UHURU satellite in the 70's (Giacconi et al., 1971; Tananbaum et al., 1972). These are NSs in close binary systems, accreting gas from their companion stars. The first conclusive evidence for periodicity was found in the sources Cen X-3 and Her X-1 (Schreier et al., 1972a,b; Tananbaum et al., 1972).

Immediately after the scientific community understood the origin of the pulsations, the problem of solving the electromagnetic Maxwell equations in the atmosphere of the NSs became a requirement to fully understand these objects, the powering of their associated nebulae, and their emission mechanisms. As the reader can read with more detail in chapter 5, the first model assumed a vacuum magnetosphere, but after that, it was understood it was not possible due to huge induction electric fields that appear when a huge magnetic field rotates (see Goldreich and Julian, 1969, and section 5.2). These huge electric fields must remove charged particles from the surface and the magnetosphere cannot be empty. This implies that a corotating magnetosphere should appear where, furthermore, electric and magnetic fields are orthogonal, $\mathbf{E} \cdot \mathbf{B} = 0$. After the work of Goldreich and Julian (1969), several efforts have been done to find a standard solution to Maxwell equations in the magnetosphere of NSs (Cerutti and Beloborodov, 2016; Contopoulos et al., 1999; Mestel and Shibata, 1994; Michel, 1973a,b, 1982; Spitkovsky, 2006).

In order to explain the emission of some single NSs in γ-rays and X-rays as well as in radio wavelengths, it was understood there must exist a region where the corotation condition $\mathbf{E} \cdot \mathbf{B} = 0$ would not be satisfied and therefore, an electric field non-ortogonal to the magnetic field $\mathbf{B}$ should accelerate charged particles along the magnetic field lines, creating γ-ray photons. In this way, different models have appeared, where different regions of emission are considered (see, for instance Venter and Harding, 2014, for a recent review of the different models proposed). Some of them can give account of certain observations in X-rays and γ-rays (Venter and Harding, 2014). But up to now, the mechanism that produces

coherent radio emission, which was the first pulsed emission detected, is still far from being understood (Melrose, 1995). So, despite all theoretical and numerical efforts, this problem is still open and not a single unified and satisfactory picture has been yet accepted.

Several problems had to be solved, such as to find a standard solution to Maxwell equations in the magnetosphere (Cerutti and Beloborodov, 2016; Contopoulos et al., 1999; Mestel and Shibata, 1994; Michel, 1973a,b, 1982; Spitkovsky, 2006), the problem of the pulsar wind (Arons, 2002, 2004; Bogovalov, 1999; Camenzind, 1986; Goldreich and Julian, 1970; Michel, 1969, 2005; Tong, 2016) and the mechanism responsible of pulsar emission in radio wavelengths (Beskin et al., 1988; Blandford, 1975; Lyutikov et al., 1999; Melrose, 2004, 1978, 1995). Today these problems are still open and not a definitive solution has been found. There are several inconsistencies in the original model (Michel, 1982; Michel and Li, 1999; Michel and Smith, 2001), the mechanism responsible for the radio emission is poorly understood (Melrose, 2004, 1995) and remains open the problem of the low braking index expected from models (Blandford and Romani, 1988; Chen and Li, 2006; Chukwude et al., 2010; Hamil et al., 2015).

While the physical properties of pulsars still remained far from being well understood, observations revealed the existence of a new class of pulsars or compact objects that with time, after several observational and theoretical studies, were called *magnetars*. What we know today as magnetars are objects that were classified either as Soft Gamma-ray repeaters (SGRs) or as Anomalous X-ray pulsars (AXPs). The first of these objects to be observed was SGR 0526-66 and was observed in 1979 (Mazets and Golenetskii, 1981; Mazets et al., 1979). These sources were originally thought to be related to the already known Gamma-ray Bursts (GRBs) (Atteia et al., 1987; Laros et al., 1986), but repeated bursts and an enormous flare detected on 5 March 1979 from the direction of the Dorado region in the Large Magellanic Cloud (Mazets et al., 1979) and from the object now known as SGR 1900+14 (Mazets and Golenetskii, 1981; Mazets et al., 1979), provided evidence that these were a new kind of objects, that belonged to a group different to the one that caused the GRBs. The SGRs had a softer spectra than most of GRBs, hence their designation as 'soft gamma repeaters'. After that a third galactic source, SGR 1806-20, underwent a burst episode (Laros et al., 1987).

Meanwhile the first AXP discovered was detected in 1981, 1E 2259+586. It had an unusual 7s period and was detected in the galactic supernova remnant CTB 109 (Fahlman and Gregory, 1981). Several researches (see Hellier, 1994; Mereghetti and Stella, 1995; Thompson and Duncan, 1996; van Paradijs et al., 1995) found distinctive and similar features in 1E 2259+586 and other sources such as 4U 0142+61 and 1E 1048.1-5937, that finally prompted to their classification as a distinct group of pulsars. Among several distinctive characteristics of AXPs are their bright X-ray pulsations in the soft X-ray range (< 10 keV) at periods of few seconds and not apparent companions from which to accrete, since

their emission in the X-ray range was thought to be initially originated from accreting binary neutron stars. Due to their emission in the X-ray range it was thought initially they were accreting binary neutron stars but further searches and observations in the optical and IR failed to detect bright companion stars (see, e.g., Thompson and Duncan, 1996, and references therein); these luminous counterparts in the optical and near infrared (NIR) were expected if these pulsars were in high-mass binaries. But also low-mass binary systems were ruled out after X-ray timing studies did not show the orbital Doppler shifts expected for binary motion (Mereghetti et al., 1998; Wilson et al., 1999). But the main reason these objects were called anomalous was that their rotational energy loss $\dot{E}_{\rm NS}$, could not explain the observed luminosity $L_{\rm obs}$,

$$\dot{E}_{\rm NS} := -4\pi^2 I_{\rm NS} \frac{\dot{P}}{P^3} < L_{\rm obs}, \tag{1.1}$$

where $I_{\rm NS}$ is the moment of inertia of a typical NS and P and $\dot{P}$ are the measured period of rotation and its time derivative, respectively. This puts a problem to the standard model of pulsars that relied on rotational energy loss to power the luminosity. In the case of normal isolated (non-accreting) pulsars the rule is that the rotational energy loss is several orders of magnitude larger than the observed luminosity ($\dot{E}_{\rm NS} > L_{\rm obs}$), whether it is radio, X-ray or γ-ray luminosity, so it can explain energetically the observed luminosity of the NS and also the bright radio/optical/X-ray emission from their nebulae, observed around the most energetic pulsars. Most of the spin-down power is lost in the stellar wind particles rather than in beamed photons from the pulsar. The efficiency ($\epsilon := L_{\rm obs}/\dot{E}_{\rm NS}$) is very low in the radio band of pulsars, $\epsilon \sim 10^{-5}$. Radio pulsars make up the majority of the discovered pulsars (over 2000). The efficiency is larger in the X-ray band, where non-thermal emission is seen around 100 pulsars (a small percentage of the radio pulsars), but still the efficiency is very small, with an average $\epsilon \sim 10^{-3}$ (Li et al., 2008; Possenti et al., 2002). Hence, the fact that AXP/SGRs do not satisfy this condition like normal pulsars do put a challenge to the pulsars' model and a different model had to be proposed.

The development of a new model of pulsars and NSs that could give account of these observations was therefore expected. While progress in the observational field showed the existence of AXPs and SGRs, in the theoretical field Duncan and Thompson (1992) stated that NSs with unusually strong magnetic dipole fields $B \sim (10^{14} - 10^{15})$ G can form when conditions for efficient dynamo action are met after the gravitational collapse that creates the NS. The conditions propitious are that they are born with initial spin periods P_0 shorter than the overturn time of $\sim (3 - 10)$ ms of the convection driven by the high neutrino luminosity $L_\nu > 10^{52}$ erg s^{-1} (Duncan and Thompson, 1992). The efficient dynamo that results in such a case can generate magnetic fields as high as $3 \times 10^{17}(P_0/1\text{ms})^{-1}$ G. Such a dynamo operates only for a few seconds but can generate magnetic fields as high as 10^{16} G, usually with multipolar structure and a strong toroidal

component in the interior (Ciolfi et al., 2010; Thompson et al., 2002). They called these high-field NSs *magnetars* and proposed that they could be the origin of the SGR emission. They also explained that these magnetars rotate initially faster, with $P_{\rm in} \sim 1$ ms, but then quickly lose most of their rotational energy thanks to magnetic dipole radiation and particle wind losses. This is important in the model because the AXPs/SGRs rotate very slowly, compared to other pulsars.

Then Thompson and Duncan (1995) showed that many of the observational characteristics of SGRs such as their bursts and their persistent emission can be explained by a model in which spontaneous magnetic field decay serves as an energy source. Thompson and Duncan (1996) argued that also AXPs are magnetars, with their X-ray luminosities powered by magnetic field decay. The detection of two SGR-like bursts in two AXPs, 1E 1048-5937 (Gavriil et al., 2002) and 1E2259+586 (Kaspi et al., 2003) then unified AXPs and SGRs observationally. Since then, the differences between these two kind of objects have diluted, as more objects of one group showed observational properties of the other; for example, bursting has now been identified as an observational property of the AXP family (Gavriil et al., 2004; Kaneko et al., 2010; Scholz and Kaspi, 2011; Woods et al., 2005) and AXP-like behaviour, e.g., absence of bursting activity for long periods of time, has been observed in objects previously identified as SGRs (Kaplan et al., 2001).

As we said before, many observational characteristics were found to be common to the members of the AXP/SGR family. The most important are the following:

- A narrow distribution of the periods, between 2 and 12 seconds, in clear contrast to normal pulsars that span a wider range of periods, between 1 ms up to 10 s.

- Regarding their spin-down, it spans a wide range, $\dot{P} \sim (10^{-13} - 10^{-10})$, much larger than the usual spin-down of normal pulsars, $\dot{P} \sim 10^{-15}$.

- Half of them are persistent X-ray sources, with luminosities in the range $L_{\rm X} \sim (10^{35} - 10^{36})$ erg s^{-1}. The other ones, most of which were detected during bright outbursts, are classified as transient sources. When bright, their X-ray spectra pulse profile and luminosity share the same features with the persistent AXPs/SGRs (Mereghetti, 2013).

- Their X-ray spectra is rather soft below 10 keV and are generally fit with two-component models, mainly a blackbody with temperature given by $kT_{\rm BB} \sim 0.5$ keV plus either a power-law with photon index in the range $\Gamma \sim 2 - 4$, or another blackbody (Olausen and Kaspi, 2014).

- Some of them have also been detected in the hard X-ray range, with power-law tails extending up to $100 - 200$ keV.

- Optical and NIR counterparts have not been firmly identified. In most cases they are too faint, a fact that immediately rules out the existence of normal companion stars or accretion disks. In three sources the optical emission is modulated with the same period observed in the X-ray range, meaning that this emission comes from the same rotating body and not from a hypothetical companion.

- Short bursts with typical luminosities $\sim (10^{38} - 10^{42})$ erg s^{-1} and durations in the range $\sim (0.01 - 1)$ s. The bursts occur sporadically, separated by long periods of time or in groups of tens or hundreds concentrated in few hours (Mereghetti, 2013).

- Extremely energetic giant flares observed to date in only three sources, SGR 0526-66 (March 5, 1979 Mazets et al., 1979), SGR 1900+14 (August 27, 1998 Hurley et al., 1999) and SGR 1806-20 (December 27, 2004 Mereghetti et al., 2005; Palmer et al., 2005).

We mentioned before that in the magnetar model the highly magnetic NS is formed when specific conditions are satisfied during the first moments of the gravitational collapse that lead to its birth. Within this model an alternative scenario has been proposed for the formation of these hypothetical highly magnetic NSs. They could be the descendants of the stars with the highest magnetic fields. Magnetic white dwarfs (MWDs) with magnetic fields as high as 10^9 G have been observed in nature (see Ferrario et al., 2015, and chapter 3). By conservation of the magnetic flux, these objects could be the progenitors of these highly magnetic NSs (Ferrario and Wickramasinghe, 2006; Hu and Lou, 2009).

In the magnetar model the magnetic field decay provides a source of internal heating that can produce a surface temperature higher than the surface temperature of a cooling NS of the same age but with a magnetic field smaller. But the magnetic field decay is also affected by the NS temperature evolution, hence a self-consistent evolution model has to be developed. Higher surface temperatures are obtained for NSs with strong internal toroidal fields, according to 2-D simulations where the magnetic field is sustained by currents in the NS crust (Pons et al., 2009).

Most of the models developed to reproduce the spectral properties of AXPs and SGRs within the magnetar model consider globally twisted magnetospheres, where dissipation of magnetic energy has been studied and even there have been obtained expressions for the evolution of the luminosity (see, for instance, Beloborodov, 2009). In this case, most of the magnetic energy is dissipated as

thermal radiation in the footprints of a bundle of twisted lines which are heated by the accelerated magnetospheric particles. The areas of these hot spots estimated in this model are consistent with the small emitting areas inferred from the blackbody fits of transient AXP/SGRs.

The outbursts and giant flares are explained in this model considering that with time, as the magnetic field evolves, the NS crust deforms, leading to low level seismic activity and storing magneto-elastic energy that powers these transient episodes when the crust cracks. In particular, for ordinary pulsars the magnetosphere could be static but for pulsars with $B \gtrsim 10^{14}$ G their magnetospheres are *dynamic*, due to crustal motions relieving internal stresses caused by the aforementioned magnetic field evolution (Kaspi, 2007; Mereghetti, 2008; Woods and Thompson, 2006). Perna and Pons (2011) were the first trying to obtain the bursting properties of these ultra-magnetic NSs taking into account the magneto-thermal evolution of the components (poloidal and toroidal) of the internal magnetic field, obtaining significant differences with observations in the energetics and the recurrence time as the magnetar evolves with time. It was found that objects with a lower toroidal field are less active. The interesting thing is that sporadic bursts were predicted for NSs with magnetic fields between 10^{12} G and 10^{13} G.

Thus, the observations and the theoretical modelling has lead to the conclusion, in the most popular model, that huge magnetic fields power the outbursts events observed in AXPs/SGRs. However, a clear definition of AXPs/SGRs is not always absolute. As we will see, some objects are classified as AXP/SGRs due to their discovery through bursting phenomena. But then it was shown that they did not satisfy the criterion $L_{\rm obs} > \dot{E}_{\rm NS}$, so they also could be modelled as rotationally powered NSs (Coelho et al., 2017). And some even don't satisfy the criterion of being highly magnetic. Let's remember that whether it be in the magnetar model or the white dwarf model, the magnetic field is always, as in the case of rotationally powered pulsars, inferred from the timing properties of the AXPs/SGRs. It is done using a very simple model for the pulsar, the *magnetic dipole* model, where an *oblique rotator* neutron star is assumed to rotate uniformly in vacuo at some frequency Ω and with a *magnetic dipole moment* $\mathbf{m}$ oriented at an angle α to the rotation axis. Let's remember that a pure magnetic dipole field at the magnetic pole of the star, $B_{\rm p}$ is related to $\mathbf{m}$ by the relation

$$|\mathbf{m}| = \frac{B_{\rm p} R^3}{2}. \tag{1.2}$$

Such a configuration radiates energy at a rate (Landau and Lifshitz, 1975; Shapiro and Teukolsky, 1986):

$$\dot{E} = -\frac{2}{3c^3}|\ddot{\mathbf{m}}|^2 = -\frac{B_{\rm p}^2 R^6 \Omega^4 \sin^2\alpha}{6c^3}. \tag{1.3}$$

This equation means that when a rotating dipole magnetic field is aligned with the axis of rotation there is no energy radiated away by it. On the other hand, when the axis of rotation is perpendicular to the dipole field axis, the radiated energy reaches its maximum value. This energy radiated originates from the rotational kinetic energy of the neutron star,

$$E = \frac{1}{2} I_{\rm NS} \Omega^2. \tag{1.4}$$

The rotational energy loss is therefore

$$\dot{E} = I_{\rm NS} \Omega \dot{\Omega}. \tag{1.5}$$

So, if we assume an angle $\alpha = 90^\circ$ we will obtain a lower limit to the magnetic field by requering the rotational energy loss due to the dipole field be equal to the electromagnetic radiation emission of the dipole:

$$B_{\rm p} = \sqrt{\frac{3c^3}{8\pi^2} \frac{I_{\rm NS}}{R^6} P\dot{P}}. \tag{1.6}$$

Using this formula, Duncan and Thompson (1992), Thompson and Duncan (1995) and Thompson and Duncan (1996) determined that AXPs and SGRs are NSs with strong magnetic fields, larger than the quantum critical field $B_{\rm QED}$ defined by:

$$B_{\rm QED} := \frac{m^2 c^3}{e\hbar} = 4.4 \times 10^{13} \text{ G}. \tag{1.7}$$

This quantum critical field is the magnetic field for which the energy of the first Landau level of an electron equals its rest mass. It was often regarded as being the boundary between ordinary pulsars and the magnetars. However, there have been found some AXPs/SGRs with inferred magnetic fields lower or slightly similar to $B_{\rm QED}$ (Turolla and Esposito, 2013). The two sources up to now discovered with a low magnetic field are SGR 0418+5729 ($B \lesssim 7.5 \times 10^{12}$ G, Rea et al. (2010)) and Swift J18822.3-1606 ($B \lesssim 2.7 \times 10^{13}$ G, Rea et al. (2012)) (see also Turolla and Esposito, 2013, and references therein). These two sources widely classified by the scientific as magnetars have dipole magnetic fields well in the range of ordinary radio pulsars. This would imply the magnetic field, considering these objects as isolated neutron stars, would not be the main responsible for the bursting activity, putting a problem to the paradigm in the magnetar model where the high magnetic fields are a requisite for the transient nature of these objects. As we know, normal radio pulsars do not show this magnetar-like activity. This fact, together with other anomalies or discrepancies with the magnetar

picture, pose a challenge to the model and opens the possibility that other models could give account of the properties of these objects.

Another observational fact is that there have been discovered normal radio pulsars with inferred magnetic fields very high (Haberl, 2007). The fact that these radio pulsars have magnetic fields similar to those of AXPs/SGRs modelled as magnetars means that not necessarily a high magnetic field is responsible for bursting activity. From a theoretical point of view we should expect that NSs with similar physical characteristics (dipolar magnetic fields of the same order of magnitude) should share similar observational properties. But high magnetic radio pulsars do not show bursting activity, while AXPs/SGRs, except in some cases, do not emit in radio. These are problems from the theoretical point of view that must be addressed in order to understand better these compact objects.

These problems show us that the magnetar model is not the only acceptable model of AXPs/SGRs and leave us with several alternative models and scenarios. One of them is the white dwarf model; this model was first proposed by Paczynski (1990), where he considered that a fast rotating, highly magnetic and massive WD could explain the AXP 1E 2259+586. The main reason behind Paczynski's hypothesis was that the rotational energy loss $\dot{E}_{\rm WD}$ of a WD can explain from the energetic point of view the observed luminosity $L_{\rm obs}$ in X-rays and γ-rays (Malheiro et al., 2012; Paczynski, 1990; Usov, 1993) detected in 1E 2259+586 (and in all other AXPs/SGRs), i.e., it does not have the problem represented by relation (1.1):

$$\dot{E}_{\rm WD} := -4\pi^2 I_{\rm WD} \frac{\dot{P}}{P^3} \gg L_{\rm obs}, \tag{1.8}$$

where $I_{\rm WD}$ is the moment of inertia of the white dwarf, P is its period of rotation and $\dot{P}$ its time derivative. We just compare equations (1.1) and (4.1) and we can see immediately that a WD behaving as a traditional rotationally powered pulsar could be a good candidate to explain the observations of all AXPs and SGRs up to now observed. Indeed, relation (4.1) is valid for all AXPs/SGRs, not just 1E 2259+586. The reason for this is that the typical moment of inertia of white dwarfs ($\approx 10^{49}$) gcm^2 is several orders of magnitude larger than the typical moment of inertia of neutron stars ($\approx 10^{45}$) gcm^2, making it possible in principle, from an energetic point of view, to explain 1E 2259+586, the first AXP detected and reported by Fahlman and Gregory (1981), as a rotationally powered pulsar-like white dwarf. However, the white dwarf hypothesis was forgotten due to the popularization of the model developed by Duncan and Thompson, the magnetar model. But after the works of Paczynski and Usov were almost forgotten, this idea has been again considered in recent papers (see, e.g. Boshkayev et al., 2013; Cáceres et al., 2017; Coelho and Malheiro, 2014; Lobato et al., 2016; Malheiro et al., 2012; Rueda et al., 2013).

The aforementioned WD model is the main motivation of this work. We

therefore proceed first studying the general theory of structure and stability of static and uniformly rotating WDs (chapter 2). As the magnetic field is important we continue in chapter 3 addressing the issue of magnetism in WDs. We give the main observational aspects of the magnetic WDs, whose most magnetic stars have magnetic fields in the range $(10^6 - 10^9)$. We take into consideration the structure and stability of WDs studied in chapter 2 to show that WDs with magnetic fields much more larger than those up to now confirmed by observations (magnetic fields as large as $\sim 10^{18}$ G) cannot exist in nature due to several instability limits.

In chapter 4 we consider again AXPs/SGRs, showing again that in the WD model the magnetic fields necessary to explain observations are in the range $(10^6 - 10^9)$ G, something which make them similar to the observed magnetic WDs addressed in chapter 3. This gives further support to the model. We continue in chapter 4 showing how the theory of unirofmly rotating WDs allow us to extract more accurate information about the masses, radii or magnetic fields for WDs modelling AXPs/SGRs. We also address the topic of the glitch-outburst connection, the optical, violet and NIR emission observed in some of these sources.

We address in chapter 5 the topic of X-ray emission in the WD model, where it is produced by the particles produced in the magnetosphere of the WD and that hit its surface, making in this way the kinetic energy be converted into thermal energy that is reradiated and observed in earth as a blackbody component in soft X-rays (2-10 keV). We show that the X-ray emission can be explained in this context, giving additional support to this hypothesis.

Finally, in chapter 6 we explore the possibility some of AXPs/SGRs can be in fact not magnetars but ordinary rotationally powered pulsars. We show that this is a viable possibility for several sources when a more realistic equation of state and structure is considered for the NS. And at the end we give the concluding remarks.

Chapter 2

Structure and Stability of non-magnetic White Dwarfs

2.1 Introduction

The structure and stability of white dwarfs is one of the most studied topics in relativistic astrophysics. From the three kind of compact objects that exist in nature, white dwarfs, neutron stars and black holes, the first ones are the best understood both from the theoretical and observational points of view. It is well known that using the quantum properties of electrons, which are fermions, Chandrasekhar (1931), following the pioneering works of Stoner (1929) and Fowler (1926), obtained for the first time a realistic interior density and pressure profile of these objects which allowed him to obtain a new mass-radius relation and consequently an improved value of the maximum stable mass $M_{\rm crit}^{\rm Ch\text{-}L}$ for the white dwarfs (see equation (2.7)). This mass-radius relation has been tested observationally (Provencal et al., 1998; Vauclair et al., 1997) and the mass limit obtained by Chandrasekhar has never been surpassed by any white dwarf reported by observations.

Salpeter (1961) improved the work of Chandrasekhar considering effects neglected by him such as corrections due to the nonuniformity of the electron distribution or the Coulomb interaction between electrons and electrons and ions. Salpeter introduced the concept of a Wigner-Seitz cell to study the electron-ion interior structure of white dwarfs through a lattice model of a point-like nucleus surrounded by a cloud of electrons, including corrections due to the nonuniformity of the electron distribution. In this way Salpeter (1961) obtained a new equation of state pointing out explicitly the relevance of the Coulomb interaction. The consequences of this equation of state on the macroscopic structure of the white dwarf were studied in a subsequent paper by Hamada and Salpeter (1961) obtaining a new critical mass of white dwarfs $M_{\rm crit}^{\rm H\&\,S}$ (see equation (2.9)) that depends in a nontrivial way on the specific nuclear composition.

More recently, Rotondo et al. (2011a) generalized the work of Salpeter by modifying several assumptions such as abandoning the point-like assumption

of the nucleus in order to ensure self-consistency with a relativistic treatment of electrons (see Ferreirinho et al., 1980; Ruffini and Stella, 1981) or the consideration of the contribution of the relativistic electrons to the energy density of the system, a contribution that had always been neglected in the previous treatments.

All these three treatments and their predictions for the mass-radius relation can be compared with the information provided by observations. This can be seen in figure 2.1, where the mass-radius relations for a white dwarf modelled with the equations of state of Chandrasekhar (1931), Salpeter (1961) and Rotondo et al. (2011a), are compared with the estimated masses and radii of white dwarfs from the Sloan Digital Sky Survey Data Release 4 (SDSS-E06 catalog) (Tremblay et al., 2011). We can see that the mass-radius relation fits more or less the observational data, with the most massive stars being the best described by the theoretical descriptions mentioned, while for white dwarfs with masses $\lesssim (0.7 - 0.8) M_{\odot}$, the deviations from these theoretical treatments are already evident. This was expected to happen because the aforementioned approaches consider a degenerate star, where the temperature effects are neglected (it is assumed a temperature $T = 0$), and this approximation of zero temperature or degenerate electron distribution is good for high densities but fails when the densities are low ($\lesssim 10^6$ g cm^{-3}). The effect of finite temperatures is worth of studying because many white dwarfs are well below the lower limiting mass or central density below which the degenerate approximation is not valid anymore; like the recent discovery of ultra-low-mass white dwarfs with masses $\lesssim 0.2\ M_{\odot}$, which are companions of neutron stars in relativistic binaries (see, e.g. Antoniadis et al., 2013, 2012). We will not consider this interesting topic here and we refer the reader to Boshkayev et al. (2016); de Carvalho et al. (2014, 2013), where the work of Rotondo et al. (2011a) is generalized to finite temperatures.

In this chapter we will review the current theoretical knowledge of the structure and stability of non-magnetic white dwarfs. First we will give a review of non-rotating white dwarfs, where briefly will be shown the main physical aspects of the structure of these compact objects and the recent theoretical progress that improved the original work of Chandrasekhar, where several additional effects are considered, such as microscopic instabilities and general relativistic effects. In particular, we will talk about the aforementioned work of Rotondo et al. (2011a), where general relativistic white dwarf equilibrium configurations were studied, considering the formulation of the relativistic Thomas-Fermi model within the Feynman-Metropolis Teller theory for compressed atoms and considering also the β-equilibrium, the nuclear and the Coulomb interactions between the nuclei and the surrounding electrons. All these effects have consequences that modify the Chandrasekhar-Landau mass limit of white dwarfs. The consequences of the different instabilities produced by phenomena such as inverse-β-decay or pycnonuclear reactions are also presented. Then we will give a review of the effects of rotation, where new instabilities appear, and also the mass-radius relation is modified depending on the period or the rotational

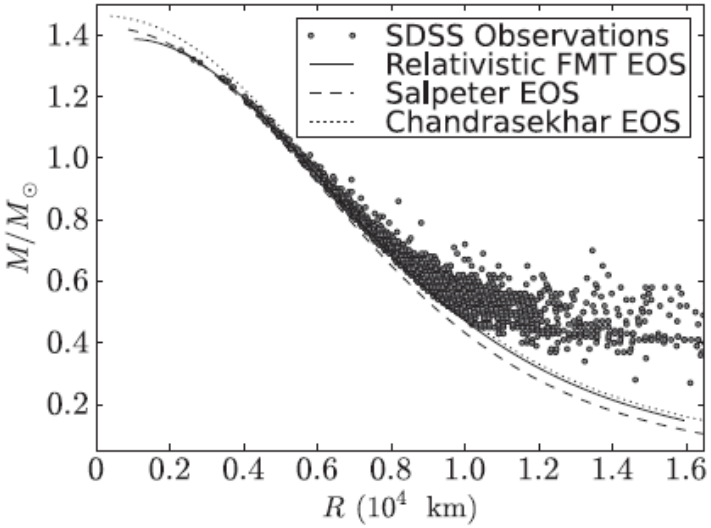

Figure 2.1: Mass-radius relation of degenerate white dwarfs obtained with the relativistic Feynman-Metropolis-Teller (solid black), Salpeter (dashed black) and Chandrasekhar (dotted black) equations of state. These mass-radius relations are compared with the estimated masses and radii of white dwarfs taken from the Sloan Digital Sky Survey Data Release 4 (SDSS-E06 catalog), which are represented by the gray circles (Tremblay et al., 2011). Figure taken from de Carvalho et al. (2014).

angular velocity of the white dwarf. We follow closely the work of Boshkayev et al. (2013), where Hartle's formalism was used to construct the internal and external solutions of the Einstein Field Equations. This work gave the mass M, radius R, angular momentum J, eccentricity ϵ and quadrupole momentum Q of uniformly rotating white dwarfs as a function of the central density ρ_c and the rotational angular velocity Ω. This work allowed to establish new limits to the minimum rotation periods of fast rotating white dwarfs, each limit depending on the chemical composition of the white dwarf.

2.2 Structure and Stability of non-rotating non-magnetic white dwarfs

Before the first theoretical calculations of the structure and stability of white dwarfs were computed, the scientific community had observational evidence of the existence of these dense and compact stars; by indirect methods the masses and the radii of stars like Sirius B were determined and it was discovered the existence of stars with the masses of the order of the solar mass ($M_\odot \sim 1.99 \times 10^{30}$ kg) but with radii of the order of the earth's radius ($\sim 10^8$ cm). Therefore, it was concluded these were very dense objects, denser than the usual stars known by the astronomical community.

The new theory of quantum mechanics allowed to establish the formulation of the Fermi-Dirac statistics and therefore allowed to understand these ob-

jects, where the traditional classical Maxwell-Boltzmann distribution was not longer valid to describe them. If we consider the gas of electrons as a Maxwell-Boltzmann gas, the volume occupied by an electron in the phase space is (Shapiro and Teukolsky, 1986):

$$(\Delta p_{\rm e} \Delta q_{\rm e}) \sim 180 h^3 \left(\frac{M}{M_\odot}\right)^{1/2} \left(\frac{R}{R_\odot}\right)^{3/2}, \tag{2.1}$$

where $R_\odot = 6.96 \times 10^{10}$ cm is the solar radius. Thus when a star with mass $M \sim M_\odot$ contracts to a radius $R \sim 3 \times 10^{-2}\ R_\odot$, the phase space volume occupied by an electron is $\sim h^3$. At such a regime of densities the quantum mechanical effects become important due to the Pauli exclusion principle and the Maxwell-Boltzmann distribution is no longer valid. Instead the Fermi-Dirac statistics must be used. This distribution allows the gas of electrons to counterbalance the gravitational collapse. At sufficiently high densities (where the approximation of zero temperature is very accurate) the gas becomes degenerate and the electrons occupy all energy levels up to the Fermi energy $E_{\rm F}$, which itself depends on the mass density of the electrons $\rho_{\rm e}$ through the relation:

$$\rho_{\rm e} = \frac{8\pi m_{\rm e}}{3h^3} p_{\rm F}^3, \tag{2.2}$$

where the *Fermi momentum* $p_{\rm F}$ has been introduced:

$$E_{\rm F} \equiv (p_{\rm F}^2 c^2 + m_{\rm e}^2 c^4)^{1/2}. \tag{2.3}$$

This concept of degenerate stars was first introduced by Fowler (1926). This concept was used by Stoner (1929), who followed Fowler's idea, but introducing, for the first time, the effects of special relativity in the Fermi-Dirac statistics obtaining a generalized equation of state of the electron gas. Stoner also assumed a constant density throughout the whole white dwarf. Stoner (1929) obtained a critical mass for white dwarfs given by:

$$M_{\rm crit}^{\rm Stoner} = \frac{15}{16}\sqrt{5\pi}\frac{M_{\rm Pl}^3}{\mu^2 m_{\rm n}^2} \approx 3.72 \frac{M_{\rm Pl}^3}{\mu^2 m_{\rm n}^2} \approx 1.714 M_\odot, \tag{2.4}$$

where $M_{\rm Pl} = \sqrt{\hbar c/G} \approx 2.18 \times 10^{-5}$ g is the Planck mass, $m_{\rm n} = 1.675 \times 10^{-24}$ g is the neutron mass, and $\mu = A/Z \approx 2$ is the average molecular weight of matter.

However, a more realistic picture must consider the gradient of the density as follows: when we consider in an appropriate way the hydrostatic Newtonian equilibrium equation:

$$\frac{dP}{dr} = -\frac{Gm(r)}{r^2}\rho, \tag{2.5}$$

and when we consider also some equation of state $P = P(\rho)$, we can obtain a differential equation for the density $\rho(r)$, whose solution will give us the structure of the star. The solutions to these hydrostatic equations (or its refinements, where several effects are considered, as we will see in this subsection) allowed to construct relations between the total mass of the star M, its radius R and its central density ρ_c (see subsection 2.2.3 for details). These solutions also allow to determine a critical mass that any white dwarf cannot surpass, otherwise it becomes unstable because electron degeneracy pressure (also known as Fermi pressure) cannot counterbalance gravitational collapse (see subsection 2.2.3 for details).

It happens that in the extreme relativistic and non-relativistic limits of the equation of state of a degenerate fermionic gas, the equation of state has a simple analytic polytropic form; a polytropic equation of state is defined by the relation:

$$P = K\rho^{\Gamma}, \tag{2.6}$$

where K and γ are constants. For the ideal Fermi gas equation of state the constant Γ has a value $\Gamma = 5/3$ for the non-relativistic limit while a value $\Gamma = 4/3$ for the ultra relativistic limit. It turns out that when the polytropic equation of state (2.6) is used in the hydrostatic Newtonian equilibrium equation (2.5), this Newtonian equilibrium equation, after making an appropriate change of variables, becomes the well-known *Lane-Emden equation*. This equation allows to obtain the radius R of the star evaluating the point where $P = 0$ and $\rho = 0$. Chandrasekhar and Landau used the method of solutions of the Lane-Emden polytropic equations, obtaining a critical mass given by (Chandrasekhar, 1931; Landau, 1932):

$$M_{\text{crit}}^{\text{Ch-L}} = 2.015\frac{\sqrt{3\pi}}{2}\frac{M_{\text{PL}}^3}{\mu^2 m_{\text{n}}^2} \approx 3.09\frac{M_{\text{PL}}^3}{\mu^2 m_{\text{n}}^2} \approx 1.427 M_{\odot}. \tag{2.7}$$

When this critical mass is surpassed the pressure of degenerate gas of electrons can not balance the gravitational collapse. So, an observational test of this analysis should be to find white dwarfs with masses larger than this critical mass, and up to now not a single white dwarf surpassing this upper bound has been observed.

One characteristic of the solution obtained by Chandrasekhar (in the extreme relativistic limit, where the polytropic index is $\Gamma = 4/3$) is that while the density increases indefinitely, the radius decreases with the density approaching to

zero while the mass remains independent of the central density (see Shapiro and Teukolsky, 1986). In this Newtonian picture of white dwarfs we can obtain arbitrarily compact objects provided the total mass satisfies the Chandrasekhar limit imposed by equation (2.7). However, this picture is not true because for a small value of compactness (which is $\propto M/R$), general relativistic effects become non-negligible. So, density cannot be arbitrarily large, firstly due to microscopic instabilities (see sections 2.2.1 and 2.3.3) and second because the solution obtained by Chandrasekhar and Landau used the Newtonian hydrostatic equilibrium equation, not valid for high densities (see below the Tolman-Oppenheimer-Volkoff equations (2.16), (2.17) and (2.18) that generalise Newtonian equation (2.5)). When General Relativity is properly considered in the equilibrium equations the density can not increase arbitrarily due to dynamical instabilities (see section 2.2.2, Shapiro and Teukolsky, 1986, and references therein).

Chandrasekhar treated the electrons as a free gas, ignoring effects due to the Coulomb interaction between nuclei and electrons and of course, between electrons. In Chandrasekhar's work the nuclei provided most of the mass density (the density of electrons was neglected) while the pressure was considered entirely due to the gas of electrons. As we said, this gas was considered free, but the electrostatic interactions make a contribution to the pressure of the electrons. For sufficiently high densities the Coulomb interaction can be considered as a small perturbation to the free gas solution (in the opposite case the Coulomb interaction is no longer a small perturbation). The electron-electron Coulomb interaction turns out to be smaller than the electron-ion interaction, hence the total effect of the electrostatic interactions is to reduce the pressure of the electron gas. The method used to approach this problem is the so-called "lattice" model which introduces the concept of Wigner-Seitz cell, where each cell is composed of a point-like nucleus of charge $+Ze$ with A nucleons located at the center and surrounded by an uniformly distributed gas of Z electrons, all completely degenerate. The global neutrality of each cell is assumed, so, there are not electrostatic interactions between the different Wigner-Seitz cells.

The first correction mentioned above considered the electrostatic interactions of an uniformly distributed cloud of degenerate electrons. However, the electron distribution cannot be uniform due to the same electrostatic interaction. So, naturally, the next correction comes into place when we consider a non-uniform distribution of electrons. These effects are considered consistently in the *Thomas-Fermi* equation, which comes from the electromagnetic Poisson equation and the fact that electrons obey the Fermi-Dirac statistics. In the Thomas-Fermi method is assumed that within each Wigner-Seitz cell the electrons move in a spherically symmetric potential $V(r)$ and that this potential is slowly varying at any point, allowing to use locally the free-particle Fermi-Dirac statistics. In order to have a spherically symmetric potential the interaction energy between electrons is assumed to be less than the kinetic or potential energies of each individual electron. The Fermi energy $E_{\rm F}$ is independent of r, ensuring in this way that electrons do not migrate to regions with smaller $E_{\rm F}$; so, the Thomas-Fermi equi-

librium condition for degenerate non-relativistic electrons in the cell is:

$$E_{\mathrm{F}} = -eV(r) + \frac{p_{\mathrm{F}}(r)}{2m_{\mathrm{e}}} = \text{constant} > 0, \tag{2.8}$$

where $p_{\mathrm{F}}(r)$ is the maximum momentum (Fermi momentum) of electrons at r.

Salpeter (1961), well aware of these effects ignored in the previous works, adopted for the study of the white dwarfs the aforementioned Wigner-Seitz cell approach. He obtained an analytic formula for the total energy in a Wigner-Seitz cell and derived the corresponding equation of state of the white dwarf modelled by such cells. The consequences of the equation of state obtained by Salpeter (1961) on the mass and radius of white dwarfs were explored in a subsequent article, Hamada and Salpeter (1961), where a new expression for the critical mass was obtained:

$$M_{\mathrm{crit}}^{\mathrm{H\&\,S}} = 2.015\frac{\sqrt{3\pi}}{2}\frac{1}{\mu_{\mathrm{eff}}^2}\frac{M_{\mathrm{Pl}}^3}{m_{\mathrm{n}}^2}, \tag{2.9}$$

where

$$\mu_{\mathrm{eff}} = \mu\left(\frac{P_{\mathrm{S}}}{P_{\mathrm{Ch}}}\right)^{-3/4}, \tag{2.10}$$

being P_{S} the pressure of the Wigner-Seitz cell obtained by Salpeter (1961) and P_{Ch} the pressure of a free-electron fluid used by Chandrasekhar. The ratio $P_{\mathrm{S}}/P_{\mathrm{Ch}}$ is a function of the number of protons Z, a direct consequence of the Coulomb interaction, that makes the critical mass now depends on the specific nuclear composition of the white dwarf, unlike in the previous simplified approaches, where it depended only on the ratio A/Z. The results of Salpeter (1961) also imply that $P_{\mathrm{S}}/P_{\mathrm{Ch}} < 1$, so the effective molecular weight satisfies $\mu_{\mathrm{eff}} > \mu$ and therefore, comparing with equation (2.7), the critical mass of white dwarfs turns out to be smaller than the original one obtained by Chandrasekhar and Landau.

We have to remember that equation (2.8) corresponds to the classical Thomas-Fermi model. This equation considers the consequences of the Fermi-Dirac statistics only on the kinetic energy of the electron. However this does not take into account the effects of the antisymmetric wave functions on the electrostatic interaction energy. Dirac (1930) was the first to point out the relevance of these exchange effects on the Thomas-Fermi model of the atom. Hence the model of Thomas-Fermi that also includes these effects is known as the Thomas-Fermi-Dirac model and modifies the equation (2.8):

$$E_{\mathrm{F}} = \frac{p_{\mathrm{F}}^2}{2m_{\mathrm{e}}} - eV - \frac{e^2}{\pi\hbar} p_{\mathrm{F}} = \text{constant} > 0. \tag{2.11}$$

This is not the only generalization of the Thomas-Fermi equation. Look that the relation between the Fermi energy and the Fermi momentum in relation (2.8) is non-relativistic. Of course, the correct relation between these two quantities at a relativistic regime is different, so the equilibrium condition for the Thomas-Fermi atom is modified in relativistic regimes by:

$$E_{\mathrm{F}} = \sqrt{(p_{\mathrm{F}})^2 + m_{\mathrm{e}}^2 c^4} - m_{\mathrm{e}}^2 c^4 - eV(r) = \text{constant}, \tag{2.12}$$

and correspondingly the relativistic Thomas-Fermi-Dirac equilibrium condition becomes:

$$E_{\mathrm{F}} = \sqrt{(p_{\mathrm{F}})^2 + m_{\mathrm{e}}^2 c^4} - m_{\mathrm{e}}^2 c^4 - eV(r) - \frac{e^2}{\pi\hbar} p_{\mathrm{F}} = \text{constant}. \tag{2.13}$$

Rotondo et al. (2011b) extended the global approach of Feynman et al. (1949) considering the relativistic Thomas-Fermi and Thomas-Fermi-Dirac models. They showed that for high densities the exchange effects become negligible so that the results of the relativistic Thomas-Fermi model alone can be considered as an excellent approximation to describe the structure of white dwarfs. The relativistic Thomas-Fermi model was solved by imposing in addition to the electromagnetic interaction also the weak equilibrium between neutrons, protons and electrons in a self-consistent way. This equilibrium condition relates the chemical potentials of electrons μ_{e}, protons μ_{p} and neutrons μ_{n} by the equation:

$$\mu_{\mathrm{e}} + \mu_{\mathrm{p}} = \mu_{\mathrm{n}}. \tag{2.14}$$

Rotondo et al. (2011b) abandoned the pointlike assumption of the nucleus introducing a finite sized nucleus, warranting in this way a self-consistent treatment with a relativistic approach of the electrons. This is because equation (2.12) (or (2.13), because the exchange effects are not significant for high densities) leads to a nonintegrable expression for the electron density near the origin.

Another contribution of Rotondo et al. (2011b) was to consider the energy density of the system as the sum of the contributions of the nuclei, the Coulomb interactions and the relativistic electrons, being the last one ignored in the previous approaches.

Then Rotondo et al. (2011a), following closely the results of Rotondo et al. (2011b), applied the approach of a compressed atom in a Wigner-Seitz cell to

describe nonrotating white dwarfs in General Relativity, obtaining the relativistic Feynman-Metropolis-Teller equation of state in GR, assuming a metric that fits a spherically symmetric system:

$$ds^2 = e^{\nu(r)}c^2dt^2 - e^{\lambda(r)}dr^2 - r^2d\theta^2 - r^2\sin^2\theta d\phi^2. \tag{2.15}$$

This metric implies that the Einstein equations can be written in the Tolman-Oppenheimer-Volkoff form (Oppenheimer and Volkoff, 1939; Tolman, 1939):

$$\frac{d\nu(r)}{dr} = \frac{2G}{c^2}\frac{4\pi r^3 P(r)/c^2 + M(r)}{r^2\left[1 - \frac{2GM(r)}{c^2 r}\right]}, \tag{2.16}$$

$$\frac{dM(r)}{dr} = 4\pi r^2\frac{\epsilon(r)}{c^2}, \tag{2.17}$$

$$\frac{dP(r)}{dr} = -\frac{1}{2}\frac{d\nu(r)}{dr}[\epsilon(r) + P(r)], \tag{2.18}$$

where $M(r)$ stands for the mass enclosed at the distance r, it has been used the relation $e^{\lambda(r)} = 1 - 2GM(r)/(c^2 r)$, $\epsilon(r)$ is the energy density and $P(r)$ is the total pressure. This equation therefore generalized the hydrostatic Newtonian equilibrium equation. The numerical integration of this set of equations allows to obtain the mass-radius relation and the mass-central density relation of the relativistic white dwarfs within the relativistic Feynman-Metropolis-Teller theory for compressed atoms. However, before showing the results of these integrations it is necessary to talk about some instabilities like the inverse β-decay instability or the General Relativity instability that constrain the range of values for the mass or the central density of the white dwarfs.

2.2.1 Inverse β-decay

At high densities the most important correction to the equation of state is due to the inverse β-decay process $(Z, A) \rightarrow (Z-1, A)$, where energetic electrons are captured:

$$^{A}_{Z}\mathrm{X} + e^- \rightarrow {}^{A}_{Z-1}\mathrm{Y} + \nu_e. \tag{2.19}$$

In this process a proton combines with an electron to give a free neutron and a neutrino, which in the case of a gas of free electrons, protons and neutrons is simply:

$$e^- + p \rightarrow n + \nu_e. \tag{2.20}$$

This reaction is possible only when the electron has enough energy to surpass the mass difference between proton and neutron, $(m_n - m_p)c^2 = 1.29$ MeV.

As we mentioned before the electron pressure is important to avoid the gravitational collapse, and when the number of electrons start to diminish, the white dwarf becomes gravitationally unstable. This makes the inverse β-decay a process that triggers the instability of the star because is an effective way to reduce the number of electrons and increase the number of free neutrons. However, it is balanced by the free neutron β-decay:

$$n \rightarrow p + e + \bar{\nu}. \tag{2.21}$$

When these two processes are counterbalanced we have an equilibrium described by equation (2.14). However, as long as we increase the density, the Fermi energy also increases up to a point where β-decay reaction (2.21) is blocked because the Fermi energy is high enough that all electron energy levels in the Fermi sea are occupied up to the one that the emitted electron would fill. Is at this point where the inverse β-decay instability makes the existence of white dwarfs with densities beyond such a critical density physically impossible.

So, when density starts to increase we reach a density where relation (3.2) is triggered ($\sim 10^7$ g cm^{-3}) but is balanced by reaction (2.21), this because free neutrons are unstable and have a mean lifetime ~ 14 min. However, there is a density ($\sim 10^{11}$ g cm^{-3}) where reaction (2.21) is blocked and the white dwarf becomes unstable. At such densities the electron Fermi energy must be larger than the mass difference between the initial nucleus (Z, A) and the final nucleus $(Z-1, A)$. Such a threshold energy is denoted by $E^{\beta}_{\mathrm{F,\,Z}}$. Usually $E^{\beta}_{\mathrm{F,Z\text{-}1}} < E^{\beta}_{\mathrm{F,Z}}$ and the initial nucleus undergoes two successive decays, i.e., $(Z, A) \rightarrow (Z-1, A) \rightarrow (Z-2, A)$ (see, e.g. Salpeter, 1961; Shapiro and Teukolsky, 1986). As we know, the electron Fermi energy is proportional to the density, so configurations with $\rho > \rho^{\beta}_{\mathrm{crit}}$, where $\rho^{\beta}_{\mathrm{crit}}$ is the density corresponding to the threshold energy $E^{\beta}_{\mathrm{F,Z}}$, are unstable.

The threshold energy can be obtained from a table reporting experimental values of atomic masses. We show in table 2.1 the threshold energies for different inverse β-decay reactions. These values were taken from Audi et al. (2003), where experimental values of atomic masses are reported. We also show in table 2.1 the corresponding critical density $\rho^{\beta}_{\mathrm{crit}}$, which was obtained solving the Thomas-Fermi equation and hence obtaining a relation between the threshold energy and the corresponding critical density. There is also a dependence on A

Decay	$E^{\beta}_{\mathrm{F,Z}}$ (MeV)	$\rho^{\beta}_{\mathrm{crit}}$ (g cm^{-3})
$^{4}\mathrm{He}\rightarrow\ ^{3}\mathrm{H}+n\rightarrow 4n$	20.596	1.39×10^{11}
$^{12}\mathrm{C}\rightarrow^{12}\mathrm{B}\rightarrow^{12}\mathrm{Be}$	13.370	3.97×10^{10}
$^{16}\mathrm{O}\rightarrow^{16}\mathrm{N}\rightarrow^{16}\mathrm{C}$	10.419	1.94×10^{10}
$^{56}\mathrm{Fe}\rightarrow^{56}\mathrm{Mn}\rightarrow^{56}\mathrm{Cr}$	3.695	1.18×10^{9}

Table 2.1: Onset for the inverse β-decay for ^{4}He, ^{12}C, ^{16}O and ^{56}Fe. The experimental values of the threshold energy $E^{\beta}_{\mathrm{F,Z}}$ have been taken from Audi et al. (2003). The corresponding critical density $\rho^{\beta}_{\mathrm{crit}}$ are for the relativistic Feynman-Metropolis-Teller equation of state (Rotondo et al., 2011a).

and Z, as we can appreciate in the table. For the case of the Salpeter equation of state corresponding to the uniform approximation an analytical expression between these quantities is obtained. However, when it comes to solve the relativistic Thomas-Fermi equation no analytical solution exists and instead a numerical integration has to be employed.

2.2.2 General Relativity instability

A white dwarf is a fluid which is subject to perturbations of its configuration. These perturbations are small and modify quantities such as the density or the pressure. The equations governing these small perturbations of a static equilibrium configuration allow to calculate the frequencies and normal modes of oscillation of the configuration and allow to address the issue of the stability of the equilibrium configuration. An instability corresponds to the unbounded growth of a small initial perturbation, so the conditions of the fluid that make it happen should set the criteria for stability.

There is a criterion to determine the onset of the instability due to perturbations. In a sequence of equilibrium stars that obey the same equation of state but that differ on the central density, the mass of a non-rotating star is limited by the first maximum of the $M-\rho_{\mathrm{c}}$ curve, i.e., the point that satisfies $\partial M/\partial\rho_{\mathrm{c}}=0$. This marks the secualr instability point and coincides with the dynamical instability point if the perturbation obeys the same equation of state the equlibrium configuration obeys (see for details, e.g. Shapiro and Teukolsky, 1986, and references therein). It applies to Newtonian configurations as well as to general relativistic configurations. When General Relativity is considered the total mass-energy of the star has to be considered. So, the density ρ_{c} that satisfies the turning-point criterion will be the critical density for the onset of instability due to general relativity in a white dwarf. This density depends on the chemical composition of the white dwarf.

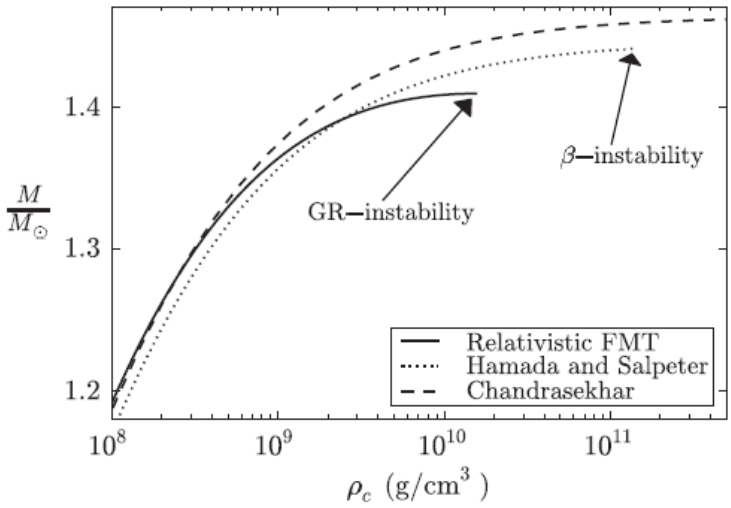

Figure 2.2: Mass in solar masses as a function of the central density for ^{4}He white dwarfs. The solid curve corresponds to the solution of the relativistic FMT approach solved in Rotondo et al. (2011a), while the dotted curve corresponds to the Newtonian configuration of Hamada and Salpeter (Hamada and Salpeter, 1961), while the dashed curve is the Newtonian configuration of Chandrasekhar. Figure taken from Rotondo et al. (2011a).

2.2.3 Mass-radius and mass-central density relations

When both β-decay equilibrium and general relativity have been considered self-consistently, it is possible to determine the critical mass and the instability that determines it. This can be seen in figures 2.2, 2.4, 2.6, 2.8, where a plot M vs. ρ_c is shown for different chemical compositions. The results of Rotondo et al. (2011a) are compared with the results of Hamada and Salpeter (1961) and the Chandrasekhar equation of state. In all of them is shown where the critical mass is reached and which instability sets it in. The same can be appreciated in figures 2.3, 2.5, 2.7, 2.9, where instead a plot M vs. R is shown for the same equations of state and the same chemical compositions.

The main result is that the white dwarfs with the lighter nuclei, ^{4}He and ^{12}C are unstable with respect to General Relativity while the white dwarfs with heavier compositions, e.g. ^{16}O and ^{56}Fe, are unstable due to inverse β-decay of the nuclei. We list in table 2.2.3 the critical densities for the different compositions, the corresponding maximum mass and the type of instability.

One of the most important contributions made by Rotondo et al. (2011a) is that they obtained a new value for the critical density of ^{12}C white dwarfs ($\sim 2.12 \times 10^{10}$) g/cm^3 that correct the value 2.65×10^{10} g/cm^3 obtained from calculations based on general relativistic corrections to the theory of polytropes (see, for instance Shapiro and Teukolsky, 1986). This is possible because unlike

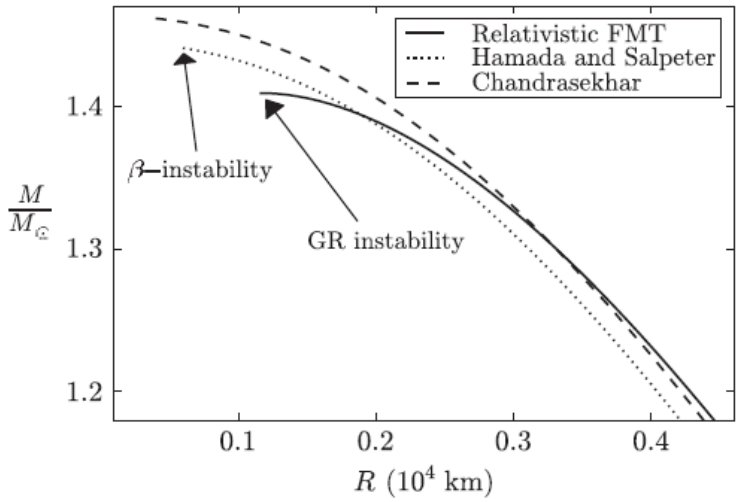

Figure 2.3: Mass in solar masses as a function of the radius for ^{4}He white dwarfs. The solid curve corresponds to the solution of the relativistic FMT approach solved in Rotondo et al. (2011a), while the dotted curve corresponds to the Newtonian configuration of Hamada and Salpeter (Hamada and Salpeter, 1961), while the dashed curve is the Newtonian configuration of Chandrasekhar. Figure taken from Rotondo et al. (2011a).

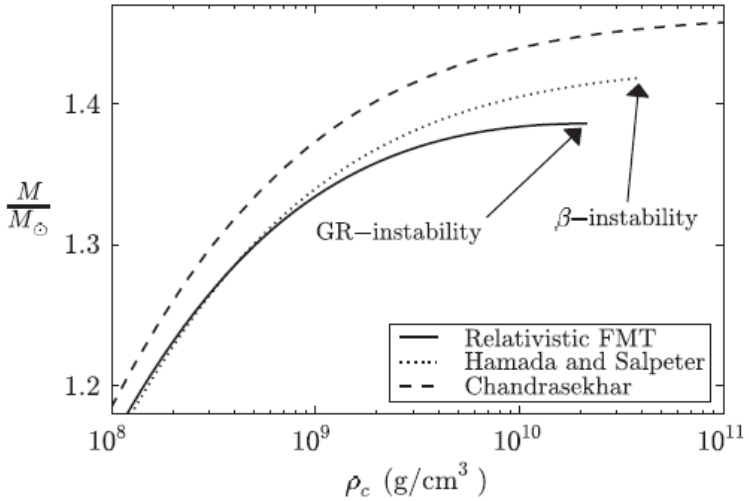

Figure 2.4: Mass in solar masses as a function of the central density for ^{12}C white dwarfs. The solid curve corresponds to the solution of the relativistic FMT approach solved in Rotondo et al. (2011a), while the dotted curve corresponds to the Newtonian configuration of Hamada and Salpeter (Hamada and Salpeter, 1961), while the dashed curve is the Newtonian configuration of Chandrasekhar. Figure taken from Rotondo et al. (2011a).

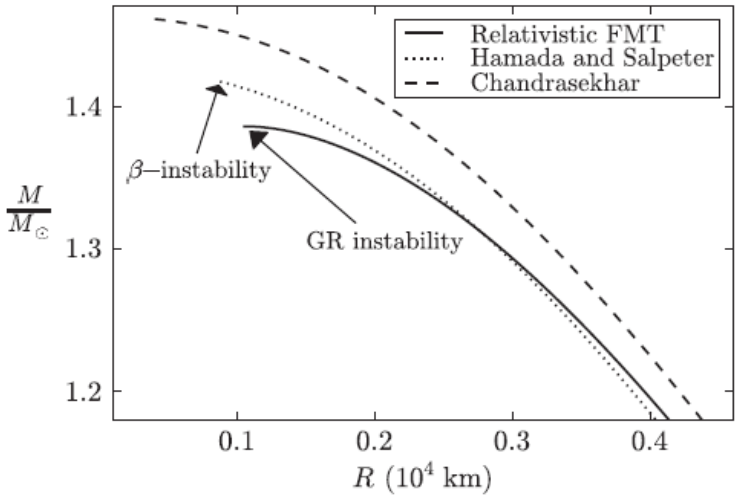

Figure 2.5: Mass in solar masses as a function of the radius for ^{12}C white dwarfs. The solid curve corresponds to the solution of the relativistic FMT approach solved in Rotondo et al. (2011a), while the dotted curve corresponds to the Newtonian configuration of Hamada and Salpeter (Hamada and Salpeter, 1961), while the dashed curve is the Newtonian configuration of Chandrasekhar. Figure taken from Rotondo et al. (2011a).

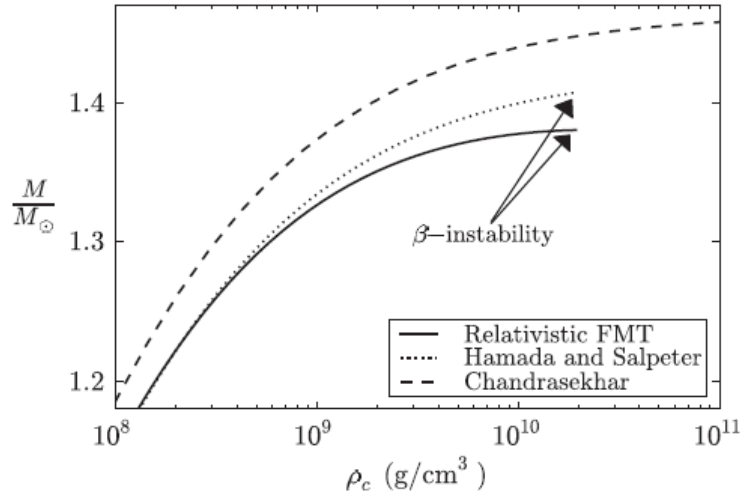

Figure 2.6: Mass in solar masses as a function of the central density for ^{16}O white dwarfs. The solid curve corresponds to the solution of the relativistic FMT approach solved in Rotondo et al. (2011a), while the dotted curve corresponds to the Newtonian configuration of Hamada and Salpeter (Hamada and Salpeter, 1961), while the dashed curve is the Newtonian configuration of Chandrasekhar. Figure taken from Rotondo et al. (2011a).

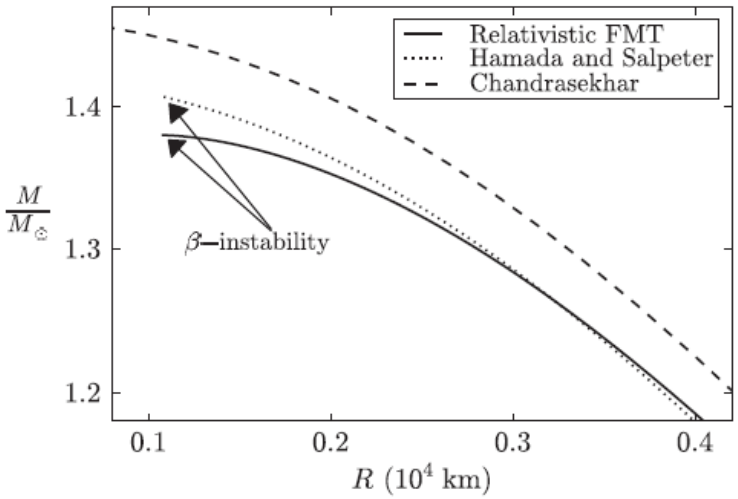

Figure 2.7: Mass in solar masses as a function of the radius for ^{16}O white dwarfs. The solid curve corresponds to the solution of the relativistic FMT approach solved in Rotondo et al. (2011a), while the dotted curve corresponds to the Newtonian configuration of Hamada and Salpeter (Hamada and Salpeter, 1961), while the dashed curve is the Newtonian configuration of Chandrasekhar. Figure taken from Rotondo et al. (2011a).

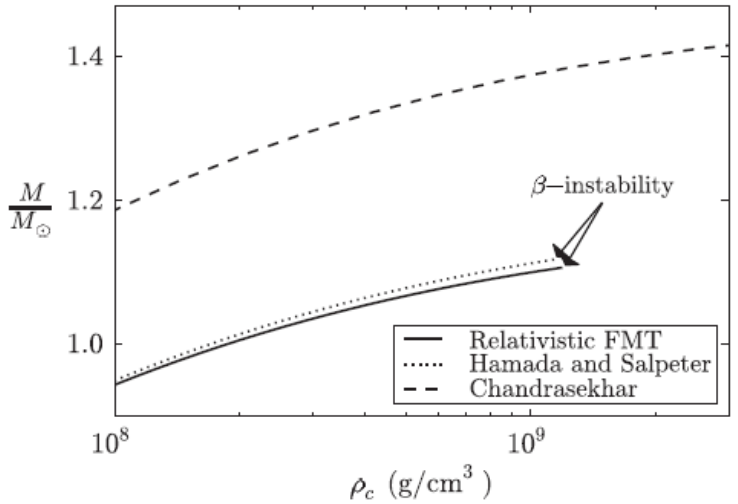

Figure 2.8: Mass in solar masses as a function of the central density for ^{56}Fe white dwarfs. The solid curve corresponds to the solution of the relativistic FMT approach solved in Rotondo et al. (2011a), while the dotted curve corresponds to the Newtonian configuration of Hamada and Salpeter (Hamada and Salpeter, 1961), while the dashed curve is the Newtonian configuration of Chandrasekhar. Figure taken from Rotondo et al. (2011a).

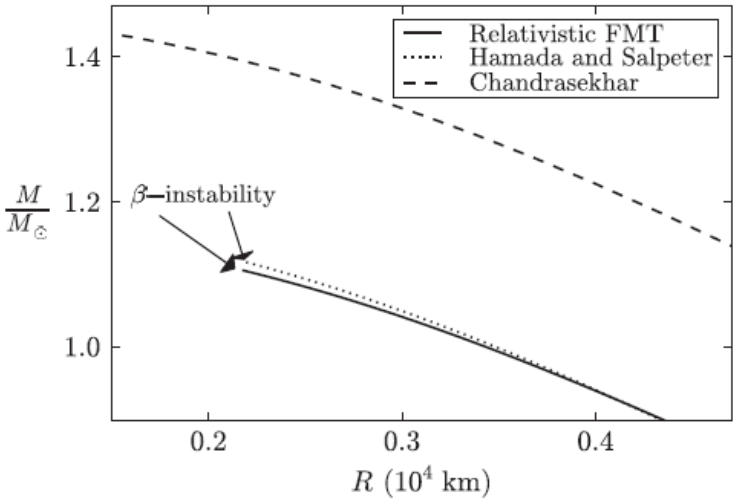

Figure 2.9: Mass in solar masses as a function of the radius for ^{56}Fe white dwarfs. The solid curve corresponds to the solution of the relativistic FMT approach solved in Rotondo et al. (2011a), while the dotted curve corresponds to the Newtonian configuration of Hamada and Salpeter (Hamada and Salpeter, 1961), while the dashed curve is the Newtonian configuration of Chandrasekhar. Figure taken from Rotondo et al. (2011a).

Composition	$\rho_{\text{crit}}^{\text{relFMT}}$	$M_{\text{crit}}^{\text{relFMT}}/M_\odot$	Instability
^{4}He	1.56×10^{10}	1.41	GR
^{12}C	2.12×10^{10}	1.39	GR
^{16}O	1.94×10^{10}	1.38	Inv. β
^{56}Fe	1.18×10^{9}	1.11	Inv. β

Table 2.2: Critical density and corresponding critical mass for the onset of gravitational collapse of ^{4}He, ^{12}C, ^{16}O and ^{56}Fe white dwarfs of the general relativistic configurations obtained in Rotondo et al. (2011a) based on the relativistic Feynman-Metropolis-Teller equation of state (Rotondo et al., 2011b). The densities are in units of g/cm^3 and the masses in units of solar masses. Values taken from Rotondo et al. (2011a).

in all previous approaches, the contribution of the electrons to the energy density of the system was considered. Otherwise, the critical density for ^{12}C white dwarfs should be determined by the inverse β-decay, whether or not the effects of General Relativity are considered.

The other significant conclusion obtained by Rotondo et al. (2011a) is that the Coulomb effects are much more pronounced in the case of white dwarfs with heavy nuclear compositions; for instance, see figures 2.8, 2.9. It can be seen that the result of Hamada and Salpeter as well as the result of Rotondo et al. (2011a) make a significant correction to the results of Chandrasekhar that neglects Coulomb effects. Neglecting these effects leads to an overestimation of the mass of the white dwarfs.

2.3 Uniformly rotating white dwarfs

The effect of rotation in the structure of uniformly rotating white dwarfs has been studied by several authors (Anand, 1965; Arutyunyan et al., 1971; Geroyannis and Hadjopoulos, 1989; James, 1964; Monaghan, 1966; Roxburgh and Durney, 1966), where it has been concluded that rotation enhance the maximum stable mass of white dwarfs. the issue of stability of uniformly and differentially rotating white dwarfs has been studied also by several authors (see, e.g. Durisen, 1975; Ostriker and Bodenheimer, 1968; Ostriker and Tassoul, 1969; Tassoul and Ostriker, 1970). All these works were considered in the framework of newtonian gravity or post-newtonian approximation. However, Arutyunyan et al. (1971) investigated uniformly rotating white dwarfs within General Relativity using the Chandrasekhar equation of state. As we saw in the previous section, the description done by Chandrasekhar is incomplete because important contributions due to the electrostatic interactions or the non-uniformity of the electron distribution.

Boshkayev et al. (2013) extended the results of Rotondo et al. (2011a), presented in the previous section, for uniformly rotating white dwarfs at zero temperatures. We could say that they also generalized the work of Arutyunyan et al. (1971) by considering an equation of state more realistic than the Chandrasekhar equation of state. However, Arutyunyan et al. (1971) used an Ω^2 approximation following a method developed by Sedrakyan and Chubaryan (1968) while Boshkayev et al. (2013) used the Hartle's approach (Hartle, 1967) to solve the Einstein equations.

In Hartle's formalism the structure of rotating objects is described approximately up to second-order in terms of the angular velocity of the star Ω. In this approach is possible to calculate the mass M, the equatorial $R_{\rm eq}$ and polar $R_{\rm p}$ radii, the angular momentum J, the quadrupole moment Q as well as the moment of inertia, depending these quantities, as expected, on the central density $\rho_{\rm c}$ and the rotational angular velocity Ω of the White Dwarf. In this approach the white dwarf is rotating uniformly and the solution of the Einstein equations

in the exterior vacuum can be written analytically in terms of M, J and Q. In this formalism the parameters M, J and Q are obtained for a given equation of state from the matching between the internal and external solutions at the surface of the rotating star.

When a rotating configuration is considered there appears the mass-shedding limit. And besides this instability limit, there are other instabilities, such as the inverse β-decay instability, the pycnonuclear instability and the secular axysimmetric instabilitiy, some of them mentioned in the previous section. As we will see, all these boundaries limit the range of possible values for the mass, the radius or the moment of inertia of an uniformly rotating white dwarf with a given rotational period P. This is important when highly rotating white dwarfs are considered as a model for AXP/SGRs.

Let's discuss some of the new instabilities not discussed in the previous section, such as the pycnonuclear reaction instability or the mass-shedding limit, that limits the mass of a rotating configuration.

2.3.1 The Mass-shedding limit

A particle on the equatorial surface of the star cannot exceed the Keplerian angular velocity of an equivalent free particle at the same location. Particles in that limit remain bound to the star only because of a balance between gravity and centrifugal forces. A star rotating at this Keplerian velocity eventually loss mass and becomes unstable (Stergioulas, 2003).

The mass-shedding angular velocity of a rotating star is computed for the Hartle's formalism calculating the four-velocity of a test particle on a circular orbit in the equatorial plane (see Boshkayev et al., 2013, for details). In this way is possible to calculate the angular velocity of corotating as well as counterrotating orbits. The result is an analytic formula for the Keplerian velocity that is a function of the mass M, the equatorial radius $R_{\rm eq}$, the angular momentum J and the quadrupole moment Q of the star (see Boshkayev et al., 2013).

The accuracy of such a result depends on the accuracy of the slow rotation approximation. Boshkayev et al. (2013) performed an analysis of the accuracy of this slow rotation approximation obtaining that the accuracy increases with the density of the white dwarf and that the Keplerian sequence of rotating white dwarfs can be described by the Ω^2 approximation within an error smaller than $\lesssim 6\%$.

2.3.2 Secular Instability in rotating and general relativistic configurations

As we mentioned in the last section, the point where $\partial M/\partial \rho_{\rm c} = 0$ marks the secular instability point for a static non-rotating configuration. This applies whether

we are considering a Newtonian or a General Relativistic configuration. For the case of a rotating configuration Friedman et al. (1988) formulated, based on previous works (Sorkin, 1981, 1982), a *turning-point method* to locate the points where secular instability sets in for uniformly rotating relativistic stars: for a sequence of rotating stars with fixed angular momentum J but variable central density ρ_c, the onset of the secular axisymmetric instability is determined by the relation:

$$\left(\frac{\partial M(\rho_c, J)}{\partial \rho_c}\right)_J = 0. \tag{2.22}$$

Boshkayev et al. (2013) constructed the boundary given by the turning points of constant angular momentum sequences given by the above equation. This boundary can be appreciated in the M vs. R or M vs. ρ_c curves.

2.3.3 Pycnonuclear Reactions

In a thermonuclear reaction the thermal energy of the reacting nuclei overcomes the Coulomb repulsion between them so that the reaction can proceed. However, nuclear reactions can take place even at zero temperature if densities are sufficiently high; this because ions fluctuating about their lattice sites with zero-point energy can penetrate the Coulomb barrier of neighbouring ions. This zero point energy is given by (Shapiro and Teukolsky, 1986):

$$E_0 = \hbar\omega_p, \qquad \omega_p = \left(\frac{4\pi e^2 Z^2 \rho}{A^2 M_u^2}\right)^{1/2}, \tag{2.23}$$

where $M_u = 1.6605 \times 10^{-24}$ g is the atomi mass unit.

In order to calculate the effect of the pycnonuclear fusion reactions on the stability of the white dwarfs a nuclear composition has to be assumed. In the case of the model presented in Boshkayev et al. (2013) an unique nuclear composition (Z,A) is assumed throughout the star.

As we mentioned before the pycnonuclear reaction depends on the density of the white dwarf star. If the density is higher the pycnonuclear reaction time will be lower. So, it is necessary to assume a time, smaller than the Hubble time, to assess whether or not a given pycnonuclear reaction is or not relevant for the stability analysis of the white dwarf. Assuming a time of 0.1 Myr, Salpeter (1961) estimated that the reaction ^{1}H $\rightarrow^4$ He happens at $\rho \sim 5 \times 10^4$ gcm^{-3}, the reaction ^{4}He $\rightarrow^{12}$ C happens at a density $\rho \sim 8 \times 10^8$ gcm^{-3} and the reaction ^{12}C $\rightarrow^{24}$ Mg happens at $\rho \sim 6 \times 10^9$ gcm^{-3}. As we can see, as we increase the atomic number the density increases. The density at which these reactions occur for the given time are smaller than the usual critical densities for the onset of the inverse β-decay instability. However, for the pycnonuclear reactions for the oxy-

gen, for the same reaction time of 0.1 Myr, the threshold density is $\rho \sim 3 \times 10^{11}$ gcm^{-3}. This density is larger than the corresponding density for the onset of inverse β-decay instability for ^{16}O, $\rho \sim 1.9 \times 10^{10}$ gcm^{-3}, making the pycnonuclear instability irrelevant for white dwarfs with nuclear compositions heavier than ^{12}C.

Another analysis allows us to dismiss the pynonuclear fusion reaction instability as essential for ^{4}He White Dwarfs, making this instability important only for ^{12}C White Dwarfs. A cold star with a mass $M > 0.5M_\odot$ has already burned an appreaciable part of helium at earlier stages, making the existence of white dwarfs with masses $M > 0.5M_\odot$ very unlikely (see Hamada and Salpeter, 1961, for details). However, from the previous analysis we know that for a ^{4}He white dwarf the density necessary to make pynonuclear instability important is $\rho_{\rm pyc} \sim 8 \times 10^8$ gcm^{-3}. But a white dwarf with such a density must have a mass $M \sim 1.35M_\odot$ (see figure 2.2). Therefore a ^{4}He white dwarf with such a mass cannot exist in nature. Instead, for ^{4}He white dwarfs with masses $M \lesssim 0.5M_\odot$ the central densities are of the order $\rho \sim 10^6$ gcm-3. These densities correspond to pycnonuclear reaction times larger than 10 Gyr, and hence, are unimportant.

Salpeter and van Horn (1969) calculated the number of reactions per unit volume per unit time for the pycnonuclear reactions:

$$R_{\rm pyc} = 3.90 \times 10^{46} Z^4 A \rho S(E_0) \lambda^{7/4} \times \exp(-2.638/\sqrt{\lambda}) \ {\rm cm}^{-3}{\rm s}^{-1}, \tag{2.24}$$

where

$$\lambda = \frac{1}{Z^2 A^{4/3}} \left(\frac{\rho}{1.3574 \times 10^{11} {\rm g \ cm}^{-3}} \right)^{1/3}, \tag{2.25}$$

and S are the astrophysical factors in units of MeV barns (1barn$= 10^{-24}$cm^2) that have to be evaluated at the energy E_0 given by equation (2.23). The astrophysical factor S depends directly on the cross-section of the repulsive Coulomb barrier between ions and hence gives account of the barrier the ions have to exceed to achieve the pycnonuclear reaction.

The S-factors are known from experiments but in some energy ranges that do not coincide with the energies found in white dwarfs. So, the S-factor has to be obtained theoretically from the extrapolation of experimental values using nuclear models.

All the nuclei (Z, A) at a given density ρ will fuse in a time $\tau_{\rm pyc}$ given by:

$$\tau_{\rm pyc} = \frac{n_{\rm N}}{R_{\rm pyc}} = \frac{\rho}{A M_{\rm u} R_{\rm pyc}}, \tag{2.26}$$

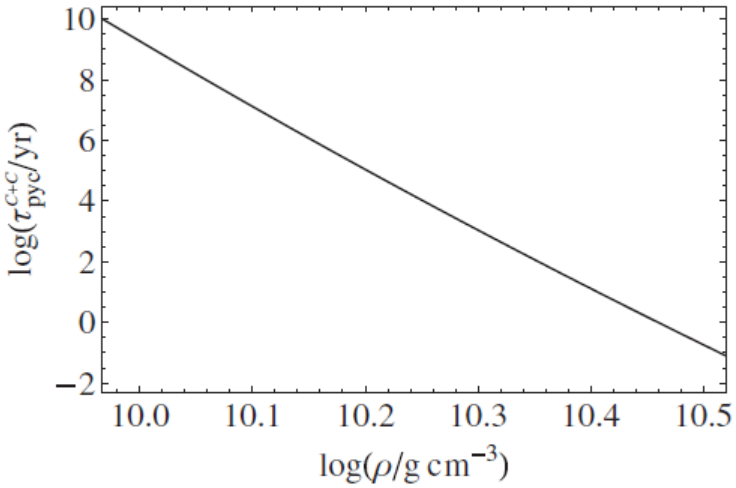

Figure 2.10: Pycnonuclear reaction times at zero temperature for C+C fusion as a function of the density. Figure taken from Boshkayev et al. (2013).

.

where $n_{\rm N} = \rho/(AM_{\rm u})$ is the ion density.

In order to compute the pycnonuclear reaction times given by equation (2.26) Boshkayev et al. (2013) used the results of Gasques et al. (2005), where the S-factors where computed using the NL2 nuclear model parametrization. The fit formula for the S-factors is appropriate for the ranges of the zero-point energies at high densities. The results of the computed pynonuclear reaction times are illustrated in figure 2.10.

2.3.4 Mass-radius and mass-central density relations

In figures 2.11, 2.12, 2.13 and 2.14 we show the mass-central density relation and the mass-radius relation of general relativistic rotating ^{12}C and ^{16}O white dwarfs. In figure 2.15 we plot also the mass-central density relation for general relativistic rotating ^{12}C, basically the same plot of 2.11 but there are also plotted the sequences of constant angular momentum J and constant angular velocities Ω. The boundaries of mass-shedding limit, secular axisymmetric instability, inverse β-decay and pycnonuclear reactions are explicitly shown. Notice that, as expected from the previous analysis, for ^{12}C white dwarfs are present all the instabilities while for ^{16}O only the inverse β-decay instability and the Keplerian sequence limit are present. This also is consistent, as expected, with the conclusions obtained from Rotondo et al. (2011a), if you follow the solid black line that corresponds to the static configuration, for the ^{12}C white dwarfs it intersects the secular axysimmetric instability boundary (static ^{12}C white dwarfs are unstable due to General Relativity) while for ^{16}O white dwarfs it intersects the inverse β-decay boundary. We can see that the main contribution of rotation is that now ^{12}C white dwarfs are also unstable due to inverse β-decay and mass-shedding limit while the ^{16}O white dwarfs are also unstable when they reach the mass-

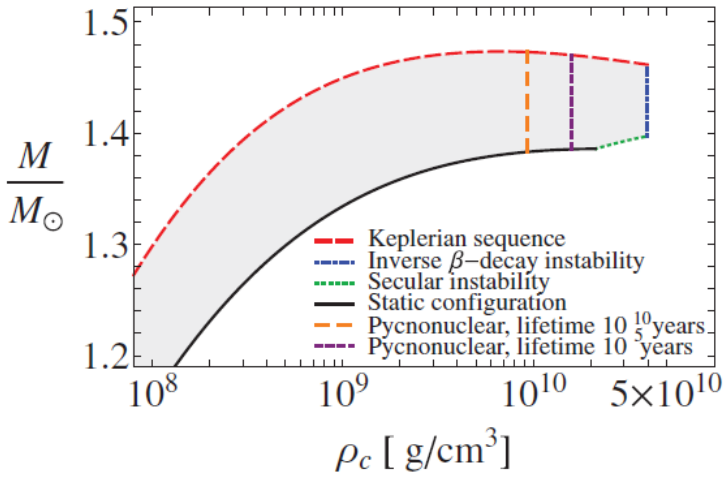

Figure 2.11: Mass vs. central density for ^{12}C white dwarfs. The solid black curve corresponds to non-rotating white dwarfs, the Keplerian sequence is the red thick dashed curve, the blue thick, dotted-dashed curve is the inverse β instability boundary and the green thick, solid curve is the axisymmetric instability boundary. The orange and purple dashed boundaries correspond to the pycnonuclear densities for reaction times $\tau_{\rm pyc} = 10$ Gyr and 0.1 Myr, respectively. All the configurations of rotating and stable white dwarfs are in the shaded region. Figure taken from Boshkayev et al. (2013).

shedding boundary.

Another difference with the non-rotating case is that the maximum mass of these rotating white dwarfs is no longer associated with a critical maximum density for gravitational collapse (inverse β-decay instability or General Relativity instability). Looking at figures 2.11 and 2.13, the curve M vs. $\rho_{\rm c}$ for the static configuration is a monotonically increasing function, so, when the critical density is reached is also reached the maximum mass. Now, considering the whole region of stable configurations, we see that in both cases the Keplerian sequence is an upper boundary to the shaded region, we can easily see that the maximum critical mass corresponds to the maximum mass of the Keplerian sequence curve. This curve, unlike the one of the static configuration, is not a monotonically increasing function, instead, it reaches a maximum $M^{J\neq0}_{\rm max}$, it is monotonically increasing up to this point, and then its derivative changes and becomes a decreasing function. In fact, it reaches a local minimum when it meets the inverse β-decay instability point. So, we can define the following relation:

$$M^{J\neq0}_{\rm max} = kM^{J=0}_{\rm max}, \tag{2.27}$$

where $M^{J=0}_{\rm max}$ is the maximum stable mass of non-rotating white dwarfs and k is a numerical factor that depends on the chemical composition. We show in table 2.3, for all chemical compositions considered, the values of $M^{J\neq0}_{\rm max}$ as well as k and the corresponding critical density $\rho^{J\neq0}_{\rm Mmax}$ that maximizes the mass.

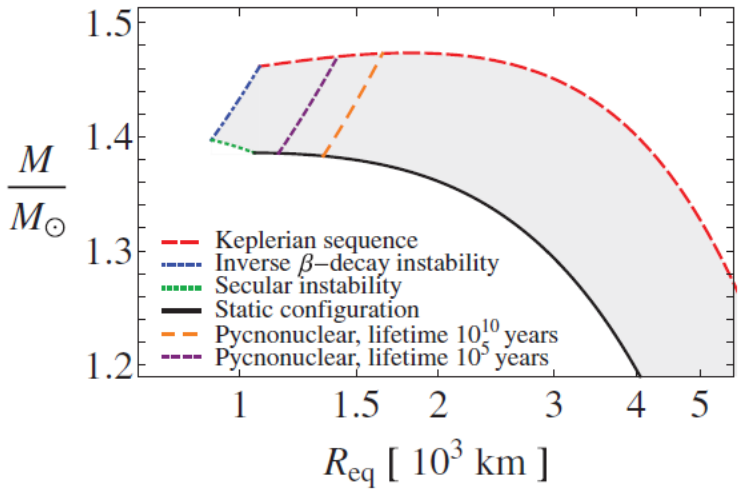

Figure 2.12: Mass vs. equatorial radius in units of 10^3 km for ^{12}C white dwarfs. The solid black curve corresponds to non-rotating white dwarfs, the Keplerian sequence is the red thick dashed curve, the blue thick, dotted-dashed curve is the inverse β instability boundary and the green thick, solid curve is the axisymmetric instability boundary. The orange and purple dashed boundaries correspond to the pycnonuclear densities for reaction times $\tau_{\rm pyc} = 10$ Gyr and 0.1 Myr, respectively. All the configurations of rotating and stable white dwarfs are in the shaded region. Figure taken from Boshkayev et al. (2013).

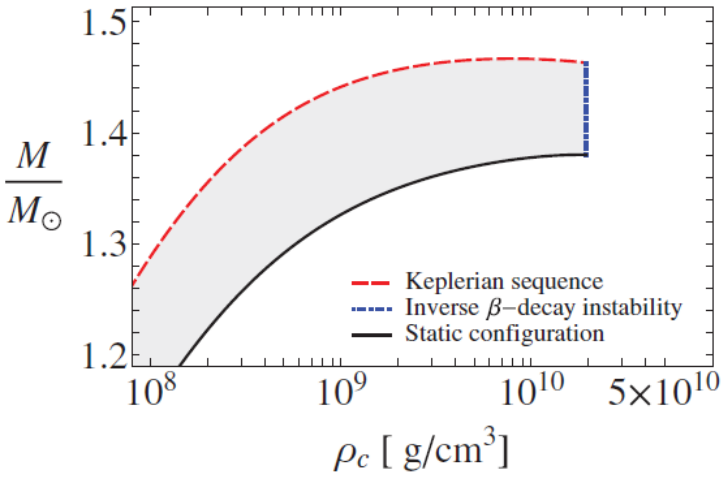

Figure 2.13: Mass vs. central density for ^{16}O white dwarfs. The solid black curve corresponds to non-rotating white dwarfs, the Keplerian sequence is the red thick dashed curve and the blue thick, dotted-dashed curve is the inverse β instability boundary. All the configurations of rotating and stable white dwarfs are in the shaded region.. Figure taken from Boshkayev et al. (2013).

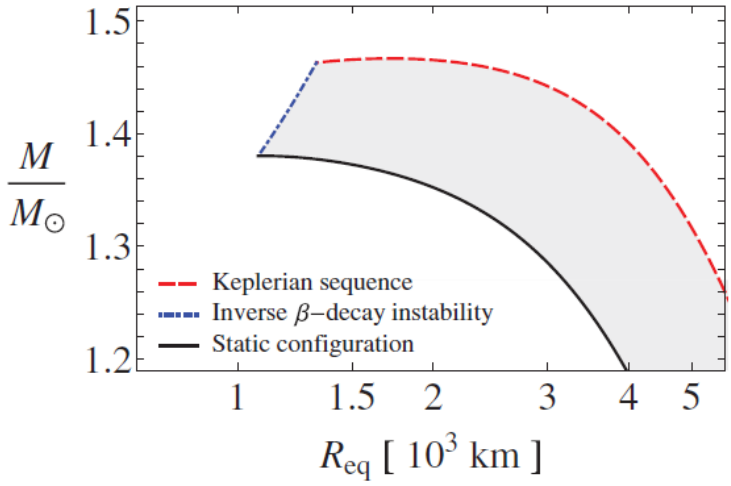

Figure 2.14: Mass vs. equatorial radius in units of 10^3 km for ^{16}O white dwarfs. The solid black curve corresponds to non-rotating white dwarfs, the Keplerian sequence is the red thick dashed curve, the blue thick, dotted-dashed curve is the inverse β instability boundary. All the configurations of rotating and stable white dwarfs are in the shaded region. Figure taken from Boshkayev et al. (2013).

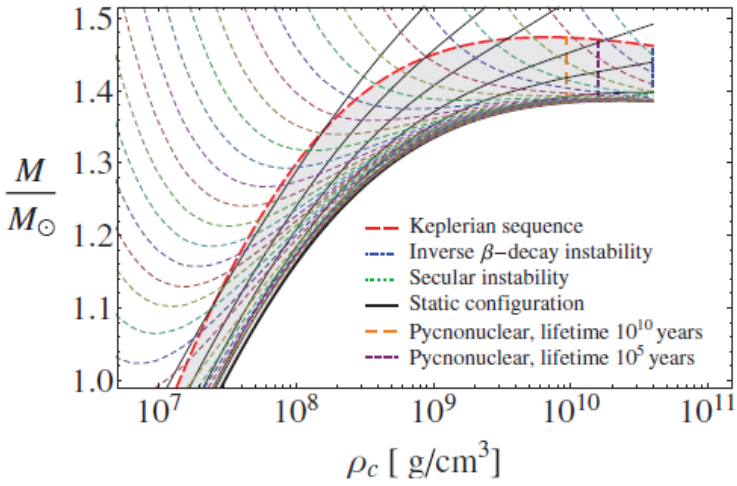

Figure 2.15: Mass vs. central density for ^{12}C white dwarfs. This is basically the same plot of figure 2.11 but with a wider range of central densities ρ_c, so the J = constant sequences (solid black curves) and the Ω = constant sequences (colored thin-dashed curves) can be fully appreciated. The solid black curve corresponds to non-rotating white dwarfs, the Keplerian sequence is the red thick dashed curve, the blue thick, dotted-dashed curve is the inverse β instability boundary and the green thick, solid curve is the axisymmetric instability boundary. The orange and purple dashed boundaries correspond to the pycnonuclear densities for reaction times $\tau_{\rm pyc}$ = 10 Gyr and 0.1 Myr, respectively. All the configurations of rotating and stable white dwarfs are in the shaded region. Figure taken from Boshkayev et al. (2013).

Composition	$\rho_{\rm Mmax}^{J\neq0}$	k	$M_{\rm max}^{J\neq0}/M_\odot$	$M_{\rm max}^{J=0}/M_\odot$	$P_{\rm min}$	$R_{\rm p}^{\rm Pmin}$	$R_{\rm eq}^{\rm Pmin}$
^{4}He	5.46	1.0646	1.50009	1.40906	0.284	5.64	7.36
^{12}C	6.95	1.0632	1.47363	1.38603	0.501	8.17	1.07
^{16}O	7.68	1.0626	1.46664	1.38024	0.687	1.00	1.32
^{56}Fe	1.18	1.0864	1.20175	1.10618	2.195	2.00	2.69

Table 2.3: Properties of uniformly rotating general relativistic ^{4}He, ^{12}C, ^{16}O and ^{56}Fe white dwarfs; $\rho_{\rm Mmax}^{J\neq0}$ is in units of 10^9 gcm^{-3}, and corresponds to the rotating maximum mass $M_{\rm max}^{J\neq0}$; k is defined by equation (2.27). $M_{\rm max}^{J=0}$ is the non-rotating maximum mass of white dwarfs, obtained in Rotondo et al. (2011a). $P_{\rm min}$ is the minimum rotation period and is obtained finding the crossing point between the mass-shedding limit and the inverse β-decay instability boundary. The polar $R_{\rm p}^{\rm Pmin}$ and the equatorial $R_{\rm eq}^{\rm Pmin}$ radii of the configuration rotating with the minimum period $P_{\rm min}$ are given in units of 10^3 km. Values obtained from Boshkayev et al. (2013).

We also can see that for a sequence of constant angular velocity Ω the maximum mass not necessarily is associated with the critical maximum density for gravitational collapse. For example, in figure 2.15 the curves with very small Ω (approaching zero) approach to the solid curve line, that corresponds to the static case (corresponds to the curve $\Omega = 0$ and also to the curve $J = 0$). In this case the maximum mass will correspond with the critical density associated with either the inverse β-decay instability or the secular axysimmetric instability in General Relativity. However, as long as we increase Ω the curves start to go up, separating from the static configuration curve and up to some point where the maximum mass will correspond not to the critical mass associated with the inverse β-decay instability or the secular axysimmetric instability but to the mass-shedding limit.

As long as we increase the angular velocity making the curves of $\Omega =$ constant move upwards, we approach the point of intersection between the mass-shedding and the critical inverse β-decay boundaries. This can be easily seen in figure 2.15. This crossing point corresponds also to the minimum rotation period $P_{\rm min}$ of the white dwarfs. This crossing point, of course, depends on the chemical composition. We show in table 2.3 the minimum periods for the 4 types of white dwarfs considered as well as the corresponding polar $R_{\rm p}^{\rm Pmin}$ and equatorial $R_{\rm eq}^{\rm Pmin}$ radii.

To conclude this chapter we have to underline the importance of these works. The refinement of the equation of state allows us to get more realistic pictures of these objects. The refinements done in the work of Rotondo et al. (2011a) allowed, for example, to determine that ^{12}C white dwarfs are unstable due to General Relativity and not to inverse β-decay. Also, new limits to the mass of static

white dwarfs were obtained. And regarding uniformly rotating white dwarfs, Boshkayev et al. (2013) refined, although using a different approach, the work of Arutyunyan et al. (1971), that also considered rotating white dwarfs in General Relativity but using only the Chandrasekhar equation of state, that, as we know, gives a maximum mass that is independent of the chemical composition of the star. Boshkayev et al. (2013) obtained new values for the maximum mass (see table 2.3), that compared to the value of $1.478 M_{\odot}$ obtained by Arutyunyan et al. (1971), are always smaller, being the maximum mass of ^{56}Fe, $1.202 M_{\odot}$, the smallest one, showing us that the chemical composition effects are important, mainly when heavy nuclei are considered.

Another important application is to confirm the importance of the instability boundaries, specially when neglecting them could lead to misleading conclusions about the maximum mass of white dwarfs. Recently Das and Mukhopadhyay (2012, 2013); Das et al. (2013) have proposed that the existence of ultra magnetic white dwarfs, with magnetic fields larger than the critical magnetic field of quantum electrodynamics, exist in nature and that the effect of these huge magnetic fields is to increase significantly the maximum mass of white dwarfs, obtaining values that surpass the traditional limit imposed by Chandrasekhar. We will show in the next chapter that the appropriate consideration of the instabilities forbids the existence of these hypothetical ultra magnetic white dwarfs.

The effects of rotation are important only for white dwarfs rotating with periods close to the minimum rotational periods. Otherwise a slow rotation imply that the non-rotating approximation is actually very good to describe the structure of these stars. Although observations have shown that magnetic or non-magnetic white dwarfs on average rotate very slowly (Ferrario et al., 2015; García-Berro et al., 2016), observations have also shown the existence of some exceptions. The famous white dwarf component of the cataclysmic Variable AE Aquarii, for example, rotates very fast, with a period of 33 s. This period of rotation is close in order of magnitude to the minimum periods calculated within this formalism. Considering also that this white dwarf has shown a pulsar-like behaviour and that AXPs/SGRs have been proposed, in an alternative model, as fast rotating highly magnetic white dwarfs, the results of this work turn out particularly useful. This will be shown in detail in chapters 4 and 5.

Chapter 3

Magnetic white dwarfs: Stability and observations

3.1 Introduction

In this chapter we will address the topic of magnetism in white dwarfs. In the first part we will review the current knowledge, both from an observational and theoretical point of view, of the observed magnetic white dwarfs. The observational evidence of the existence of white dwarfs with magnetic fields in the range $(10^6 - 10^9)$ G shows us that they constitute about $\sim$ 10% of all white dwarfs (Wickramasinghe and Ferrario, 2005). Hence the importance of magnetism in white dwarfs.

On the other hand, in the second part of the chapter we will address the issue of highly magnetic white dwarfs, e.g., the hypothetical existence of white dwarfs with magnetic fields much larger than even the strongest magnetic fields measured ($\sim 10^9$ G) in white dwarfs. We address this issue because in the last years ultra-magnetic and super-Chandrasekhar white dwarfs have been proposed as a possibility to explain the observations of some peculiar superluminous type Ia supernovae, which need white dwarf progenitors with masses $(2.1 - 2.8)M_\odot$, mass that in turn depends on the amount of nickel needed to successfully explain both the low kinetic energies and the high luminosity of these supernovae (Hicken et al., 2007; Howell et al., 2006; Scalzo et al., 2010; Silverman et al., 2011; Taubenberger et al., 2011; Yamanaka et al., 2009). These hypothetical white dwarfs should have interior fields up to 10^{18} G and a critical mass limit $M_{\rm max} \approx 2.58\ M_\odot$, which surpasses the traditional Chandrasekhar mass limit $M_{\rm Ch} \approx 1.44 M_\odot$. In this case we show that several stability criteria and fundamental physical aspects (some of them studied in the preceding chapter), that take place when huge magnetic fields and high densities are present, have been neglected in the determination of such a new mass limit for white dwarfs, invalidating that result.

In the first part we will review the current status of the research on magnetic white dwarfs, both in the observational as well as in the theoretical fields. So, in

section 3.2.1 we will give a brief introduction to this interesting topic. Then in section 3.2.2 we will give a review of the most significant historical discoveries that gave birth to this research field in the observational field. We proceed in section 3.2.3 addressing the mass distribution in magnetic white dwarfs, talking about their difference with their non-magnetic white dwarfs and how this could help to ellucidate their origin and evolution. Then, in section 3.2.4 we will address the topic of the rotational periods reported from observations of magnetic white dwarfs. We proceed in section 3.2.5 talking about the hypotheses proposed to explain the origin and the observational facts mentioned before of magnetic white dwarfs. Finally, we give in section 3.2.7 the conclusions. This is just a brief review of this interesting topic, where I follow closely the main ideas exposed in García-Berro et al. (2016) and Ferrario et al. (2015); for a recent and complete review of this subject I suggest the reader to check the aforementioned references.

In the second part, as we mentioned before, we address the topic of ultramagnetic white dwarfs. In section 3.3.1 we give a brief introduction to the reasons that lead some authors (Das and Mukhopadhyay, 2012, 2013) recently to propose the existence ultra-magnetic white dwarfs with interior fields up to 10^{18} G and with significantly super-Chandrasekhar masses. We specifically point out that the existence of these ultra-magnetic white dwarfs is forbidden due to several stability reasons ignored by such authors, physical considerations that are considered in the different sections. So, in section 3.3.2 we show the main hypotheses and considerations behind the aforementioned model, how these considerations lead them to obtain a theoretical structure and stability of magnetic white dwarfs that can reach masses as large as $M \sim 2.58 M_{\odot}$, an upper limit significantly larger than the super-Chandrasekhar mass limit of $M_{\rm Ch} \approx 1.44 M_{\odot}$. Then, in section 3.3.3 we show how these ultra-magnetic white dwarfs significantly violate the virial theorem, a stability criterion very well known in the theory of structure of white dwarfs (Shapiro and Teukolsky, 1986). Then, in section 3.3.4 we address the topic of microscopic instabilities, a topic already considered in the previous chapter; we address the inverse β-decay instability and then we point out the relevance of the pycnonuclear fusion reactions in the stability of white dwarfs. In section 3.3.5 we remark that such huge magnetic white dwarfs will seriously break the spherical symmetry assumed in the model of Das and Mukhopadhyay (2012, 2013), something that leads to an inconsistency. This departure from spherical symmetry can be measured with an eccentricity, which, by the way, cannot be arbitrarily large due to dynamical instabilities (Shapiro and Teukolsky, 1986). In section 3.3.6 we point out the relevance of the general relativistic effects, which are nonnegligible considering the energy density of the magnetic field, which overcomes the matter density, and considering the compactness of these white dwarfs, which is similar to the compactness of a typical neutron star, where general relativistic effects can no longer be ignored. These general relativistic effects were neglected in the treatment of Das and Mukhopadhyay (2012, 2013). In section 3.3.7 we address the evolutionary path, proposed by the aforementioned authors in order to explain the existence of these ultra-magnetic white dwarfs. We show that these white

dwarfs will be subjected to several of the above mentioned instability effects before reaching such hypothetical stages of ultra-magnetism. In section 3.3.8 we discuss the recent discussion between the authors of the hypothesis of ultra-magnetic white dwarfs and the different articles, included our articles (Cáceres et al., 2014; Coelho et al., 2014), that criticized their work. Despite this feedback allowed the authors of this hypothesis to improve their model, we still point out their proposal lacks the consideration of several physical issues relevant for the physics of magnetic white dwarfs. Finally, in section 3.2.7 we expose the conclusions.

3.2 Observations of magnetic white dwarfs

3.2.1 Introduction

The existence of magnetic white dwarfs (with fields $\gtrsim$ 1 MG) has been shown since the beggining of the 70's. In order to analyze their spectra it has been important to find the solution to the Schrödinger equation of atoms in strong magnetic fields (Forster et al., 1984; Garstang, 1977; Roesner et al., 1984; Ruder et al., 1994). This problem has not a general solution since there are two competing effects, the electric Coulomb force between the nucleus and the electron in the atom (could be, for example, a hydrogen or a helium atom), and the magnetic force acting on a free electron. The first case has spherical symmetry, while the second one has cylindrical symmetry. In the case both forces are present there is not a general solution, and the problem has to be solved numerically. If the magnetic field is weak compared to the electric field of the nucleus, the magnetic field can be treated just as a perturbation. The same happens in the opposite case, the Coulomb force can be treated as a perturbation to the magnetic field. The case where both electric and magnetic forces are of the same magnitude is the most difficult to solve. The range of magnetic fields of the highly magnetic white dwarfs $(10^6 - 10^9)$G corresponds to this case and the numerical work to solve this problem and the advances in the observational field have triggered the research of atoms in strong magnetic fields. So, the first magnetic white dwarfs reported had hydrogen atoms in their atmosphere but when numerical calculations for Helium atoms were available, it was possible to identify magnetic white dwarfs with Helium (Ferrario et al., 2015).

Depending on the chemical composition of their atmosphere, white dwarfs can exhibit different spectral features. This prompted to their classification in different spectral types; so, for example, DA are rich in hydrogen, DB are rich in helium, DQ are rich in carbon and DZ white dwarfs have metal rich atmospheres. Most of the magnetic white dwarfs belong to the DA spectral type. This is because more than 80% of normal white dwarfs also belong to that spectral class. The measurements of the magnetic field rely on the spectroscopic determination of the Zeeman splitting of the Balmer series of hydrogen. For sufficiently low magnetic fields these splittings are linear, but with increasing the magnetic field this is not anymore true because nonlinear terms in the Hamiltonian of the

atom become more relevant for the determination of the magnetic field strength. More precisely, quadratic terms are important for field strengths ~ 1 MG (Wickramasinghe and Ferrario, 2000). Today the astronomical community has determined reliably the magnetic fields of several isolated magnetic white dwarfs with magnetic field strengths as large as 800 MG (Ferrario et al., 2015).

For the white dwarfs of spectral type DB, the determination of the field strength became more difficult (Jordan et al., 1998), until numerical calculations allowed to associate the absorption features in spectra of several magnetic white dwarfs with stationary line transitions of HeI. Regarding the white dwarfs of spectral type DQ, there is a recently discovered population of hot DQs, with carbon-dominated atmospheres (Dufour et al., 2007); about half of them are magnetic. Finally, there is also a group of magnetic DZ white dwarfs (Hollands et al., 2015; Kepler et al., 2016).

Another technique used to determine the magnetic field of white dwarfs consists of measuring the continuum circular polarization (Kemp, 1970), but this technique is useful only for white dwarfs with magnetic field strengths exceeding 10^8 G.

Now, there are reported more than 600 magnetic white dwarfs (see Ferrario et al., 2015; Kepler et al., 2013, 2015, and references therein) since the first magnetic white dwarf was reported in 1970 (Kemp et al., 1970). This number allows to make statistical analysis regarding their average masses, average rotational periods or magnetic field strength, something that can give information and hints that could help to solve the question of their origin and their evolutionary channels. But despite this is a very interesting research field, with many applications to other areas, the progress on the observational side has not been followed by a similar progress on its theoretical counterpart. This is due to the intrinsic difficulty of modelling magnetic fields, something that in most cases requires full three-dimensional (3D) simulations. This vacuum in our theoretical understanding of magnetic white dwarfs is due also to the uncertainty about the full evolutionary picture of the progenitors of magnetic white dwarfs. There are two main hypotheses: either magnetic fields are inherited from a progenitor star (fossil field hypothesis) or are originated by the evolution in a binary system. Both hypotheses have advantages and drawbacks and this debate has still not been solved. And besides these two hypotheses there are other proposed competing scenarios which challenge those two previously mentioned.

Magnetic white dwarfs can also be found in Cataclysmic Variables, which are close binary systems where a white dwarf accretes matter from a late-type main sequence companion. Their orbital periods are less than a day and the typical orbital separations are of the order of the solar radius, making these binaries relatively compact. Those cataclysmic binaries with white dwarfs that host strong magnetic fields ($B \gtrsim 1$ MG) allow also to study accretion and emission processes in a strong magnetic field environment and help to improve the understanding

of the influence of magnetic fields in close binary evolution.

The cataclysmic variables with the most magnetic white dwarfs are known as *Polars* or *AM Herculis Stars*. This name is due to the name of the first source of this kind discovered, AM Herculis, a red dwarf variable star located in the constellation Hercules. An important consequence of the high magnetism in these binaries is that it synchronizes the rotational period of the white dwarf with the rotational period of the binary to first order (Cropper, 1990; Hellier, 2001). Besides the polars, that are the cataclysmic variables with the strongest magnetic fields in their white dwarfs, there is another type of cataclysmic variables with magnetic fields not so large as those of polars but large enough to differentiate them from the non-magnetic cataclysmic variables. These binaries are known as *Intermediate Polars (IP)*.

The number of known magnetic Cataclysmic Variables has also increased dramatically in the last years. Wickramasinghe and Ferrario (2000) listed around 60 cataclysmic variables but this number has recently increased to about 170 (Ferrario et al., 2015). But only about half of those magnetic cataclysmic variables have measured magnetic fields, mostly in the range $\sim (7 - 230)$ MG (Ferrario et al., 2015).

The magnetic field distribution of White Dwarfs (WDs) seems to be bimodal with a high field population (1-1000 MG) and a low field population $(< 0.1MG)$. This is because observations seem to point to the existence of a peculiarly low percentage of MWDs in the field range $(0.1 - 1)$ MG (Kawka and Vennes, 2012; Koester et al., 2001). This fact could be useful to ellucidate the different evolutionary channels followed by the magnetic white dwarfs that exist in nature.

3.2.2 Historical background

Kemp et al. (1970) published the discovery of the first highly magnetic ($\sim 10^7$G) white dwarf through the discovery of the circularly polarized continuum radiation of Grw$+70^\circ$8247. For magnetic fields in these highly magnetic white dwarfs the quadratic Zeeman effect is non-negligible, so, the discovery of these highly magnetic white dwarfs led to several further investigations on this subject. Precisely, the spectral features of Grw$+70^\circ$8247 remained unidentified until the first computations of the hydrogen transitions in strong magnetic fields became available in the mid of 80's. Similarly, the spectral features of another magnetic white dwarf, GD229, were interpreted as stationary line transitions of helium in a magnetic field of 300-700 MG (Jordan et al., 1998; Wickramasinghe et al., 2002).

The work of Kemp et al. (1970) was followed by the detection of many more magnetic white dwarfs (see, e.g., Angel, 1978; Angel et al., 1981; Ferrario et al., 2015; Wickramasinghe and Ferrario, 2000). Angel and Landstreet (1971a) detected circular polarisation in a second white dwarf, G195-19 and Angel and

Landstreet (1971b) published the detection of the third one, GD99-37.

After the discovery of Kemp in 1970 the number of known Magnetic White Dwarfs has increased dramatically in the last decades. Wickramasinghe and Ferrario (2000) listed 65 isolated magnetic white dwarfs and later, thanks to the Sloan Digital Sky Survey (York et al., 2000), the list increased in the last years up to approximately 600 (see Ferrario et al., 2015; Kepler et al., 2013, 2015, and references therein).

Regarding the Cataclysmic Variables, AM Her was the first source of this kind discovered to emit soft X-rays by the *UHURU* and *SAS-3* satellites in 1976 (Hearn et al., 1976). Then optical observations revealed variable linear (up to 7%) and circular (up to 9%) polarisation in the V and I spectral bands (Tapia, 1977), revealing in this way the presence of a compact star with a magnetic field $B \sim 2 \times 10^8$ G and a rotational period of 3.09 h, which is synchronized with the orbital period. The unpolarized radiation in the U band revealed instead the presence of a hot source, companion to the compact star and unaffected by its magnetic field. Systems with similar characteristics were named *AM Her-type* variables. The name *polar* was introduced later for these AM Her objects and other X-ray sources where the main feature is polarised optical light (see Warner, 1995).

The binary system DQ Her was discovered in the mid-50s and was the first *Intermediate Polar* detected, which as we said before, is a magnetic cataclysmic variable not so magnetic as a *Polar*. Observations detected a 71 s periodic variability (Walker, 1956) and two decades later it was also found to be weakly polarised (Swedlund et al., 1974). In 1978, optical pulsations of 33 s were detected in AE Aqr, but not in polarised light (Patterson, 1979). Then, in the following years, fast optical periodic variations at periods much shorter than the orbital one ($P_{\rm rot} \ll P_{\rm orb}$) were found in other CVs, a characteristic that differentiated them from the above mentioned polars. All cataclysmic variables that shared the same characteristics of DQ Her were first called DQ Her-type variables, but then were called *Intermediate Polars* (Patterson, 1994; Patterson and Steiner, 1983; Warner, 1995). Later it was recognized there were two types fo magnetic cataclysmic variables, Polars and Intermediate Polars.

Because of their strong soft X-ray emission, soft X-ray surveys increased the number of reported Polars, and in particular thanks to the survey conducted in the nineties by the *ROSAT* satellite (Beuermann, 1999). To date, ~ 110 of these systems are known hosting white dwarfs with surface field strengths $B \sim (7 - 230)$ MG (see Ferrario et al., 2015, for a complete list of known systems up to December 2014). On the other hand, Intermediate Polars remained elusive objects until the recent hard X-ray surveys conducted by the *INTEGRAL*/IBIS and *Swift*/BAT satellites (Baumgartner et al., 2013; Bird et al., 2010). The number of reported Intermediate Polars has now increased to ~ 55 systems (see Bernardini et al., 2012, 2013; Ferrario et al., 2015) and ~ 60 candidates are still awaiting

confirmation through X-ray follow-ups with facilities such as XMM-Newton and NuSTAR.

3.2.3 Mass distribution of magnetic white dwarfs

Mass estimates of isolated magnetic white dwarfs with fields $\gtrsim 1$ MG are available only for a small number of objects (Ferrario et al., 2015). This is due to the poor knowledge of the magnetic field effects on the atmospheres of the magnetic white dwarfs. The derived effective temperatures often remain uncertain and hence, also the implied magnetic white dwarf masses (Külebi et al., 2010). The mass estimates are few also because the procedure of fitting the Balmer lines for $T_{\rm eff}$ and $\log g$ can only be applied to white dwarfs with magnetic fields below a few MG, and even in such cases the results must be treated with some caution (Dupuis et al., 2003; Ferrario et al., 1998). For higher field strengths, mass estimates are derived from the combination of effective temperatures, parallaxes and a mass-radius relation. Estimates of the distance can be done for the small number of magnetic white dwarfs with accurate parallax estimations, for the magnetic white dwarfs that have non-degenerate white dwarf companions (Dobbie et al., 2012, 2013; Girven et al., 2010), or for magnetic white dwarfs in open clusters (Külebi et al., 2013).

Despite the limited number of magnetic white dwarfs whose mass could be inferred from observations, it has been possible to determine that the mean mass of high field isolated magnetic white dwarfs (with $B \gtrsim 1$ MG) is 0.784 ± 0.047 $M_\odot$ (Ferrario et al., 2015). The distribution of high field magnetic white dwarfs also exhibits a strong tail that extends to the Chandrasekhar mass limit. Meanwhile, the most recent estimate for the mean mass of non-magnetic DA white dwarfs is 0.663 ± 0.136 $M_\odot$ (Tremblay et al., 2013). The fact that magnetic white dwarfs are, on average, heavier than their non-magnetic counterparts was something first noted by Liebert (1988). The comparison between the mass distributions of magnetic and non-magnetic white dwarfs can be appreciated in figure 3.1.

3.2.4 Spin periods of isolated magnetic white dwarfs

Like nonmagnetic white dwarfs, their magnetic counterparts rotate very slowly (Fontaine and Brassard, 2008). There is weak evidence for a bimodal distribution of the rotational periods, with a group of magnetic white dwarfs rotating with periods of the order of hours (see, for instance, the sources analysed in Barstow et al., 1995; Ferrario et al., 1997), while a second group rotates very slowly, with periods very large, typically of the order of years, with lower limits of decades, if not centuries (Berdyugin and Piirola, 1999; Beuermann and Reinsch, 2002). This should give useful information regarding their origin, something still not completely elucidated. Within the group of magnetic white dwarfs it seems very long period magnetic white dwarfs tend to possess high fields while short pe-

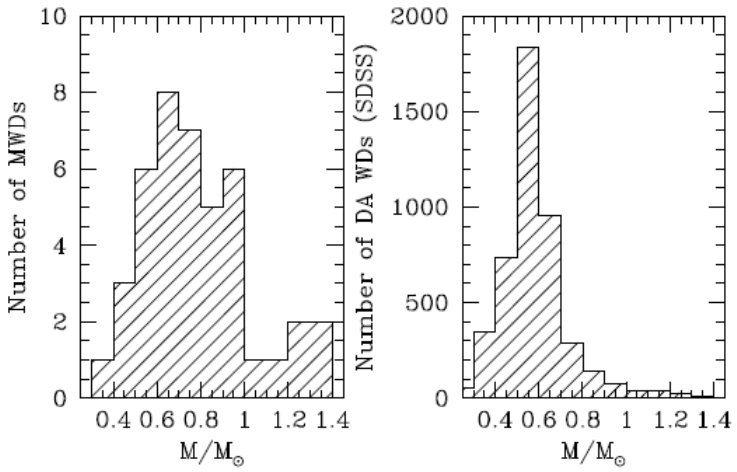

Figure 3.1: *Left panel*: The mass distribution of magnetic white dwarfs (Ferrario and Wickramasinghe, 2010). *Right panel*: The mass distribution of non-magnetic DA white dwarfs from SDSS (Kepler et al., 2007).

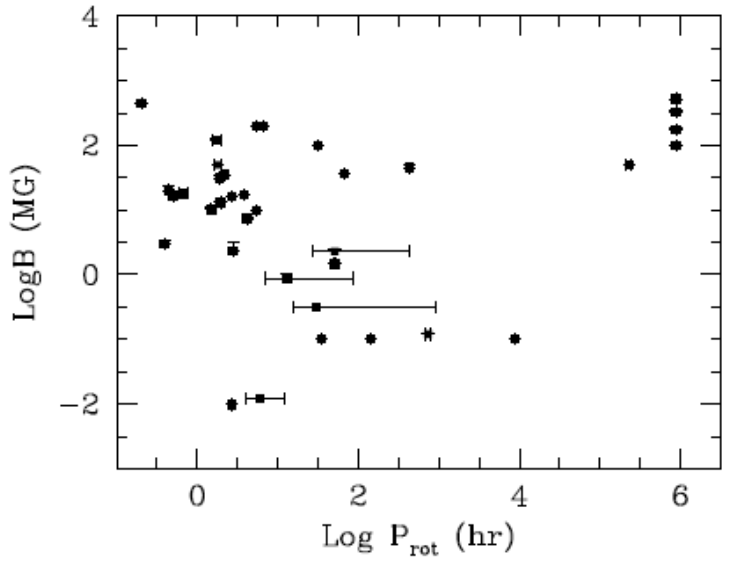

Figure 3.2: Rotation periods of isolated magnetic white dwarfs against their magnetic field strength. Figure taken from Ferrario et al. (2015).

riod ones do not show any preferred field strength (see figure 3.2). Slow rotators could be the descendants of the magnetic main sequence stars Ap/Bp stars, which means their magnetic field has a fossil origin, whereas fast rotators could be the outcome of binary interaction. However, Külebi et al. (2013) argued that in such kind of mergers the interaction between the magnetosphere of the white dwarf and the debris disk may slow down the rotation rather quickly.

In the case of magnetic white dwarfs in cataclysmic variables, the spin period is influenced by the interaction between the magnetic field of the magnetic white

dwarf and that of the secondary and/or by the torque of the accretion flow. For magnetic white dwarfs with strong magnetic fields the rotation period is locked to the orbital period, a characteristic of these objects known as polars, while for white dwarfs with weaker magnetic fields the magnetic white dwarf rotates faster than the orbit. These are knwon as Intermediated Polars.

3.2.5 The origin of the magnetic field

As we mentioned before there is not still reached a general consensus in the astronomical community about the origin of the magnetic white dwarfs. The different scenarios proposed to explain their existence have to explain several observational facts such as:

1. The high-field magnetic white dwarfs are on average more massive than their nonmagnetic counterparts (see subsection 3.2.3).

2. Most of magnetic white dwarfs with reported rotational periods are slow rotators (see subsection 3.2.4).

3. For nonmagnetic white dwarfs there exists a well known population of binaries in which one of the members of the pair is a main-sequence star while the other one is the white dwarf (Rebassa-Mansergas et al., 2013). However, magnetic white dwarfs are predominantly single stars (Liebert et al., 2015). For the magnetic white dwarfs in binary systems it has been found that the white dwarf companion in cataclysmic variables is magnetic in about 25% of those systems. All this is strong evidence that binarity is fundamental in the origin of at least some fraction of the presently observed magnetic white dwarfs.

There are two competing scenarios which could explain the formation of the field of magnetic white dwarfs, the fossil field hypothesis and the binary scenario. In the fossil field hypothesis the magnetic field in the white dwarf is simply a consequence of the evolution of a single progenitor along the standard stellar evolutionary phases, specifically the white dwarfs should descend from rotating Ap and Bp stars, which are the only class of main-sequence stars known to have magnetic fields between 10^3 and 10^5 G. Neglecting the mass loss and assuming the magnetic flux is conserved, their field will be amplified by a factor of $\sim 10^4$ when the progenitor becomes a white dwarf. But even if we consider the effects of the mass loss, it is expected that the magnetic field of the resulting white dwarf would be comparable to those typically found in the magnetic white dwarfs (García-Berro et al., 2016).

On the other hand, in the binary hypothesis, the magnetic field is the product of the interaction of the future magnetic white dwarf with a companion during

its previous evolution. In this scenario Tout et al. (2008); Wickramasinghe and Ferrario (2005) suggested that the strong magnetic fields are produced during a common envelope episode in a close binary system. During that stage, the spiral-in of the secondary induces differential rotation in the extended convective envelope, producing a stellar dynamo responsible for the magnetic field. However (Potter and Tout, 2010) showed that the magnetic field produced in this way does not penetrate into the white dwarf and decays rapidly when the common envelope is ejected. It has also been recently demonstrated that the hot, differentially rotating convective corona resulting from the merger of two degenerate cores produces strong magnetic fields that are confined to the outer layers of the resulting remnant and it also has been shown that they do not decay over very long timescales (García-Berro et al., 2012; Lorén-Aguilar et al., 2009). And detailed 3D numerical simulations have shown that a very small magnetic field is amplified during the merger episode and that the remnant of the merger is strongly magnetized (Ji et al., 2013). All this would make of this scenario a good candidate to explain some of the most properties of the high-field magnetic white dwarfs. However, this scenario may be in conflict with the observational fact that most magnetic white dwarfs are slow rotators. However, it has also been shown that the interaction between the magnetosphere and the debris region that results from the disruption of the secondary star during the merger episode can brake the magnetic white dwarf and bring the rotation periods to values similar to those observationally found (Külebi et al., 2013).

3.2.6 Applications

The theory of magnetic white dwarfs has numerous applications to astrophysical phenomena occurring in cataclysmic variables. However, it can also be applied to solve various questions in astrophysics, one of them directly related with the topic addressed in this thesis. Various of those applications are the following (García-Berro et al., 2016):

1. Millisecond pulsars are a special group of pulsars with characteristic magnetic fields of the order $10^8 - 10^9$ G, smaller than the average strength of radio pulsars ($B \lesssim 10^{13}$ G). They are frequently found in binary systems ($\sim$ 75%) (Hurley et al., 2010). It is believed they originated in a core-collapse supernova event in a binary system. In this scenario, in order to explain the large prevalence of low-field millisecond pulsars in binary systems, it has been hypothesized that white dwarfs with initially small magnetic fields ($\sim 10^4$ G) can explain naturally the observed properties of these pulsars by simply assuming that the magnetic field is amplified by flux conservation during the gravitational collapse this star will face due to the accretion of material expected in a binary system. The evolutionary route should be an accreting massive white dwarf whose degenerate core reaches super-Chandrasekhar stages, something ensuring the gravitational collapse and the formation of a neutron star (Gutiérrez et al., 2005; Gutierrez et al., 1996). This massive white dwarf sholuld have a core made of

oxygen and neon, reaches the threshold density to enable electron captures on ^{24}Mg and ^{24}Na first, and later on ^{20}Ne and ^{20}F, to finally ignite Ne and O explosively at central densities higher than $\sim 2 \times 10^{10}$ g cm^3, densities high enough to trigger the electron captures. However, recent population synthesis studies have concluded that the birth rates of binary millisecond pulsars formed through accretion-induced collapse are comparable to and can exceed those of core collapse (Hurley et al., 2010). Nevertheless these studies are not yet conclusive and further research is needed to clarify this issue (García-Berro et al., 2016).

2. Magnetic double degenerates are very rare systems which are composed of two degenerate stars, a magnetic white dwarf and a non-magnetic one. In these systems the stars are sufficiently separated so they have evolved independently and the age and the distance of the system can be evaluated studying the nonmagnetic star (Girven et al., 2010). These systems also allow to study the origin of the magnetic field. However, the fact that very few of these systems have been observed and reported makes it difficult to reach definite conclusions, but this is a promising line of future research.

3. Finally is the application of these magnetic white dwarfs to the study of Anomalous X-ray pulsars. We will explain this application in chapters 4 and 5

3.2.7 Conclusions

Despite the determination of mass for most high-field white dwarfs is uncertain, there is a curious characteristic difference between magnetic $(B > 1)$ MG and non-magnetic white dwarfs. The average mass of magnetic white dwarfs has a value of $0.784 \pm 0.047 M_\odot$ (Ferrario et al., 2015) whereas for non-magnetic white dwarfs the average mass is $0.643 \pm 0.136 M_\odot$ (Tremblay et al., 2013). This observational fact could give us valuable information regarding the different evolutionary channels that follow magnetic and non-magnetic white dwarfs.

Regarding the rotational properties, both magnetic and non-magnetic white dwarfs rotate slowly (Fontaine and Brassard, 2008). For the case of magnetic white dwarfs, despite the difficulties for measuring accurately the periods using photometry and polarimetric variability, it has been discovered that the rotational periods of isolated white dwarfs encompass a wide interval, with a lower limit of $\sim$ 700 s and with the the longest rotation periods being of the order of about 100 yr (Brinkworth et al., 2013; Jordan and Friedrich, 2002). There is a weak evidence for a bimodal distribution of rotational periods, but some magnetic white dwarfs rotate with periods clustered around hours while a second and more numerous group rotate with periods much more longer, of typically hundreds of years. Therefore we could conclude that most of magnetic white dwarfs are slow rotators, if we compare them with the non-magnetic ones. This

observational fact can give hints to the question of the progenitors of the magnetic white dwarfs.

So, the most important observational facts are that magnetic white dwarfs are more massive and much slower than non-magnetic ones. Any theory or hypothesis has to give account of these observational properties of the ensemble of the white dwarfs. An origin and an evolutionary channel has to be proposed and elaborated in order to explain satisfactorily these facts. The origin or the progenitors of the magnetic white dwarfs is still an open issue and still not a definitive answer has been given to this question. There are two scenarios that could explain the formation of magnetic white dwarfs, the fossil field hypothesis and the binary hypothesis. In the first the evolutionary channel of the magnetic field of white dwarfs is the consequence of the evolution of a single progenitor along the different stellar evolutionary phases (Angel et al., 1981; Wickramasinghe and Ferrario, 2005) while in the binary scenario the magnetic field arises from the interaction of the future white dwarfs with a companion during its previous evolution. Both of them have their advantages and drawbacks (García-Berro et al., 2016).

In the fossil field hypothesis the magnetic white dwarfs descend from rotating Ap and Bp stars, which are the only stars in the main-sequence with significantly high magnetic fields $(10^3 - 10^5)$ G. Assuming that the magnetic flux is conserved and neglecting the effects of mass loss the magnetic field will be amplified by a factor of $\sim 10^4$ when the progenitor becomes a white dwarf. So, these magnetic stars would become white dwarfs with magnetic fields in the range $(10^6 - 10^9)$ G. This happens even if mass loss is considered (García-Berro et al., 2016).

In the binary scenario several proposals for the evolutionary channel have been proposed. For example, it has been proposed (see, e. g. Nordhaus et al., 2011; Tout et al., 2008) that strong magnetic fields are produced during a common envelope episode in a close binary system in which one of the components is a degenerate star. The spiral-in of the secondary star induces differential rotation in the extended convective envelope, creating a stellar dynamo that produces the magnetic field. However, this magnetic field does not penetrate into the white dwarf and decays very fast when the common envelope is ejected (Potter and Tout, 2010). On the other hand, another proposed channel has turn out to be more plausible after research has shown more its feasibility; the merger of two degenerate stars produce a hot differentially rotating convective corona capable of producing strong magnetic fields that are confined to the outer layers of the resulting remnant and do not decay for very long timescales (see García-Berro et al., 2012; Lorén-Aguilar et al., 2009). It has also been shown that the magnetosphere couples with the debris region producing a torque that brakes the final magnetic white dwarf and brings the rotational periods to values comparable to those that have been observationally found (see Külebi et al., 2013). So, this scenario should be the most plausible to explain the existence of mag-

netic white dwarfs.

3.3 Stability of Magnetic White Dwarfs

3.3.1 Introduction

Super-Chandrasekhar white dwarfs with high magnetic fields have been recently used to explain some properties of supernovae. These hypothetical white dwarfs may surpass the Chandrasekhar mass limit,

$$M_{\rm Ch} = 2.015 \frac{\sqrt{3\pi}}{2} \frac{m_{\rm PL}^3}{(\mu_e m_u)^2} \approx 1.44\ M_\odot, \tag{3.1}$$

where $\mu_e \approx 2$ is the mean molecular weight per electron, $m_{\rm H}$ is the mass of hydrogen atom, and $m_{\rm PL} = \sqrt{\hbar c/G}$ is the Planck mass.

Since such objects should be metastable, the magnetic breaking of magnetic $B \sim 10^6 - 10^8$ G, super-Chandrasekhar white dwarfs with $M \sim 1.5 M_\odot$ have been adopted to explain the delayed time distribution of type Ia supernovae (see Ilkov and Soker, 2012, for details). The explosion would be delayed for a time typical of the spin-down timescale due to magnetic braking, providing the result of the merging process is a magnetic super-Chandrasekhar white dwarf rather than a sub-Chandrasekhar one.

It has also been claimed that super-Chandrasekhar white dwarfs could explain the observations of some peculiar superluminous type Ia supernovae which need white dwarf progenitors with masses $(2.1 - 2.8) M_\odot$, mass that in turn depends on the amount of nickel needed to successfully explain both the low kinetic energies and the high luminosity of these supernovae (Hicken et al., 2007; Howell et al., 2006; Scalzo et al., 2010; Silverman et al., 2011; Taubenberger et al., 2011; Yamanaka et al., 2009).

Following this idea, Das and Mukhopadhyay (2012, 2013) have recently proposed that white dwarfs could hold in their interiors magnetic fields $B \sim 10^{18}$ G, something never proposed before. The effect of these hypothetical huge magnetic fields should be to increase the mass limit of the white dwarfs:

$$M_{\rm max} = \pi^{3/2} \frac{m_{\rm PL}^3}{(\mu_e m_{\rm H})^2} \approx 2.58 M_\odot, \tag{3.2}$$

significantly exceeding the Chandrasekhar limit (3.1). This result would imply these hypothetical objects would be viable progenitors of the above superluminous type Ia supernovae. Such a new mass limit would be reached, in principle,

for extremely large interior magnetic fields of the order of 10^{18} G.

It is therefore necessary to assess the validity of the assumption of the existence of these objects following a theoretical approach. We show that the approach followed in Das and Mukhopadhyay (2013) and Das and Mukhopadhyay (2012) ignores several macro and micro physical effects needed for a complete and accurate description of ultra-magnetic white dwarfs. The virial theorem, gravitational and dynamical instabilities, the breaking of spherical symmetry, General Relativity, inverse β-decay, and pycnonuclear reactions render invalid the new mass limit and therefore confirm the validity of the traditional Chandrasekhar mass limit. We already considered these effects in the previous chapter, following closely the cases of static (Rotondo et al., 2011a) and uniformly rotating (Boshkayev et al., 2013) white dwarfs. Our analysis in this chapter, that exposes the analysis in Coelho et al. (2014) and Cáceres et al. (2014), leads to two major conclusions:

- For the sub-Chandrasekhar white dwarfs (or slightly super-Chandrasekhar when we consider, for example, rotation) with surface magnetic fields in the observed range of the most magnetic white dwarfs, i.e., $B \sim (10^6 - 10^9)$ G (Ferrario et al., 2015), the non-magnetic approximation for the description of the structure parameters is approximately correct and therefore, the results of Rotondo et al. (2011a) and (Boshkayev et al., 2013) can be used to obtain the structure parameters such as mass and radius, for the static and uniformly rotating cases, respectively.

- When all the above mentioned macro and micro physical aspects relevant for the self-consistent description of the structure and stability of white dwarfs are considered, they lead to the conclusion that the existence of such ultra-magnetic white dwarfs in nature is very unlikely due to the violation of the requirements for stability. All these ignored effects make improbable that a white dwarf could reach such a hypothetical extreme case either in single or binary evolution.

This implies that the canonical Chandrasekhar mass limit of white dwarfs still has to be applied and consequently the proposed ultra-magnetic white dwarfs cannot be used as progenitors of superluminous supernovae.

3.3.2 Ultra-magnetic white dwarfs

We now summarise how the new mass limit for ultra-magnetic white dwarfs was obtained in Das and Mukhopadhyay (2013) and Das and Mukhopadhyay (2012). The equation of state of a degenerate electron gas in the presence of a magnetic field B directed along the z-axis in the limit of high magnetic fields, $B \to \infty$, where all electrons are constrained to the lowest Landau level, obeys a polytrope-like form (with polytropic index $\gamma = 2$) (Das and Mukhopadhyay, 2012, 2013):

$$P = K_{\rm m}\rho^2, \tag{3.3}$$

where

$$K_{\rm m} = m_e c^2 \pi^2 \lambda_e^3/(\mu_e^2 m_{\rm H}^2 B_{\rm D}), \tag{3.4}$$

with λ_e being the electron Compton wavelength and with $B_{\rm D} \equiv B/B_c$ being the magnetic field in units of the critical magnetic field of quantum electrodynamics:

$$B_c = m_e^2 c^3/(e\hbar) = 4.41 \times 10^{13}\ \text{G}. \tag{3.5}$$

To obtain the aforementioned equation of state in Das and Mukhopadhyay (2013), the density of the system was assumed to be given by $\rho = \mu_{\rm e} m_{\rm H} n_{\rm e}$, so, determined only by the nuclei component, where $n_{\rm e}$ is the electron number density.

Then, the Newtonian equations of hydrostatic equilibrium in spherical symmetry were integrated for this equation of state using the Lane-Emden solution of Newtonian self-gravitating polytropes of index $n = 1$, obtaining the radius

$$R = \sqrt{\pi K_{\rm m}/2G}, \tag{3.6}$$

and the corresponding mass

$$M = 4\pi^2 \rho_{\rm c} (K_{\rm m}/2\pi G)^{3/2}, \tag{3.7}$$

where $\rho_{\rm c}$ is the central density.

In the present limit of one Landau level with high-electron Fermi energies $E_e^{\rm F}$, $E_e^{\rm F} = E_{\rm max}^{\rm F} \gg m_e c^2$, with

$$E_{\rm max}^{\rm F} = m_e c^2 \sqrt{1 + 2B_{\rm D}} \approx m_e c^2 \sqrt{2B_{\rm D}} \gg m_e c^2, \tag{3.8}$$

the maximum possible value of $E_e^{\rm F}$. In this limit the central density $\rho_{\rm c}$ is given by (Das and Mukhopadhyay, 2012, 2013):

$$\rho_c = \frac{\mu_e m_{\rm H} B_D^{3/2}}{\sqrt{2}\pi^2 \lambda_e^3}. \tag{3.9}$$

Substituting (3.9) in (3.7) we obtain the new upper mass limit independent of $\rho_{\rm c}$

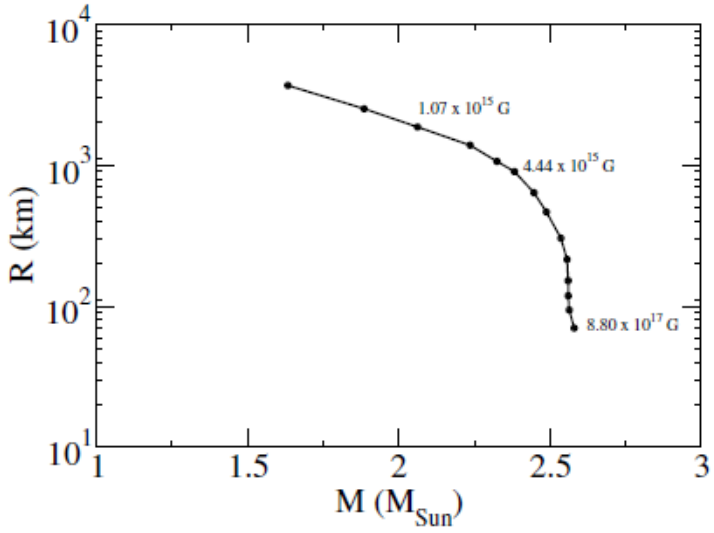

Figure 3.3: Mass-radius relation of magnetic white dwarfs - the curve represents the evolutionary track of the white dwarf with the increase of the uniform magnetic field inside the star obtained in Das and Mukhopadhyay (2013).

and B_D (corresponds to the limits $\rho_c \to \infty$, $B_{\rm D} \to \infty$ and $R \to 0$):

$$M_{\rm max} = \pi^{3/2} \frac{m_{\rm PL}^3}{(\mu_e m_{\rm H})^2} \approx 2.58 M_\odot \tag{3.10}$$

In figure 3.3 is reproduced the evolutionary track of the white dwarf proposed in Das and Mukhopadhyay (2012, 2013). It is possible to see how the star reaches the maximum mass limit (3.10) while reducing its radius. The magnetic field is increasing along the curve as a consequence of accretion onto the star.

At this point we can address some of the assumptions made in the model presented by Das and Mukhopadhyay (2013) which, as we will show, are unjustified and therefore, render invalid all their conclusions regarding the existence of the so-called super-Chandrasekhar ultra-magnetic white dwarfs. These assumptions are:

- The equation of state assumed in the limit of very intense magnetic fields, $B \to \infty$.
- An uniform magnetic field is adopted.
- The virial theorem is ignored, hence the huge magnetic fields and the mass-radius relation they obtained are not realistic.

- Dynamical instabilities due to quadrupole deformation are not taken into account.

- Spherical symmetry is assumed for all values of the magnetic field.

- The role of the magnetic field in the hydrostatic equilibrium equations is neglected.

- General relativistic effects are ignored, even if the final configuration is almost as compact as a neutron star and the magnetic energy is larger than the matter energy density.

- Microphysical effects such as inverse β-decay and pycnonuclear fusion reactions, important in a regime where electrons are highly relativistic, $E_e^{\rm F} \gg m_e c^2$, are ignored.

- The magnetic field, the density and the electron Fermi energy are assumed to increase with time inside the star as a consequence of a continuos accretion process onto the white dwarf.

3.3.3 Equation of state and virial theorem violation

Following Chandrasekhar and Fermi (1953), there existes a maximum magnetic field $B_{\rm max}$ above which an equilibrium configuration is impossible because the electromagnetic energy $W_{\rm B}$ exceed the gravitational energy $W_{\rm G}$, therefore becoming gravitationally unbound. If one includes the forces derived from the magnetic field, one can write the virial scalar relation for an equilibrium configuration as (Chandrasekhar and Fermi, 1953):

$$3\Pi + W_{\rm B} + W_{\rm G} = 0, \tag{3.11}$$

where $\Pi = \int P {\rm d}V$, with P the pressure of the system, $W_{\rm B}$ the positive magnetic energy and $W_{\rm G}$ the negative gravitational potential energy. The quantity Π satisfies $\Pi = (\gamma - 1)U$ for a polytrope ($P = K\rho^{\gamma}$), where U is the total kinetic energy of particles. Since the total energy of the configuration can be written as $E = U + W_{\rm B} + W_{\rm G}$, then one can eliminate U from equation (3.11) to obtain $E = -[(\gamma - 4/3)/(\gamma - 1)](|W_{\rm G}| - W_{\rm B})$, and therefore the necessary condition for the stability of the star, $E < 0$, is given by:

$$(3\gamma - 4)|W_{\rm G}| \left(1 - \frac{W_{\rm B}}{|W_{\rm G}|}\right) > 0. \tag{3.12}$$

From this expression we can recover, in the case of an absent magnetic field ($W_B = 0$), the known condition for bound non-magnetic polytropes $\gamma < 4/3$, or $n < 3$ in terms of the polytrope index n defined by $\gamma = 1 + 1/n$. The presence of a magnetic field weakens the stability and no matter the value of γ, the star becomes gravitationally unbound when the magnetic energy exceed the gravitational one, i.e., $W_B > |W_G|$. This condition implies an upper bound for the magnetic field obtained by the condition $W_B = |W_G|$. In order to determine such a limit we first consider the expression of W_B for a constant magnetic field throughout the whole star, which is the type of magnetic field assumed by Das and Mukhopadhyay (2013). This expression for the magnetic field energy is:

$$W_B = \frac{B^2}{8\pi}\frac{4\pi R^3}{3} = \frac{B^2 R^3}{6}. \tag{3.13}$$

As we have already mentioned before, Das and Mukhopadhyay (2013) adopts for the equation of state of the magnetic white dwarf a polytrope model with $\gamma = 2\,(n+1)$, assumption that is valid for extreme magnetic fields such that only one Landau level is occupied and the electron Fermi energy satisfies $E^F \gg m_e c^2$. This implies that the gravitational energy density of the spherical star configuration is (Shapiro and Teukolsky, 1986):

$$W_G = -\frac{3}{5-n}\frac{GM^2}{R} = -\frac{3}{4}\frac{GM^2}{R}. \tag{3.14}$$

Using the above expressions and expressing M and R in units of solar mass $M_\odot$ and solar radius $R_\odot$ respectively, we find that the maximum value of the magnetic field, B_{max}, is given by:

$$B_{max} = 2.24 \times 10^8 \frac{M}{M_\odot}\left(\frac{R_\odot}{R}\right)^2 \text{ G}. \tag{3.15}$$

In the case of a Chandrasekhar white dwarf with the maximum mass $M = 1.44 M_\odot$ and a radius of 3000 km, consistent with the recent calculation of massive and rotating white dwarfs (Boshkayev et al., 2013), we obtain $B_{max} \sim 1.7 \times 10^{13}$ G. This values is lower than the critical field $B_c = 4.4 \times 10^{13}$ G.

We can see from equation (3.15) that if we know the mass-radius relation we can obtain B_{max} as a function of either the mass M or the radius R. We therefore use the mass-radius relation calculated by Das and Mukhopadhyay (2013) and shown in figure 3.3, to plot B_{max} vs. M in figure 3.4. In the same figure we can appreciate three points that correspond to the magnetic fields of three configurations (shown in table 3.1) of the model of Das and Mukhopadhyay (2013), that correspond to different masses $M = (2.06, 2.38, 2.58) M_\odot$ and that lie in the region of high-mass configuration. We compare these values of B

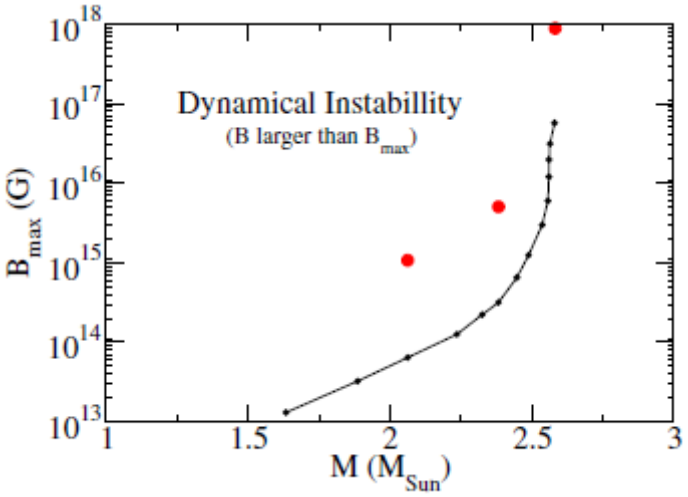

Figure 3.4: Maximum magnetic field $B_{\max}$ as a function of the star mass. We show (red dots) the three values of the magnetic field of table 3.1. that are above the $B_{\max}$ line in the dynamical instability region.

with the maximum value, $B_{\max}$, allowed by the virial theorem, equation (3.15). In figure 3.4 we show that such extreme magnetic fields with $B > B_{\max}$ and the magnetic white dwarfs of table 3.1 are in the instability region, violating the virial theorem. We also show in that table the corresponding magnetic energy W_B and gravitational energy $|W_{\rm G}|$ of each configuration. These results indicate that the magnetic field obtained in Das and Mukhopadhyay (2013) are at least one order of magnitude larger than the maximum magnetic field allowed $B_{\max}$. Also for these configurations we have $W_B/|B_{\rm G}| \sim 250$, well above the stability condition that requires $W_B/|B_{\rm G}| \sim 1$. These results imply these hypothetical ultra-magnetic white dwarfs are indeed unstable and unbound.

$M(M_\odot)$	R(km)	B(G)	$B_{\rm max}$(G)	$W_{\rm B}(\times 10^{51}$ erg)	$\lvert W_G\rvert(\times 10^{51}$ erg)	$W_{\rm B}/\lvert W_G\rvert$	$\rho_{\rm B}$(g cm^{-3})	ϵ/R
2.58	7.02×10^1	8.80×10^{17}	5.70×10^{16}	4.43×10^4	1.88×10^2	235	3.40×10^{13}	-195.14
2.38	9.60×10^2	4.44×10^{15}	2.81×10^{14}	2.90×10^3	1.17×10^1	248	8.71×10^8	-204.16
2.026	1.86×10^3	1.07×10^{15}	6.49×10^{13}	1.23×10^3	4.52	273	5.10×10^7	-223.03

Table 3.1: Mass radius configurations of magnetic white dwarfs of Das and Mukhopadhyay (2013) with the corresponding magnetic field B, the maximum virial magnetic field $B_{\rm max}$, the magnetic energy $W_{\rm B}$, the gravitational energy W_G, the ratio $W_{\rm B}/|W_G|$, the magnetic field contribution to the total energy density $\rho_{\rm B}$, and the values of the eccentricity in units of the spherical star radius.

It is worth noting that equation (3.15) can be also expressed as a limit to the magnetic flux: $\Phi_{\max} \sim B_{\max} R^2 \approx 1.1 \times 10^{30} (M/M_\odot)$ G cm^2. In the case of the maximum mass given by equation (3.10), $M = 2.58 M_\odot$, this maximum magnetic flux is $\Phi_{\max} \approx 2.8 \times 10^{30}$ G cm^2. The equations of the solution obtained by Das and Mukhopadhyay (2013) imply a constant value of the magnetic flux:

$$\frac{\Phi_{\text{frozen}}}{B_{\text{c}}} \sim B_{\text{D}} R^2 = \pi^3 \left(\frac{\hbar c}{G}\right) \frac{1}{(\mu_e m_{\text{H}})^2} \lambda_e^2 \approx 2 \times 10^{18} \text{ cm}^2, \Rightarrow \tag{3.16}$$

$$\Phi_{\text{frozen}} \sim B R^2 \approx 8.74 \times 10^{31} \text{ G cm}^2. \tag{3.17}$$

This constant value highly overcomes the maximum possible magnetic flux $\Phi_{\max}$, something that shows in a different way the violation of the stablity limit imposed by the virial theorem by the solution presented in Das and Mukhopadhyay (2013).

3.3.4 Microscopic instabilities

We turn now to show how such well-known processes as the inverse β-decay and pycnonuclear reactions lead to an instability region of these ultra-magnetic white dwarfs. These processes were also considered in Chamel et al. (2013), and a conclusion that these white dwarfs could not exist in nature was presented.

Inverse β-decay instability

As we saw in the previous chapter, inverse β-decay by capture of energetic electrons is known to cause an instability in a white dwarf, thereby inducing its gravitational collapse. The process is triggered once the electron Fermi energy reaches the threshold energy, $\epsilon_{\text{Z}}^{\beta}$, given by the difference in nuclear binding energies between the initial (Z, A) and the final $(Z-1, A)$ nucleus. Such a process destabilizes the star because the electrons are the main responsible for the pressure in a white dwarf (Harrison et al., 1965; Shapiro and Teukolsky, 1986). This threshold Fermi energy for the non-magnetic case corresponds to a critical density $\rho_{\text{c}}^{\text{non-mag}}$ which of course, also depends on the composition, as can be appreciated in table 3.2 and in table 2.1 of section 2.2.1. And for the magnetic case this process also sets a limit on the maximum electron Fermi energy $E_{\max}^{\text{F}}$. Using equation (3.8), it can be seen that the electron capture process limits the magnetic field to values lower than (see, e.g., Chamel et al., 2013):

$$B_{\text{D}}^{\beta} = \frac{1}{2} \left(\frac{\epsilon_{\text{Z}}^{\beta}}{m_e c^2}\right)^2, \tag{3.18}$$

and on the density of the white dwarf through equation (3.9). These quantities, the maximum magnetic field and the corresponding critical density $\rho_{\text{c}}^{\text{mag}}$ are also

Comp.	$E^{\beta}_{\rm th}$ (MeV)	$B^{\beta}_{\rm max}$ (G)	$\rho_{\rm c}^{\rm mag}$ (g$\cdot$ cm^{-3})	$\rho_{\rm c}^{\rm non\text{-}mag}$ (g$\cdot$ cm^{-3})
Carbon	13.370	1.51×10^{16}	$2.6{\times}10^{10}$	$2.12{\times}10^{10}$
Oxygen	10.419	9.18×10^{15}	$1.2{\times}10^{10}$	$1.94{\times}10^{10}$
Iron	3.695	1.16×10^{15}	$5.7{\times}10^{8}$	$1.18{\times}10^{9}$

Table 3.2: Depending on the composition, we have different threshold energies for the triggering of electron capture. The corresponding maximum magnetic field $B^{\beta}_{\rm max}$ and central density $\rho_c^{\rm mag}$ (g$\cdot$ cm^{-3}) will vary as shown. Just compare with the respective critical density in the non-magnetic case, $\rho_c^{\rm non\text{-}mag}$ (g$\cdot$ cm^{-3}).

shown in table 3.2. We can see that the critical densities for the magnetic case are even smaller than the corresponding critical densities for the non-magnetic case. All these densities are much smaller than the ones of the massive ultra-magnetic white dwarfs considered by Das and Mukhopadhyay (2013). The configurations reaching the maximum mass limit (3.10), according to Das and Mukhopadhyay (2013), have fields $B \gtrsim 4 \times 10^{17}$ G and densities $\rho_c \gtrsim 4 \times 10^{12}$ g cm^{-3}. Indeed, inverse β-decay in a ^{12}C white dwarf ($\epsilon_Z^{\beta} \approx 13.4$ MeV) will take place for a magnetic field $B \approx 1.5 \times 10^{16}$ G at a corresponding density $\rho_c \gtrsim 2.6 \times 10^{10}$ g cm^{-3}. Similar conclusions are obtained for other possible compositions such as ^{4}He, ^{16}O or ^{56}Fe, as shown in table 3.2.

For the configurations that approach the maximum mass (3.10) $B_{\rm D} \gtrsim 10^4$ ($B \gtrsim 4 \times 10^{17}$ G) and $\rho_{\rm c} \gtrsim 4 \times 10^{12}$ g cm^{-3}. At such high densities, higher than the neutron drip value ($\rho_{\rm drip} \approx 4.3 \times 10^{11}$ g cm^{-3}), the less bound neutrons in nuclei start to drip out forming a free Fermi gas (Baym et al., 1971). The neutron drip process then starts when $\rho_c = \rho_{\rm drip}$, where $\rho_{\rm c}$ is given by equation (3.9). For a carbon composition it happens for a magnetic field $B_{\rm D} \approx 531$, or $B \approx 2.3 \times 10^{16}$ G (see, e.g., Chamel et al., 2013). It is important to clarify that extremely large magnetic fields ($> 10^{17}$ G) are needed to modify the neutron drip value appreaciably and we refer to Chamel et al. (2012) for an analysis of the influence of strong magnetic fields on the precise value of the neutron drip density and pressure.

Pycnonuclear Instability

As discussed by Chamel et al. (2013), pycnonuclear fusion reactions might establish a more stringent limit than inverse β-decay in an ultramagnetic white dwarf. Carbon fusion leads to ^{24}M, which undergoes electron capture and thus inverse β-decay instability at a density of approximately $\rho^{\beta}_{\rm crit,Mg} \approx 3 \times 10^9$ g cm^{-3} (see section 2.3.3 for further details). Therefore, if C+C fusion occurs at rates high enough at densities lower than $\rho^{\beta}_{\rm crit,Mg}$ to produce appreciable amounts of ^{24}Mg in times shorter than a Hubble time, then this process imposes a more tight constraint to the density of the white dwarf. Based on the up-to-date astrophysical

$\tau_{\rm pyc}$ (Myr)	ρ_c (g cm^{-3})	$B^{\rm pyc}_{\rm max}$ (G)
10^3	9.3×10^9	7.5×10^{15}
0.1	1.6×10^{10}	1.1×10^{16}

Table 3.3: The corresponding central densities and maximum magnetic fields are shown for the reaction ^{12}C+^{12}C$\rightarrow^{24}$Mg$\overset{\beta}{\rightarrow}{}^{24}Na\overset{\beta}{\rightarrow}{}^{24}$Ne for different timescales.

S-factors computed in Gasques et al. (2005) and Yakovlev et al. (2006), Boshkayev et al. (2013) computed the pycnonuclear reaction times for C+C fusion as a function of the density. They determined that for a timescale of $\tau^{\rm C+C}_{\rm pyc} = 10$ Gyr, $\rho_{\rm pyc} \sim 9.26\times10^9$ g cm^{-3} while for $\tau^{\rm C+C}_{\rm pyc} = 0.1$ Myr, $\rho_{\rm pyc} \sim 1.59\times10^{10}$ g cm^{-3}; see figure 2.10 and table 3.3. These densities are larger than the inverse β-decay threshold density of ^{24}Mg, ^{24}Mg$\rightarrow^{24}$Na$\rightarrow^{24}$Ne, $\rho \sim 3.2\times10^9$g cm^{-3} see Salpeter (1961); Shapiro and Teukolsky (1986). Thus, pycnonuclear ^{12}C+^{12}C fusion produces unstable ^{24}Mg, which decays due to electron capture, thus, the white dwarf becomes β-unstable.

Since $\rho^{\rm C+C}_{\rm pyc} < \rho^{\rm C+C}_{\rm crit,C} \approx 2.6\times10^{10}$ g cm^{-3}, this implies that C+C pycnonuclear fusion does not limit further the magnetic field strength with respect to the inverse β-decay instability of carbon. Indeed, using equation (3.9) we obtain that such a density is reached for a magnetic field $B^{\rm C+C}_{\rm D,pyc} \approx 246.6$, or $B^{\rm C+C}_{\rm pyc} \approx 1.1\times10^{16}$ G, a value lower than $B^{\beta,{\rm C}}_{\rm D} \approx 342.3$ or $B^{\beta}_{\rm C} \approx 1.5\times10^{16}$ G. Longer reaction times imply lower densities and thus lower magnetic fields.

It is important to note that the above limits to the magnetic field are estimated assuming that the density of the system is given by equation (3.9); however, more realistic estimates of these limiting fields have to account for the contribution of the magnetic field to the mass-energy density (see section 3.3.6) and the self-consistent value of the electron density accounting for the real number of Landau levels populated, which will be higher than one. The above microscopic limits to the magnetic field are higher than the maximal values allowed by the virial theorem. Therefore, the macroscopic dynamical instabilities appear to set in before both electron captures and pycnonuclear reactions.

3.3.5 Breaking of spherical symmetry

In Chandrasekhar and Fermi (1953) (see also the errata Chandrasekhar and Fermi (1955)), the figure of equilibrium of an incompressible fluid sphere with an internal uniform magnetic field that matches an external dipole field was shown to be represented by an oblate spheroid instead of a sphere. The star becomes oblate by contracting along the direction of the magnetic field. The bounding surface of this spheroid is given by

$$r(\cos\theta) = R + \epsilon P_l(\cos\theta), \tag{3.19}$$

where $\epsilon \ll R$, θ is the polar angle and $P_l(\cos\theta)$ denotes the Legendre polynomial of order l.

The deviation from the spherical configuration is given by the term $P_l(\cos\theta)$, thus in Chandrasekhar and Fermi (1953) such a perturbation was called "P_l-deformation". They have also concluded that the term with $l = 2$ contributes to the corresponding change in the internal magnetic energy density, while for the all other values of l the change in the magnetic energy is of the second order in ϵ. The quantity ϵ satisfies $\epsilon \ll R$ and measures the deviations from a spherical configuration. The polar and equatorial radii are $R_p = R + \epsilon P_l(1)$ and $R_{\rm eq} = R + \epsilon P(0)$, respectively, thus $\epsilon = -(2/3)(R_{\rm eq} - R_{\rm p})$ and therefore $\epsilon/R = -(2/3)(R_{\rm eq} - R_{\rm p})/R$ for the axisymmetric deformed configuration with $l = 2$.

It was shown by Chandrasekhar and Fermi (1953) that such an axisymmetrically deformed object is favorable energetically with respect to the spherical star. Thus the star becomes unstable and proceeds to collapse along the magnetic field axis, turning into an oblate spheroidal with $\epsilon < 0$. For a "P_2-deformation" ($l = 2$) the contraction continues until the configuration reaches a value of ϵ/R given by (see: Chandrasekhar and Fermi, 1953, 1955):

$$\frac{\epsilon}{R} = -\frac{35}{24}\frac{B^2R^4}{GM^2}. \tag{3.20}$$

Using the expression for $B_{\rm max}$ given by equation (3.15) one obtains:

$$\frac{\epsilon}{R} = -\frac{315}{384}\left(\frac{B}{B_{\rm max}}\right)^2 \simeq -0.8\left(\frac{B}{B_{\rm max}}\right)^2. \tag{3.21}$$

Therefore, when the internal magnetic field is close to the limit set by the virial theorem, the star deviates to a highly oblate shape.

We show in the last column of table 3.1 the "P_l-deformation" ϵ/R calculated for the three configurations discussed before. The results show that $|\epsilon/R| \gtrsim 2 \times 10^2$, which implies that the star has a highly oblate shape and thus the spherical symmetry is strongly broken. Therefore, in order to consider the effect of the deformation caused by the presence of the magnetic field a more consistent calculation that considers cylindrical symmetry (see, e.g. Chandrasekhar and Fermi, 1953; Ostriker and Hartwick, 1968) is mandatory. It is worth mentioning that if we consider the quantum nature of the equation of state of a Fermi gas subjected at fields $B \gg B_{\rm c}$, the actual shape of equilibrium is defined by the

total (matter+field) pressures parallel and perpendicular to the magnetic field, pressures that are different and that vanish at the star surface (Chaichian et al., 2000; Pérez Martínez et al., 2003, 2008; Strickland et al., 2012).

3.3.6 General Relativistic effects

As we mentioned before the solution obtained by Das and Mukhopadhyay (2013) used the hydrostatic equilibrium equations of a magnetic fluid, something which can be used only when the contribution of the magnetic field to the total energy density is negligible compared with the matter density. However, it is easy to check that this requirement is violated by the configurations considered by Das and Mukhopadhyay (2013), where the magnetic fields are so intense that their contribution to the energy density turns out to be equal or greater than the contribution of the matter, making invalid the Newtonian approach. To see this we can calculate for the maximum white dwarf mass of Das and Mukhopadhyay (2013), equation (3.10), which is obtained for a magnetic field $B \approx 10^8$ G, the contribution of the magnetic field to the total energy density, which turns out to be $\rho_{\text{B}} \approx B^2/(8\pi c^2) \approx 4.4 \times 10^{13}$ g cm^{-3}. This value is larger than the matter density of the configuration and cannot be neglected in the energy-momentum tensor of the system. However, as we have shown before, due to different instability effects, such large magnetic fields cannot be reached in the star.

On the other hand, when the maximum mass (equation (3.10)) is approached for magnetic fields $B_{\text{D}} \gtrsim 10^4$, the central density of the system is given $\rho_c \gtrsim 4 \times 10^{12}$ g cm^{-3}, according to equation (3.9). In particular, the maximum mass configuration would have a radius $R \approx 70$ km and therefore a central density $\rho_c \approx 1.2 \times 10^{13}$ g cm^{-3}, only one order of magnitude less than the nuclear saturation density. These values imply that the mass, radius and density of the ultra-magnetic white dwarfs considered by Das and Mukhopadhyay (2013) are much more similar to the typical parameters of a neutron star rather than those of a white dwarf. Therefore we could ask whether or not the compactness of the star is such to require a full general relativistic treatment. For the above star parameters close to the maximum mass configuration, it is obtained a compactness $GM/(c^2R) \approx 0.05$, a value in clear contrast with a Newtonian treatment of the equilibrium equations.

In this line, the results of Rotondo et al. (2011a) become relevant. It was found there that in the case of carbon white dwarfs, general relativistic instability sets in at a density $\rho_{\text{crit}} \approx 2 \times 10^{10}$ g cm^{-3}, before the onset of the inverse β-decay instability. Such a density is much lower than the densities of the ultra-magnetic white dwarfs of Das and Mukhopadhyay (2013).

3.3.7 Evolutionary path

In order to explain how those white dwarfs with such huge magnetic fields could exist in nature, Das and Mukhopadhyay (2013); Das et al. (2013) proposed that

the star by accretion could increase its central density and its magnetic field owing to magnetic flux conservation. However, it is unlikely that such an accretion could bring the white dwarf to such extreme regimes without passing through the instability channels we have analysed before.

Flux conservation implies that an uniform magnetic field, as the one assumed by Das and Mukhopadhyay (2013), satisfies $B_f/B_0 = (R_0/R_f)^2$, where the subscripts 0 and f stand for initial and final values. It is known that in the Newtonian treatment the critical mass is reached at infinite densities, so when the radius tends to zero it causes an unphysical large increase of the above magnetic field when approaching the critical mass value. Therefore it is essential for this computation to take into due account the general relativistic and microscopic instabilities leading to a finite critical density and radius for the critical mass configuration. For this purpose, we use the mass-radius relation obtained by Rotondo et al. (2011a). If we start an accretion process on a carbon white dwarf with an initial mass $M \sim M_\odot$ ($R_0 \approx 5587.43$ km), a mass typical of white dwarfs with high magnetic field (see Ferrario et al., 2005, for details), we obtain that the magnetic field increases only by a factor $B_f/B_0 \approx 28$ up to the final mass $M_f = M_{\rm crit} \approx 1.39\ M_\odot$ ($R_f \approx 1051.44$km). Indeed, the magnetic flux is $\Phi_{\rm acc} \sim B_0 R_0^2 \approx 3.1 \times 10^{25} (B_0/10^8)$ G cm^2, to be contrasted with the much higher value of the frozen value $\Phi_{\rm frozen} \approx 8.7 \times 10^{31}$ G cm^2, inferred in section 3.3.3 for the maximum mass solution of Das and Mukhopadhyay (2013). This implies that the accretion most likely will lead to the triggering of the white dwarf gravitational collapse either to a neutron star or to an ordinary Type Ia supernova before reaching a stage where the magnetic field can cause and appreciable changes to the equation of state and to the structure of the star.

One could think that the white dwarf has already a huge magnetic field ($\gtrsim 10^{15}$ G) before starting the accretion process. However, we know from what we have shown in section 3.3.3 that the virial theorem imposes a limit to the magnetic flux of $\Phi_{\rm max} \approx 1.1 \times 10^{30} \sqrt{4/(5-n)} (M/M_\odot)$ G cm^2, where n is the polytropic index. In addition, huge seed magnetic fields in the interior of a solas mass white dwarf appear to be in contradiction with observations since the non-magnetic mass-radius relation reproduces with appreciable accuracy the observational data (see, e.g., Provencal et al., 1998; Vauclair et al., 1997).

3.3.8 Recent discussion on ultra-magnetic white dwarfs

Besides this work, other works have also pointed out the stability problems of the ultra-magnetic white dwarfs proposed in Das and Mukhopadhyay (2013) (see Chamel et al., 2013; Dong et al., 2014; Nityananda and Konar, 2014, 2015, for further details on some of the same points considered in this chapter and on other issues such as the neglected effect of the Lorentz force, i.e., the magnetic field gradient).

More recently Das and Mukhopadhyay (2014), taking into account some of

the criticisms raised by us and several researchers, obtained new solutions for ultra-magnetic super-Chandrasekhar white dwarfs, improving in this way the previous treatment exposed in Das and Mukhopadhyay (2013). They solved the general relativistic equations of hydrostatic equilibrium within the assumption of spherical symmetry, including the magnetic pressure gradient. The effect of the magnetic field gradient was introduced through a phenomenological magnetic field profile. They solved the equations for two different conditions on the parallel pressure:

1. That the spherically averaged paralled pressure be positive throughout the star (case 1).

2. The parallel pressure be positive throughout (case 2).

The total pressure was assumed to be isotropic and increased by an *isotropized* magnetic field contribution given by:

$$\frac{1}{3}\frac{B^2}{8\pi} = \frac{B^2}{24\pi}. \tag{3.22}$$

Clearly this isotropic increase of the matter pressure could give, in principle, systems with higher masses than those of the non-magnetic case, something indeed obtained by Das and Mukhopadhyay (2014). They find that:

1. For case 1, for some choice of the phenomenological parameters that characterize the magnetic field profile, the maximum mass could be as high as $M_{\rm max} \approx 3.3 M_\odot$.

2. For case 2, $M_{\rm max} \approx 2.1 M_\odot$.

The magnetic field at the center in these configurations is $B_{\rm center} \approx 6.8 \times 10^{14}$ G. Those solutions, although interesting, use a phenomenological magnetic field not coming from the self-consistent solution of the Maxwell equations coupled to the Einstein equations. It is not clear that the self-consistent solution will have a distribution of the magnetic field similar to the one employed in that work and with a value showing such a high excursion from the center of the surface. A good example for the latter is the self-consistent solution presented by Ferraro (1954), for which the magnetic field at the center is only five times larger than its value at the surface. Possibly a more self-consistent calculation has been recently performed by Bera and Bhattacharya (2014), which includes the break of the spherical symmetry and the effect of the quantum pressure anisotropy. they obtain white dwarf masses as large as $1.9 M_\odot$. However, the maximum mass solution they obtained corresponds to an electron Fermi energy that overcomes the

limiting value for the inverse β-decay analysed in this work and in Chamel et al. (2013).

As a positive support for their model, Das and Mukhopadhyay (2014) recalled the recent mathematical analysis of Federbush et al. (2015), who showed that there exist solutions for magnetic self-gravitating $n = 1$ polytropes for a specific ansatz of the current $J = \beta r \rho$, where r is the cylindrical coordinate, ρ is the matter density and β is a constant. For the case of constant density, the above ansatz redusces to the one introduced by Ferraro (1954). Federbush et al. (2015) proved that there exist solutions providing the constant β is properly bound by a sufficiently small value. However, the solutions found by Das and Mukhopadhyay (2013) do not conform to such an ansatz of the current and therefore the analysis of Federbush et al. (2015) does not apply to such a specific solution. It is noteworthy that, in addition, Federbush et al. (2015) provides a simple proof of the non-existence of magnetic stars in the spherically symmetric case since the only possible solution has a magnetic field with a singularity as the center.

3.3.9 Concluding remarks

There are some restrictions coming from the virial theorem and general relativity. For a Chandrasekhar white dwarf with $M = 1.44 M_\odot$, $R \sim 3000$ km, consistent with the recent calculation of massive white dwarfs computed by Boshkayev et al. (2013), the maximum magnetic field permitted by the virial theorem is $B_{\rm max} \sim 1.7 \times 10^{13}$ G$< B_{\rm c} = 4.4 \times 10^{13}$ G $\ll 10^{18}$ G. Besides, for the magnetic fields considered considered in Das and Mukhopadhyay (2012, 2013), e.g. $B \approx 10^{18}$ G, the contribution of the magnetic field to the total energy density of the system is $\rho_B \approx B^2/(8\pi c^2) \approx 4.4 \times 10^{13}$ g cm^{-3}. This value is, indeed, larger than the matter density of the configuration and, therefore, cannot be neglected in the energy-momentum tensor of the system. This invalidates the treatment used in Das and Mukhopadhyay (2013) based on the Newtonian hydrostatic equilibrium equations because the general relativistic effects are ignored.

As a larger magnetic field is considered, the eccentricity it generates, the dynamical instabilities that come into play, and the microscopic instabilities, relevant when the electron energies increase significantly, make very unlikely the existence of such extremely magnetic white dwarfs since they would make a white dwarf either collapse or explode long before reaching such a hypothetical structure. The construction of equilibrium configurations of ultra-magnetic white dwarfs needs the inclusion of several effects not accounted for in Das and Mukhopadhyay (2013), and therefore the acceptance of such ultra-magnetic white dwarfs as possible astrophysical objects has to be considered with caution On the contrary, sub-Chandraselhar white dwarfs (or those that slightly exceed the Chandrasekhar limiting value thanks, for example, to rotation) with surface magnetic fields in the observed range, i.e., $B \sim 10^6 - 10^{10}$ G, can be safely described using a non-magnetic approximation for the calculation of the structure parameters such as the mass or the radius.

We would also like to mention that in Nityananda and Konar (2014), the importance of the gradient of the magnetic pressure, which was also neglected in Das and Mukhopadhyay (2012, 2013), was pointed out. The results of this work confirm the traditional Chandrasekhar mass limit and invalidate the recently proposed new mass limit for white dwarfs.

Chapter 4

Soft Gamma-ray repeaters and Anomalous X-ray Pulsars in the White Dwarf Model

As we saw in the preceding chapter, the increasing data from observational campaigns leave no room for doubts on the existence of massive ($M \sim 1$ M$_\odot$) white dwarfs (WDs) with magnetic fields comprised in the range $B \sim (10^6 - 10^9)$ G (Ferrario et al., 2015; Kepler et al., 2010, 2013, 2015; Külebi et al., 2009). The observed magnetic white dwarfs (MWDs) are usually massive, for example, REJ 0317-853 with $M \sim 1.35$ M$_\odot$ and $B \sim (1.7 - 6.6) \times \times 10^8$ G (Barstow et al., 1995; Külebi et al., 2010); PG 1658+441 with $M \sim 1.31$ M$_\odot$ and $B \sim 2.3 \times 10^6$ G (Liebert et al., 1983; Schmidt et al., 1992); and PG 1031+234 with $B \sim 10^9$ G (Külebi et al., 2009; Schmidt et al., 1986).

The highly magnetic white dwarfs (MWDs) observed up to now have very large periods (compared with those of pulsars), something that make them inactive as pulsars. However, Usov (1988) advanced the possibility that MWDs (he assumed, for instance, $B \sim 10^8$ G) that rotate very fast (with angular velocities $\Omega \sim 1$ rad/sec) would behave like a pulsar. However, due to the lack of observational evidence of fast rotating and highly MWDs, this possibility was dismissed or at least, considered highly improbable. But the discovery of pulsed emission in the white dwarf (WD) primary of AE Aquarii (Terada et al., 2008), a cataclysmic variable binary, brought back the attention to the idea of a pulsar-like WD, which was the first of these objects reported with such a behaviour. Notice that the reported period of this WD is $P \sim 33$ s, one of the smallest of all the periods reported in rotating white dwarfs (RWDs), and close to the range of periods of AXPs/SGRs and of course, of some slow and rotationally powered pulsars (RPPs).

More recently, Marsh et al. (2016) pointed to the pulsar behaviour of another MWD, AR Scorpii (AR Sco). It is interesting that, as in the well known case of AE Aquarii, also this WD belongs to a binary system. It is well known from observations that isolated WDs emit most of their electromagnetic emission from

ultraviolet to near-infrared wavelengths, while when they are in close orbits with a binary companion the resulting mass transfer due to gravitational strip generates atomic line emission (Szkody et al., 2011), emission in X-ray wavelengths (Revnivtsev et al., 2008) and in the case the WD is also magnetic they emit near and mid-infrared radiation (Parsons et al., 2013). However, whether the WDs are isolated or in binaries, it is highly unusual they be detected at far-infrared or radio frequencies. But the WD of AR Scorpii is detected in these wavelenghts, specifically from X-ray to radio wavelengths (Marsh et al., 2016).

Besides those characteristics that make the WD analyzed in Marsh et al. (2016) unique among WDs, it was also discovered that the emission in radio and optical was pulsed and the period of the pulsations is ~ 1.97 min, similar to the period of the WD of AE Aquarii. Marsh et al. (2016) associated this pulsation with the spin of the MWD. Furthermore, Marsh et al. (2016) concluded that the emission was rotationally powered because the spin-down power of the WD is an order of magnitude larger than the power of the electromagnetic radiation. So, up to now, two well known WDs have shown a pulsar-like behaviour and both happen to belong to binary systems, while the ordinary RPPs either belong to a binary system or are isolated. We remark that the pulsar-like behaviour can be observed from WDs in binaries when they can be considered approximately as isolated objects, as in the case of detached binaries, or in binaries in a propeller case.

The aforementioned discoveries are a fundamental support for the WD pulsar model for AXPs/SGRs. However, despite a WD could not be the only explanation for AXPs/SGRs because there are several proposed models, this raises the possibility that more pulsar WDs could be discovered in the future. WDs with a pulsar-like behaviour must be a very tiny percentage of the total MWDs due to the fact the conditions on the rotational period are extremely restrictive.

In this chapter we will review the main progress done on the WD model for AXPs/SGRs, beggining with the original idea and the first papers that proposed the model. Then we will talk about the bounds on the parameters of the WD of this model that come out from the structure and stability of an uniformly RWD, following closely chapter 2. Then we will talk about the glitches and outbursts observed in AXPs/SGRs and how the WD model can explain them from the energetic point of view. Finally we will talk about the emission in optical and near infra-red of some of these objects, where we will also mention a key ingredient of this model, the fact that in the case AXPs/SGRs are WDs they are most likely the outcome of a merger of two WDs. This is important in the model because several AXPs/SGRs have been associated with supernovae remnants and in the case of this model this remnant should come from the merger of these two WD progenitors.

4.1 Rotationally powered pulsar-like white dwarfs: structure and stability

Despite always pulsars were indisputably assumed to be neutron stars (NSs), the idea that a WD could have a pulsar-like behaviour was advanced, although not much attention was given to it because most of highly MWDs rotate very slowly (see chapter 3). From several considerations of the different pulsar models it was concluded that fast rotation is a requirement to have a pulsar-like behaviour. How much a star has to rotate to become an active pulsar will depend on the magnetospheric emission model and on parameters such as the rotational period (given directly by observations) and the surface magnetic field (inferred indirectly through the dipole formula (1.6)). These conditions will determine a condition called *death line* (see chapter 5).

NSs usually rotate fast thanks to the conservation of angular momentum after the collapse of a normal star to a neutron star (NS). On the contrary WDs rotate slower because they are bigger, but in principle, if they possess an appropriate rotational angular velocity, they can behave also as active pulsars. This possibility made Usov to be the first to advance this hypothesis in 1988 (Usov, 1988), where he assured that WDs with magnetic fields of the order $B \sim 10^8$ G and rotational velocities $\Omega \sim 1$ rad/sec would behave like a pulsar. In that paper Usov showed that under these conditions the WD becomes a source of γ-rays like an active pulsar, suggesting also for the first time the existence of pulsar-like WDs. Then, in the same year, Morini et al. (1988) were the first to suggest that the pulsar 1E 2259+586, that was associated with the supernova remnant G109.1-1.0, could be a fast RWD, proposing that any work on this direction could give a good explanation to the apparent anomaly observed in this pulsar (e.g., when assumed as a canonical NS satisfy the relation (1.1)). However, they did not enter into further details of this proposed WD model.

Then, Paczynski (1990) explored more the possibility of 1E 2259+586 as a fast rotating highly MWD, suggesting that in such a case it would be a WD formed from the merger of two WDs. Such a merger scenario was proposed before to explain Type Ia Supernovae (Iben and Tutukov, 1984; Paczynski, 1985). Different works point to a likely result of a final WD and a stellar remnant coming out from these kind of mergers (Benz et al., 1990; Iben, 1990; Mochkovitch and Livio, 1989) and these results were known when Paczynski addressed this hypothesis for 1E 2259+586.

The main reason behind Paczynski's hypothesis was that the rotational energy loss $\dot{E}_{\rm WD}$ of a WD can explain from the energetic point of view the observed luminosity $L_{\rm obs}$ in X-rays and γ-rays (Malheiro et al., 2012; Paczynski, 1990; Usov, 1993) detected in 1E 2259+586 (and in all other AXPs/SGRs), i.e., it

does not have the problem represented by relation (1.1); instead:

$$\dot{E}_{\rm WD} := -4\pi^2 I_{\rm WD} \frac{\dot{P}}{P^3} \gg L_{\rm obs}, \tag{4.1}$$

where $I_{\rm WD}$ is the moment of inertia of the WD, P is its period of rotation and $\dot{P}$ its time derivative. Just compare this to the relation obtained if we consider 1E 2259+586 (and in most of AXPs/SGRs) as a NS, i.e., to relation (1.1):

$$\dot{E}_{\rm NS} := -4\pi^2 I_{\rm NS} \frac{\dot{P}}{P^3} < L_{\rm obs},$$

where, we just remind, $I_{\rm NS}$ is the moment of inertia of a typical NS. The reason for this is that the typical moment of inertia of WDs ($\approx 10^{49}$ g cm^2) is several orders of magnitude larger than the typical moment of inertia of NSs ($\approx 10^{45}$ g cm^2), making possible in principle, from an energetic point of view, to explain 1E 2259+586, the first AXP detected and reported by Fahlman and Gregory (1981), as a rotationally powered pulsar-like WD. However, the WD hypothesis was forgotten due to the popularization of the model developed by Duncan and Thompson, the magnetar model. But after the works of Paczynski and Usov were almost forgotten, this idea has been again considered in recent papers (see, e.g. Boshkayev et al., 2013; Cáceres et al., 2017; Coelho and Malheiro, 2014; Lobato et al., 2016; Malheiro et al., 2012; Rueda et al., 2013).

Malheiro et al. (2012) checked if the relation (1.1) holds for all AXPs/SGRs up to now observed. They used fiducial parameters of typical NSs, $I \approx 10^{45}$ g cm^2, $M = 1.4$ M$_\odot$ and $R = 10$ km. They discovered that this relation was true for all the sources, except for 4, as can be seen in figure 4.1. These 4 sources are 1E 1547.0-5408, SGR 1627-41, PSR J1622-4950 and XTE J1810-197. The reason for this is that there is not an unique criterion to define AXPs/SGRs. Some of them were defined because they satisfied relation (1.1). Others were defined as AXPs/SGRs thanks to their transient emission. This means these four sources could in principle be modelled as rotationally powered NSs. Indeed, after that paper, Coelho et al. (2017) explored further this possibility. That work is explained in chapter 6.

Malheiro et al. (2012) also checked if the WD hypothesis could explain energetically all AXPs/SGRs. Like in the case for NSs, they considered fiducial values of a typical massive WD: $M = 1.4$ M$_\odot$, $R = 10^3$ km and $I \approx 10^{49}$ g cm^2. As we can see from figure 4.2, taken from Malheiro et al. (2012), the rotational energy loss of a typical WD is well above any observed luminosity in X-rays for all AXPs/SGRs observed up to now. So, the original hypothesis proposed by Paczynski (1990) to explain 1E 2259+586 as a WD can be applied also to the other members of the AXPs/SGRs family.

A crucial question for the model is the stability of WDs that rotate as fast

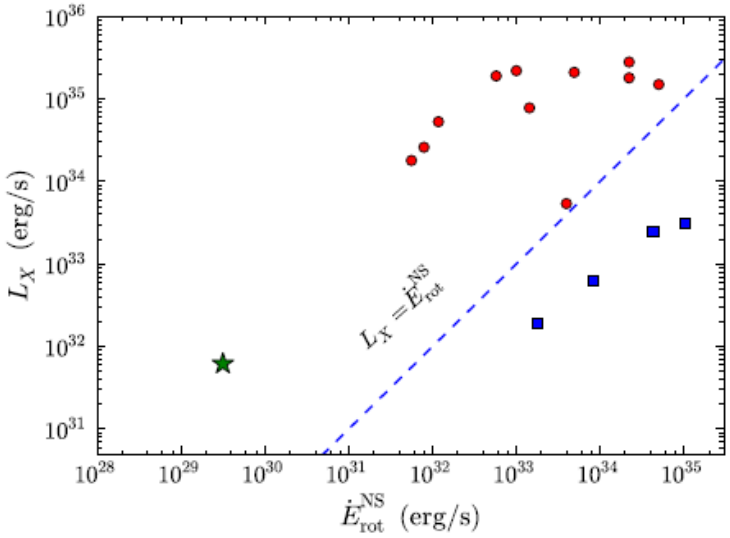

Figure 4.1: Luminosity in X-rays (L_X) compared with the loss of rotational energy of AXPs/SGRs when they are considered as Neutron Stars. This figure is taken from Malheiro et al. (2012). The green star corresponds to SGR 0418+5729, using an observational upper limit for the time derivative of the period $(\dot{P} < 6.0 \times 10^{-15})$. However, this value is outdated because now we have a more accurate measurement of $\dot{P} = 4(1) \times 10^{-15}$, not an upper limit (Rea et al., 2013). The blue squares are the four sources that satisfy $L_X < \dot{E}_{rot}^{NS}$.

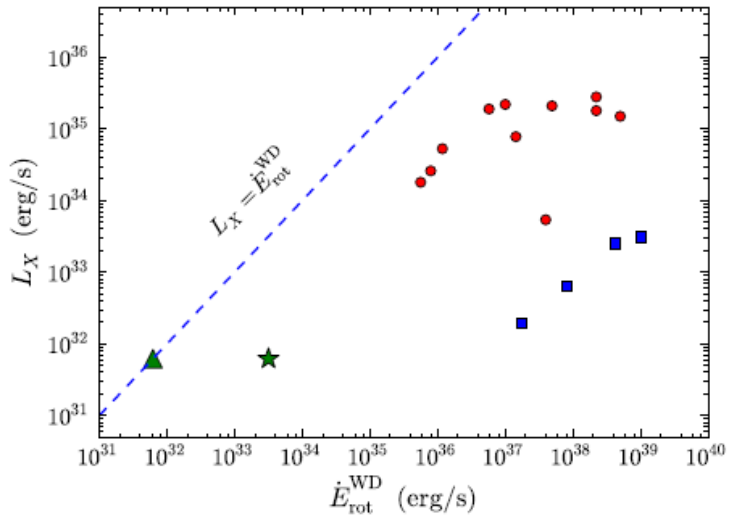

Figure 4.2: Luminosity in X-rays (L_X) compared with the loss of rotational energy of a WD model of AXPs/SGRs. This figure is taken from (Malheiro et al., 2012). The green star and the green triangle correspond to SGR 0418+5729, using respectively an upper limit and a lower limit for $\dot{P}$, respectively. The upper limit corresponds to an observational upper limit of $\dot{P} < 6.0 \times 10^{-15}$, while the lower limit is $\dot{P} \geq 1.18 \times 10^{-16}$, which is obtained when we make $\dot{E}_{rot}^{NS} = L_X$. However, this is updated because now we have a more accurate measurement of $\dot{P}$, not an upper limit (Rea et al., 2013). The blue squares are the four sources that satisfy $L_X < \dot{E}_{rot}^{NS}$ (see figure 4.1).

as AXPs/SGRs. This is one of the main criticisms done to the model, because, as we know from chapter 2, when WDs rotate too fast they approach the mass-shedding limit and when they overcome that limit they are rotationally unstable. Therefore a confirmation of their stability is important to determine whether or not a WD model can be applied to these objects. The question of the stability was implicitly assumed in Malheiro et al. (2012). However, this question was addressed later by Boshkayev et al. (2013), who improved the analysis done by Malheiro et al. (2012) considering the structure and stability of uniformly RWDs following closely the model constructed in Boshkayev et al. (2013). As we saw in chapter 2, Boshkayev et al. (2013) constructed solutions to the Einstein Field Equations within the Hartle's formalism for uniformly RWDs and used the relativistic Feynman-Metropolis-Teller equation of state to describe their matter properties.

Within the formalism developed by Boshkayev et al. (2013) we can determine whether or not hypothetical WDs could rotate with the rotational periods of AXPs/SGRs. To answer that question let's remember (see chapter 2) that in this formalism, for each nuclear composition (^{4}He, ^{12}C, ^{16}O and ^{56}Fe WDs are considered), a minimum rotational period $P_{\rm min}$ is determined; this minimum rotational period of WDs is obtained when we consider a configuration rotating at Keplerian angular velocity and at a critical density for the onset of inverse β-decay instability. This extreme configuration corresponds to the point of intersection between the mass-shedding and the inverse β-decay boundaries. These boundaries and their corresponding intersection point can be appreciated in figure 4.3, taken from Boshkayev et al. (2013). The minimum rotation periods for all the four compositions can be seen in table 2.3. As we can see, the minimum rotational periods, considering the different compositions, are in the range $(0.3 - 2)$ s. This allows us to conclude that WDs that rotate as fast as AXPs/SGRs are dynamically stable.

With the stability analysis that this formalism allows us to do it is possible to obtain and constrain the range of possible parameters for quantities such as the radius, the mass or the moment of inertia for a given period and of course, for a given nuclear composition. As we mentioned before, in figure 4.3 is plotted the mass versus the equatorial radius of RWDs with ^{12}C as nuclear composite. Besides the Keplerian sequence and the inverse β-decay instability boundaries, there are plotted other instability limits such as the secular and pycnonuclear instabilities. Also are plotted sequences of constant period of rotation, these sequences are represented by the thin dashed colored lines. These curves of constant period or angular velocity intersect the Keplerian sequence and the instability boundaries of inverse β-decay or secular instability. We can see that there can exist sequences of constant period that would not intersect the gray dashed region, this is because their rotational velocity would be below the minimum reported in table 2.3.

The intersections of configurations of constant period $P > P_{\rm min}$ with the

different boundary limits determine the range of possible values for the mass, radius and magnetic field (calculated indirectly using equation (4.2)) for an uniformly rotating and MWD; the constant period curves determine all the possible configurations for that given period of rotation within the limits imposed by instability boundaries. Looking at figure 4.3, the curves of constant but large periods are very close to the static configuration curve, as it should be. As long as we increase the angular velocity (or decrease the period), the curves of constant period start to go up and separate from the static curve. We can appreciate that the mass M is monotonically decreasing with the equatorial radius $R_{\rm eq}$, but as long as we decrease the period this tendency is gradually reversed and at some point the curves are monotonically increasing. This happens for curves of very small periods, close to the limit period $P_{\rm min}$. We can also appreciate that the minimum equatorial radius $R_{\rm eq}^{\rm min}$ will be given by the intersection between the curve of constant period and the boundary curve of either the secular axysimmetric instability or the inverse β-decay instability while the maximum radius $R_{\rm eq}^{\rm max}$ will be given by the intersection with the Keplerian sequence curve. For the case of WDs rotating with velocities similar to those of AXPs/SGRs, despite their very small period, they still behave more like WDs described by the curves close to the static curve, i.e., they are similar to the curves that are monotonically decreasing. Therefore $R_{\rm eq}^{\rm min}$ will correspond to a maximum mass while $R_{\rm eq}^{\rm max}$ will correspond to a minimum mass. Therefore, for each curve of constant period it is possible to obtain these intersections and find these limiting values for the mass and the radius. In this way Rueda et al. (2013) calculated the maximum and minimum masses, the equatorial $R_{\rm eq}$ and mean $\bar{R}$ radii ($\bar{R} = (2R_{\rm eq} + R_{\rm p})/3$, where $R_{\rm p}$ is the polar radius of the star), the corresponding minimum and maximum moments of inertia and the corresponding maximum and minimum dipole magnetic field of 4U 0142+61, assuming ^{12}C WD, while Boshkayev et al. (2013) did it for three sources, SGR 0418+5729, Swift J 1822.3-1606 and 1E 2259+586, but for WDs with the four compositions considered (^4He, ^{12}C, ^{16}O and ^{56}Fe). In table 4.1 we report all these values for ^{12}C for all these four sources. The dipole magnetic field was calculated using equation (1.6), but as we are considering non-spherical WDs (see section 2.3) we have to use the mean radius $\bar{R}$, i.e.:

$$B_{\rm dp} = \sqrt{\frac{3c^3}{8\pi^2}\frac{I}{\bar{R}^6}P\dot{P}}. \tag{4.2}$$

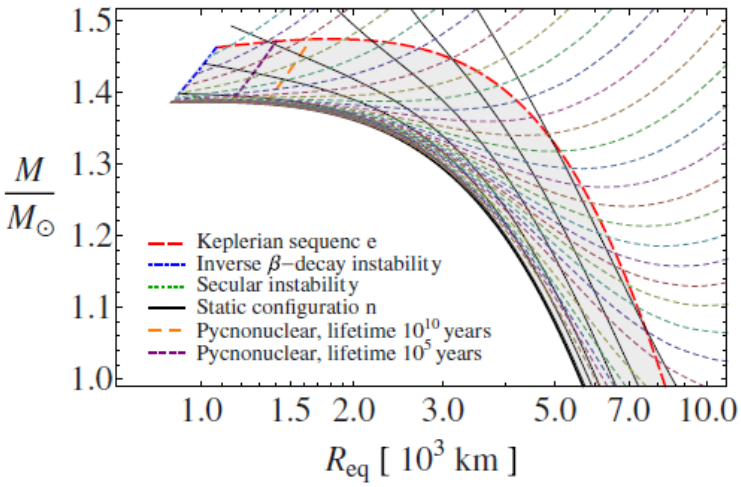

Figure 4.3: Mass versus equatorial radius of rotating ^{12}C white dwarfs (taken from Boshkayev et al., 2013). The gray region denotes the region of stability, all the points in this region describe all possible configurations allowed in this model. This region is bounded by the sequence of static configurations (denoted by the black thick line) and by the different instabilities such as the secular instability, the inverse β-decay instability, the Keplerian seuence or mass shedding limit and the pycnonuclear instabilities of C+C fusion with reaction mean times $\tau_{\text{pyc}} = 10$ Gyr and $\tau_{\text{pyc}} = 0.1$ Myr. The thin dashed colored lines correspond to sequences of constant period of rotation. In this picture we can see that these curves corresponding to a constant period or angular velocity intersect the Keplerian sequence and the instability boundaries of inverse β-decay or secular instability. These intersections will determine the range of possible values of the mass, radius and magnetic field for a MWD rotating with a particular angular velocity.

Source	$R_{\rm eq}^{\rm max}$	$R_{\rm eq}^{\rm min}$	$\bar{R}_{\rm max}$	$\bar{R}_{\rm min}$	$M_{\rm min}$	$M_{\rm max}$	$I_{48}^{\rm min}$	$I_{50}^{\rm max}$	$B_{\rm min}$	$B_{\rm max}$
SGR 0418+5729	6.82	1.05	6.18	1.05	1.15	1.39	2.86	1.42	1.19×10^7	3.49×10^8
Swift J 1822.3-1606	6.55	1.05	5.93	1.05	1.17	1.39	2.86	1.32	4.87×10^7	1.31×10^9
1E 2259+586	5.88	1.04	5.34	1.04	1.24	1.39	2.84	1.08	1.27×10^8	2.76×10^9
4U 0142+61	6.66	1.05	6.03	1.05	1.16	1.39	2.90	1.40	2.30×10^8	6.26×10^9

Table 4.1: Bounds on the properties of four different AXPs/SGRs modelled as ^{12}C white dwarfs. The radii $R_{\rm eq}^{\rm max}$, $R_{\rm eq}^{\rm min}$, $\bar{R}_{\rm max}$ and $\bar{R}_{\rm min}$ are given in units of 10^8 cm. The masses $M_{\rm min} = M(R_{\rm eq}^{\rm max})$ and $M_{\rm max} = M(R_{\rm eq}^{\rm min})$ are given in units of $M_\odot$, and the moments of inertia $I_{48}^{\rm min} = I(R_{\rm eq}^{\rm min})$ and $I_{50}^{\rm max} = I(R_{\rm eq}^{\rm max})$ are given in units of 10^{48} g cm^2 and 10^{50} g cm^2 respectively. The magnetic fields $B_{\rm min} = B_{\rm dp}(\bar{R}_{\rm max})$ and $B_{\rm max} = B_{\rm dp}(\bar{R}_{\rm min})$ were calculated using formula (4.2) and are in units of G. These values are taken from Boshkayev et al. (2013) and Rueda et al. (2013).

4.2 Glitches and outbursts in SGRs and AXPs

Usov (1994) showed that starquakes could be the reason for the decrease of the mean spin-down rate observed for the source 1E 2259+586, considering it again as a MWD. The main idea behind it is that when a fast rotating MWD slows down due to the electromagnetic torque and the stellar wind, centrifugal forces on the core decrease and gravity, pulling it to a less oblate more spherical shape, stresses it. This stress accumulates until a critical value is reached, then it is released, generating a starquake. This idea was borrowed from previous works studying the glitches observed in pulsars (Baym and Pines, 1971; Pines et al., 1972; Ruderman, 1969). The release of those stresses leads to a decrease of the moment of inertia, and hence, by conservation of angular momentum, to an increase of rotational velocity:

$$\frac{\Delta I}{I} = 2\frac{\Delta R}{R} = \frac{\Delta P}{P} = -\frac{\Delta \Omega}{\Omega}. \tag{4.3}$$

This change in the period of rotation and the moment of inertia lead to a change of gravitational energy and a gain of rotational energy in the spin-up process during the glitch given respectively by:

$$\Delta E_{\rm g} = \frac{GM^2}{R}\frac{\Delta R}{R} \sim 2.5 \times 10^{51}\frac{\Delta P}{P}\ {\rm erg}, \tag{4.4}$$

$$\Delta E_{\rm rot} = -\frac{2\pi^2 I}{P^2}\frac{\Delta P}{P} = -1.98 \times 10^{50}\frac{\Delta P}{P^3}\ {\rm erg}. \tag{4.5}$$

Using formulae for starquakes in NSs and extrapolating it to the WD Usov (1994) showed that glitches would occur in magnetic white dwarfs with regular periodic times given by the characteristc time (Baym and Pines, 1971; Usov, 1994):

$$\delta t_{\rm q} = \frac{2D^2}{B}\frac{|\Delta P|}{P|\dot{E}_{\rm rot}|}, \tag{4.6}$$

where $\dot{E}_{\rm rot}$ is the loss of rotational energy, $B = 0.33(4\pi/3)R_{\rm c}^3 e^2 Z^2[\bar{\rho}_{\rm c}/Am_{\rm p}]^{4/3}$, $D = (3/25)GM_{\rm c}^2/R_{\rm c}$, $M_{\rm c}$, $R_{\rm c}$ and $\bar{\rho}_{\rm c}$ are the mass, the radius and the mean density of the solid core respectively, and $m_{\rm p}$ is the proton mass. This equation was obtained assuming the solid core is a rotating self-gravitating sphere composed of incompressible matter of uniform shear modulus (Usov, 1994).

Using this equation and assuming 1E 2259+586 is a WD with parameters $M = 1.45\,{\rm M}_\odot$, $R \simeq 3 \times 10^8$ cm, $M_{\rm c} \simeq 1\,{\rm M}_\odot$, $R_{\rm c} \simeq 2 \times 10^8$ cm, $\bar{\rho}_{\rm c} = M_{\rm c}/(4\pi/3)R_{\rm c}^3$, and $I_{\rm WD} \simeq 10^{50}$ g cm^2, Usov (1994) estimated a recurrence time for glitches:

$$\delta t_{\rm q} \simeq 7 \times 10^6 \frac{\Delta P}{P} \text{ yr}. \tag{4.7}$$

Assuming the existence of glitches as the main cause of the instability of $\dot{P}$ with $\Delta P = -(1-2) \times 10^{-5}$, Usov (1994) estimated a recurrence time $\delta t_{\rm q} \simeq 10 - 20$ yr, with an uncertainty of a factor of 2 or 3. As can be seen on figure 4.4, this value of $t_{\rm q}$ is consistent with data on the evolution of the pulse period of 1E 2259+586. So, he concluded that if this object is a WD within some years a glitch with such characteristics could be observed in that object. And indeed, Kaspi et al. (2003); Woods et al. (2004) reported the observation in 2002 of changes of the order $\Delta P/P \approx -4 \times 10^{-6}$ associated with an outburst (see figure 4.5). In this case, equation (4.5) gives us a change in the rotational energy of $|\Delta E_{\rm rot}| \sim 1.7 \times 10^{43}$ erg, which can explain energetically the energy released in the outburst, $\sim 3 \times 10^{41}$ erg. Another glitch was observed on 26 March 2007 in the source 1E 1048.1-5937 (Dib et al., 2009). In that case the observed change in the period was $\Delta P/P \sim -1.63 \times 10^{-5}$, which imply $|\Delta E_{\rm rot}| \sim 7.73 \times 10^{43}$ erg, large enough to be able to explain energetically the energy released in the outburst, $\sim 4.3 \times 10^{42}$ erg (Dib et al., 2009).

As we saw in the previous section, Boshkayev et al. (2013) and Rueda et al. (2013) calculated more accurate values for the mass, the radius and the moment of inertia of SGRs/AXPs modelled as white dwarfs, instead of using fiducial values. The central density is also calculated, and therefore, this can improve the estimate of the recurrence time. For the case of 1E 2259+586 we have a recurrence time for the maximum and minimum mass configurations given by (Boshkayev et al., 2013):

$$\delta t_{\rm q} > \begin{cases} 4.5 \times 10^7 (|\Delta P|/P) \text{ yr} & M = M_{\rm min} \\ 1.2 \times 10^{10} (|\Delta P|/P) \text{ yr} & M = M_{\rm max}, \end{cases} \tag{4.8}$$

which for typical changes of period $|\Delta P|/P \sim 10^{-6}$ gives $\delta t_{\rm q} > 45$ yr and $\delta t_{\rm q} > 1.2 \times 10^4$ yr for $M_{\rm min}$ and $M_{\rm max}$ respectively. These values indicate that 1 E 2259+586 is a very active source in which glitches and outbursts occur with a frequency of years, if we consider our configuration is closer to the minimum mass. It changes drastically if we are near the maximum mass. Notice also that glitches of minor intensity, $|\Delta P/P| \sim 10^{-7}$ occur with more frequency, $\delta t_{\rm q} \lesssim 4$ yr.

In the case of giant flares there has not been found evidence linking them to glitches. Considering that they are energetically in the range $(10^{44} - 10^{47})$ erg, fractional changes in the period of the order $\Delta P/P \sim -(10^{-5} - 10^{-3})$ could explain them.

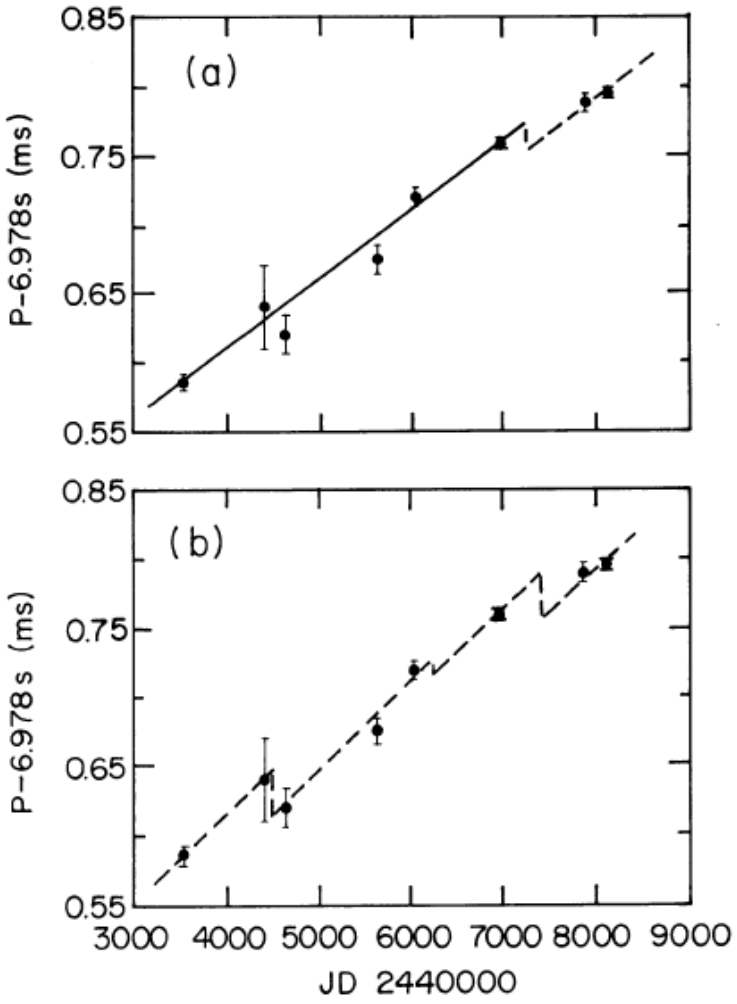

Figure 4.4: Pulse period history of 1E 2259+586 from 1978 to 1990. The solid line represents the best fit before 1989 assuming no glitches. The dashed lines show the fit with glitches. The amplitude of the glitches is in the range $(1-2)\times 10^{-5}$ s. The characteristic time between glitches seem to be in agreement with the predicted one by Usov (1994), paper from which we have taken this figure. This is an argument in favor of the WD model.

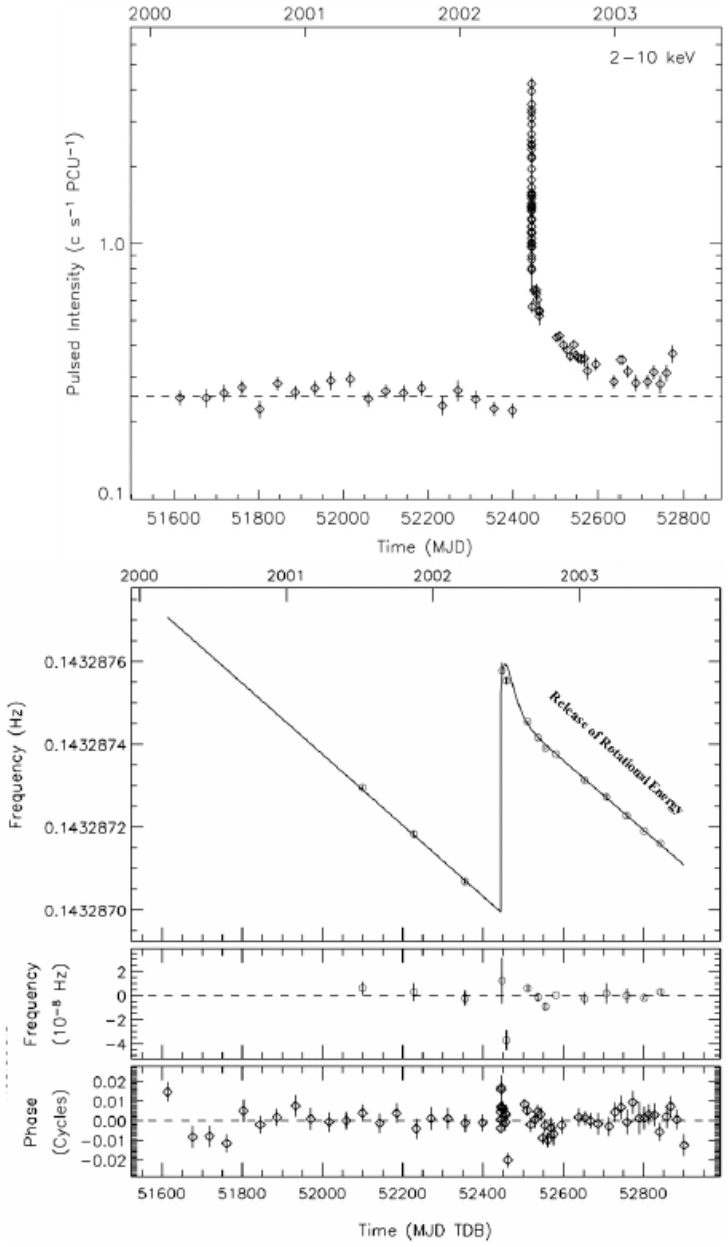

Figure 4.5: Timing and pulsed emission of the glitch-outburst episode observed on 1E 2259+586 on June 2002. The reported energy release during the outburst is $\sim 3 \times 10^{41}$ erg and the change in the rotational period reported was $\Delta P/P = -\Delta\Omega/\Omega \sim -4 \times 10^{-6}$ (Woods et al., 2004). Figure taken from (Malheiro et al., 2012).

4.3 Infrared, Optical and Ultraviolet emission

AXPs/SGRs are variable sources at optical and near-infrared wavelengths. Up to now only seven AXPs/SGRs have been confirmed 4U 0142+61, SGR 0501+4516, 1E 1048.1-5937, 1E 1547.0-5408, SGR 1806-20 XTE J1810-190 and 1E 2259+586 (see Olausen and Kaspi, 2014, and references therein). There are also suggested, but yet unconfirmed, optical counterparts for CXOU J010043.1-721134, 1E 1841-045 and SGR 1900+14.

Two sources, 1E 2259+586 and 4U 0142+61, have been detected in the K band, indicating an excess in the near-infrared, something that, in the traditional magnetar model, has been atributed to the presence of a fallback disk around a NS. But this emission has also been explained in the WD model, in particular for these two sources, in Boshkayev et al. (2013) and Rueda et al. (2013).

Let's remember that the white dwarfs that model AXPs/SGRs are massive and very magnetic. In the WD model it is necessary also to explain that some of these sources are associated with supernovae remnants. This prompted Paczynski (1990) to suggest that these massive and highly magnetic white dwarfs should come from the merger of two white dwarfs. Well before he formulated his hypothesis, these mergers were already proposed as an explanation for Type Ia supernova outbursts (Iben and Tutukov, 1984; Webbink, 1984). More recent smoothed particle hydrodynamics (SPH) simulations of the coalescence process of double degenerate stars indicate that the outcome of the merging process is a WD that contains the mass of the undisrupted primary surrounded by a hot corona made of about half of the mass of the disrupted secondary (Lorén-Aguilar et al., 2009). This rapidly rotating corona is convective and an efficient $\alpha\omega$ dynamo can produce magnetic fields as large as $B \approx 10^{10}$ G (García-Berro et al., 2012). And a rapidly rotating Keplerian disk is formed with the rest of the material of the secondary. In this scenario the WD model could explain the near-infrared excess coming from this Keplerian disk.

We mention that besides the binary WD merger scenario proposed by Paczynski (1990), another scenario was proposed by Malheiro et al. (2012) where a late-evolved star, gravitationally bound to a WD, collapses gravitationally either to a NS or a black hole. In the case the loss of mass in the supernova explosion is $M_{\rm loss} < M/2$, where M is the total mass of the binary, the system remains bound and therefore the object will remain close to the center of the supernova remnant (see Ruffini, 1973, for details). So, we have two different scenarios to give account for the existence of supernova remnants for AXPs/SGRs that have been associated with them.

Boshkayev et al. (2013) and Rueda et al. (2013) analyzed the infrared, optical and ultraviolet observation of four sources. Two sources were observed in one or more of these wavelength ranges, 1E 2259+586 (Boshkayev et al., 2013) and 4U 0142+61 (Rueda et al., 2013), while two sources were undetected, SGR

0418+5729 and *Swift* J1822.3-1606 (see Boshkayev et al., 2013), which allowed to put observational upper limits to their intrinsic luminosity. The observations or the observational upper limits (in the case of the undetected sources) are analyzed and compared with the expected emission from the system composed of the WD and the aforementioned disk produced during the merger. The infrared emission is in these cases associated with the blackbody emission of the disk, but when this infrered emission is not detected is assumed the surface emission of the single WD. We now present the analysis for the four aforementioned sources.

4.3.1 4U 0142+61

As we mentioned before, this source has a confirmed infrared excess (Hulleman et al., 2000). This source has been detected also in the optical bands. Assuming a WD this emission should be explained as the sum of two components, a blackbody coming from the surface of the WD and a blackbody disk model. The first is given by:

$$F_{\rm BB} = \pi \frac{2h}{c^2} \left(\frac{R_{\rm WD}}{d} \right)^2 \frac{\nu^3}{e^{h\nu/(k_{\rm B})T_{\rm eff}}}, \tag{4.9}$$

where $R_{\rm WD}$ and $T_{\rm eff}$ are, respectively, the radius and effective temperature of the WD. Regarding the disk emission, Rueda et al. (2013) adopted the model of Chiang and Goldreich (1997), a model of a passive, opaque, flat circumstellar disk initially proposed by the authors for T Tauri stars, but then adopted also to white dwarfs (García-Berro et al., 2007; Jura, 2003). In this disk model the energy absorbed by the disk is reemitted in infrared, which would explain the infra-red excess emission from T Tauri stars (see Adams et al., 1987; Mendoza V., 1968; Shu et al., 1987, and references therein), an idea then extended to explain also the infrared excess emission in some white dwarfs (García-Berro et al., 2007; Jura, 2003). The emission from this disk model is given by:

$$F_{\rm disk} = 12\pi^{1/3} \cos i \left(\frac{R_{\rm WD}}{d} \right)^2 \left(\frac{2k_{\rm B}T_{\rm eff}}{3h\nu} \right)^{8/3} \left(\frac{h\nu^3}{c^2} \right) \times \int_{x_{\rm in}}^{x_{\rm out}} \frac{x^{5/3}}{e^x - 1} dx, \tag{4.10}$$

where i is the inclination angle of the disk and $x = h\nu/(k_{\rm B}T)$. In this model the disk's temperature T varies as $r^{-3/4}$, with r the distance from the center of the WD.

Using the data in ultraviolet and infrared, Rueda et al. (2013) fitted the spectrum within this WD+disk model. The best fit is shown in figure 4.6, where the spectrum parameters corresponding to this best fit are: $R_{\rm WD} \approx 0.006 R_\odot$, $T_{\rm eff} \approx 1.31 \times 10^5$, inner and outer disk radii $R_{\rm in} = 0.97 R_\odot$, $R_{\rm out} = 51.1 R_\odot$ and inner and outer disk temperatures $T_{\rm in} \approx 1950$ K and $T_{\rm out} \approx 100$ K. We can see the excellent agreement between the composite spectrum and the observational

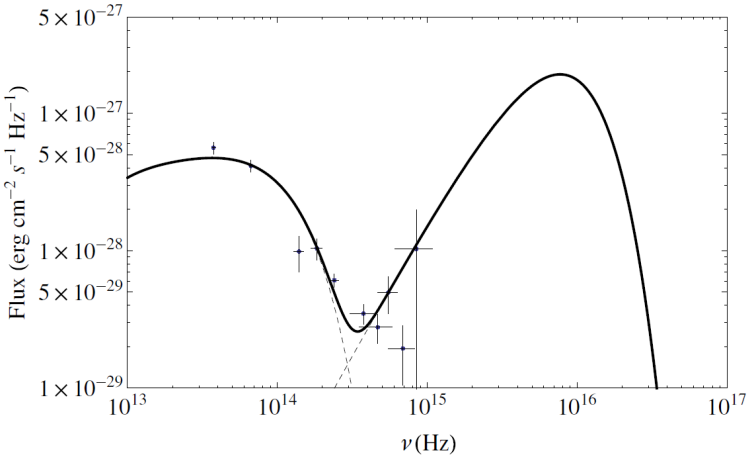

Figure 4.6: Observed and fitted spectrum of 4U 0142+61 shown in Rueda et al. (2013). It is shown the average of all the existing data of the sources in the different bands, this due to the high variability of the source in the optical bands. The data come from observations between 1994 October 1994 and 2005 July 26 (Dhillon et al., 2005; Durant and van Kerkwijk, 2006; Hulleman et al., 2000, 2004; Morii et al., 2005, 2009). For further details see (Rueda et al., 2013).

data, proving in this way that the WD model is compatible with the observed photometry. However, keep in mind that these data is extremely variable, and this variability can lead to changes in the optical fluxes of up to one order of magnitude (Durant and van Kerkwijk, 2006).

We remind that the simulations of the coalescence process of two degenerate stars show that the result of the merger is a WD that contains the mass of the undisrupted primary, surrounded by a hot corona made of about half of the mass of the disrupted secondary and a rapidly rotating Keplerian disk, which contains the rest of the material of the secondary, and with a little mass ejected from the system during the merging process. Therefore, in order to check whether the double degenerate merger hypothesis is a realistic and consistent model for 4U 0142+61, Rueda et al. (2013) ran a Smoothed Particle Hydrodynamics (SPH) simulation of the merger of a 0.6+1.0 $M_\odot$ binary WD, which resulted in a central remnant of $\approx 1.1 M_\odot$, with a radius $R_{\rm WD} \approx 0.006 R_\odot$, and a surrounding disk of mass $M_{\rm disk} \approx 0.5 M_\odot$. The value of the radius, as we can see, is in good agreement with the photometric value. Moreover, the rotation period is $P \approx 15.7$ s, of the same order of the reported period for this source (8.69 s, Dib et al., 2007).

4.3.2 1E 2259+586

Hulleman et al. (2001) established a near-infrared counterpart of 1E 2259+586 of magnitude $K = 21.7 \pm 0.2$. Unlike in the case of 4U 0142+61, for this source were obtained only upper limits in the optical band, given by: $R = 26.4$, $I = 25.6$ and $J = 23.8$. Like for the previous source, the spectrum was fitted using equations

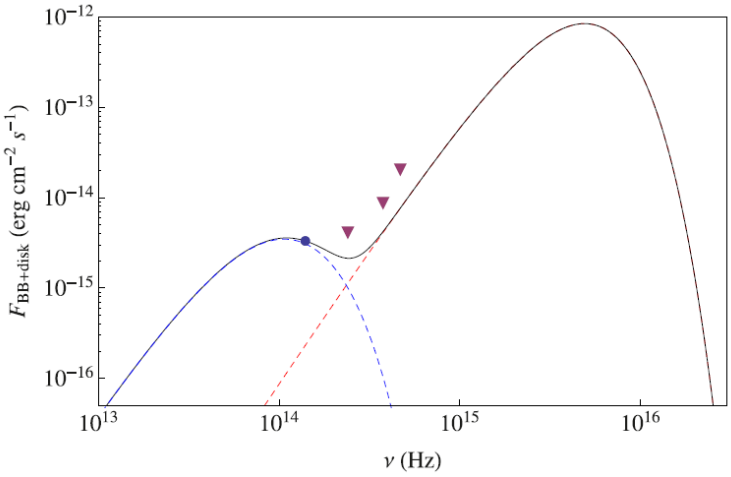

Figure 4.7: Observed and fitted spectrum of 1E 2259+586. The circle is the observed flux in the K band (infrared), while the triangles correspond to upper limits in the R, I and J bands. The parameters of the blackbody+disk spectrum are $R_{\mathrm{WD}} = 3 \times 10^8$ cm, $T = 7 \times 10^4$ K, $T_{\mathrm{in}} = 2 \times 10^3$ K and $R_{\mathrm{out}} = R_\odot$. The blue-dashed curve is the contribution of the disk and the red-dashed curve is the contribution from the surface of the , that is modelled by a blackbody. The sum of these two gives the total spectrum that is represented by the black curve. Figure taken from Boshkayev et al. (2013).

(4.9) and (4.10). For this case the fit is more complicated because we don't have enough data and we have just upper limits in the optical band. To overcome this inconvenience Boshkayev et al. (2013) assumed a value for the WD $R_{\mathrm{WD}} = 3 \times 10^8$ cm, a value in the interval of stability, and a value for the outer disk of $R_{\mathrm{out}} = R_\odot$. They found that the good fitting values of the other parameters are $T = 7.0 \times 10^4$ K and $T_{\mathrm{in}} = 2.0 \times 10^3$ K. We show in figure 4.7 the observed spectrum in the optical, infrared and ultraviolet bands and the corresponding fit spectrum of the blackbody+disk model. This implies that further observations with lower limits could confirm or reject the model. Up to now, we only can assure that the infrared excess can be well explained with a disk surrounding a WD.

4.3.3 SGR 0418+5729

Using the information provided by Rea et al. (2010) about the position (and its positional error circle) of SGR 0418+5729, Durant et al. (2011) observed this source with two wide filters of the *Hubble Space Telescope*, F606W (well approximated by the V-band, $\lambda \sim 588$ nm, in the visible part of the electromagnetic spectrum) and F110W (well approximated by the j-band, $\lambda \sim 1159$ nm, in the near-infrared part of the electromagnetic spectrum). The derived upper limits for the apparent magnitudes are $m_{\mathrm{F606W}} > 28.6$ and $m_{\mathrm{F110W}} > 27.4$. This allowed Boshkayev et al. (2013) to obtain upper limits for the luminosity, $L_{\mathrm{F606W}} < 5 \times 10^{28}$ erg s^{-1} and $L_{\mathrm{F110W}} < 6 \times 10^{28}$ erg s^{-1}. Considering that the emission from the surface is very well approximated by a blackbody and

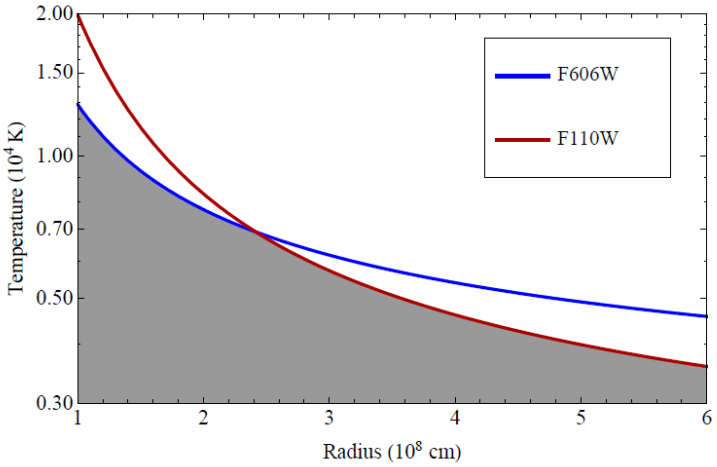

Figure 4.8: Constraint on temperature according to equation (4.11). The gray region corresponds to the possible values of temperature and radius in the case SGR 0418+5729 is an uniformly RWD. The range of values for the radius corresponds to the limits obtained in the first section of this chapter, where the instability boundaries were consistently taken into account. Figure taken from Boshkayev et al. (2013).

that the luminosity of a blackbody depends directly on the temperature, we can realise that these upper limits also imply limits on the temperature. Specifically, they put upper limits on the temperature, which in terms of the radius R of the star are given by (see Boshkayev et al., 2013, for details):

$$T < \begin{cases} 1.3 \times 10^4 [\ln(1 + 0.44 R_8^2)]^{-1} \text{ K}, & \text{F110W} \\ 2.4 \times 10^4 [\ln(1 + 6.35 R_8^2)]^{-1} \text{ K}, & \text{F606W}, \end{cases} \tag{4.11}$$

where R_8 is R in units of 10^8 cm. As we saw before in this chapter, the values for the mass or radius of the WD that model each AXP/SGR are constrained according to their rotational angular velocity. Following the previous equation we can plot the upper limits on the temperature as a function of radius within the limits imposed by the stability criteria. We show this in figure 4.8. The gray region corresponds to the possible values of temperature and radius and this region has the following upper limits:

$$T < \begin{cases} 4.3 \times 10^3 \text{ K}, & R = R_{\text{max}}, \text{ F101W}, \\ 1.2 \times 10^4 \text{ K}, & R = R_{\text{min}}, \text{ F606W}. \end{cases} \tag{4.12}$$

The minimum upper limit for the temperature corresponds to the maximum radius and the upper limit imposed by the measurement of the F110W filter, while the opposite maximum upper limit corresponds to the minimum radius and the upper limit imposed by the measurement done by the F606W filter. We have to remark also that this upper limits for the temperature are similar to

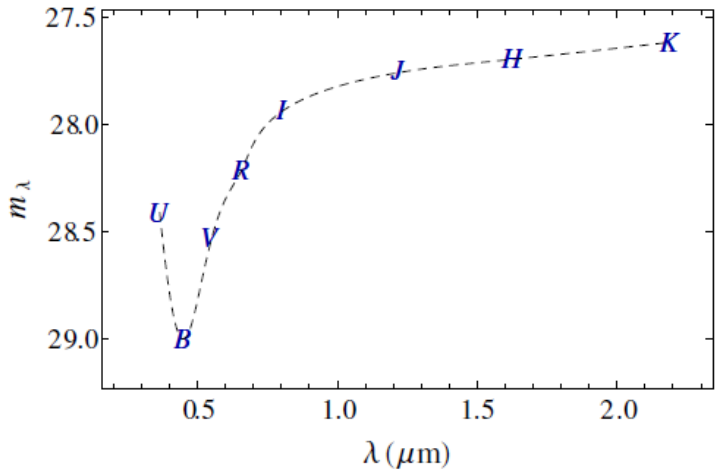

Figure 4.9: Expected optical magnitudes of SGR 0418+5729 assuming a blackbody spectral emission with temperature $T = 10^4$ K and radius $R = 1.5 \times 10^8$ cm. Figure taken from Boshkayev et al. (2013).

the observed surface temperatures of massive and isolated white dwarfs. For example, Ferrario et al. (2005) report values in the range 1.14×10^4 K $< T < 5.52 \times 10^4$ K.

Given a temperature and radius is possible to obtain the expected optical magnitude. Choosing the smallest radius (that corresponds in figure 4.8 to the maximum upper limit), $R = 1.5 \times 10^8$ cm, a temperature of $T = 10^4$ K, and a distance of 2 kpc, is obtained the expected optical magnitude shown in figure 4.9.

4.3.4 Swift J1822.3-1606

Three sources were detected in the J, H and K bands associated with the position determined for SGR 1822-1606. However, all these three sources are too luminous to be associated with a WD at such a distance (≈ 5 kpc). In this case due to the very large distance associated with this source, we don't have strong constraints on the temperature or the radius of the WD. Therefore, there can be assumed values of $T = 10^4$ K and $R = 1.5 \times 10^8$ cm, like in the previous case, obtaining an expected optical magnitude shown in figure 4.10.

4.4 The age and magnetic field of 4U 0142+61

The predictions of the proposed scenario of the formation of massive and highly MWDs due to the merging of two degenerate stars can be compared with the information provided by observations of AXPs/SGRs, in particular, of 4U 0142+61. After their merger the interaction of the disk formed with the MWD will play a key role in the evolution of its rotation period. As we will see, its main role is played at the beggining of the life of the WD recently born from the coa-

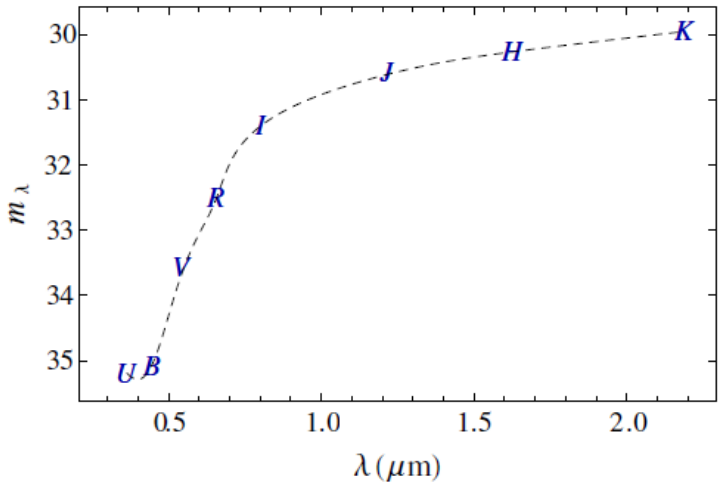

Figure 4.10: Expected optical magnitudes of SGR 1822-1606 assuming a blackbody spectral emission with temperature $T = 10^4$ K and radius $R = 1.5 \times 10^8$ cm. Figure taken from Boshkayev et al. (2013).

lescence. However, this interaction disappears after a certain time and the WD will spin-down like any other isolated WD, i.e., only thanks to the traditional magneto-dipole braking.

In order to model the evolution of the rotational period of 4U 0142+61, Rueda et al. (2013) adopted the phenomenological model of Armitage and Clarke (1996), which assumes that the magnetic field lines threading the disk are closed. In this model the evolution of the angular velocity ω is governed by the equation:

$$\dot{\omega} = -\frac{2B^2\langle T\rangle^6\omega^3}{3Ic^3}\sin^2\theta + \frac{B^2\bar{R}^6}{3I}\left[\frac{1}{R_{\rm mag}^3} - \frac{2}{(R_{\rm c}R_{\rm mag})^{3/2}}\right] + \frac{\dot{M}R_{\rm mag}^2\omega}{I}, \quad (4.13)$$

where θ is the angle between the rotation axis and the magnetic dipole moment,

$$R_{\rm mag} = \left[\frac{B^2\bar{R}^6}{\dot{M}\sqrt{2GM}}\right]^{2/7} \quad (4.14)$$

is the magnetospheric radius (Chatterjee et al., 2000; Matt et al., 2012; Rueda and Ruffini, 2012; Toropina et al., 2012), and

$$R_{\rm c} = \left(\frac{GM}{\omega^2}\right)^{1/3} \quad (4.15)$$

is the corotation radius. The first term in equation (4.13) corresponds to the traditional magneto-dipole braking, the second one is the star-disk coupling and

the last one describes the angular momentum transfer from the disk to the WD.

The integration of equation (4.13) allowed Rueda et al. (2013) to obtain P and $\dot{P}$ as a function of time. Adopting a misalignment angle $\theta = \pi/2$ they obtained that for a wide range of magnetic fields, at early stages $R_{\rm mag} \approx R_{\rm WD}$. The integration of equation (4.13) can be appreciated in figure 4.11. We can see that initially the star is spun-up, this because of the large accretion rates. However, after approximately 1 kyr the disk cannot torque any more the WD and from that moment the disk and the star evolve independently and accretion onto the magnetic poles stops. This is because the inner radius of the disk, which is given approximately by the magnetospheric radius, becomes larger than the light cylinder radius, $R_{\rm lc} = c/\omega$. When the interaction between the disk and the star stops, the star spins-down by magneto-dipole radiation (Chatterjee et al., 2000; Lamb et al., 1973).

We can see from figure 4.11 that approximately at an age of $\tau_{\rm sd} = 64$ kyr the star will reach the values of P and $\dot{P}$ reported in the literature. It is remarkable this age estimate is comparable with the characteristic age $P/(2\dot{P}) \approx 68$ kyr. When a mass $M = 1.2 M_{\odot}$ is adopted, the surface magnetic field needed to fit the observed values of P and $\dot{P}$ is $B \approx 2.3 \times 10^8$ G, at the aforementioned age $\tau_{\rm sd} = 64$ kyr. We can compare this surface magnetic field with the magnetic field obtained with the magnetic dipole formula (4.2). From the observed values $P = 8.69$ s and $\dot{P} = 2.03 \times 10^{-12}$ (Hulleman et al., 2000), we obtain $B = 2.3 \times 10^8$ G for $M_{\rm min}$, and 6.2×10^9 G for $M_{\rm max}$ (see table 4.1), in agreement with the result obtained integrating equation (4.13).

4.5 Concluding Remarks

We have seen in this chapter how different works have confirmed the first hypotheses of the WD model for AXPs/SGRs. Specifically it has been possible to determine that white dwarfs rotating as fast as AXPs/SGRs are within the limits stablished by the instability boundaries. We have also seen that more accurate values for the radius and mass of these highly rotating white dwarfs have been obtained. From the values obtained for the mass it is concluded that these highly rotating and magnetic white dwarfs are also very massive, something remarkable, considering that also, on average, magnetic white dwarfs are more massive than their non-magnetic counterparts (see chapter 3).

On the other hand, both the persistent and transient emission of these objects could be explained from the energetic point of view in the WD model. We saw that spin-down power of these hypothetical highly rotating white dwarfs can explain the luminosity observed coming from AXPs/SGRs, so the persistent emission can be explained within a rotationally powered pulsar model. And the transient emission represented by the outbursts observed can be explained also with a WD subjected to strain forces produced by the spin-down of the star because the outbursts have been associated with glitches that have changed the

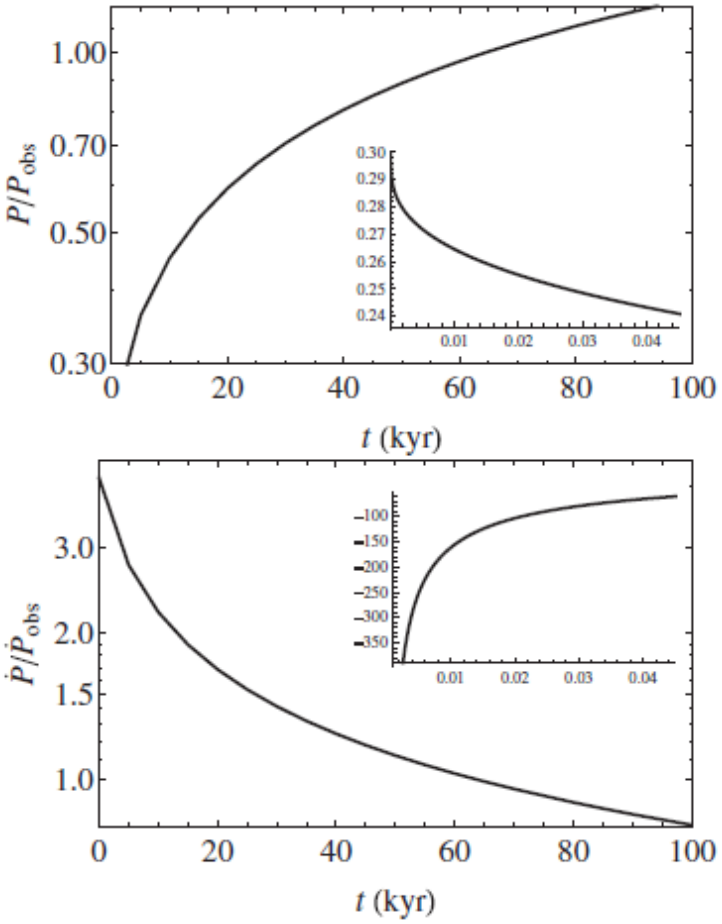

Figure 4.11: Time evolution of the period (top panel) and period derivative (bottom panel) of 4U 0142+61. The insets show the early evolutionary phases of the system. Figure taken from Rueda et al. (2013).

rotational period of the compact object.

In the last part we saw that the hypothesis of formation of these highly massive and magnetic white dwarfs can give account of an infrared excess detected in some AXPs/SGRs. Besides this infrared excess, in some cases there has been detected emission in the optical and ultraviolet spectrum. In the WD model this emission is naturally associated with the surface emission coming from the WD. An important factor that makes it difficult to detect a possible optical emission is the distance, the usual distances of AXPs/SGRs are of the order of 1 or more kpc, while most of the observed WDs, more exactly a 98%, are at a distance less than 1 kpc (Napiwotzki, 2009). This severely limits the possibility to check the theory with a direct observational evidence of the existence or not of the blackbody surface emission of the WD.

This difficulty to detect observationally the surface emission from the WD, as we previously saw where only upper limits were obtained for some cases, constrains us to find other methods to validate or dismiss the WD hypothesis. As we know, the AXPs/SGRs were observed in the X-ray wavelengths. In the next chapter we will deal with part of this emission, considering always a rotationally powered model and using several ideas used in the traditional rotationally powered pulsar model.

Chapter 5

Surface thermal X-ray emission of highly magnetic white dwarfs: Application to Anomalous X-ray Pulsars

5.1 Introduction

We saw in the previous chapter how the white dwarf model of AXPs/SGRs can be tested considering the association between glitches and outbursts, one of the main characteristics of AXPs/SGRs that distinguish them from normal radio pulsars, and also considering the emission in the optical, infrared and ultraviolet bands. Is in these wavelengths where the surface emission of white dwarfs is detected and observations in these wavelengths with lower thresholds could easily rule out or keep alive this model or hypothesis. However, the X-ray emission was not considered and the purpose of this chapter is to examine it within the proposed white dwarf model.

As it was mentioned briefly in chapter 1, if a white dwarf is rotating fast enough, there are some conditions on the magnetosphere that will render it similar to the magnetosphere of pulsars. This magnetosphere creates propitious conditions for the production of electron-positron pairs and for the generation of high energy photons through different radiative processess such as curvature radiation, inverse Compton scattering or synchrotron radiation. In this chapter we will review the main aspects of the traditional pulsar model and we will examine the X-ray emission within the framework of this model applied to the white dwarf hypothesis. So, in section 5.2 a brief summary of the pulsar magnetosphere model will be presented. Then, in section 5.3 an application of a specific emission model will be applied to some AXPs/SGRs, more specifically, will be considered the thermal X-ray emission produced by the particles produced in the magnetosphere that hit the surface of the star. Then, in section 5.4 we consider the pulsed fraction caused by this emission and finally in section 5.5 we give the concluding remarks.

5.2 Pulsar-like White Dwarf magnetosphere

After the hypothesis of a rotating neutron star became the most plausible explanation to the observed pulsed emission, there appeared a series of papers directed to solve the magnetosphere and hence, the problem of explaining the emission mechanism of pulsars. Hoyle et al. (1964) and Pacini (1967, 1968), considering the small density scale height ($\sim$ 1 cm) and the huge gravitational binding energies for electrons ($\sim 8 \times 10^4$ eV) and protons ($\sim 1.4 \times 10^8$ e V) at the surface of a typical neutron star, concluded that the plasma density surrounding a rotating magnetic neutron star must be very low, practically empty. If that were the case, the most appropiate solution to the Maxwell equations in the magnetosphere should be the one calculated by Deutsch (1955). In fact, this solution has been taken as a reference point for other studies of pulsar magnetospheres (Bonazzola et al., 2015; Pétri, 2013, 2015, 2016). However, Goldreich and Julian (1969) showed that this was not correct and instead a corotating plasma must surround the star. This due to the existence of huge electric fields (due to unipolar induction) that easily overcome the huge gravitational binding fields. However, the idea of a corotating magnetosphere was not new (see Davis, 1947; Ferraro and Bhatia, 1967; Ferraro and Unthank, 1949; Gold, 1962; Hones and Bergeson, 1965).

A rotating conducting star modelled as a rotating magnetic dipole field **B** creates an induction (quadrupole) electric field **E** in a vacuum whose parallel component is given by:

$$E_{\parallel} = \frac{\mathbf{E} \cdot \mathbf{B}}{B} \sim R\Omega B_0 \left(\frac{R}{r}\right)^4 \cos^3\theta. \tag{5.1}$$

where $B = |\mathbf{B}|$, Ω is the angular velocity, R is the radius of the star, B_0 is the magnetic field at the surface and r and θ are the spherical coordinates, where the origin is considered at the center of the pulsar. Here the z axis is defined by the axis of the magnetic dipole field.

This electric field gives a force greatly exceding gravity on any charged particle near the pulsar surface. For example, for a typical pulsar such as the famous Crab pulsar whose estimated magnetic field is $\sim 4 \times 10^{12}$ G and has a measured period of $\sim$ 33 ms, for a singly ionized iron ion, the ratio of gravitational to electric force would be $mg/(eE_{\parallel}) \sim 1.5 \times 10^{-9}$. This makes the gravitational force negligible compared to the electrical force, making the charged particles on the surface to be pulled out and replenish the exterior of the neutron star. So, in this way, Goldreich and Julian (1969) set the "standard" picture of pulsar magnetospheres.

The Goldreich Julian model considers an aligned neutron star, i.e., the axis of the magnetic dipole field aligned with the rotational axis. As done in previous

articles that treated the case of a generic magnetic star (Davis, 1947; Hones and Bergeson, 1965), not necessarily a neutron star, they assumed that the star is immersed in a tenuous plasma of infinite conductivity parallel to the external magnetic field lines and of zero conductivity normal to these lines. This anisotropic conductivity of the plasma is equivalent to the condition $\mathbf{E} \cdot \mathbf{B} = 0$, where $\mathbf{E}$ and $\mathbf{B}$ are the external electric and magnetic fields. This is also known as the exact Magneto Hydrodynamic (MHD) condition. One consequence of this condition is that the magnetic field lines become electric equipotentials, and as mentioned before, a corotating magnetosphere is enforced up to a maximum distance given by $R_{\rm lc} = c/\Omega = cP/(2\pi)$, known as *light cylinder radius*, where c is the speed of light and Ω is the angular velocity of the star. Corotation at larger distances would imply superluminal velocities for the magnetospheric particles. And with this MHD condition it is also possible to calculate from Maxwell equations the local density of charged plasma, which within the corotating magnetosphere is given by the famous Goldreich-Julian density (Goldreich and Julian, 1969):

$$\rho_{\rm GJ} = -\frac{\mathbf{\Omega} \cdot \mathbf{B}}{2\pi c} \frac{1}{1 - (\Omega r_\perp / c)^2}, \tag{5.2}$$

where $r_\perp = r \sin\theta$. A general picture of this model is shown in figure 5.2. The last B-field line closing within the corotating magnetosphere can be easily located from the equation for a magnetic dipole:

$$r / \sin^2\theta = \text{constant} = R_{\rm lc}, \tag{5.3}$$

and is located at an angle from the star's magnetic pole given by:

$$\theta_{\rm pc} = \arcsin\left(\sqrt{R/R_{\rm lc}}\right) \approx \sqrt{R/R_{\rm lc}} = \sqrt{R\Omega/c} = \sqrt{2\pi R/(cP)}, \tag{5.4}$$

with R the radius of the star. The B-field lines that originate in the region between $\theta = 0$ and $\theta = \theta_{\rm pc}$ (known as *magnetic polar cap*) cross the light cylinder and are called *open field lines*. The size of the polar cap is given approximately by the polar cap radius

$$R_{\rm pc} = R\theta_{\rm pc} \approx R\sqrt{2\pi R/(cP)}. \tag{5.5}$$

By symmetry reasons, there are two antipodal polar caps on the stellar surface.

From the picture it can be seen that contrary to the open field lines, the *close field lines* do not cross the light cylinder and are characterized by having a polar angle larger than $\theta_{\rm pc}$. The particles that are attached to these closed magnetic field lines corotate on average and comprise what is called the corotating mag-

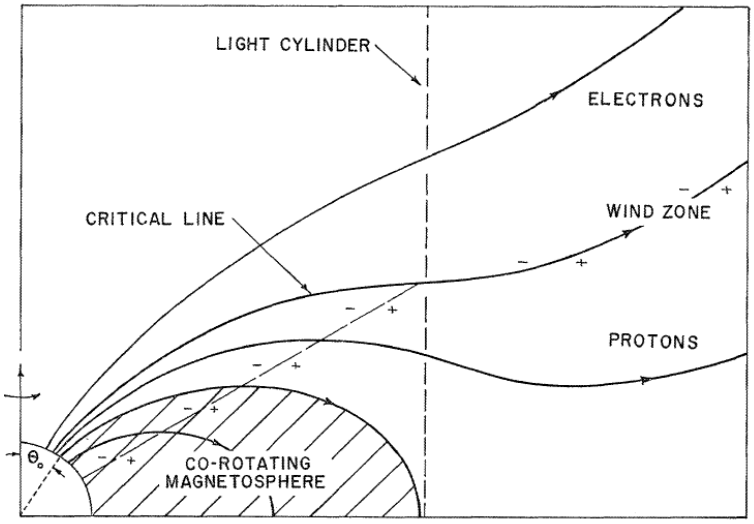

Figure 5.1: Schematic figure showing the standard picture of the Goldreich-Julian model. We can see that the light cylinder serves as a limit for the corotating magnetosphere, where magnetic lines are closed. On the other hand, the magnetic field lines coming from the polar cap are open and particles from the surface of the star follow these lines emitting radiation. Figure taken from Goldreich and Julian (1969).

netosphere. On the contrary, particles in the open field line region stream out along the magnetic field lines. The lines are called open but in fact, they should close in the boundary region, a region full of plasma that comes from the supernova remnant that came out at the birth of the neutron star. The feet of the *critical* magnetic field lines are at the same electric potential as the interstellar medium. This critical magnetic field line divides the open field lines into *electron lines* (higher-latitude lines) and *proton lines* (lower-latitude lines).

5.3 Vacuum inner gap model and polar cap heating

The different models that intend to explain pulsar emission rely on particle acceleration in regions where the corotation condition (equivalent to $\mathbf{E} \cdot \mathbf{B} = 0$) is no longer satisfied. So, different models were elaborated to deal with this problem of particle acceleration defining different regions where a deficit of charge would lead to the departure of corotation and hence to $E_{\parallel} := \mathbf{E} \cdot \mathbf{B} \neq 0$. Basically there are two kinds of models, the Polar Cap (PC) models and the Outer Gap (OG) models. The PC models consider the accelerating electric field $E_{\parallel}$ (parallel to the magnetic field), and hence the particle acceleration, in the open field region near the surface of the neutron star. There are two models of PC acceleration, the *vacuum gap* model, proposed by Ruderman and Sutherland (1975), and the *space-charge limited flow* model (Arons and Scharlemann, 1979; Harding and Muslimov, 1998, 2001, 2002; Harding et al., 2002; Zhang and Harding, 2000). The first of these models assumes the ions are trapped in the Neutron Star crust (a

high work function due to the huge magnetic fields present) while the second one assumes the surface temperature is high enough to overcome the binding or cohesive forces on charged particles due to the lattice structure in the strong magnetic field. On the other hand, OG models consider that particle acceleration takes place in the outer magnetosphere (Cheng et al., 1986a,b; Hirotani, 2006, 2013; Zhang and Cheng, 1997).

After the famous article of Goldreich and Julian of 1969, Sturrock (1971) showed that due to the huge magnetic fields present in the star, an avalanche of electron-positron pairs is expected to occur in the magnetosphere, thanks to the electrodynamical process $\gamma + B \rightarrow e^+ + e^-$ of the neutron stars and this avalanche screens the electric field. The PC models rely on the avalanche of electron-positron pairs produced as an essential phenomenon to explain not only the detected emission in radio (the first pulsars detected were radio pulsars) but also in X-rays and γ-rays of isolated non-accreting neutron stars. In the same way, the OG models consider the avalanche of electron-positron pairs to model the electromagnetic pulsed emission coming fron Neutron Stars, but, unlike in the case of the PC models, the electrodynamical process $\gamma + B \rightarrow e^+ + e^-$ is no longer possible because at high altitudes the magnetic field B is not high enough to trigger this process. Instead a $\gamma - \gamma$ pair production comes into place where γ-rays produced in the outer gap interact with the X-ray photons coming from the surface of the neutron star producing electron-positron pairs (see Viganò et al., 2015; Zhang and Cheng, 1997, for details). But despite the different models varied on their fundamental assumptions, they relied on the rotational energy as the energy source to explain the observed emission.

In the *vacuum inner gap* model proposed by Ruderman and Sutherland (1975) the potential drop generated by the unipolar effect and that accelerates the electrons along the open B-field lines above the surface is given by:

$$\Delta V = \frac{B_S \Omega h^2}{c}, \tag{5.6}$$

where h is the height of the vacuum gap and B_S is the surface magnetic field, which does not necessarily coincide with the dipole field B_{dp}.

The electrons (or positrons) accelerated through this potential and following the B-field lines will emit curvature photons whose energy depends on the γ-factor, $\gamma = e\Delta V/(mc^2)$, and on the B-field line curvature radius r_c, i.e. $\omega_c = \gamma^3 c/r_c$. Following Chen and Ruderman (1993), we adopt the constraint on the potential ΔV for pair production via $\gamma + B \rightarrow e^- + e^+$,

$$\frac{1}{2}\left(\frac{e\Delta V}{mc^2}\right)^3 \frac{\lambda}{r_c}\frac{h}{r_c}\frac{B_S}{B_c} \approx \frac{1}{15}, \tag{5.7}$$

or in terms of a condition on the value of the potential,

$$\Delta V \approx \left(\frac{2}{15}\right)^{2/7} \left(\frac{r_c}{\lambda}\right)^{4/7} \left(\frac{\lambda\Omega}{c}\right)^{1/7} \left(\frac{B_S}{B_c}\right)^{-1/7} \frac{mc^2}{e}, \tag{5.8}$$

where we have used Eq. (5.6), and where $\lambda = \hbar/(mc)$ is the "'reduced"' Compton wavelength of the electron and $B_c \equiv m^2c^3/(e\hbar) = 4.4 \times 10^{13}$ G is the quantum electrodynamic field, with $\hbar$ the reduced Planck's constant.

For a magnetic dipole geometry, i.e. $B_S = B_{dp}$ and $r_c = \sqrt{Rc/\Omega}$. The potential drop ΔV cannot exceed the maximum potential (i.e. the potential for $h = h_{max} = R_{pc}/\sqrt{2}$), which for a magnetic dipole field will be given by:

$$\Delta V_{max} = \frac{B_{dp}\Omega^2 R^3}{2c^2}. \tag{5.9}$$

We are here interested in the possible magnetospheric mechanism of X-ray emission from magnetized WDs, thus we will consider the heating of the polar caps by the inward flux of pair-produced particles in the magnetosphere. These particles of opposite sign to the parallel electric field move inward and deposit most of their kinetic energy on an area

$$A_{spot} = f A_{pc}, \tag{5.10}$$

i.e. a fraction $f \leq 1$ of the polar cap area $A_{pc} = \pi R_{pc}^2$. The temperature T_{spot} of this surface hotspot can be estimated from the condition that it re-radiates efficiently the kinetic energy deposited, as follows: the rate of particles flowing to the polar cap is $\dot{N} = JA_{pc}/e$, where $J = \eta\rho_{GJ}c$ is the current density in the gap, and $\eta < 1$ is a parameter that accounts for the reduction of the particle density in the gap with respect to the Goldreich-Julian value (Cheng and Ruderman, 1977 used $\eta = 1$ for order-of-magnitude estimates). In this model the filling factor f is not theoretically constrained and it has been estimated from pulsar's observations in X-rays that its value can be much smaller than unity (Cheng and Ruderman, 1977). The condition that the hotspot luminosity equals the deposited kinetic energy rate reads

$$A_{spot}\sigma T_{spot}^4 = e\Delta V\dot{N} = JA_{pc}\Delta V = \eta\rho_{GJ}(R)cA_{pc}\Delta V, \tag{5.11}$$

where σ is the Stefan-Boltzmann constant. From Eqs. (5.2), (5.10) and (5.11) we obtain the spot temperature

$$T_{spot} = \left(\eta\frac{B_{dp}\Delta V}{\sigma f P}\right)^{1/4}. \tag{5.12}$$

It is worth mentioning that in the above estimate we have assumed a full effi-

ciency in the conversion from the deposited kinetic energy to the hotspot emission. This assumption is accurate if the heating source, namely the energy deposition, occurs not too deep under the star's surface and it is not conducted away to larger regions being mainly re-radiated from the surface area filled by the penetrating particles (Cheng and Ruderman, 1980). In appendix A we estimate the cooling and heating characteristic times and the heating and re-radiation efficiency. For the densities and temperatures of interest here we show that the polar cap surface re-radiates efficiently most of the kinetic energy deposited by the particle influx, validating our assumption.

Now, considering the application of this polar cap model to two sources, 1E 2259+586 and 4U 0142+61, we need an estimate of the white dwarf magnetic dipole field. For this we use the traditional dipole formula, that has been already mentioned in previous chapters:

$$B_{\rm dp} = \left(\frac{3c^3}{8\pi^2} \frac{I}{R^6} P\dot{P} \right)^{1/2}, \tag{5.13}$$

where I is the moment of inertia of the star, P is the rotation period, $\dot{P} \equiv dP/dt$ is its first time derivative (spin-down rate), and an inclination angle of $\pi/2$ between the magnetic dipole and the rotation axis has been adopted. It is worth recalling that the estimate of the B-field by equation (5.13) is not necessarily in contrast, from the quantitative point of view, with an estimate using an aligned field but introducing a breaking from the particles escaping from the magnetosphere, since also in this case a quantitatively and qualitatively similar energy loss is obtained (see, e.g., Contopoulos and Spitkovsky, 2006; Harding et al., 1999; Spitkovsky, 2006).

As we already learned from chapters 2 and 4, for a given rotation period P, the WD structure parameters such as mass M, radius R, and moment of inertia I are bounded from below and above if the stability of the WD is requested (Boshkayev et al., 2013). From those bounds are established the lower and upper bounds for the field $B_{\rm dp}$ of the WD.

5.3.1 1E 2259+586

We apply the above theoretical framework to a specific source, AXP 1E 2259+586. This source, with a rotation period $P = 6.98$ s (Fahlman and Gregory, 1981) and a spin-down rate $\dot{P} = 4.8 \times 10^{-13}$ (Davies et al., 1990), has a historical importance since Paczynski (1990) was the first to point out the possibility this object could be a WD. This object produced a major outburst in 2002 (Kaspi et al., 2003; Woods et al., 2004), in which the pulsed and persistent fluxes rose suddenly by a factor of ≥ 20 and decayed on a time-scale of months. Coincident with the X-ray brightening, the pulsar suffered a large glitch of rotation frequency fractional change 4×10^{-6} (Kaspi et al., 2003; Woods et al., 2004). It is worth recalling that the observed temporal coincidence of glitch/bursting activity, as first pointed

out by Usov (1994) in the case of 1E 2259+586, and then extended in Malheiro et al. (2012) and Boshkayev et al. (2013), can be explained as due to the release of the rotational energy gained in a starquake occurring in a total or partially crystallized WD. Since we are interested in the quiescent behaviour, we will not consider this interesting topic here. Therefore, only X-ray data prior to this outburst event will be used in this work (Zhu et al., 2008).

The soft X-ray spectrum of 1E 2259+586 is well fitted by a blackbody plus a power-law model. The blackbody is characterised by a temperature $kT_{\rm bb} \approx 0.37$ keV ($T_{\rm bb} \approx 4.3 \times 10^6$ K) and an emitting surface area $A_{\rm bb} \approx 1.3 \times 10^{12}$ cm^2 (Zhu et al., 2008). These values of temperature and area are inconsistent (too high and too small, respectively) with an explanation based on the cooling of a hot WD, and therefore such a soft X-ray emission must be explained from a spotty surface due to magnetospheric processes, as the one explored in this work.

The stability of the WD for such a rotation period constrains the WD radius to the range $R \approx (1.04\text{–}4.76) \times 10^8$ cm. For example, in the case of a WD with radius $R \approx 10^8$ cm, the polar cap area is $A_{\rm pc} = 6.6 \times 10^{14}$ cm, hence using equation (5.10) we have $f \approx 0.002$. From equation (5.12) the spot temperature $kT_{\rm spot} \approx 0.37$ keV can be obtained using $B_{\rm dp} \approx 6 \times 10^9$ G from the dipole formula (5.13), a potential drop $\Delta V \approx 3.5 \times 10^{11}$ Volts (lower than $\Delta V_{\rm max} \approx 5.4 \times 10^{12}$ Volts), and using the typical value $\eta = 1/2$ of the reduced particle density in the gap adopted in the literature. These parameters suggest a height of the gap, obtained with equation (5.6), $h \approx 0.11 R_{\rm pc}$.

The smallness of the filling factor, which appears to be not attributable to the value of h, could be explained by a multipolar magnetic field near the surface. It is interesting that the existence of a complex multipolar magnetic field close to the surface of white dwarfs is observationally supported (see, e.g., Ferrario et al., 2015). It is important to clarify that the above defined filling factor has only a physical meaning when besides a strong non-dipolar surface field, the physical parameters of the star (magnetic field and rotational velocity) fulfill the requirement for the creation of electron-positron pairs in such a way that an avalanche of particles hits the surface. This is given by the request that the potential drop (5.8) does not exceed the maximum value (5.9). For example, for the largest magnetic field measured in White Dwarfs, $B \sim 10^9$G, and for white dwarf radii $(10^8 - 10^9)$ cm, the maximum period that allows the avalanche of electron-positron pairs is $P \sim (4 - 100)$s, values much shorter thatn the value of typical rotation periods measured in most of magnetic white dwarfs, $P \gtrsim 725$ s (see, e.g., Ferrario et al., 2015). It is interesting to note that the condition of e^+e^- pair creation in the white dwarf magnetosphere could explain the narrow range of observed rotation periods of SGRs/AXPs, $P \sim 2 - 12$ s. Such a local, strong non-dipolar field in the surface, diminishes the area bombarded by the incoming particles and, via magnetic flux conservation, the filling factor establishes the intensity of the multipolar magnetic field component as (see, e.g., Cheng

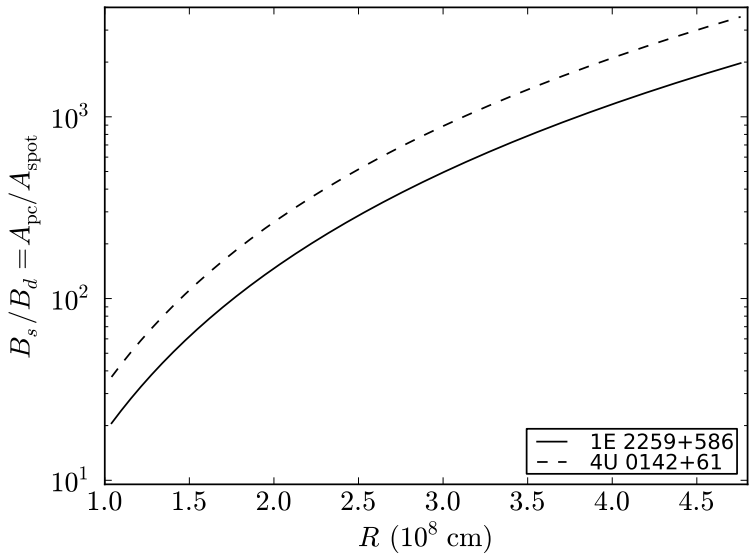

Figure 5.2: Surface to dipole magnetic field ratio given by magnetic flux conservation (5.14) for the AXPs 1E 2259+586 and 4U 0142+61.

and Zhang, 1999; Gil and Melikidze, 2002; Gil and Sendyk, 2000, and references therein):

$$B_{\rm S} = \frac{B_{\rm dp}}{f}, \tag{5.14}$$

which implies that, close to the surface, there could be small magnetic domains with magnetic field intensities as large as $(10^{11} - 10^{12})$ G (see figure 5.2).

5.3.2 4U 0142+61

We can repeat the above analysis for the case of 4U 0142+61. This source, with a rotation period $P \approx 8.69$ s, was first detected by *Uhuru* (Forman et al., 1978). The measured period derivative of this source is $\dot{P} = 2.03 \times 10^{-12}$ (Hulleman et al., 2000). The time-integrated X-ray spectrum of 4U 0142+61 is also described by a blackbody plus a power-law model. The blackbody component shows a temperature $kT_{\rm bb} = 0.39$ keV ($T_{\rm bb} \approx 4.6 \times 10^6$ K) and a surface area $A_{\rm bb} \approx 5.75 \times 10^{11}$ cm^2 (Göhler et al., 2005). As for the above case of 1E 2259+5726, such a blackbody cannot be explained from the cooling of a white dwarf but instead from a magnetospheric hotspot created by the heating of the polar cap.

For a white dwarf radius $R = 10^8$ cm and a magnetic field $B_{\rm dp} \approx 10^{10}$ G for a rotating dipole (5.13), we have a filling factor $f \approx 0.001$, a potential drop $\Delta V \approx 1.4 \times 10^{11}$ V (smaller than $\Delta V_{\rm max} \approx 5.8 \times 10^{12}$ Volts) and a gap height $h \approx 0.06 R_{\rm pc}$. Again a filling factor suggest the presence of a strong multipolar component as shown in figure 5.2.

We show in figures 5.3 and 5.4 the potential drop inferred from equation

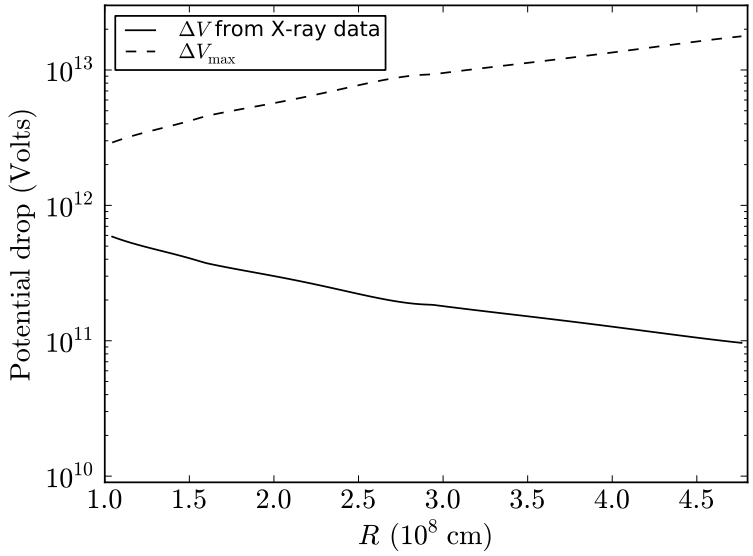

Figure 5.3: White dwarf polar gap potential drop ΔV inferred via equation (5.12) using the blackbody observed in soft X-rays of 1E 2259+586. In this plot, we check the potential drop developed in the white dwarf polar gap does not exceed the maximum potential reachable $\Delta V_{\rm max}$ given by equation (5.9).

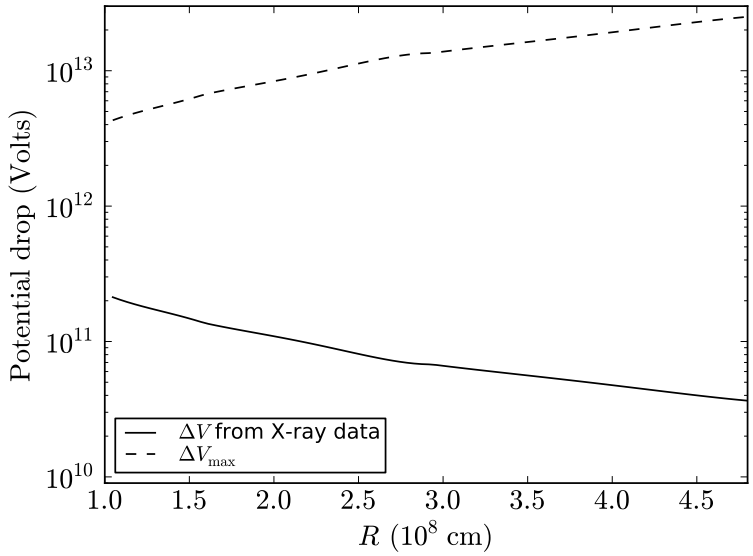

Figure 5.4: White dwarf polar gap potential drop ΔV inferred via equation (5.12) using the blackbody observed in soft X-rays of 4U 0142+61. In this plot, we check the potential drop developed in the white dwarf polar gap does not exceed the maximum potential reachable $\Delta V_{\rm max}$ given by equation (5.9).

(5.12) using the X-ray blackbody data for the above two sources. We check that for all the possible stable white dwarf configurations, the potential drop satisfies the self-consistent condition $\Delta V < \Delta V_{\rm max}$, where the latter is given by equation 5.9.

5.4 Flux profiles and pulsed fraction

We now show the effect of these hotspots on the flux profile following the treatment exposed in Turolla and Nobili (2013). In this treatment general relativistic effects are considered and it is assumed that the exterior of the star can be described, with very good approximation, by the Schwarschild metric. We consider General Relativity despite the gravitational field of white dwarfs is not very strong.

In figure 5.4 we can appreciate the photon trajectory from the surface of the star to the observer. We assume the star has a mass M and a radius R. Assuming a (r, θ, ϕ) spherical coordinate system centred on the star and the line-of-sight (LOS) being the polar axis, we consider the observer is located at $r \to \infty$ and a photon arising from the star's surface making an angle α with the local surface normal, with $0 \leq \alpha \leq \pi/2$. Due to space-time curvature, the photon path is bended an additional angle β, so it reaches the observer with an angle $\psi = \alpha + \beta$. Due to the spherical coordinate system we have defined, we have that $\psi = \theta$ (see figure 5.4). Beloborodov (2002) showed that a simple approximate formula relates the emission angle α to the final angle θ:

$$1 - \cos\alpha = (1 - \cos\theta)\left(1 - \frac{R_s}{R}\right), \tag{5.15}$$

where $R_s = 2GM/c^2$ is the Schwarschild radius and G is the gravitational constant.

For an emission with a local Planck spectrum, the intensity is given by a blackbody of temperature T, $B_\nu(T)$, where ν is the photon frequency. The flux is proportional to the visible area of the emitting region (S_V) plus a relativistic correction proportional to the surface, given by the equation

$$\begin{aligned} F_\nu &= \left(1 - \frac{R_S}{R}\right) B_\nu(T) \int \cos\alpha \frac{\mathrm{d}\cos\alpha}{\mathrm{d}(\cos\theta)} \mathrm{d}s \\ &= \left(1 - \frac{R_S}{R}\right)^2 B_\nu(T)(I_p + I_s) \end{aligned} \tag{5.16}$$

where

$$I_p = \int_{S_V} \cos\theta \sin\theta d\theta d\phi, \quad I_s = \int_{S_V} \sin\theta d\theta d\phi. \tag{5.17}$$

In polar coordinates, the circular spot has its center at θ_0 and a semi-aperture θ_c. The spot is bounded by the function $\phi_b(\theta)$, where $0 \leq \phi_b \leq \pi$, and since we must consider just the star visible part, the spot must be also limited by a constant θ_F.

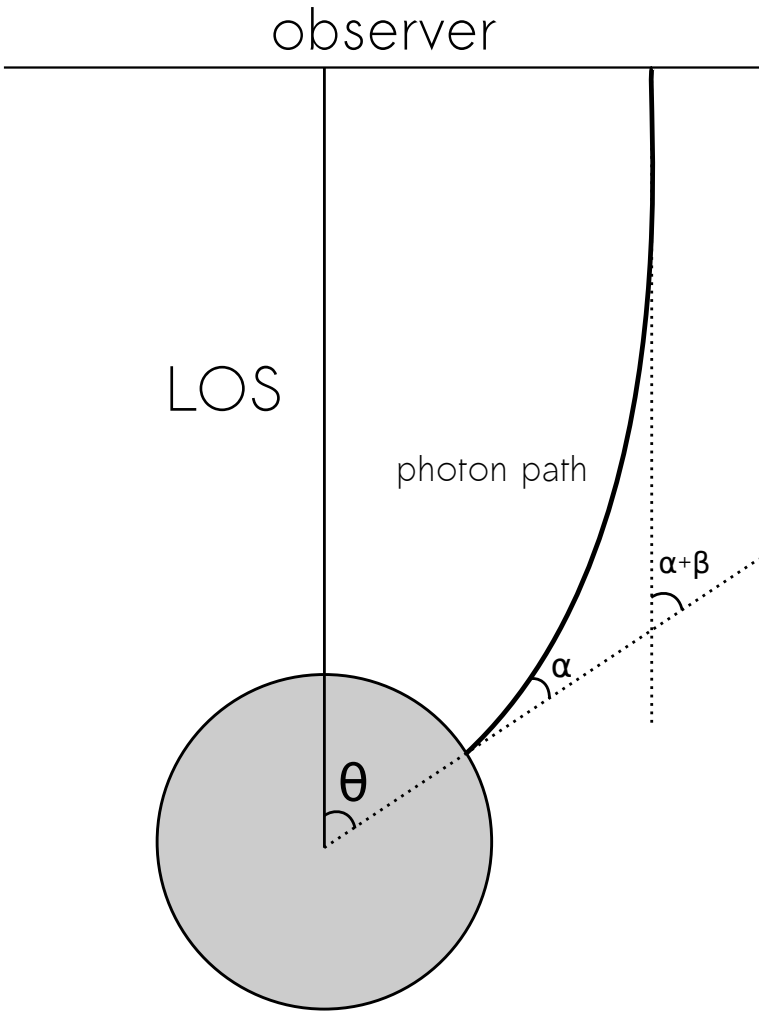

Figure 5.5: View of the photon trajectory and angles θ, α and β.

For a given bending angle β, the maximum θ_F is given by the maximum emission angle α, i.e. $\alpha = \pi/2$. One can see that in Newtonian gravity, where $\beta = 0$, the maximum visible angle is $\theta_F = \pi/2$ which means half of the star is visible, while in a relativistic star, values $\theta_F > \pi/2$ are possible, as expected. Then

$$I_p = 2\int_{\theta_{\rm min}}^{\theta_{\rm max}} \cos\theta \sin\theta \phi_b(\theta) d\theta,$$
$$I_s = 2\int_{\theta_{\rm min}}^{\theta_{\rm max}} \sin\theta \phi_b(\theta) d\theta, \tag{5.18}$$

where $\theta_{\rm min}$, $\theta_{\rm max}$ are the limiting values to be determined for the spot considered. Turolla and Nobili (2013) showed how to solve these integrals and how to treat carefully the limiting angles. The I_p and I_s integrals can be then written as $I_{p,s} = I_{1,2}(\theta_{\rm max}) - I_{1,2}(\theta_{\rm min})$ and we refer the reader to that work for the precise expressions.

Finally, the flux (5.16) is written as

$$F_\nu = \left(1 - \frac{R_{\rm S}}{R}\right)^2 B_\nu(T) A_{\rm eff}(\theta_c, \theta_0) \ , \tag{5.19}$$

where $A_{\rm eff}$ is the effective area, given by

$$A_{\rm eff}(\theta_c, \theta_0) = R^2 \left[\frac{R_{\rm S}}{R} I_s + \left(1 - \frac{R_{\rm S}}{R}\right) I_p\right]. \tag{5.20}$$

The total flux produced by two antipodal spots, with semi-apertures $\theta_{c,i}$ and temperatures T_i (i=1,2), can be calculated by adding each contribution, so we have

$$F_\nu^{\rm TOT} = \left(1 - \frac{R_{\rm S}}{R}\right)^2 [B_\nu(T_1) A_{\rm eff}(\theta_{c,1}, \theta_0) + B_\nu(T_2) A_{\rm eff}(\theta_{c,2}, \theta_0 + \pi/2)]. \tag{5.21}$$

Besides, the pulse profile in a given energy band $[\nu_1, \nu_2]$ for one spot is given by

$$F(\nu_1, \nu_2) = \left(1 - \frac{R_{\rm S}}{R}\right)^2 A_{\rm eff}(\theta_c, \theta_0) \int_{\nu_1}^{\nu_2} B_\nu(T) {\rm d}\nu \ . \tag{5.22}$$

The star rotates with a period P (angular velocity $\Omega = 2\pi/P$), so we consider $\hat{\mathbf{r}}$ the unit vector parallel to the rotating axis. It is useful to introduce the angles ξ, the angle between the LOS (unit vector $\hat{\mathbf{l}}$) and the rotation axis, and the angle χ between the spot axis (unit vector $\hat{\mathbf{c}}$) and the rotation axis, i.e., $\cos\xi = \hat{\mathbf{r}} \cdot \hat{\mathbf{l}}$ and $\cos\chi = \hat{\mathbf{r}} \cdot \hat{\mathbf{c}}$. As the star rotates, the spot's center θ_0 changes. Let $\gamma(t) = \Omega t$ be the rotational phase, thus by geometrical reasoning we have

$$\cos\theta_0(t) = \cos\xi\cos\chi - \sin\xi\sin\chi\cos\gamma(t) \ , \tag{5.23}$$

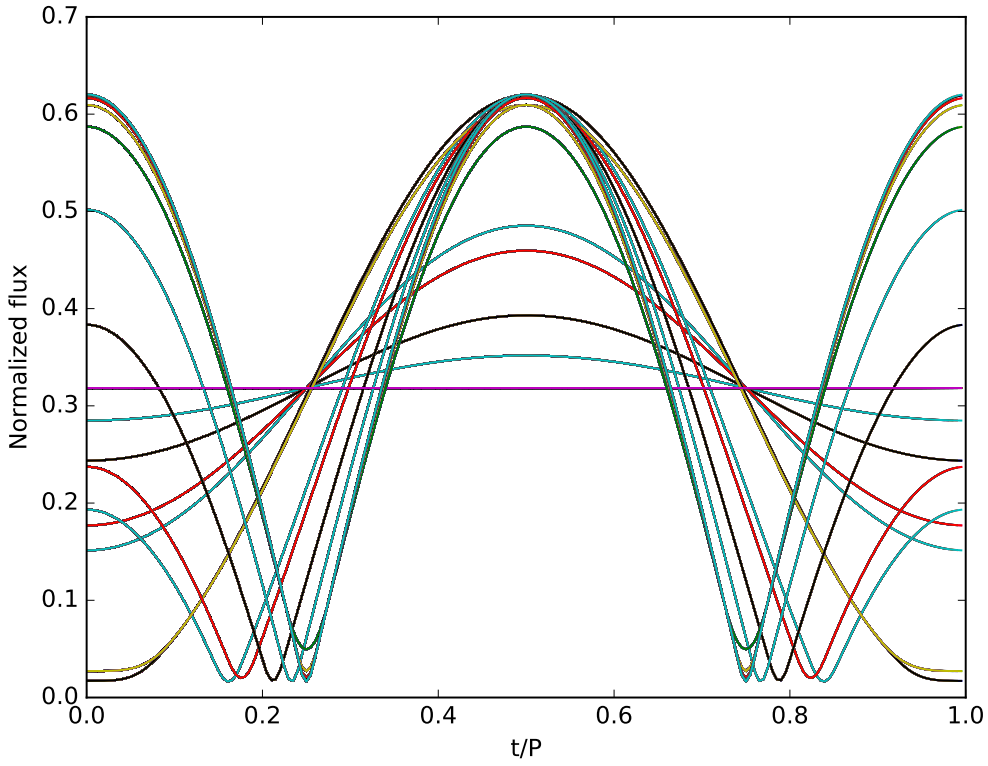

Figure 5.6: Flux profiles for different configurations of antipodal spots as a function of the phase. The semi-aperture for all the lines is $\theta_c = 3^\circ$. The WD parameters correspond to the ones of the WD of minimum radius adopted for AXP 1E 2259+586.

where it is indicated that ξ and χ do not change in time. When the total flux (5.21) is calculated for a given configuration (ξ, χ) in the whole period of time, the typical result is a pulsed flux with a maximum ($F_{\rm max}$) and a minimum flux ($F_{\rm min}$). As an example, we show in Fig. 5.6 flux profiles for different configurations of antipodal spots as a function of the phase for the WD of minimum radius in the case of AXP 1E 2259+586 used in section 5.3.

We can measure the amount of pulsed emission by defining the *pulsed fraction*

$$\mathrm{PF} = \frac{F_{\rm max} - F_{\rm min}}{F_{\rm max} + F_{\rm min}}, \tag{5.24}$$

which is shown in figure 5.7 as a function of the angles ξ and χ, for AXP 1E 2259+586. In the left panel of this figure we consider only the flux given by the blackbody produced by the two antipodal hotspots on the WD. We can see that indeed pulsed fractions as small as the above values can be obtained from magnetic WDs, for appropriate values of the geometric angles ξ and χ. However, the soft X-ray spectrum shows a non-thermal power-law component,

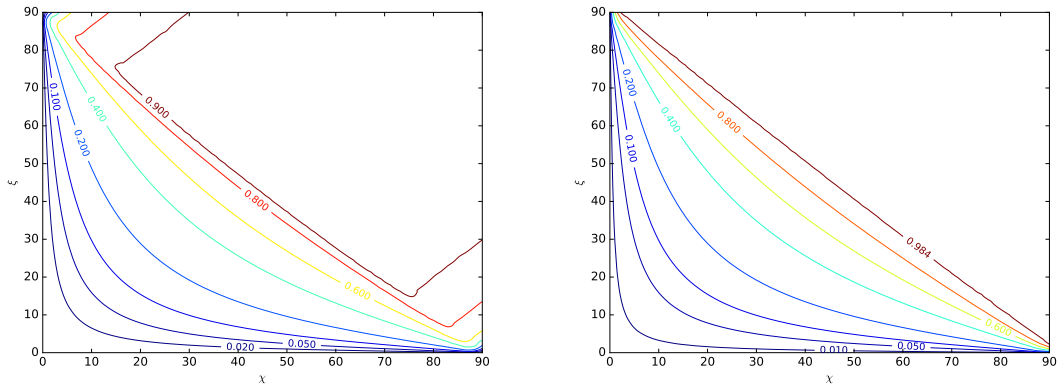

Figure 5.7: Theoretical PF as a function of the angles ξ and χ, computed in this work for the source 1E 2259+586 modelled as a WD of radius $R_{\rm min} \approx 1.04 \times 10^8$ cm. The left-hand panel shows the results of the PF produced by the blackbody given by the two antipodal hotspots. The right-hand panel shows the results for the total flux given by the blackbody plus the non-thermal power-law component, both pulsed. The observed total PF of this source in the 2–10 keV is about 20 per cent (Zhu et al., 2008).

additional to the blackbody one. As we have shown, the blackbody itself can contribute to the PF if produced by surface hotspots and thus the observed total PF of a source in those cases includes both contributions, mixed. It is thus of interest to explore this problem from the theoretical point of view. To do this we first recall that total intrinsic flux of this source in the 2–10 keV band is $F_{\rm tot} \approx 1.4 \times 10^{-11}$ erg cm^{-2} s^{-1}, and the power-law flux is $F_{\rm PL} \approx 1.8 F_{\rm bb} \approx 8.5 \times 10^{-12}$ erg cm^{-2} s^{-1} (Zhu et al., 2008). The right panel of Fig. 5.7 shows the PF map for this source taking into account both the blackbody and the power-law components. By comparing this PF map with the one in the left panel which considers only the pulsed blackbody we can see that they are very similar each other. This means that in these cases where both pulsed components are in phase and have comparable fluxes it is difficult (although still possible if good data are available), to disentangle the single contributions.

5.5 Conclusions

We exploited the analogy with pulsars to investigate whether or not massive, highly magnetic, fast rotating WDs, can behave as neutron star pulsars and emit observable high-energy radiation. We conclude the following:

1. We showed that WDs can produce $e^- e^+$ pairs in their magnetosphere from the decay of curvature radiation photons, i.e., we infer the structure parameters for which they are located above the WD pulsar death-line. We evaluated the rate of such a process. Then, we calculated the thermal emission produced by the polar cap heating by the pair-created particles that flow back to the WD surface due to the action of the induction electric field.

2. In order to give a precise example of the process, we applied the theoretical results to the case of the WD model of SGRs and AXPs. We have shown that the inferred values of the WD parameters obtained from fitting with this magnetospheric emission, the blackbody spectrum observed in the soft X-rays of SGRs and AXPs, are in agreement with our previous estimates using the IR, optical, and UV data, and fall within the constraints imposed by the gravitational stability of the WD.

3. We have related the size of the spot with the size of the surface under the polar cap filled by the inward particle bombardment. We have shown that the spot area is much smaller than the polar cap area pointing to the existence of strong non-dipolar magnetic fields close to the WD surface.

4. We have used the heat transport and energy balance equations to show that, for the actual conditions of density and temperature under the polar cap, the hot spot re-radiates efficiently the heat proportioned by the inward particle bombardment.

5. The spot, which is aligned with the magnetic dipole moment of the WD, produces a pulsed emission in phase with the rotation period of the object. We showed that the theoretically inferred pulsed fraction of the WD spans from very low values all the way to unity depending on the viewing angles. Therefore it can also account for the observed pulsed fraction in SGRs and AXPs for appropriate choices of the viewing angles. In addition, the low-energy tail of the blackbody spectrum of the hotspot could produce a non-null pulsed fraction of the flux in the optical bands as well. However, this depends on the flux produced by the surface temperature of the WD which certainly dominates the light curve at low energies. From the quantitative point of view, the size of the surface area of the spots is crucial for the explanation of the observed pulsed fraction in soft X-rays.

6. We have also shown that the addition of a pulsed power-law component as the one observed in SGRs/AXPs does not modify appreciably the above result. The reason for this is that the non-thermal power-law component and the blackbody due to the surface hotspot have comparable fluxes and are in phase with each other. In those cases it is difficult to disentangle the single contributions to the pulsed fraction.

We have shown that, as advanced in Rueda et al. (2013), indeed the blackbody observed in the optical wavelengths of SGRs and AXPs can be due to the surface temperature of the WD, while the one observed in the X-rays can be of magnetospheric origin. For the power-law component, also observed in the soft X-rays, a deeper analysis of processes such as curvature radiation, inverse Compton scattering, as well as other emission mechanisms, is currently under study.

There is also room for application and extension of the results presented in this work to other astrophysical phenomena. WD mergers can lead to a system

formed by a central massive, highly magnetic, fast rotating WD, surrounded by a Keplerian disk (see Rueda et al., 2013, and references therein). At the early stages, the WD and the disk are hot and there is ongoing accretion of the disk material onto the WD. In such a case, the WD surface shows hot regions that deviate from the spotty case, e.g. hot surface rings. That case is also of interest and will be presented elsewhere.

Chapter 6

Soft Gamma-ray Repeaters and Anomalous X-ray Pulsars as Rotationally Powered Neutron Stars

6.1 Introduction

As we mentioned in chapter 4, Malheiro et al. (2012) could check that in 4 AXPs/SGRs (1E 1547.0-5408, SGR 1627-41, PSR J1622-4950 and XTE J1810-197), when they are considered as neutron stars with a fiducial value for the moment of inertia of $I_{\rm NS} \approx 10^{45}$ g cm^2, the observed luminosity was less than the spin-down power:

$$L_{\rm obs} < \dot{E}_{\rm NS} = -4\pi^2 I_{\rm NS} \frac{\dot{P}}{P^3}. \tag{6.1}$$

This would make these four sources similar to the canonical rotationally powered pulsars. One of the main criteria to define a pulsar as a member of the family AXPs/SGRs is that precisely equation (6.1) is not satisfied. However, this is not the only criterion that defines AXPs/SGRs, being the transient activity, not seen in common pulsars, as one of the main characteristics of these objects.

On the other hand several works (Belvedere et al., 2014, 2012; Rotondo et al., 2011c; Rueda et al., 2011) considered the equations of equilibrium of neutron stars taking into account strong, weak, electromagnetic and gravitational interactions within the framework of General Relativity. These works allowed to obtain realistic neutron star parameters (such as mass M, radius R or moment of inertia I) which can differ significantly from the fiducial values adopted in Malheiro et al. (2012) and in most of estimates done in the literature of the magnetic field or efficiency of any pulsar (usually are assumed neutron stars with mass $M = 1.4 M_\odot$, radius $R = 10$ km and moment of inertia $I = 10^{45}$ g cm^2).

In this way, using the realistic parameters of uniformly rotating neutron stars

obtained in Belvedere et al. (2014) and using a formula that generalised the dipole formula taking into account the effects of General Relativity (see section 6.3), Belvedere et al. (2015) showed that the estimates of the magnetic field and radiation efficiency $L_X/\dot{E}_{\rm rot}$ lead to values that are very different from estimates based on the fiducial parameters usually assumed for pulsars. They focused on objects that belong to the high-magnetic field pulsars class (see, e.g. Ng and Kaspi, 2011). One of the characteristics of this class of pulsars is that usually they have magnetic fields of the order or larger than the critical field for quantum electrodynamical effects (Ng and Kaspi, 2011; Zhu et al., 2011),

$$B_{\rm c} = \frac{m_{\rm e}^2 c^2}{e\hbar} = 4.41 \times 10^{13}\ {\rm G}. \tag{6.2}$$

and they also, in some cases have luminosities higher than the rotational power of the neutron star, $L_X > |\dot{E}^{\rm f}_{\rm rot}|$, where the f stands for fiducial values. As we can see, they have properties similar to magnetars, but unlike these, they emit in radio wavelengths. For this reason it has been suggested that these high-magnetic field pulsars should be a transition class between rotationally powered pulsars and the so called magnetars.

The formula (6.4), obtained by Rezzolla and Ahmedov (2004), generalises the dipole formula (6.3) and the classical solution in vacuum obtained by Deutsch (1955) by taking into account the effects of General Relativity. Belvedere et al. (2015), using the aforementioned equation (6.4) and using the results from Belvedere et al. (2014), calculated the surface magnetic field and the efficiencies $L_X/|\dot{E}_{\rm rot}|$ for several high-magnetic field pulsars as we said before, obtaining in this way estimates smaller than the magnetic field using fiducial values. They also concluded that the use of the classical Newtonian formula (6.3) can overestimate the surface magnetic field of up to one order of magnitude with respect to the general relativistic one. This made that several pulsars that were considered overcritical actually turn out to be undercritical, when they are calculated with the new formula and with the realistic neutron star parameters.

Coelho et al. (2017) following closely Belvedere et al. (2015), applied realistic parameters of the neutron star to model the AXPs/SGRs, in this way generalising the analysis of Malheiro et al. (2012). Coelho et al. (2017) also completed the work of (Boshkayev et al., 2013) and (Rueda et al., 2013), which also generalised the treatment of Malheiro et al. (2012), but instead considering realistic values of highly rotating white dwarfs. And the main contribution of Coelho et al. (2017) was to extend the group of the 4 aforementioned AXPs/SGRs that could be rotationally powered pulsars to other 5 sources, i.e., that the equation (6.1) also apply to 5 additional AXPs/SGRs.

Radio emission, which is usually absent in AXPs/SGRs but very common in rotationally powered pulsars, has been also observed in four of these sources (Camilo et al., 2007, 2006; Eatough et al., 2013; Halpern et al., 2005; Levin et al.,

2010, 2012). And it was also shown in Coelho et al. (2017) that the energetics of the observed outbursts can be explained from the gain of rotational energy during an accompanied glitch. This test is crucial for the model of AXPs/SGRs as ordinary rotationally powered pulsars. All these results make that the model of these AXPs/SGRs as rotationally powered pulsars should not be completely dismissed. Although this explanation is not possible for the other sources, It can not be completely dismissed as a possible explanation for the 9 aforementioned sources.

Here we will show the main results presented in Coelho et al. (2017). First we will give a review in section 6.2 of the Neutron Star structure properties, which are based mostly on the model developed in Rotondo et al. (2011c), Rueda et al. (2011), Belvedere et al. (2012) and Belvedere et al. (2014). Then in section 6.3 are presented the estimates of the surface magnetic field, where is used the recently generalization of the famous magnetic dipole formula where are considered general relativistic effects (Rezzolla and Ahmedov, 2004). For the calculation of the magnetic field are used the realistic structure parameters presented in section 6.2. After this we proceed in section 6.4 to estimate the efficiencies of AXPs/SGRs as rotationally powered pulsars calculating the ratio $L_X/\dot{E}_{\rm rot}$ in all the range of possible values for the masses of the Neutron Star masses, something which allows us to conclude, as we stated before, that only 9 sources could be considered as rotationally powered Neutron Stars. After this we proceed in section 6.5 to analyze the glitch/outburst connection in this model. Finally we present the main conclusions of this analysis in section 6.7.

6.2 Neutron star structure

In several works (Belvedere et al., 2014, 2012; Rotondo et al., 2011c; Rueda et al., 2011), the equations of equilibrium of neutron stars taking into account strong, weak, electromagnetic and gravitational interactions within the framework of genera relativity were considered. Considering previous works, where the possible existence of overcritical electric fields at the core of neutron stars (see Ruffini, 2008), the Einstein-Maxwell system of equations coupled to the general relativistic Thomas-Fermi equations of equilibrium were assumed, giving rise to what has been called the Einstein-Maxwell-Thomas-Fermi (EMTF) equations (see Belvedere et al., 2014, 2012; Rotondo et al., 2011c; Rueda et al., 2011). Rotondo et al. (2011c) showed that in the most simple case, where strong interactions are neglected, the local charge neutrality condition was incompatible with matter made of neutrons, protons and electrons in β-equilibrium and modelled by the EMTF equations. This because these equations imply that the neutron Fermi energy would be constant throughout the configuration as well as the sum of the electron and proton Fermi energies, but not the individual Fermi energies of these two components. As we know from chapter 2, the Fermi energy has to be constant throughout the whole star, whether the star is a white dwarf or a neutron star, otherwise this would lead to a microscopic instability. This imply that for these systems a less restrictive condition of *global charge neutral-*

ity has to be imposed instead of the usual *local charge neutrality*, which is used when the neutron stars are modelled through the Tolman-Oppenheimer-Volkoff (TOV) system of equations (Oppenheimer and Volkoff, 1939; Tolman, 1939). In this chapter we present the effects of both the local and global charge neutrality on the structure of the star.

Several works generalised the treatment of Rotondo et al. (2011c) considering the strong interaction in a static (Belvedere et al., 2012; Rueda et al., 2011) or an uniformly rotating neutron star (Belvedere et al., 2014), which is important to describe the properties of the core of the neutron star. The neutron star interior is made up of a core and a crust. The core has densities higher than the nuclear density, $\rho_{\rm nuc} \approx 3 \times 10^{14}$ g cm^{-3} and is composed of a degenerate gas of baryons (e.g.. neutrons, protons or hyperons) and leptons (e.g. electrons and muons). In this high density range the physical properties of matter are still uncertain. It is so not only because the correct form of the nuclear potential is still uncertain but also because a totally satisfactory many-body computational method to solve the Schrödinger equation, given the potential, is still not completely developed. On the other hand, the properties of matter in the crust are reasonably well understood because there are not significant uncertainties on the knowledge of the equation of state in the density regime that applies to the crust. The inner region of the crust is composed of ions, electrons and free neutrons and its density satisfies $\rho_{\rm drip} < \rho < \rho_{\rm nuc}$, where $\rho_{\rm drip} \approx 4.3 \times 10^{11}$ g cm^{-3} is the neutron drip density; this density defines when the ratio n/p reaches such a critical level that neutrons start to "drip" from the nuclei and become free. And finally, in the outer region we have densities that satisfy $\rho \leqslant \rho_{\rm drip}$ and the matter is composed of ions and electrons.

For the crust can be adopted the Baym-Pethick-Sutherland (BPS) equations of state (EOS) (Baym et al., 1971), which is based on Baym et al. (1971). For the core were adopted the relativistic mean-field (RMF) theory models, specifically an extension of the Boguta and Bodmer (1977) formulation with a massive scalar meson (σ) and two vector mesons (ω and ρ) mediators, and possible interactions amongst them. Three sets of parameterizations of these models were adopted (see table 6.1): the NL3 (Lalazissis et al., 1997), the TM1 (Sugahara and Toki, 1994), and the GM1 Glendenning and Moszkowski (1991) equations of state. The behaviour of these three different equations of state can be appreciated in figure 6.1.

As AXPs/SGRs are rotating it is natural to model their structure with the model of uniformly rotating neutron stars presented in Belvedere et al. (2014), where are considered small rotation perturbations from the spherically symmetric configuration using the Hartle's formalism (Hartle, 1967). In this method are computed rotating configurations, accurate up to second-order in Ω, with the same central density as the seed static non-rotating configurations. But given

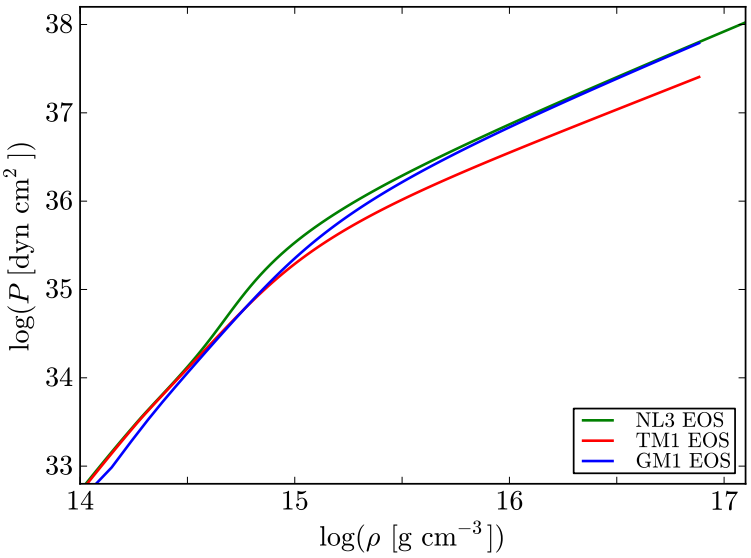

Figure 6.1: Equation of state of the models NL3, TM1 and GM1 (see table 6.1). The behaviour is shown at sub and supranuclear densities. This figure appears in Coelho et al. (2017).

	NL3	TM1	GM1
M(MeV)	939.00	938.00	938.93
m_σ(MeV)	508.194	511.198	512.000
m_ω(MeV)	782.501	783.000	783.000
m_ρ(MeV)	763.000	770.000	770.000
g_σ	10.2170	10.0289	8.9073
g_ω	12.8680	12.6139	10.6089
g_ρ	4.4740	7.2325	4.0972

Table 6.1: Meson masses and coupling constants in the parameterizations NL3, TM1 and GM1.

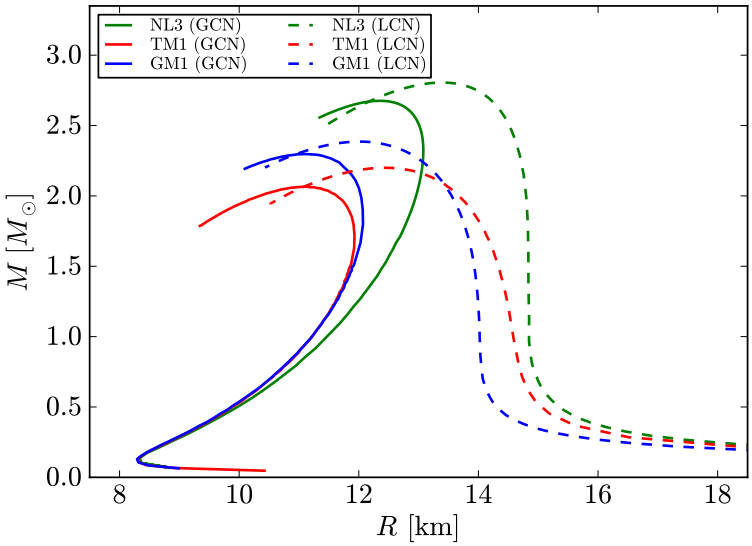

Figure 6.2: Mass-radius relation for the NL3, TM1 and GM1 equations of state in the cases of global (solid curves) and local (dashed curves) charge neutrality. This figure appears in Coelho et al. (2017).

that the rotational periods are very large for a neutron star, the effects of rotation are almost negligible and the mass-radius relation, in both global and local charge neutrality cases, is practically identical to the one for non-rotating configurations (see figure 1 of Belvedere et al. (2015)). Therefore, we can use as a good approximation the non-rotating configurations to model AXPs/SGRs. In figure 6.2 we can see the mass-radius relation for non-rotating configurations in the cases of global and local charge neutrality and where are considered the three aforementioned equations of state, NL3, TM1 and GM1. We can appreciate that the general effect of the global charge neutrality is to make the stars less dense, for a given mass the radius in the global charge neutrality configuration is larger than in the local charge neutrality one.

Another important quantity besides mass and equatorial radius is the moment of inertia I. In figures 6.3 and 6.4 we can see the moment of inertia as a function of the neutron star mass for global and local charge neutrality, respectively. Again, there are shown the three equations of state. This quantity is important to estimate the dipole magnetic field, which we will talk about in the next section

6.3 Estimate of the magnetic field

The simplest model that has allowed astrophysicists to estimate the magnetic field of the neutron stars is the one that assumes a magnetic dipole $\mu = BR^3$ at the center of the star of radius R and which rotates with angular velocity Ω. If an angle of $\pi/2$ is assumed between the dipole axis and the axis of rotation, then the magnetic field, according to this simple model is estimated with the relation

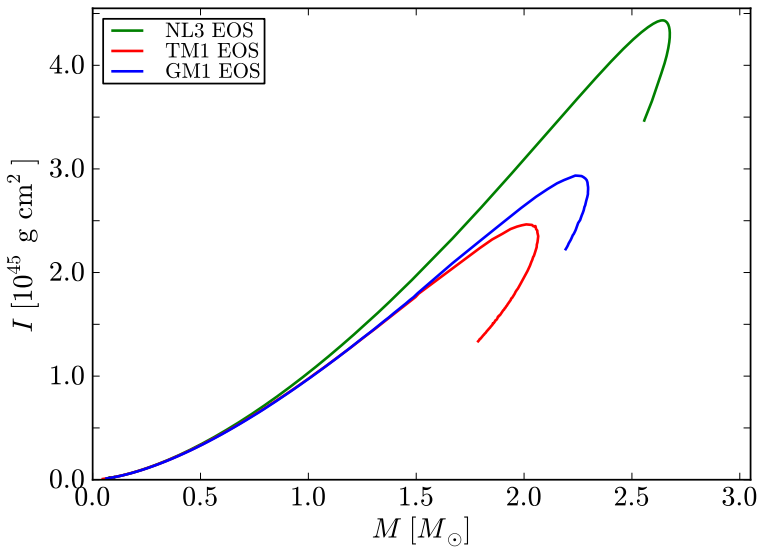

Figure 6.3: Moment of inertia I as a function of the neutron star mass for the NL3, TM1 and GM1 equations of state in the case of global charge neutrality. Compare with the case of local charge neutrality shown in figure 6.4. This figure appears in Coelho et al. (2017).

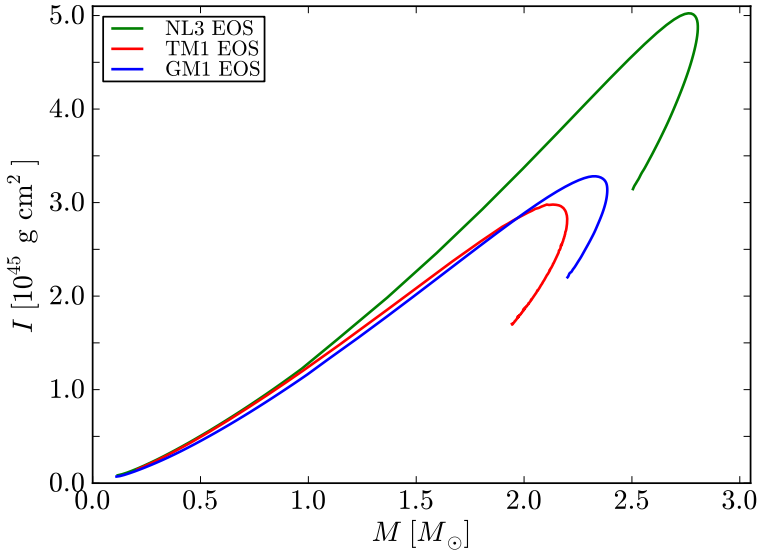

Figure 6.4: Moment of inertia I as a function of the neutron star mass for the NL3, TM1 and GM1 equations of state in the case of local charge neutrality. Compare with the case of global charge neutrality shown in figure 6.3. This figure appears in Coelho et al. (2017).

(Landau and Lifshitz, 1975):

$$B_{\rm dp} = \left(\frac{3c^3}{8\pi^2} \frac{I}{R^6} P\dot{P} \right)^{1/2}, \tag{6.3}$$

where $P = 2\pi/\Omega$ is the period of rotation and $\dot{P}$ is its time derivative. But this is the simplest formula and several improvements have been calculated. For example, the famous classical solution of Deutsch (1955) generalizes the dipole model considering the solution to the Maxwell equations of an uniformly rotating perfectly conducting star with a misaligned magnetic dipole. Deutsch (1955) obtained the exterior electromagnetic field, assuming the exterior is completely vacuum. The generalization of the Deutsch's solution to the general relativistic case in the slow rotation regime, and for a general misaligned dipole was obtained in analytic form in the *near zone* ($r \ll c/\Omega = 1/k = \lambda/2\pi$) by Rezzolla et al. (2001, 2003) and, for the *wave zone* by Rezzolla and Ahmedov (2004). This allowed them to obtain a formula for the magnetic field that generalised equation (6.3):

$$B_{\rm GR} = \frac{N^2}{f} \left(\frac{3c^3}{8\pi^2} \frac{I}{R^6} P\dot{P} \right)^{1/2}, \tag{6.4}$$

where

$$f = -\frac{3}{8} \left(\frac{R}{M} \right)^3 \left[\ln(N^2) + \frac{2M}{R} \left(1 + \frac{M}{R} \right) \right], \tag{6.5}$$

and

$$N = \sqrt{1 - \frac{2M}{R}}. \tag{6.6}$$

We have to remind that equation (6.4) has been obtained for a rotating magnetic dipole in electrovacuum, neglecting the torque produced by the magnetospheric plasma. The effect of this torque certainly leads to values still lower of the magnetic field.

In figures 6.5 and 6.6 we can appreciate the theoretical prediction for the surface magnetic fields of the SGRs/AXPs as a function of the neutron star mass, using equation (6.4). We show it only for the GM1 equation of state and for the global and local charge neutrality cases, respectively. In both cases some of the sources have inferred magnetic fields lower than the critical value $B_{\rm c}$ of quantum electrodynamics, for some range of neutron star masses. This set of sources

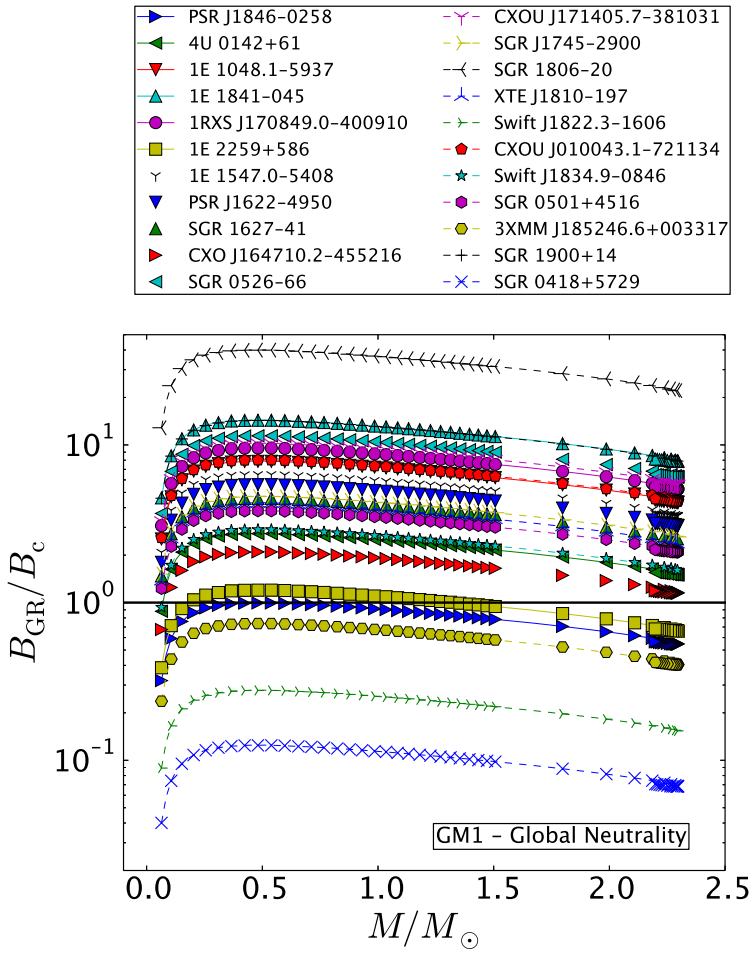

Figure 6.5: Magnetic field B_{GR} given by equation (6.4), in units of $B_c = m_e c^3/(e\hbar) = 4.4 \times 10^{13}$ G, as a function of the mass (in solar masses) in the global charge neutrality case. This figure appears in Coelho et al. (2017).

includes SGR 0418+5729, *Swift* J1822.3-1606 and 3XMM J185246.6+003317, which already before gave magnetic fields lower than B_c where instead of the realistic parameters are used fiducial parameters and where is used the classical magnetic dipole equation (6.3) (see, e.g., Olausen and Kaspi, 2014).

6.4 Efficiency of SGRs and AXPs as rotationally powered neutron stars

The spin-down power depends proportionally on the moment of inertia:

$$\dot{E}_{rot} = -4\pi^2 I \frac{\dot{P}}{P^3}. \tag{6.7}$$

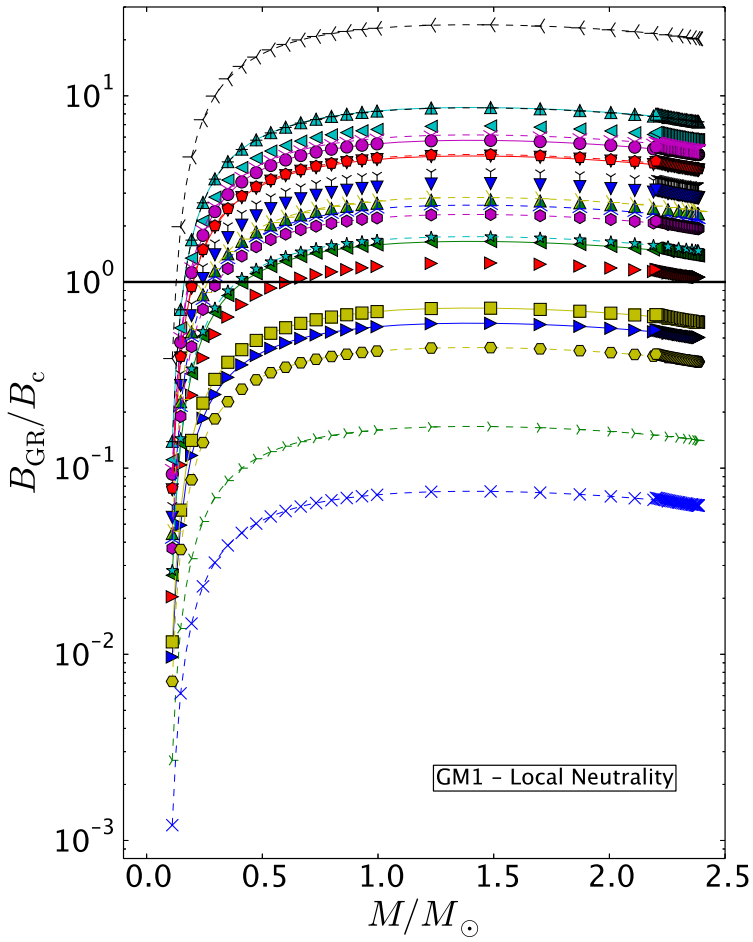

Figure 6.6: Magnetic field B_{GR} given by equation (6.4), in units of $B_c = m_e c^3/(e\hbar) = 4.4 \times 10^{13}$ G, as a function of the mass (in solar masses) in the local charge neutrality case. This figure appears in Coelho et al. (2017).

For pulsars P and $\dot{P}$ are given by observations but the moment of inertia will depend on the model and the equation of state. We can appreciate in figures 6.3 and 6.4 that the moment of inertia is larger than the assumed fiducial values of 10^{45} g cm^2. This means that the efficiency, given by $L_X/\dot{E}_{\rm rot}$ will be smaller and this makes that some sources could now classify as potential rotationally powered pulsars. All we have to do is to plot this efficiency in the range of all possible values of mass for all sources. As we know, the dominant emission of these objects is in X-rays, that is why we consider the luminosity L_X in soft X-rays to calculate the efficiency, which is plotted in figures 6.7 and 6.8 for global and local charge neutrality, respectively, and considering only the GM1 equation of state. We can see that some SGRs/AXPs allow a wide range of masses for which $L_X/\dot{E}_{\rm rot} \lesssim 1$, implying a possible rotation-powered nature for those sources. We can see from figures 6.7 and 6.8 that 9 out of 23 AXPs/SGRs could have masses in which $L_X < \dot{E}_{\rm rot}$ is satisfied. Such sources are: *Swift* J1834.9-0846, PSR J1846-0258, 1E 1547.0-5408, SGR J1745-2900, XTE J1810-197, PSR J1622-4950, SGR 1627-41, SGR 0501+4516 and CXOU J171405.7381031. It is possible to see the properties of these sources in table 6.2.

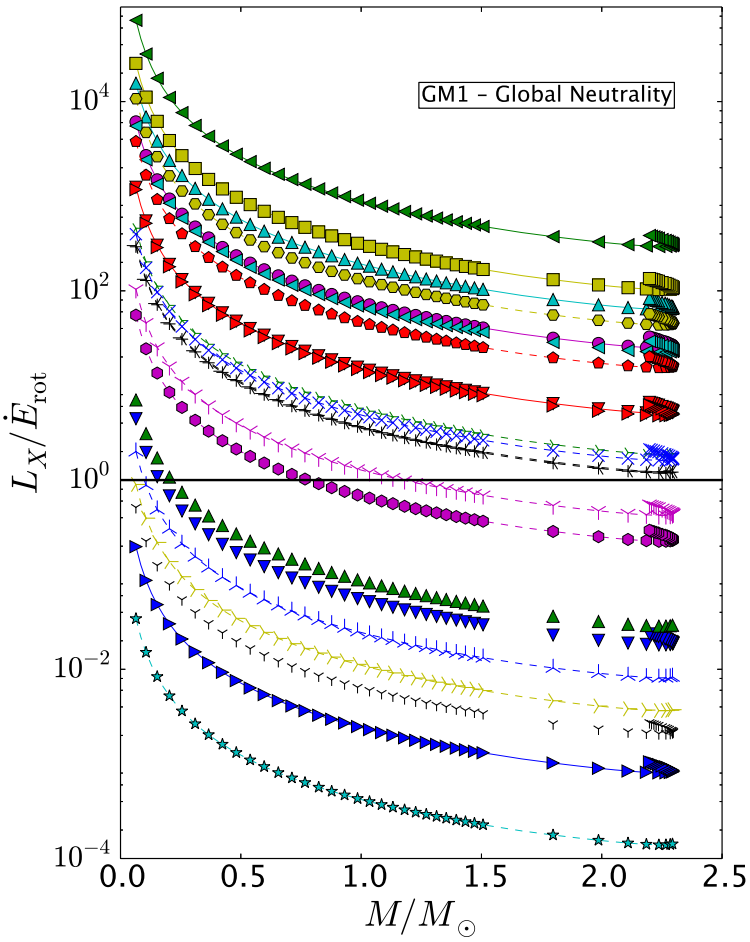

Figure 6.7: Radiation efficieny $L_X/\dot{E}_{\rm rot}$ as a function of the neutron star mass, in solar masses, for the global charge neutrality case and with the GM1 equation of state. This figure appears in Coelho et al. (2017).

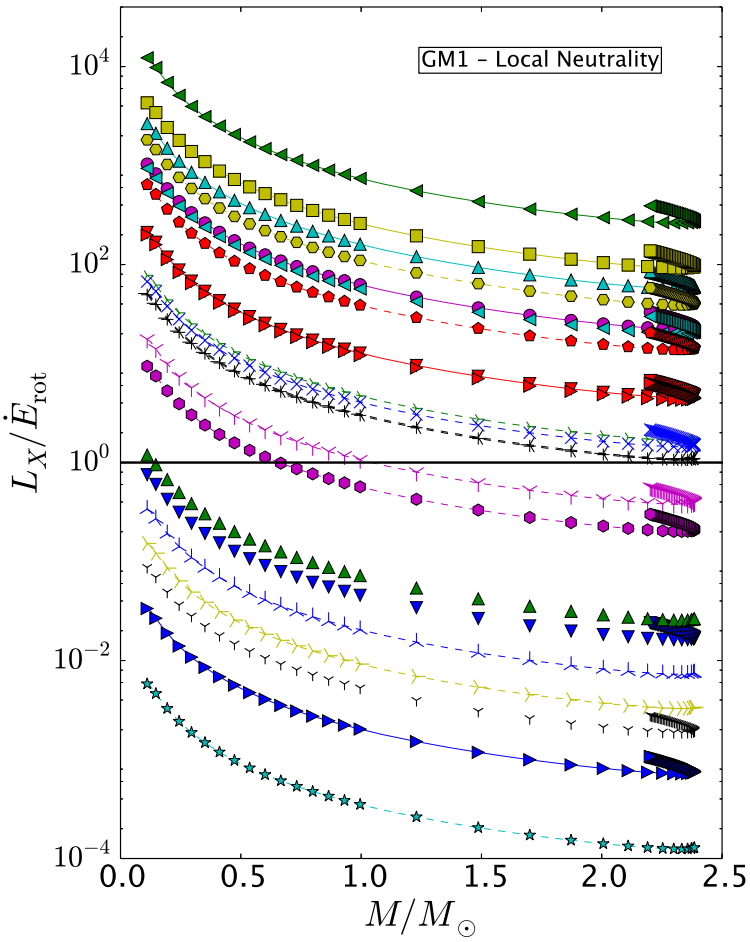

Figure 6.8: Radiation efficieny $L_X/\dot{E}_{\rm rot}$ as a function of the neutron star mass, in solar masses, for the local charge neutrality case and with the GM1 equation of state. This figure appears in Coelho et al. (2017).

Source	P	$\dot{P}$	d	L_X	L_X^{hard}	Obs. gltchs.	Burst	SNR. ass.	Transient	L_{radio}
SGR 0501+4516	5.8	0.59	2	0.81	40.2	No	Yes	HB 9(?)	Yes	-
1E 1547.0-5408	2.07	4.77	4.5	1.3	193.9	Yes	Yes	G327.24-0.13	Yes	1.19
PSR J1622-4950	4.33	1.7	9	0.44	-	No	No	G333.9+0.0	Yes	5.18
SGR 1627-41	2.59	1.9	11	3.6	-	No	Yes	G337.0-0.1	Yes	-
CXOU J171405.7-381031	3.8	6.4	13.2	56	-	No	No	CTB 37B	No	-
SGR J1745.2900	3.76	1.38	8.5	0.11	57.9	No	Yes	-	Yes	84.6
XTE J1810-197	5.54	0.77	3.5	0.043	-	No	Yes	-	Yes	0.98
Swift J1834.9-0846	2.48	0.79	4.2	0.0084	-	No	Yes	W41	Yes	-
PSR J1846-0258	0.33	0.71	6	19	-	Yes	Yes	Kes 75	No	-

Table 6.2: Some properties of the 9 AXPs/SGRs potential rotation-powered neutron stars. In column 2 the period is in seconds and in column 3 $\dot{P}$ is in units of 10^{-11}. In column 4 the distance to the source is in units of kpc. In column 5 the X-ray luminosity in the soft band (2-10) keV is in units of 10^{33} erg s^{-1}. In column 6 the hard X-ray luminosity (20-150 keV) is in units of 10^{33} erg s^{-1}. In columns 7 and 8 we report if there have been observed glitches and outbursts, respectively. in column 9 we report if the source has a reported associated supernova and in column 10 if it is considered as a transient X-ray luminosity in the sense that show flux variations by a factor $\sim (10 - 1000)$ over the quiescent level (Turolla et al., 2015). Finally we report in column 11 the radio luminosity per solid angle at the frequency $f_0 = 1.4$ GHz, i.e., $L_{radio} = S_{1.4}d^2$ in units of 10^{28} sr^{-1} erg s^{-1}, where $S_{1.4}$ is the measured flux density at f_0. In the case of SGR J1745-2900 we report the luminosity per beam at the frequency of 41 GHz according to Yusef-Zadeh et al. (2015). Data taken from Olausen and Kaspi (2014).

Due to the poorly constrained determination of the distance to the sources there is still the possibility that SGR 1900+14 and SGR 1806-20 could be considered as rotationally powered pulsars due to their proximity (but from above) of these sources to the line $L_X = \dot{E}_{rot}$. This would enlarge the list from 9 to 11 sources. But this can only be clarified when better estimates of the distances will be available. And we have to consider also that the soft X-ray spectra of AXPs/SGRs are usually fitted with a blackbody + power-law spectrum model (Mereghetti, 2008). The blackbody temperature is usually of the order $kT_{BB} \sim 0.5$ keV and the surface radii of the emitting region is usually ~ 1 km. When these objects are modelled as neutron stars, it is possible to interpret such a thermal component as due to the surface temperature of the star. On the other hand, the power-law component must still be considered as a consequence of the rotational power of the star and produced by several magnetospheric processes, which are connected themselves with the rotational energy. In this way we should consider only the power-law component to calculate the efficiency because the thermal component is clearly not of rotational origin. Following this line of thought, we proceed to calculate the new efficiencies considering only the power-law component of these two sources in order to explore more the possibility these sources could still be rotationally powered.

SGR 1900+14: The blackbody component of the spectrum is characterised by $kT_{BB} = 0.47$, and a surface radius of $R_{BB} = 4.0$ km, assuming a distance of 15 kpc (Mereghetti et al., 2006). The total flux in the (2-10) keV energy band is $F_X = 4.8 \times 10^{-12}$ erg cm^{-2} s^{-1}. With the above data, we infer that the blackbody and the power-law components contribute respectively 28% and 72% to the total flux, i.e., $F_X^{BB} = 0.28F_X$ and $F_X^{PL} = 0.72F_X$. This leads to $L_X^{PL} = 9.3 \times 10^{34}$ erg s^{-1}.

SGR 1806-20: In this case we have $kT_{BB} = 0.55$ keV and $R_{BB} = 3.7$ km, assuming a distance of 15 kpc (Esposito et al., 2007). For this source $F_X = 1.8 \times 10^{-11}$ erg cm^{-2} s^{-1}, and we infer $F_X^{BB} = 0.16F_X$ and $F_X^{PL} = 0.84F_X$. This leads to $L_X^{PL} = 4.1 \times 10^{35}$ erg s^{-1}. If we use instead the revised distance of 8.7 kpc (Bibby et al., 2008), we have $L_X^{PL} = 1.4 \times 10^{35}$ erg s^{-1}.

In figures 6.9 and 6.10 we show the ratio $L_X^{PL}/\dot{E}_{rot}$ as a function of the neutron star mass in the case of the two above mentioned sources, SGR 1900+14 and SGR 1806-20, adopting the GM1 equation of state and assuming a distance of 15 kpc for both sources. It is clear that the substraction of the contribution from the thermal component to the total flux in soft X-rays can be important for the correct identification of the nature of these sources. We should remark that besides the fact the distances to the sources are not well known, something that could diminish (or increase) the efficiency, the spectrum of both sources could be equally well fitted by a different spectral model, for instance a double blackbody, and this fact would change completely the interpretation. And another factor that adds uncertainty to these calculations is the fact that the equation of state of the neutron star is still unknown, making the moment of inertia and the radius could be different. All these effects could alter significantly the value of

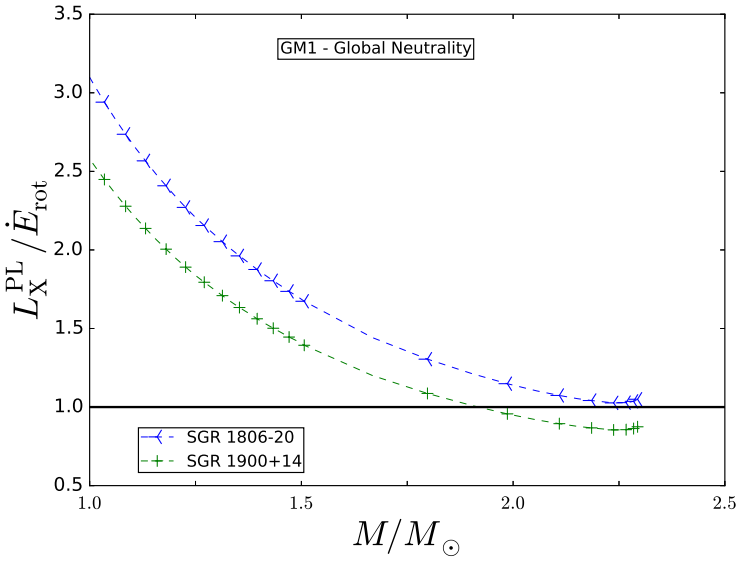

Figure 6.9: Radiation efficiency $L_X^{PL}/\dot{E}_{rot}$ as a function of the neutron star mass, in solar masses, for the global charge neutrality case and with the GM1 equation of state. This figure appears in Coelho et al. (2017).

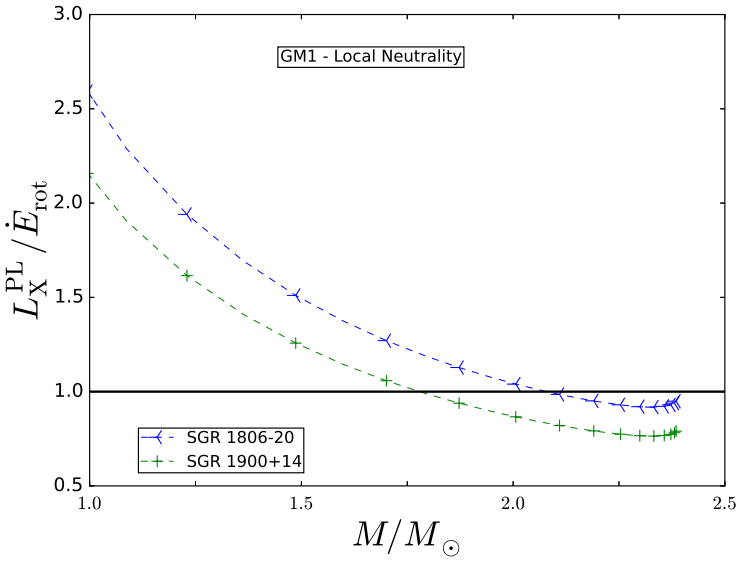

Figure 6.10: Radiation efficiency $L_X^{PL}/\dot{E}_{rot}$ as a function of the neutron star mass, in solar masses, for the local charge neutrality case and with the GM1 equation of state. This figure appears in Coelho et al. (2017).

the efficiency and of course, of the inferred magnetic field.

We have to mention that besides the emission in the soft X-ray band that is detected in all AXPs/SGRs, some sources have shown non-thermal hard X-ray emission (above 10 keV). This emission has been revealed by missions such as RXTE, INTEGRAL, *Suzaku* and *NuSTAR*. From the aforementioned 9 sources that satisfy $L_X < \dot{E}_{rot}$ for a determined range of values of the mass, only three

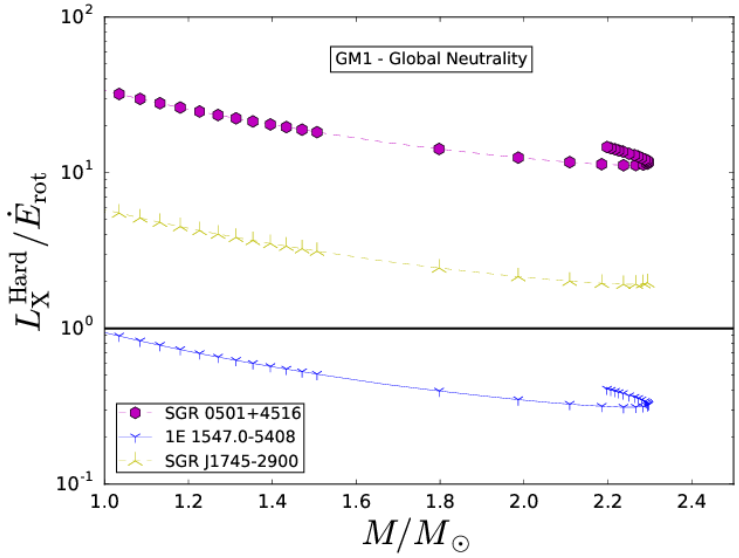

Figure 6.11: Radiation efficiency $L_X^{Hard}/\dot{E}_{rot}$ as a function of the neutron star mass, in solar masses, for the global charge neutrality case and with the GM1 equation of state. This figure appears in Coelho et al. (2017).

have shown persistent hard X-ray emission (see again table 6.2): SGR 0501+4516, 1E 1547.0-5408 and SGR J1745-2900. It is therefore necessary to check if also the emission in hard X-rays satisfies the requirement $L_X^{hard} < \dot{E}_{rot}$. In figures 6.11 and 6.12 we show the ratio $L_X^{Hard}/\dot{E}_{rot}$ as a function of the neutron star mass in the case of SGR 0501+4516, 1E 1547.0-5408 and SGR J1745-2900. After including the hard X-ray component in these three sources, 1E 1547.0-5408 stands still below the line $L_X/\dot{E}_{rot} = 1$, while the other two sources appear above it. This would exclude these sources from the group of potential rotationally powered pulsars.

We have to point out that the mechanisms responsible for the hard X-ray emission are still poorly understood and still considered an open issue. We have to remark that since these sources that emit in hard X-rays are also associated with supernova remnants (see Olausen and Kaspi, 2014, and references therein), the emission in these bands could be contaminated by the remnant emission. The disentanglement of the contributions of the remnant and the central pulsar to the total emission is an issue that should be explored, in addition to the refinement of the estimates of the distances to these sources. If the above numbers are confirmed, then, as we said in the previous paragraph, this would imply that the number of potential rotation-powered AXPs/SGRs should be only 7.

6.5 Glitches and outbursts

Following Malheiro et al. (2012), we also intend to explore the possibility that rotational power of neutron stars could give account not only of the persistent emission but also could explain, from the energetic point of view, the tran-

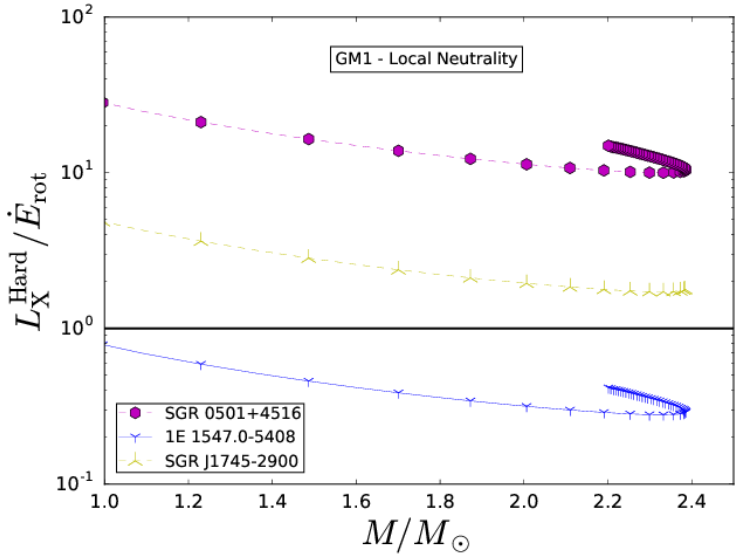

Figure 6.12: Radiation efficiency $L_X^{Hard}/\dot{E}_{rot}$ as a function of the neutron star mass, in solar masses, for the local charge neutrality case and with the GM1 equation of state. This figure appears in Coelho et al. (2017).

sient phenomena observed in these sources. The key idea in this discussion is the glitch-outburst connection. We therefore scrutinize the outburst data of AXPs/SGRs to seek for associated glitches and compare the energetics of the bursting activity with the gain of rotational energy during an associated (observed or unobserved) glitch.

We therefore remember concepts and equations exposed in chapter 4. In a glitch, the release of the accumulated stress leads to a sudden decrease of the moment of inertia and hence, because angular momentum is conserved, we have the relation:

$$J = I\Omega = (I + \Delta I)(\Omega + \Delta\Omega) = \text{constant}. \tag{6.8}$$

We have also a decrease of both the rotational period (e.g., a spin-up) and the radius:

$$\frac{\Delta I}{I} = 2\frac{\Delta R}{R} = \frac{\Delta P}{P} = -\frac{\Delta\Omega}{\Omega}. \tag{6.9}$$

The sudden spin-up leads to a gain of rotational energy:

$$\Delta E_{rot} = -\frac{2\pi^2 I}{P^2}\frac{\Delta P}{P}, \tag{6.10}$$

energy gain that is paid by the gravitational energy gain by the star's contraction (see chapter 4 and Malheiro et al. (2012)).

We therefore proceed to infer theoretically the fractional change of rotation period $|\Delta P|/P$, which explains energetically the bursts of the nine AXPs/SGRs that satisfy $L_X < \dot{E}_{rot}$ and that we have presented in this chapter. We assume that $|\Delta E_{rot}|$, given by equation (6.10), equals the observed energy of the burst event, E_{burst}, i.e.:

$$\frac{|\Delta P|}{P} = \frac{E_{burst} P^2}{2\pi^2 I}. \tag{6.11}$$

It is clear from table 6.2 that from the set of 9 potential rotation-powered pulsars only two have a firmly established glitch-outburst connection. These two sources are also the only sources with glitches detected and are: PSR J1849-0258 with a measured fractional change of period $|\Delta P|/P \sim (2 - 4.4) \times 10^{-6}$ (Kuiper and Hermsen, 2009) and 1E 1547.0-5408 with $|\Delta P|/P \approx 1.9 \times 10^{-6}$ (Kuiper et al., 2012). One way to compare the theory with observations is to plot the value of $\Delta P/P$ as a function of the neutron star mass (according to equation (6.11)) and compare the values theoretically predicted with the value given by observations. In figures 6.13 and 6.14 we plot this equation (6.11) as a function of the mass for the 7 of the 9 sources for which have been reported the observation of outbursts (see table 6.2). Is also plotted the observed value (gray-shaded area) of PSR J1846-0258 with the corresponding uncertainty. From this is possible infer a minimum mass for the neutron star by requiring that the entire moment of inertia is involved in the glitch and that the theoretical value of $|\Delta P|/P$ coincides with the observed value. For the case of PSR J1846-0258 are obtained two minimum masses, $M_{min} = 0.72 M_\odot$ and $M_{min} = 0.61 M_\odot$, for the global and local charge neutrality cases, respectively.

Another way to compare the theory with the observational data is substituting in equation (6.11) the moment of inertia I by $I_{glitch} = \eta I$, where $\eta \leq 1$, being I_{glitch} the moment of inertia powering the glitch. This allows to obtain a lower limit for the parameter η, $\eta_{min} = 0.20$ for the global charge neutrality case and $\eta = 0.18$ for the local charge neutrality case. In table 6.3 we show the theoretically predicted value of $|\Delta P|/P$ for the seven sources with known bursts energy, assuming the mass of the neutron star is larger than 1 $M_\odot$ and $\eta = 1$, in the cases of global and local charge neutrality.

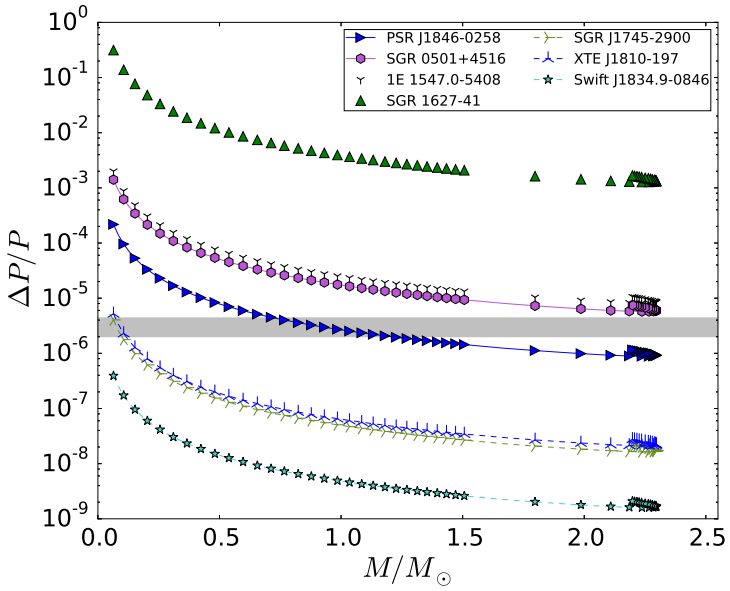

Figure 6.13: Inferred fractional change of rotation period during the glitch, $\Delta P/P$, obtained by equating the rotational energy gained during the glitch, $\Delta E_{\rm rot}$, to the energy of the burst, for globally neutral neutron stars that obey the GM1 equations of state. The gray-shaded area corresponds to the value of $|\Delta P|/P$ in the observed glitch of PSR J1846-0258 in June 2006 (Kuiper and Hermsen, 2009). This figure appears in Coelho et al. (2017).

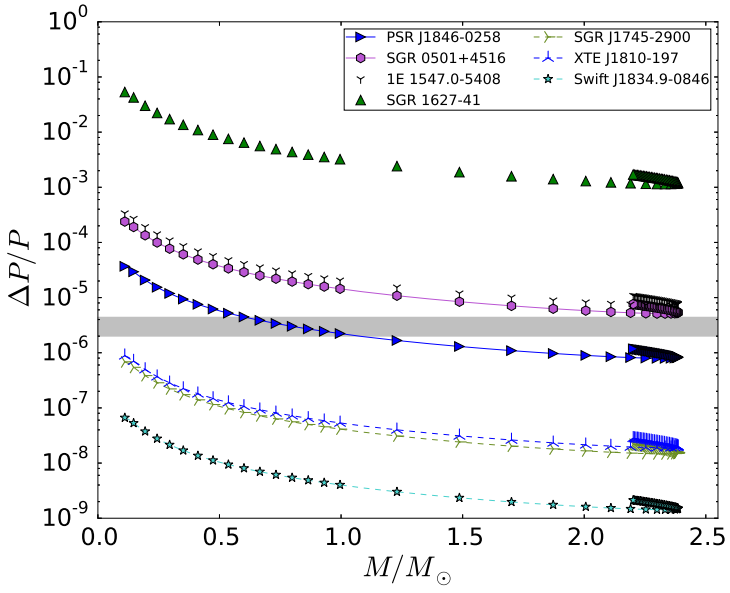

Figure 6.14: Inferred fractional change of rotation period during the glitch, $\Delta P/P$, obtained by equating the rotational energy gained during the glitch, $\Delta E_{\rm rot}$, to the energy of the burst, for locally neutral neutron stars that obey the GM1 equations of state. The gray-shaded area corresponds to the value of $|\Delta P|/P$ in the observed glitch of PSR J1846-0258 in June 2006 (Kuiper and Hermsen, 2009). This figure appears in Coelho et al. (2017).

Source	Year of burst	Tot. isot. burst en. (erg)	$\lvert\Delta P\rvert/P$ ($M > 1M_\odot$, GCN)	$\lvert\Delta P\rvert/P$ ($M > 1M_\odot$, LCN)
PSR J1846-0258	2006	4.8×10^{41}	$8.8 \times 10^{-7} - 2.6 \times 10^{-6}$	$7.9 \times 10^{-7} - 2.2 \times 10^{-6}$
1E 1547.0-5408	2009	1.1×10^{41}	$8.1 \times 10^{-6} - 2.4 \times 10^{-5}$	$7.2 \times 10^{-6} - 2.0 \times 10^{-5}$
XTE J1810-197	2004	4.0×10^{37}	$2.1 \times 10^{-8} - 6.3 \times 10^{-8}$	$1.9 \times 10^{-8} - 5.3 \times 10^{-8}$
SGR 1627-41	1998	1.0×10^{41}	$1.0 \times 10^{-5} - 3.8 \times 10^{-5}$	$1.1 \times 10^{-5} - 3.2 \times 10^{-5}$
SGR 0501+4516	2008	1.0×10^{40}	$5.7 \times 10^{-6} - 1.7 \times 10^{-5}$	$5.0 \times 10^{-6} - 1.4 \times 10^{-5}$
Swift J1834.9-0846	2011	1.5×10^{37}	$1.6 \times 10^{-9} - 4.8 \times 10^{-9}$	$1.4 \times 10^{-9} - 3.0 \times 10^{-9}$
SGR 1745.2900	2013	6.7×10^{37}	$1.61 \times 10^{-8} - 4.0 \times 10^{-8}$	$1.4 \times 10^{-8} - 4.1 \times 10^{-8}$

Table 6.3: Predicted values of $\lvert\Delta P\rvert/P$ assuming a rotationally powered model for global (GCN, column 4) and local (LCN, column 5) charge neutrality.

As we mentioned before, in table 6.2 we can appreciate that of the seven sources for which have been observed outburst explosions only two have observed glitches, i.e., there have been established a clear glitch-outburst connection. For the other sources which have not such a connection there are two possibilities: 1.) The glitch is missing due to the absence of timing monitoring of the source, as is the case of sources detected thanks to an outburst. 2.) The source timing was monitored and indeed the glitch was not detected when the outburst was observed. In this case, the outburst should have a magnetospheric origin.

By the way, we remind that there are also observed glitches without associated outburst activity (Pons and Rea, 2012). We remind also that a recent systematic analysis of the glitch-outburst connection in 5 AXPs done by Dib and Kaspi (2014) concluded: 1.) Glitches associated and not associated with outbursts or radiative changes show similar timing properties, i. e., outburst activity is not necessarily associated with large glitches. 2.) All glitches observed point to have their origin in the neutron star interior. This conclusion gives theoretical support to our interpretation of glitches associated to cracking occurring in the neutron star's interior. Whether a glitch can or not lead to observable radiative changes depends on specific properties of the phenomenon such as the energy budget and the localisation of the event in the star's interior (Dib and Kaspi, 2014), as well as the efficiency in converting mechanical energy into radiation, being this last aspect analysed in this chapter.

This glitch-outburst connection remains one of the most fundamental problems in the physics of AXPs/SGRs. We have seen that several issues deserve further investigation, whether observational or theoretical.

6.6 Possible additional evidence

Four of the nine sources considered here as potential rotationally-powered pulsars, namely 1E 1547.0-5408, SGR J1745-2900, XTE J1810-197 and PSR J1622-4950, are the only AXPs/SGRs with detected radio emission (see, e.g. Camilo et al., 2007, 2006, 2008; Eatough et al., 2013; Halpern et al., 2005; Kramer et al., 2007; Levin et al., 2010, 2012; Lobato et al., 2015; Olausen and Kaspi, 2014; Yusef-Zadeh et al., 2015). This property is common but not always present in ordinary rotationally powered pulsars, and in general is absent in AXPs/SGRs. In the case of the radio emission observed in these 4 AXPs/SGRs we have $L_{\rm radio} \ll L_{\rm X}$, a characteristic shared with ordinary rotationally powered pulsars. New observational facilities such as the Square Kilometer Array (SKA) are expected to bring light to the differences and similarities between different sources of radio emission such as rotating radio transients (RRATS), high field pulsars, AXPs/SGRs and ordinary radio pulsars (Tauris et al., 2015).

Eleven AXPs/SGRs have been identified as *transient* sources, showing flux variations by a factor $\sim (10 - 1000)$ over the quiescent level in timescales from days to months (see, for instance, Turolla et al., 2015). Seven of the nine potential

rotationally powered sources shown in table 6.2 are transient sources. The theoretical analysis of the evolution of the X-ray flux can constrain the properties of the neutron star and the emission geometry (see, e.g. Albano et al., 2010). Such constraints can help to constrain also the properties of the radio emission. Such an analysis is out of the scope of the present work and opens a window of new research which is worthy to be explored.

Another observational fact that gives support to the hypothesis of a neutron star nature for these 9 sources of table 6.2 is that six of them have possible associations with supernova remnants. If these associations are fully confirmed, then it is clear that the neutron star was born from the core-collapse of a massive star which triggered the supernova explosion. Further analysis of the supernova remnant and/or pulsar wind nebulae energetics and emission properties is ncessary to check their consistency with the hypothesis presented here of neutron star rotationally powering these sources.

6.7 Conclusions

Just as the analysis of Malheiro et al. (2012) was later improved by works like (Boshkayev et al., 2013) and (Rueda et al., 2013), where instead of assuming fiducial values it is assumed the structure of uniformly rotating white dwarfs to determine in a more accurate way the range of values for the radius or mass, in a similar way the analysis of Malheiro et al. (2012) of AXPs/SGRs as neutron stars with fiducial values was improved by the recent work of Coelho et al. (2017) where the entire range of Neutron Star parameters was explored considering the conditions of stability of the star.

It was found that fiducial parameters overestimate both the radiation efficiency and the surface magnetic field of pulsars. The number of potential rotationally powered pulsars was enlarged from 4 to 9. It was also obtained lower mass limits from the request $\dot{E}_{\rm rot} \geq L_X$. Then, an analysis was done of the hard X-ray emission, allowing to dismiss two sources, SGR J1745-2900 and SGR 0501+4516. However, in order to fully confirm these sources cannot longer be considered as potential rotationally powered pulsars, it is necessary to verify the accuracy of the estimated distances and to explore the possible contribution of their associated supernova remnants to the hard X-ray emission.

We also showed that if it is assumed that the blackbody component in the soft X-ray band of two additional sources, SGR 1900+14 and SGR 1806-20, is produced by the thermal reservoir of the neutron star, then the rotational energy loss is enough to cover their non-thermal X-ray luminosity. This implies that up to 11 AXPs/SGRs could be rotationally powered neutron stars. this argument could also, in principle, be applied to the other sources, lowering even more their radiation efficiency $L_X/\dot{E}_{\rm rot}$. We therefore argue that the observational uncertainties in the determination of the distances and/or luminosities, as well as the uncertainties in the neutron star nuclear equation of state, and as well as the

different interpretations of the observed spectrum still leave room for a possible explanation of the observed spectrum in terms of spin-down power for additional sources.

The transient activity was also checked within this model. It was explored the possibility that the energy released in outbursts, $E_{\rm burst}$, could be explained from the rotational energy gained in an associated glitch, $\Delta E_{\rm rot}$. The fact that this glitch outburst connection could be explained within this model reinforces the hypothesis that these sources are indeed rotationally powered (e.g., the cases of PSR J1846-0258 and PSR J1119-6127).

Finally, in section 6.6 we discussed possible additional evidence that supports the rotation-power nature of these sources: the radio emission is observed in four of the AXPs/SGRs and all of them are part of these nine sources. The radio emission is typical of ordinary pulsars but generally is absent in AXPs/SGRs. We also point out that seven of the nine sources belong to the group of the so-called transient sources (which are eleven in total). Within these seven transient rotation-powered objects we find four showing radio emission. We argue that the analysis of the varying X-ray flux can provide information on the neutron star properties and its magnetospheric geometry, improving also our understanding of the properties of the radio emission.

All this work shows us that, despite not all AXPs/SGRs are describable as rotationally powered pulsars, the fact that some of them do and some of them share properties with the traditional rotationally powered pulsars invites to proceed with the exploration of this possibility as a solution to solve the puzzle posed by these sources. Further investigation on the magnetospheric activity of these objects from a theoretical point of view could help to clarify many of the properties of these objects. It still remains open the explanation of the other objects that are not rotationally powered pulsars.

General conclusions

We have shown that the hypothetical ultra-magnetic super-Chandrasekhar WDs proposed by Das and Mukhopadhyay (2012, 2013) cannot exist in nature. Before reaching those stages where magnetic fields could have a significant non-negligible impact on the equation of state and the structure of the WD, they will be subjected to several instabilities that will forbid them to reach such levels of ultra-magnetism ($B \sim 10^{18}$ G). Several effects come into play, such as the inverse β-decay, the pynonuclear fusion reactions, the General Relativity instabilities, the breaking of the spherical symmetry or the General Relativity effects on the equation of state, as well as the violation of the Virial theorem. All these effects were ignored by the aforementioned authors, effects that have always been considered in the traditional treatment of WDs. Despite this analysis was done following the relativistic Feynman-Metropolis-Teller equation of state that does not consider the effects of the magnetic field, the instabilities come to place well before the magnetic field can have an appreciable or significant effect on the equation of state.

The magnetic WDs and their observational properties give us information about their possible origin and evolutionary channel. The answer is not unique and several models have been proposed. One of these evolutionary channels, the double degenerate merger, has been proposed as the most likely origin for the pulsar-like WD that could explain AXPs/SGRs. Despite not necessarily a WD could be the only explanation for AXPs/SGRs, as we have several proposed models besides this model and the magnetar model, the possibility of the existence of pulsar-like WDs could not be completely dismissed. Most of magnetic WDs, however, are very slow rotators, but at the beggining of their lifes, if they are the product of the merger of two white dwarfs, they should rotate relatively fast.

We have seen how the consideration of WD configurations with the most realistic equations of state can greatly improve the analysis on the parameters of the WD model. We therefore saw how we can get more precise values of the mass, radii, moment of inertia or magnetic field of WDs that rotate as fast as some of the reported AXPs/SGRs. This analysis shows us, for example, that the WDs rotating like AXPs/SGRs must be among the most massive WDs. We could see this as a consequence to ensure stability, the faster a WD rotates more mass is required to keep it gravitationally bound. This fact is also something remarkable, considering that also, on average, MWDs are more massive than their

non-magnetic counterparts (see chapter 3).

However, there is a limit where gravitation cannot longer counterbalance rotation and beyond it rotation tears up the star, being this limit known as the mass-shedding limit. We could verify that non of the reported AXPs/SGRs would violate this limit if they were WDs because their periods of rotation are clustered in the range $(2-12)$ s, while the minimum rotational periods for WDs obeying the relativistic Feynman-Metropolis-Teller equation of state are $\sim 0.3, 0.5, 0.7$ and 2.2 s for ^{4}He, ^{12}C, ^{16}O and ^{56} Fe WDs. So, the WDs rotating as fast as AXPs/SGRs are within the limits stablished by the instability boundaries.

The hypothesis of formation of these highly massive and MWDs as the outcome of double degenerate mergers can give account of an infrared excess detected in some AXPs/SGRs (see chapter 4). Besides this infrared excess, in some cases there is reported emission in the optical and ultraviolet spectrum. In the WD model this emission is naturally associated with the surface emission. However, it is difficult to detect a possible optical emission (if the WD model is correct) because of the large distances of AXPs/SGRs, their usual distances are of the order of several kpc, while most of the observed WDs, more exactly a 98%, are at a distance less than 1 kpc (Napiwotzki, 2009). This severely limits the possibility to check the theory with a direct observational evidence of the existence or not of the blackbody surface emission of the WD.

We showed that highly rotating WDs can produce $e^{-}e^{+}$ pairs in their magnetosphere from the decay of curvature radiation photons, i.e., we infered the structure parameters for which they are located above the WD pulsar deathline. We calculated the thermal emission produced by the polar cap heating by the pair-created particles that flow back to the WD surface due to the action of the induction electric field. Then, regarding the application to the WD model of AXPs/SGRs and to the emission in X-rays of these objects, we have shown that the inferred values of the WD parameters obtained from fitting with the magnetospheric emission, i.e. the blackbody spectrum observed in the soft X-rays of SGRs and AXPs, are in agreement with our previous estimates using the IR, optical, and UV data, and fall within the constraints imposed by the gravitational stability of the WD.

We have related the size of the spot of the blackbody component of AXPs/SGRs in X-rays with the size of the surface under the polar cap filled by the inward particle bombardment. We have shown that the spot area is much smaller than the polar cap area pointing to the existence of strong non-dipolar magnetic fields close to the WD surface.

We have used the heat transport and energy balance equations to show that, for the actual conditions of density and temperature under the polar cap, the hot spot re-radiates efficiently the heat proportioned by the inward particle bombardment.

The spot, which is aligned with the magnetic dipole moment of the WD, produces a pulsed emission in phase with the rotation period of the object. We showed that the theoretically inferred pulsed fraction of the WD spans from very low values all the way to unity depending on the viewing angles. Therefore it can also account for the observed pulsed fraction in SGRs and AXPs for appropriate choices of the viewing angles. In addition, the low-energy tail of the blackbody spectrum of the hotspot could produce a non-null pulsed fraction of the flux in the optical bands as well. However, this depends on the flux produced by the surface temperature of the WD which certainly dominates the light curve at low energies. We have also shown that the addition of a pulsed power-law component as the one observed in SGRs/AXPs does not modify appreciably the above result. The reason for this is that the non-thermal power-law component and the blackbody due to the surface hotspot have comparable fluxes and are in phase with each other. In those cases it is difficult to disentangle the single contributions to the pulsed fraction.

We therefore have shown that, as advanced in Rueda et al. (2013), indeed the blackbody observed in the optical wavelengths of SGRs and AXPs can be due to the surface temperature of the WD, while the one observed in the X-rays can be of magnetospheric origin. For the power-law component, also observed in the soft X-rays, a deeper analysis of processes such as curvature radiation, inverse Compton scattering, as well as other emission mechanisms, could be done in a future work.

Just as the analysis of Malheiro et al. (2012) was later improved by works like (Boshkayev et al., 2013) and (Rueda et al., 2013), where instead of assuming fiducial values it is assumed the structure of uniformly rotating white dwarfs to determine in a more accurate way the range of values for the radius or mass, in a similar way the analysis of Malheiro et al. (2012) of AXPs/SGRs as neutron stars with fiducial values was improved by the recent work of Coelho et al. (2017) where the entire range of Neutron Star parameters was explored considering the conditions of stability of the star.

It was found that fiducial parameters of NSs overestimate both the radiation efficiency and the surface magnetic field of pulsars. The number of potential rotationally powered pulsars (NSs) was enlarged from 4 to 9. It was also obtained lower mass limits from the request $\dot{E}_{\rm rot} \geq L_{\rm X}$. Then, an analysis was done of the hard X-ray emission, allowing to dismiss two sources, SGR J1745-2900 and SGR 0501+4516. However, in order to fully confirm these sources cannot longer be considered as potential rotationally powered pulsars, it is necessary to verify the accuracy of the estimated distances and to explore the possible contribution of their associated supernova remnants to the hard X-ray emission.

We also showed that if it is assumed that the blackbody component in the soft X-ray band of two additional sources, SGR 1900+14 and SGR 1806-20, is

produced by the thermal reservoir of the NS, then the rotational energy loss is enough to cover their non-thermal X-ray luminosity. This implies that up to 11 AXPs/SGRs could be rotationally powered neutron stars. this argument could also, in principle, be applied to the other sources, lowering even more their radiation efficiency $L_X/\dot{E}_{\rm rot}$. We therefore argue that the observational uncertainties in the determination of the distances and/or luminosities, as well as the uncertainties in the neutron star nuclear equation of state, and as well as the different interpretations of the observed spectrum still leave room for a possible explanation of the observed spectrum in terms of spin-down power for additional sources.

The transient activity was also checked within this model. It was explored the possibility that the energy released in outbursts, $E_{\rm burst}$, could be explained from the rotational energy gained in an associated glitch, $\Delta E_{\rm rot}$. The fact that this glitch outburst connection could be explained within this model reinforces the hypothesis that these sources are indeed rotationally powered (e.g., the cases of PSR J1846-0258 and PSR J1119-6127).

In section 6.6 we discussed possible additional evidence that support the rotation-power nature of these sources: the radio emission is observed in four of the AXPs/SGRs and all of them are part of these nine sources. The radio emission is typical of ordinary pulsars but generally is absent in AXPs/SGRs. We also point out that seven of the nine sources beling to the group of the so-called transient sources (which are eleven in total). Within these seven transient rotation-powered objects we find four showing radio emission. We argue that the analysis of the varying X-ray flux can provide information on the neutron star properties and its magnetospheric geometry, improving also our understanding of the properties of the radio emission.

Despite not all AXPs/SGRs are describable as rotationally powered pulsars, the fact that some of them do and some of them share properties with the traditional rotationally powered pulsars invites to proceed with the exploration of this possibility as a solution to solve the puzzle posed by these sources. Further investigation on the magnetospheric activity of these objects from a theoretical point of view could help to clarify many of the properties of these objects. It still remains open the explanation of the other objects that are not rotationally powered pulsars.

Appendix A

Heating and cooling of particle influx bombardment

We estimate in this appendix the efficiency of the particle bombardment in heating (and re-radiating) the surface area they hit. We follow the discussion in Gil and Melikidze (2002) and Gil et al. (2003) for the heat flow conditions in the polar cap surface of neutron stars, and extend it to the present case of magnetic WDs.

The particles arriving to the surface penetrate up to a depth that can be estimated using the concept of *radiation length* (Cheng and Ruderman, 1980). For a carbon composition, the radiation length is $\Sigma \approx 43$ g cm^{-2} (Tsai, 1974), so an electron would penetrate the WD surface up to a depth

$$\Delta z \approx \frac{\Sigma}{\rho} = 4.3 \times 10^{-3}\,\mathrm{cm}\left(\frac{10^4\,\mathrm{g\,cm^{-3}}}{\rho}\right). \tag{A.1}$$

With the knowledge of the thickness of the layer under the surface where the energy deposition occurs, we can proceed to estimate the properties of the diffusion and re-radiation of the kinetic energy of the particle influx using the heat transport and energy balance equations on the star's surface corresponding to the polar cap. The typically small distances (see equation (A.1)) allow us to introduce a plane-parallel approximation in the direction parallel to the magnetic field lines, say in the direction z orthogonal to the surface.

The energy balance can be simply written as

$$F_{\mathrm{rad}} = F_{\mathrm{heat}} + F_{\mathrm{cond}}, \tag{A.2}$$

where $F_{\mathrm{heat}} = e\Delta V \eta \rho_{\mathrm{GJ}} c$, $F_{\mathrm{cond}} = -\kappa \partial T/\partial z$ and $F_{\mathrm{rad}} = \sigma T^4$, with κ the thermal conductivity (along the z-direction).

Let us first estimate the characteristic cooling time. To do this, we switch off energy losses and heating terms in the energy balance equation (A.2), i.e., the

radiation flux is only given by conduction:

$$\sigma T^4 = -\kappa \frac{\partial T}{\partial z}, \tag{A.3}$$

which leads to the heat transport equation

$$c_v \frac{\partial T}{\partial t} = \frac{\partial}{\partial z}\left(\kappa \frac{\partial T}{\partial z}\right). \tag{A.4}$$

where c_v is the heat capacity per unit volume. We can therefore obtain the characteristic (e-folding) cooling and heating time assuming the quantities are uniform within the penetration depth Δz, i.e.

$$\Delta t_{\rm cool} = \frac{\Delta z^2 c_v}{\kappa}, \qquad \Delta t_{\rm heat} = \frac{c_v \Delta z}{\sigma T^3}. \tag{A.5}$$

We can now introduce the radiation to heating efficiency parameter

$$\epsilon \equiv \frac{F_{\rm rad}}{F_{\rm heat}} = \frac{1}{1 + \Delta t_{\rm heat}/\Delta t_{\rm cool}} = \frac{1}{1 + \kappa/(\sigma T^3 \Delta z)}, \tag{A.6}$$

which shows that in equilibrium, $\Delta t_{\rm heat} = \Delta t_{\rm cool}$, we have $\epsilon = 1/2$.

In estimating the spot temperature (5.12) we have assumed in equation (5.11) full re-radiation of the influx, namely we assumed $\epsilon = 1$. We proceed now to estimate the realistic values of ϵ from equation (A.6) to check our assumption. We compute the thermal conductivity from Itoh et al. (1993) and the heat capacity from Chabrier and Potekhin (1998); Potekhin and Chabrier (2000). For example, at a density $\rho = 10^3$ g cm^{-3} and $T = 10^6$ K, we have $c_v = 2.7 \times 10^{10}$ erg cm^{-3} K^{-1} and $\kappa \approx 4 \times 10^{11}$ erg cm^{-1} s^{-1} K^{-1}, and equation (A.6) gives $\epsilon \approx 0.86$. At $T = 10^7$ K, we have $c_v = 3.8 \times 10^{11}$ erg cm^{-3} K^{-1} and $\kappa \approx 3.4 \times 10^{13}$ erg cm^{-1} s^{-1} K^{-1} and $\epsilon \approx 1$.

Bibliography

Adams, F. C., C. J. Lada, and F. H. Shu (1987, January). Spectral evolution of young stellar objects. *ApJ 312*, 788–806.

Albano, A., R. Turolla, G. L. Israel, S. Zane, L. Nobili, and L. Stella (2010, October). A Unified Timing and Spectral Model for the Anomalous X-ray Pulsars XTE J1810-197 and CXOU J164710.2-455216. *ApJ 722*, 788–802.

Ambartsumyan, V. A. and G. S. Saakyan (1960, October). The Degenerate Superdense Gas of Elementary Particles. *Soviet Ast. 4*, 187.

Anand, S. P. S. (1965, July). On Chandrasekhar's Limiting Mass for Rotating White Dwarf Stars. *Proceedings of the National Academy of Science 54*, 23–26.

Angel, J. R. P. (1978). Magnetic white dwarfs. *ARA&A 16*, 487–519.

Angel, J. R. P., E. F. Borra, and J. D. Landstreet (1981, March). The magnetic fields of white dwarfs. *ApJS 45*, 457–474.

Angel, J. R. P. and J. D. Landstreet (1971a, February). Detection of Circular Polarization in a Second White Dwarf. *ApJ 164*, L15.

Angel, J. R. P. and J. D. Landstreet (1971b, May). Discovery of Periodic Variations in the Circular Polarization of the White Dwarf G195-19. *ApJ 165*, L71.

Antoniadis, J., P. C. C. Freire, N. Wex, T. M. Tauris, R. S. Lynch, M. H. van Kerkwijk, M. Kramer, C. Bassa, V. S. Dhillon, T. Driebe, J. W. T. Hessels, V. M. Kaspi, V. I. Kondratiev, N. Langer, T. R. Marsh, M. A. McLaughlin, T. T. Pennucci, S. M. Ransom, I. H. Stairs, J. van Leeuwen, J. P. W. Verbiest, and D. G. Whelan (2013, April). A Massive Pulsar in a Compact Relativistic Binary. *Science 340*, 448.

Antoniadis, J., M. H. van Kerkwijk, D. Koester, P. C. C. Freire, N. Wex, T. M. Tauris, M. Kramer, and C. G. Bassa (2012, July). The relativistic pulsar-white dwarf binary PSR J1738+0333 - I. Mass determination and evolutionary history. *MNRAS 423*, 3316–3327.

Armitage, P. J. and C. J. Clarke (1996, May). Magnetic braking of T Tauri stars. *MNRAS 280*, 458–468.

Arons, J. (2002). Theory of pulsar winds. In *34th COSPAR Scientific Assembly*, Volume 34 of *COSPAR Meeting*.

Arons, J. (2004). Theory of pulsar winds. *Advances in Space Research 33*, 466–474.

Arons, J. and E. T. Scharlemann (1979, August). Pair formation above pulsar polar caps - Structure of the low altitude acceleration zone. *ApJ 231*, 854–879.

Arutyunyan, G. G., D. M. Sedrakyan, and É. V. Chubaryan (1971, July). Rotating white dwarfs in the general relativity theory. *Astrophysics 7*, 274–280.

Atteia, J.-L., M. Boer, K. Hurley, M. Niel, G. Vedrenne, E. E. Fenimore, R. W. Klebesadel, J. G. Laros, A. V. Kuznetsov, R. A. Sunyaev, O. V. Terekhov, C. Kouveliotou, T. Cline, B. Dennis, U. Desai, and L. Orwig (1987, September). Localization, time histories, and energy spectra of a new type of recurrent high-energy transient source. *ApJ 320*, L105–L110.

Audi, G., A. H. Wapstra, and C. Thibault (2003, December). The AME2003 atomic mass evaluation . (II). Tables, graphs and references. *Nuclear Physics A 729*, 337–676.

Baade, W. and F. Zwicky (1934a, May). Cosmic Rays from Super-novae. *Proceedings of the National Academy of Science 20*, 259–263.

Baade, W. and F. Zwicky (1934b, May). On Super-novae. *Proceedings of the National Academy of Science 20*, 254–259.

Baade, W. and F. Zwicky (1934c, July). Remarks on Super-Novae and Cosmic Rays. *Physical Review 46*, 76–77.

Baade, W. and F. Zwicky (1934d, January). Super-Novae and Cosmic Rays. *Physical Review 45*, 138.

Barstow, M. A., S. Jordan, D. O'Donoghue, M. R. Burleigh, R. Napiwotzki, and M. K. Harrop-Allin (1995, December). RE J0317-853: the hottest known highly magnetic DA white dwarf. *MNRAS 277*, 971–985.

Baumgartner, W. H., J. Tueller, C. B. Markwardt, G. K. Skinner, S. Barthelmy, R. F. Mushotzky, P. A. Evans, and N. Gehrels (2013, August). The 70 Month Swift-BAT All-sky Hard X-Ray Survey. *ApJS 207*, 19.

Baym, G., H. A. Bethe, and C. J. Pethick (1971, November). Neutron star matter. *Nuclear Physics A 175*, 225–271.

Baym, G., C. Pethick, and P. Sutherland (1971, December). The Ground State of Matter at High Densities: Equation of State and Stellar Models. *ApJ 170*, 299.

Baym, G. and D. Pines (1971). Neutron starquakes and pulsar speedup. *Annals of Physics 66*, 816–835.

Beloborodov, A. M. (2002, February). Gravitational Bending of Light Near Compact Objects. *ApJ 566*, L85–L88.

Beloborodov, A. M. (2009, September). Untwisting Magnetospheres of Neutron Stars. *ApJ 703*, 1044–1060.

Belvedere, R., K. Boshkayev, J. A. Rueda, and R. Ruffini (2014, January). Uniformly rotating neutron stars in the global and local charge neutrality cases. *Nuclear Physics A 921*, 33–59.

Belvedere, R., D. Pugliese, J. A. Rueda, R. Ruffini, and S.-S. Xue (2012, June). Neutron star equilibrium configurations within a fully relativistic theory with strong, weak, electromagnetic, and gravitational interactions. *Nuclear Physics A 883*, 1–24.

Belvedere, R., J. A. Rueda, and R. Ruffini (2015, January). On the Magnetic Field of Pulsars with Realistic Neutron Star Configurations. *ApJ 799*, 23.

Benz, W., A. G. W. Cameron, W. H. Press, and R. L. Bowers (1990, January). Dynamic mass exchange in doubly degenerate binaries. I - 0.9 and 1.2 solar mass stars. *ApJ 348*, 647–667.

Bera, P. and D. Bhattacharya (2014, December). Mass-radius relation of strongly magnetized white dwarfs: nearly independent of Landau quantization. *MNRAS 445*, 3951–3958.

Berdyugin, A. V. and V. Piirola (1999, December). Polarization variability in magnetic white dwarfs GD 229 and G 240-72. *A&A 352*, 619–622.

Bernardini, F., D. de Martino, M. Falanga, K. Mukai, G. Matt, J.-M. Bonnet-Bidaud, N. Masetti, and M. Mouchet (2012, June). Characterization of new hard X-ray cataclysmic variables. *A&A 542*, A22.

Bernardini, F., D. de Martino, K. Mukai, M. Falanga, I. Andruchow, J.-M. Bonnet-Bidaud, N. Masetti, D. H. G. Buitrago, M. Mouchet, and G. Tovmassian (2013, November). On the nature of the hard X-ray sources SWIFT J1907.3-2050, IGR J12123-5802 and IGR J19552+0044. *MNRAS 435*, 2822–2834.

Beskin, V. S., A. V. Gurevich, and I. N. Istomin (1988, July). Theory of the radio emission of pulsars. *Ap&SS 146*, 205–281.

Beuermann, K. (1999). Magnetic cataclysmic variables: the state of the art after ROSAT. In B. Aschenbach and M. J. Freyberg (Eds.), *Highlights in X-ray Astronomy*, Volume 272, pp. 410.

Beuermann, K. and K. Reinsch (2002, January). The high-field magnetic white dwarf LP790-29: Not a fast rotator. *A&A 381*, 487–490.

Bibby, J. L., P. A. Crowther, J. P. Furness, and J. S. Clark (2008, May). A downward revision to the distance of the 1806-20 cluster and associated magnetar from Gemini Near-Infrared Spectroscopy. *MNRAS 386*, L23–L27.

Bird, A. J., A. Bazzano, L. Bassani, F. Capitanio, M. Fiocchi, A. B. Hill, A. Malizia, V. A. McBride, S. Scaringi, V. Sguera, J. B. Stephen, P. Ubertini, A. J. Dean, F. Lebrun, R. Terrier, M. Renaud, F. Mattana, D. Götz, J. Rodriguez, G. Belanger, R. Walter, and C. Winkler (2010, January). The Fourth IBIS/ISGRI Soft Gamma-ray Survey Catalog. *ApJS 186*, 1–9.

Blandford, R. D. (1975, March). Amplification of radiation by relativistic particles in a strong magnetic field. *MNRAS 170*, 551–557.

Blandford, R. D. and R. W. Romani (1988, October). On the interpretation of pulsar braking indices. *MNRAS 234*, 57P–60P.

Bogovalov, S. V. (1999, September). On the physics of cold MHD winds from oblique rotators. *A&A 349*, 1017–1026.

Boguta, J. and A. R. Bodmer (1977, December). Relativistic calculation of nuclear matter and the nuclear surface. *Nuclear Physics A 292*, 413–428.

Bonazzola, S., F. Mottez, and J. Heyvaerts (2015, January). General solution for the vacuum electromagnetic field in the surroundings of a rotating star. *A&A 573*, A51.

Boshkayev, K., L. Izzo, J. A. Rueda Hernandez, and R. Ruffini (2013, July). SGR 0418+5729, Swift J1822.3-1606, and 1E 2259+586 as massive, fast-rotating, highly magnetized white dwarfs. *A&A 555*, A151.

Boshkayev, K., J. A. Rueda, R. Ruffini, and I. Siutsou (2013, January). On General Relativistic Uniformly Rotating White Dwarfs. *ApJ 762*, 117.

Boshkayev, K. A., J. A. Rueda, B. A. Zhami, Z. A. Kalymova, and G. S. Balgymbekov (2016, March). Equilibrium structure of white dwarfs at finite temperatures. In *International Journal of Modern Physics Conference Series*, Volume 41 of *International Journal of Modern Physics Conference Series*, pp. 1660129.

Brinkworth, C. S., M. R. Burleigh, K. Lawrie, T. R. Marsh, and C. Knigge (2013, August). Measuring the Rotational Periods of Isolated Magnetic White Dwarfs. *ApJ 773*, 47.

Cáceres, D. L., S. M. de Carvalho, J. G. Coelho, R. C. R. de Lima, and J. A. Rueda (2017, March). Thermal X-ray emission from massive, fast rotating, highly magnetized white dwarfs. *MNRAS 465*, 4434–4440.

Cáceres, D. L., J. A. Rueda, and R. Ruffini (2014, September). On the stability of ultra-magnetized white dwarfs. *Journal of Korean Physical Society 65*, 846–849.

Camenzind, M. (1986, July). Hydromagnetic flows from rapidly rotating compact objects. I - Cold relativistic flows from rapid rotators. *A&A 162*, 32–44.

Cameron, A. G. (1959, November). Neutron Star Models. *ApJ 130*, 884.

Camilo, F., I. Cognard, S. M. Ransom, J. P. Halpern, J. Reynolds, N. Zimmerman, E. V. Gotthelf, D. J. Helfand, P. Demorest, G. Theureau, and D. C. Backer (2007, July). The Magnetar XTE J1810-197: Variations in Torque, Radio Flux Density, and Pulse Profile Morphology. *ApJ 663*, 497–504.

Camilo, F., S. M. Ransom, J. P. Halpern, J. Reynolds, D. J. Helfand, N. Zimmerman, and J. Sarkissian (2006, August). Transient pulsed radio emission from a magnetar. *Nature 442*, 892–895.

Camilo, F., J. Reynolds, S. Johnston, J. P. Halpern, and S. M. Ransom (2008, May). The Magnetar 1E 1547.0-5408: Radio Spectrum, Polarimetry, and Timing. *ApJ 679*, 681–686.

Cerutti, B. and A. M. Beloborodov (2016, December). Electrodynamics of Pulsar Magnetospheres. *Space Sci. Rev.*.

Chabrier, G. and A. Y. Potekhin (1998, October). Equation of state of fully ionized electron-ion plasmas. *Phys. Rev. E 58*, 4941–4949.

Chaichian, M., S. S. Masood, C. Montonen, A. Pérez Martínez, and H. Pérez Rojas (2000, June). Quantum Magnetic Collapse. *Physical Review Letters 84*, 5261–5264.

Chamel, N., A. F. Fantina, and P. J. Davis (2013, October). Stability of super-Chandrasekhar magnetic white dwarfs. *Phys. Rev. D 88*(8), 081301.

Chamel, N., R. L. Pavlov, L. M. Mihailov, C. J. Velchev, Z. K. Stoyanov, Y. D. Mutafchieva, M. D. Ivanovich, J. M. Pearson, and S. Goriely (2012, November). Properties of the outer crust of strongly magnetized neutron stars from Hartree-Fock-Bogoliubov atomic mass models. *Phys. Rev. C 86*(5), 055804.

Chandrasekhar, S. (1931, July). The Maximum Mass of Ideal White Dwarfs. *ApJ 74*, 81.

Chandrasekhar, S. and E. Fermi (1953, July). Problems of Gravitational Stability in the Presence of a Magnetic Field. *ApJ 118*, 116.

Chandrasekhar, S. and E. Fermi (1955, September). Errata. *ApJ 122*, 208.

Chatterjee, P., L. Hernquist, and R. Narayan (2000, May). An Accretion Model for Anomalous X-Ray Pulsars. *ApJ 534*, 373–379.

Chen, K. and M. Ruderman (1993, January). Pulsar death lines and death valley. *ApJ 402*, 264–270.

Chen, W. C. and X. D. Li (2006, April). Why the braking indices of young pulsars are less than 3? *A&A 450*, L1–L4.

Cheng, A. F. and M. A. Ruderman (1977, June). Pair-production discharges above pulsar polar caps. *ApJ 214*, 598–606.

Cheng, A. F. and M. A. Ruderman (1980, January). Particle acceleration and radio emission above pulsar polar caps. *ApJ 235*, 576–586.

Cheng, K. S., C. Ho, and M. Ruderman (1986a, January). Energetic radiation from rapidly spinning pulsars. I - Outer magnetosphere gaps. II - VELA and Crab. *ApJ 300*, 500–539.

Cheng, K. S., C. Ho, and M. Ruderman (1986b, January). Energetic Radiation from Rapidly Spinning Pulsars. II. VELA and Crab. *ApJ 300*, 522.

Cheng, K. S. and L. Zhang (1999, April). Multicomponent X-Ray Emissions from Regions near or on the Pulsar Surface. *ApJ 515*, 337–350.

Chiang, E. I. and P. Goldreich (1997, November). Spectral Energy Distributions of T Tauri Stars with Passive Circumstellar Disks. *ApJ 490*, 368–376.

Chukwude, A. E., A. A. Baiden, and C. C. Onuchukwu (2010, June). Measurements of radio pulsar braking indices. *A&A 515*, A21.

Ciolfi, R., V. Ferrari, and L. Gualtieri (2010, August). Structure and deformations of strongly magnetized neutron stars with twisted-torus configurations. *MNRAS 406*, 2540–2548.

Coelho, J. G., D. L. Cáceres, R. C. R. de Lima, M. Malheiro, J. A. Rueda, and R. Ruffini (2017, March). The rotation-powered nature of some soft gamma-ray repeaters and anomalous X-ray pulsars. *A&A 599*, A87.

Coelho, J. G. and M. Malheiro (2014, February). Magnetic dipole moment of soft gamma-ray repeaters and anomalous X-ray pulsars described as massive and magnetic white dwarfs. *PASJ 66*, 14.

Coelho, J. G., R. M. Marinho, M. Malheiro, R. Negreiros, D. L. Cáceres, J. A. Rueda, and R. Ruffini (2014, October). Dynamical Instability of White Dwarfs and Breaking of Spherical Symmetry Under the Presence of Extreme Magnetic Fields. *ApJ 794*, 86.

Contopoulos, I., D. Kazanas, and C. Fendt (1999, January). The Axisymmetric Pulsar Magnetosphere. *ApJ 511*, 351–358.

Contopoulos, I. and A. Spitkovsky (2006, June). Revised Pulsar Spin-down. *ApJ 643*, 1139–1145.

Cropper, M. (1990, December). The Polars. *Space Sci. Rev. 54*, 195–295.

Das, U. and B. Mukhopadhyay (2012, August). Strongly magnetized cold degenerate electron gas: Mass-radius relation of the magnetized white dwarf. *Phys. Rev. D 86*(4), 042001.

Das, U. and B. Mukhopadhyay (2013, February). New Mass Limit for White Dwarfs: Super-Chandrasekhar Type Ia Supernova as a New Standard Candle. *Physical Review Letters 110*(7), 071102.

Das, U. and B. Mukhopadhyay (2014, June). Maximum mass of stable magnetized highly super-Chandrasekhar white dwarfs: stable solutions with varying magnetic fields. *J. Cosmology Astropart. Phys. 6*, 050.

Das, U., B. Mukhopadhyay, and A. R. Rao (2013, April). A Possible Evolutionary Scenario of Highly Magnetized Super-Chandrasekhar White Dwarfs: Progenitors of Peculiar Type Ia Supernovae. *ApJ 767*, L14.

Davies, S. R., M. J. Coe, and K. S. Wood (1990, July). HEAO-1 observations of the X-ray pulsar 1E2259 + 586. *MNRAS 245*, 268–274.

Davis, L. (1947, October). Stellar Electromagnetic Fields. *Physical Review 72*, 632–633.

de Carvalho, S. M., M. Rotondo, J. A. Rueda, and R. Ruffini (2014, January). Relativistic Feynman-Metropolis-Teller treatment at finite temperatures. *Phys. Rev. C 89*(1), 015801.

de Carvalho, S. M., J. A. Rueda, M. Rotondo, C. Argüelles, and R. Ruffini (2013, January). The Relativistic Feynman Metropolis Teller Theory at Zero and Finite Temperatures. In *International Journal of Modern Physics Conference Series*, Volume 23 of *International Journal of Modern Physics Conference Series*, pp. 244–247.

Deutsch, A. J. (1955, January). The electromagnetic field of an idealized star in rigid rotation in vacuo. *Annales d'Astrophysique 18*, 1.

Dhillon, V. S., T. R. Marsh, F. Hulleman, M. H. van Kerkwijk, A. Shearer, S. P. Littlefair, F. P. Gavriil, and V. M. Kaspi (2005, October). High-speed, multicolour optical photometry of the anomalous X-ray pulsar 4U 0142+61 with ULTRACAM. *MNRAS 363*, 609–614.

Dib, R. and V. M. Kaspi (2014, March). 16 yr of RXTE Monitoring of Five Anomalous X-Ray Pulsars. *ApJ 784*, 37.

Dib, R., V. M. Kaspi, and F. P. Gavriil (2007, September). 10 Years of RXTE Monitoring of the Anomalous X-Ray Pulsar 4U 0142+61: Long-Term Variability. *ApJ 666*, 1152–1164.

Dib, R., V. M. Kaspi, and F. P. Gavriil (2009, September). Rossi X-Ray Timing Explorer Monitoring of the Anomalous X-ray Pulsar 1E 1048.1 - 5937: Long-term Variability and the 2007 March Event. *ApJ 702*, 614–630.

Dirac, P. A. M. (1930). Note on Exchange Phenomena in the Thomas Atom. *Proceedings of the Cambridge Philosophical Society 26*, 376.

Dobbie, P. D., R. Baxter, B. Külebi, Q. A. Parker, D. Koester, S. Jordan, N. Lodieu, and F. Euchner (2012, March). Two new young, wide, magnetic + non-magnetic double-degenerate binary systems. *MNRAS 421*, 202–212.

Dobbie, P. D., B. Külebi, S. L. Casewell, M. R. Burleigh, Q. A. Parker, R. Baxter, K. A. Lawrie, S. Jordan, and D. Koester (2013, January). High-field magnetic white dwarfs as the progeny of early-type stars? *MNRAS 428*, L16–L20.

Dong, J. M., W. Zuo, P. Yin, and J. Z. Gu (2014, January). Comment on "New Mass Limit for White Dwarfs: Super-Chandrasekhar Type Ia Supernova as a New Standard Candle". *Physical Review Letters 112*(3), 039001.

Dufour, P., J. Liebert, G. Fontaine, and N. Behara (2007, November). White dwarf stars with carbon atmospheres. *Nature 450*, 522–524.

Duncan, R. C. and C. Thompson (1992, June). Formation of very strongly neutron stars - Implications for gamma-ray bursts. *ApJ 392*, L9–L13.

Dupuis, J., P. Chayer, S. Vennes, N. F. Allard, and G. Hébrard (2003, November). Far Ultraviolet Spectroscopic Explorer Observation of the Ultramassive White Dwarf PG 1658+441. *ApJ 598*, 486–491.

Durant, M., O. Kargaltsev, and G. G. Pavlov (2011, December). Search for the Optical Counterpart to SGR 0418+5729. *ApJ 742*, 77.

Durant, M. and M. H. van Kerkwijk (2006, November). Multiwavelength Variability of the Magnetar 4U 0142+61. *ApJ 652*, 576–583.

Durisen, R. H. (1975, July). Upper mass limits for stable rotating white dwarfs. *ApJ 199*, 179–183.

Eatough, R. P., H. Falcke, R. Karuppusamy, K. J. Lee, D. J. Champion, E. F. Keane, G. Desvignes, D. H. F. M. Schnitzeler, L. G. Spitler, M. Kramer, B. Klein, C. Bassa, G. C. Bower, A. Brunthaler, I. Cognard, A. T. Deller, P. B. Demorest, P. C. C. Freire, A. Kraus, A. G. Lyne, A. Noutsos, B. Stappers, and N. Wex (2013, September). A strong magnetic field around the supermassive black hole at the centre of the Galaxy. *Nature 501*, 391–394.

Esposito, P., S. Mereghetti, A. Tiengo, S. Zane, R. Turolla, D. Götz, N. Rea, N. Kawai, M. Ueno, G. L. Israel, L. Stella, and M. Feroci (2007, December). SGR 1806-20 about two years after the giant flare: Suzaku, XMM-Newton and INTEGRAL observations. *A&A 476*, 321–330.

Fahlman, G. G. and P. C. Gregory (1981, September). An X-ray pulsar in SNR G109.1-1.0. *Nature 293*, 202–204.

Federbush, P., T. Luo, and J. Smoller (2015, February). Existence of Magnetic Compressible Fluid Stars. *Archive for Rational Mechanics and Analysis 215*, 611–631.

Ferrario, L., D. de Martino, and B. T. Gänsicke (2015, October). Magnetic White Dwarfs. *Space Sci. Rev. 191*, 111–169.

Ferrario, L., S. Vennes, and D. T. Wickramasinghe (1998, August). 1RXS J0823.6-2525: a new ultramassive magnetic white dwarf. *MNRAS 299*, L1–L4.

Ferrario, L., S. Vennes, D. T. Wickramasinghe, J. A. Bailey, and D. J. Christian (1997, November). EUVE J0317-855 A rapidly rotating, high-field magnetic white dwarf. *MNRAS 292*, 205.

Ferrario, L. and D. Wickramasinghe (2006, April). Modelling of isolated radio pulsars and magnetars on the fossil field hypothesis. *MNRAS 367*, 1323–1328.

Ferrario, L., D. Wickramasinghe, J. Liebert, and K. A. Williams (2005, August). The open-cluster initial-final mass relationship and the high-mass tail of the white dwarf distribution. *MNRAS 361*, 1131–1135.

Ferrario, L. and D. T. Wickramasinghe (2010, November). White dwarf pairing functions. In K. Werner and T. Rauch (Eds.), *American Institute of Physics Conference Series*, Volume 1273 of *American Institute of Physics Conference Series*, pp. 378–383.

Ferraro, V. C. A. (1954, March). On the Equilibrium of Magnetic Stars. *ApJ 119*, 407.

Ferraro, V. C. A. and V. B. Bhatia (1967, January). Corotation and Solar Wind in the Solar Corona and Interplanetary Medium. *ApJ 147*, 220.

Ferraro, V. C. A. and H. W. Unthank (1949). On the Solar Electric Field Engendered by the Rotation of the Sun in its Magnetic Field. *MNRAS 109*, 462.

Ferreirinho, J., R. Ruffini, and L. Stella (1980, April). On the relativistic Thomas-Fermi model. *Physics Letters B 91*, 314–316.

Feynman, R. P., N. Metropolis, and E. Teller (1949, May). Equations of State of Elements Based on the Generalized Fermi-Thomas Theory. *Physical Review 75*, 1561–1573.

Fontaine, G. and P. Brassard (2008, October). The Pulsating White Dwarf Stars. *PASP 120*, 1043.

Forman, W., C. Jones, L. Cominsky, P. Julien, S. Murray, G. Peters, H. Tananbaum, and R. Giacconi (1978, December). The fourth Uhuru catalog of X-ray sources. *ApJS 38*, 357–412.

Forster, H., W. Strupat, W. Rosner, G. Wunner, H. Ruder, and H. Herold (1984, April). Hydrogen atoms in arbitrary magnetic fields. II. Bound-bound transitions. *Journal of Physics B Atomic Molecular Physics 17*, 1301–1319.

Fowler, R. H. (1926, December). On dense matter. *MNRAS 87*, 114–122.

Friedman, J. L., J. R. Ipser, and R. D. Sorkin (1988, February). Turning-point method for axisymmetric stability of rotating relativistic stars. *ApJ 325*, 722–724.

García-Berro, E., M. Kilic, and S. O. Kepler (2016, January). Magnetic white dwarfs: Observations, theory and future prospects. *International Journal of Modern Physics D 25*, 1630005.

García-Berro, E., P. Lorén-Aguilar, G. Aznar-Siguán, S. Torres, J. Camacho, L. G. Althaus, A. H. Córsico, B. Külebi, and J. Isern (2012, April). Double Degenerate Mergers as Progenitors of High-field Magnetic White Dwarfs. *ApJ 749*, 25.

García-Berro, E., P. Lorén-Aguilar, A. G. Pedemonte, J. Isern, P. Bergeron, P. Dufour, and P. Brassard (2007, June). Evidence of a Merger of Binary White Dwarfs: The Case of GD 362. *ApJ 661*, L179–L182.

Garstang, R. H. (1977, February). REVIEW: Atoms in high magnetic fields (white dwarfs). *Reports on Progress in Physics 40*, 105–154.

Gasques, L. R., A. V. Afanasjev, E. F. Aguilera, M. Beard, L. C. Chamon, P. Ring, M. Wiescher, and D. G. Yakovlev (2005, August). Nuclear fusion in dense matter: Reaction rate and carbon burning. *Phys. Rev. C 72*(2), 025806.

Gavriil, F. P., V. M. Kaspi, and P. M. Woods (2002, September). Magnetar-like X-ray bursts from an anomalous X-ray pulsar. *Nature 419*, 142–144.

Gavriil, F. P., V. M. Kaspi, and P. M. Woods (2004, June). A Comprehensive Study of the X-Ray Bursts from the Magnetar Candidate 1E 2259+586. *ApJ 607*, 959–969.

Geroyannis, V. S. and A. A. Hadjopoulos (1989, July). Models of white dwarfs under rapid uniform or differential rotation - Numerical results. *ApJS 70*, 661–677.

Giacconi, R., H. Gursky, E. Kellogg, E. Schreier, and H. Tananbaum (1971, July). Discovery of Periodic X-Ray Pulsations in Centaurus X-3 from UHURU. *ApJ 167*, L67.

Gil, J. and G. I. Melikidze (2002, October). On the Formation of Inner Vacuum Gaps in Radio Pulsars. *ApJ 577*, 909–916.

Gil, J., G. I. Melikidze, and U. Geppert (2003, August). Drifting subpulses and inner accelerationregions in radio pulsars. *A&A 407*, 315–324.

Gil, J. A. and M. Sendyk (2000, September). Spark Model for Pulsar Radiation Modulation Patterns. *ApJ 541*, 351–366.

Girven, J., B. T. Gänsicke, B. Külebi, D. Steeghs, S. Jordan, T. R. Marsh, and D. Koester (2010, May). PG1258+593 and its common proper motion magnetic white dwarf counterpart. *MNRAS 404*, 159–165.

Glendenning, N. K. and S. A. Moszkowski (1991, October). Reconciliation of neutron-star masses and binding of the Lambda in hypernuclei. *Physical Review Letters 67*, 2414–1417.

Göhler, E., J. Wilms, and R. Staubert (2005, April). XMM-Newton observation of the anomalous X-ray pulsar 4U 0142+61. *A&A 433*, 1079–1083.

Gold, T. (1962). Interchange and Rotation of the Earth Field Lines. *Journal of the Physical Society of Japan Supplement 17*, 187.

Gold, T. (1968, May). Rotating Neutron Stars as the Origin of the Pulsating Radio Sources. *Nature 218*, 731–732.

Gold, T. (1969, January). Rotating Neutron Stars and the Nature of Pulsars. *Nature 221*, 25–27.

Goldreich, P. and W. H. Julian (1969, August). Pulsar Electrodynamics. *ApJ 157*, 869.

Goldreich, P. and W. H. Julian (1970, June). Stellar Winds. *ApJ 160*, 971.

Gutiérrez, J., R. Canal, and E. García-Berro (2005, May). The gravitational collapse of ONe electron-degenerate cores and white dwarfs: The role of ^{24}Mg and ^{12}C revisited. *A&A 435*, 231–237.

Gutierrez, J., E. Garcia-Berro, I. Iben, Jr., J. Isern, J. Labay, and R. Canal (1996, March). The Final Evolution of ONeMg Electron-Degenerate Cores. *ApJ 459*, 701.

Haberl, F. (2007, April). The magnificent seven: magnetic fields and surface temperature distributions. *Ap&SS 308*, 181–190.

Halpern, J. P., E. V. Gotthelf, R. H. Becker, D. J. Helfand, and R. L. White (2005, October). Discovery of Radio Emission from the Transient Anomalous X-Ray Pulsar XTE J1810-197. *ApJ 632*, L29–L32.

Hamada, T. and E. E. Salpeter (1961, November). Models for Zero-Temperature Stars. *ApJ 134*, 683.

Hamil, O., J. R. Stone, M. Urbanec, and G. Urbancová (2015, March). Braking index of isolated pulsars. *Phys. Rev. D 91*(6), 063007.

Harding, A. K., I. Contopoulos, and D. Kazanas (1999, November). Magnetar Spin-Down. *ApJ 525*, L125–L128.

Harding, A. K. and A. G. Muslimov (1998, November). Particle Acceleration Zones above Pulsar Polar Caps: Electron and Positron Pair Formation Fronts. *ApJ 508*, 328–346.

Harding, A. K. and A. G. Muslimov (2001, August). Pulsar Polar Cap Heating and Surface Thermal X-Ray Emission. I. Curvature Radiation Pair Fronts. *ApJ 556*, 987–1001.

Harding, A. K. and A. G. Muslimov (2002, April). Pulsar Polar Cap Heating and Surface Thermal X-Ray Emission. II. Inverse Compton Radiation Pair Fronts. *ApJ 568*, 862–877.

Harding, A. K., A. G. Muslimov, and B. Zhang (2002, September). Regimes of Pulsar Pair Formation and Particle Energetics. *ApJ 576*, 366–375.

Harrison, B. K., K. S. Thorne, M. Wakano, and J. A. Wheeler (1965). *Gravitation Theory and Gravitational Collapse*.

Hartle, J. B. (1967, December). Slowly Rotating Relativistic Stars. I. Equations of Structure. *ApJ 150*, 1005.

Hearn, D. R., J. A. Richardson, and G. W. Clark (1976, November). Detection of soft X-ray emission from an unidentified source at high galactic latitude. *ApJ 210*, L23–L26.

Hellier, C. (1994, November). A ROSAT observation of the X-ray pulsars X0142+614 and X0146+612. *MNRAS 271*, L21–L24.

Hellier, C. (2001, January). *Cataclysmic Variable Stars*.

Hewish, A., S. J. Bell, J. D. H. Pilkington, P. F. Scott, and R. A. Collins (1968, February). Observation of a Rapidly Pulsating Radio Source. *Nature 217*, 709–713.

Hicken, M., P. M. Garnavich, J. L. Prieto, S. Blondin, D. L. DePoy, R. P. Kirshner, and J. Parrent (2007, November). The Luminous and Carbon-rich Supernova 2006gz: A Double Degenerate Merger? *ApJ 669*, L17–L20.

Hirotani, K. (2006, December). Particle Accelerator in Pulsar Magnetospheres: Super-Goldreich-Julian Current with Ion Emission from the Neutron Star Surface. *ApJ 652*, 1475–1493.

Hirotani, K. (2013, April). Luminosity Evolution of Gamma-Ray Pulsars. *ApJ 766*, 98.

Hollands, M. A., B. T. Gänsicke, and D. Koester (2015, June). The incidence of magnetic fields in cool DZ white dwarfs. *MNRAS 450*, 681–690.

Hones, Jr., E. W. and J. E. Bergeson (1965, October). Electric Field Generated by a Rotating Magnetized Sphere. *J. Geophys. Res. 70*, 4951–4958.

Howell, D. A., M. Sullivan, P. E. Nugent, R. S. Ellis, A. J. Conley, D. Le Borgne, R. G. Carlberg, J. Guy, D. Balam, S. Basa, D. Fouchez, I. M. Hook, E. Y. Hsiao, J. D. Neill, R. Pain, K. M. Perrett, and C. J. Pritchet (2006, September). The type Ia supernova SNLS-03D3bb from a super-Chandrasekhar-mass white dwarf star. *Nature 443*, 308–311.

Hoyle, F., J. V. Narlikar, and J. A. Wheeler (1964, August). Electromagnetic Waves from Very Dense Stars. *Nature 203*, 914–916.

Hu, R.-Y. and Y.-Q. Lou (2009, June). Magnetized massive stars as magnetar progenitors. *MNRAS 396*, 878–886.

Hulleman, F., A. F. Tennant, M. H. van Kerkwijk, S. R. Kulkarni, C. Kouveliotou, and S. K. Patel (2001, December). A Possible Faint Near-Infrared Counterpart to the Anomalous X-Ray Pulsar 1E 2259+586. *ApJ 563*, L49–L52.

Hulleman, F., M. H. van Kerkwijk, and S. R. Kulkarni (2000, December). An optical counterpart to the anomalous X-ray pulsar 4U0142+61. *Nature 408*, 689–692.

Hulleman, F., M. H. van Kerkwijk, and S. R. Kulkarni (2004, March). The Anomalous X-ray Pulsar 4U 0142+61: Variability in the infrared and a spectral break in the optical. *A&A 416*, 1037–1045.

Hurley, J. R., C. A. Tout, D. T. Wickramasinghe, L. Ferrario, and P. D. Kiel (2010, March). Formation of binary millisecond pulsars by accretion-induced collapse of white dwarfs. *MNRAS 402*, 1437–1448.

Hurley, K., T. Cline, E. Mazets, S. Barthelmy, P. Butterworth, F. Marshall, D. Palmer, R. Aptekar, S. Golenetskii, V. Il'Inskii, D. Frederiks, J. McTiernan, R. Gold, and J. Trombka (1999, January). A giant periodic flare from the soft γ-ray repeater SGR1900+14. *Nature 397*, 41–43.

Iben, Jr., I. (1990, April). On the consequences of low-mass white dwarf mergers. *ApJ 353*, 215–235.

Iben, Jr., I. and A. V. Tutukov (1984, February). Supernovae of type I as end products of the evolution of binaries with components of moderate initial mass (M not greater than about 9 solar masses). *ApJS 54*, 335–372.

Ilkov, M. and N. Soker (2012, January). Type Ia supernovae from very long delayed explosion of core-white dwarf merger. *MNRAS 419*, 1695–1700.

Itoh, N., H. Hayashi, and Y. Kohyama (1993, November). Electrical and Thermal Conductivities of Dense Matter in the Crystalline Lattice Phase. III. Inclusion of Lower Densities. *ApJ 418*, 405.

James, R. A. (1964, August). The Structure and Stability of Rotating Gas Masses. *ApJ 140*, 552.

Ji, S., R. T. Fisher, E. García-Berro, P. Tzeferacos, G. Jordan, D. Lee, P. Lorén-Aguilar, P. Cremer, and J. Behrends (2013, August). The Post-merger Magnetized Evolution of White Dwarf Binaries: The Double-degenerate Channel of Sub-Chandrasekhar Type Ia Supernovae and the Formation of Magnetized White Dwarfs. *ApJ 773*, 136.

Jordan, S. and S. Friedrich (2002, February). Search for variations in circular-polarization spectra of the magnetic white dwarf LP 790-29. *A&A 383*, 519–523.

Jordan, S., P. Schmelcher, W. Becken, and W. Schweizer (1998, August). Evidence for helium in the magnetic white dwarf GD 229. *A&A 336*, L33–L36.

Jura, M. (2003, February). A Tidally Disrupted Asteroid around the White Dwarf G29-38. *ApJ 584*, L91–L94.

Kaneko, Y., E. Göğüş, C. Kouveliotou, J. Granot, E. Ramirez-Ruiz, A. J. van der Horst, A. L. Watts, M. H. Finger, N. Gehrels, A. Pe'er, M. van der Klis, A. von Kienlin, S. Wachter, C. A. Wilson-Hodge, and P. M. Woods (2010, February). Magnetar Twists: Fermi/Gamma-Ray Burst Monitor Detection of SGR J1550-5418. *ApJ 710*, 1335–1342.

Kaplan, D. L., S. R. Kulkarni, M. H. van Kerkwijk, R. E. Rothschild, R. L. Lingenfelter, D. Marsden, R. Danner, and T. Murakami (2001, July). Hubble Space Telescope Observations of SGR 0526-66: New Constraints on Accretion and Magnetar Models. *ApJ 556*, 399–407.

Kaspi, V. M. (2007, April). Recent progress on anomalous X-ray pulsars. *Ap&SS 308*, 1–11.

Kaspi, V. M., F. P. Gavriil, P. M. Woods, J. B. Jensen, M. S. E. Roberts, and D. Chakrabarty (2003, May). A Major Soft Gamma Repeater-like Outburst and Rotation Glitch in the No-longer-so-anomalous X-Ray Pulsar 1E 2259+586. *ApJ 588*, L93–L96.

Kawka, A. and S. Vennes (2012, September). A study of high proper-motion white dwarfs - I. Spectropolarimetry of a cool hydrogen-rich sample. *MNRAS 425*, 1394–1412.

Kemp, J. C. (1970, October). Circular Polarization of Thermal Radiation in a Magnetic Field. *ApJ 162*, 169.

Kemp, J. C., J. B. Swedlund, J. D. Landstreet, and J. R. P. Angel (1970, August). Discovery of Circularly Polarized Light from a White Dwarf. *ApJ 161*, L77.

Kepler, S. O., S. J. Kleinman, A. Nitta, D. Koester, B. G. Castanheira, O. Giovannini, A. F. M. Costa, and L. Althaus (2007, March). White dwarf mass distribution in the SDSS. *MNRAS 375*, 1315–1324.

Kepler, S. O., S. J. Kleinman, I. Pelisoli, V. Peçanha, M. Diaz, D. Koester, B. G. Castanheira, and A. Nitta (2010, November). Magnetic White Dwarfs in the SDSS and Estimating the Mean Mass of Normal DA and DB WDs. In K. Werner and T. Rauch (Eds.), *American Institute of Physics Conference Series*, Volume 1273 of *American Institute of Physics Conference Series*, pp. 19–24.

Kepler, S. O., I. Pelisoli, S. Jordan, S. J. Kleinman, D. Koester, B. Külebi, V. Peçanha, B. G. Castanheira, A. Nitta, J. E. S. Costa, D. E. Winget, A. Kanaan, and L. Fraga (2013, March). Magnetic white dwarf stars in the Sloan Digital Sky Survey. *MNRAS 429*, 2934–2944.

Kepler, S. O., I. Pelisoli, D. Koester, G. Ourique, S. J. Kleinman, A. D. Romero, A. Nitta, D. J. Eisenstein, J. E. S. Costa, B. Külebi, S. Jordan, P. Dufour, P. Giommi, and A. Rebassa-Mansergas (2015, February). New white dwarf stars in the Sloan Digital Sky Survey Data Release 10. *MNRAS 446*, 4078–4087.

Kepler, S. O., I. Pelisoli, D. Koester, G. Ourique, A. D. Romero, N. Reindl, S. J. Kleinman, D. J. Eisenstein, A. D. M. Valois, and L. A. Amaral (2016, February). New white dwarf and subdwarf stars in the Sloan Digital Sky Survey Data Release 12. *MNRAS 455*, 3413–3423.

Koester, D., R. Napiwotzki, N. Christlieb, H. Drechsel, H.-J. Hagen, U. Heber, D. Homeier, C. Karl, B. Leibundgut, S. Moehler, G. Nelemans, E.-M. Pauli,

D. Reimers, A. Renzini, and L. Yungelson (2001, November). High-resolution UVES/VLT spectra of white dwarfs observed for the ESO SN Ia progenitor survey (SPY). I. *A&A 378*, 556–568.

Kramer, M., B. W. Stappers, A. Jessner, A. G. Lyne, and C. A. Jordan (2007, May). Polarized radio emission from a magnetar. *MNRAS 377*, 107–119.

Kuiper, L. and W. Hermsen (2009, July). High-energy characteristics of the schizophrenic pulsar PSR J1846-0258in Kes 75. Multi-year RXTE and INTEGRAL observations crossing the magnetar-like outburst. *A&A 501*, 1031–1046.

Kuiper, L., W. Hermsen, P. R. den Hartog, and J. O. Urama (2012, April). Temporal and Spectral Evolution in X- and γ-Rays of Magnetar 1E 1547.0-5408 since its 2008 October Outburst: The Discovery of a Transient Hard Pulsed Component after its 2009 January Outburst. *ApJ 748*, 133.

Külebi, B., K. Y. Ekşi, P. Lorén-Aguilar, J. Isern, and E. García-Berro (2013, May). Magnetic white dwarfs with debris discs. *MNRAS 431*, 2778–2788.

Külebi, B., S. Jordan, F. Euchner, B. T. Gänsicke, and H. Hirsch (2009, November). Analysis of hydrogen-rich magnetic white dwarfs detected in the Sloan Digital Sky Survey. *A&A 506*, 1341–1350.

Külebi, B., S. Jordan, E. Nelan, U. Bastian, and M. Altmann (2010, December). Constraints on the origin of the massive, hot, and rapidly rotating magnetic white dwarf RE J 0317-853 from an HST parallax measurement. *A&A 524*, A36.

Külebi, B., J. Kalirai, S. Jordan, and F. Euchner (2013, June). The progenitors of magnetic white dwarfs in open clusters. *A&A 554*, A18.

Lalazissis, G. A., J. König, and P. Ring (1997, January). New parametrization for the Lagrangian density of relativistic mean field theory. *Phys. Rev. C 55*, 540–543.

Lamb, F. K., C. J. Pethick, and D. Pines (1973, August). A Model for Compact X-Ray Sources: Accretion by Rotating Magnetic Stars. *ApJ 184*, 271–290.

Landau, L. D. (1932, December). To the Stars theory. *Phys. Zs. Sowjet., vol.1, p.285, 1932 (English and German) 1*, 285.

Landau, L. D. and E. M. Lifshitz (1975). *The classical theory of fields*.

Laros, J. G., E. E. Fenimore, M. M. Fikani, R. W. Klebesadel, and C. Barat (1986, July). The soft gamma-ray burst GB790107. *Nature 322*, 152.

Laros, J. G., E. E. Fenimore, R. W. Klebesadel, J.-L. Atteia, M. Boer, K. Hurley, M. Niel, G. Vedrenne, S. R. Kane, C. Kouveliotou, T. L. Cline, B. R. Dennis, U. D. Desai, L. E. Orwig, A. V. Kuznetsov, R. A. Sunyaev, and O. V. Terekhov (1987, September). A new type of repetitive behavior in a high-energy transient. *ApJ 320*, L111–L115.

Levin, L., M. Bailes, S. Bates, N. D. R. Bhat, M. Burgay, S. Burke-Spolaor, N. D'Amico, S. Johnston, M. Keith, M. Kramer, S. Milia, A. Possenti, N. Rea, B. Stappers, and W. van Straten (2010, September). A Radio-loud Magnetar in X-ray Quiescence. *ApJ 721*, L33–L37.

Levin, L., M. Bailes, S. D. Bates, N. D. R. Bhat, M. Burgay, S. Burke-Spolaor, N. D'Amico, S. Johnston, M. J. Keith, M. Kramer, S. Milia, A. Possenti, B. Stappers, and W. van Straten (2012, May). Radio emission evolution, polarimetry and multifrequency single pulse analysis of the radio magnetar PSR J1622-4950. *MNRAS 422*, 2489–2500.

Li, X.-H., F.-J. Lu, and Z. Li (2008, August). Nonthermal X-Ray Properties of Rotation-powered Pulsars and Their Wind Nebulae. *ApJ 682*, 1166–1176.

Liebert, J. (1988, November). Searches for magnetic fields in white dwarfs since Babcock. *PASP 100*, 1302–1305.

Liebert, J., L. Ferrario, D. T. Wickramasinghe, and P. S. Smith (2015, May). Enigmas from the Sloan Digital Sky Survey DR7 Kleinman White Dwarf Catalog. *ApJ 804*, 93.

Liebert, J., G. D. Schmidt, R. F. Green, H. S. Stockman, and J. T. McGraw (1983, January). Two hot, low-field magnetic DA white dwarfs. *ApJ 264*, 262–272.

Lobato, R. V., J. Coelho, and M. Malheiro (2015, July). Particle acceleration and radio emission for SGRs/AXPs as white dwarf pulsars. In *Journal of Physics Conference Series*, Volume 630 of *Journal of Physics Conference Series*, pp. 012015.

Lobato, R. V., M. Malheiro, and J. G. Coelho (2016, July). Magnetars and white dwarf pulsars. *International Journal of Modern Physics D 25*, 1641025.

Lorén-Aguilar, P., J. Isern, and E. García-Berro (2009, June). High-resolution smoothed particle hydrodynamics simulations of the merger of binary white dwarfs. *A&A 500*, 1193–1205.

Lyutikov, M., R. D. Blandford, and G. Machabeli (1999, April). On the nature of pulsar radio emission. *MNRAS 305*, 338–352.

Malheiro, M., J. A. Rueda, and R. Ruffini (2012, June). SGRs and AXPs as Rotation-Powered Massive White Dwarfs. *PASJ 64*, 56.

Marsh, T. R., B. T. Gänsicke, S. Hümmerich, F.-J. Hambsch, K. Bernhard, C. Lloyd, E. Breedt, E. R. Stanway, D. T. Steeghs, S. G. Parsons, O. Toloza, M. R. Schreiber, P. G. Jonker, J. van Roestel, T. Kupfer, A. F. Pala, V. S. Dhillon, L. K. Hardy, S. P. Littlefair, A. Aungwerojwit, S. Arjyotha, D. Koester, J. J. Bochinski, C. A. Haswell, P. Frank, and P. J. Wheatley (2016, September). A radio-pulsing white dwarf binary star. *Nature 537*, 374–377.

Matt, S. P., G. Pinzón, T. P. Greene, and R. E. Pudritz (2012, January). Spin Evolution of Accreting Young Stars. II. Effect of Accretion-powered Stellar Winds. *ApJ 745*, 101.

Mazets, E. P. and S. V. Golenetskii (1981, March). Recent results from the gamma-ray burst studies in the KONUS experiment. *Ap&SS 75*, 47–81.

Mazets, E. P., S. V. Golenetskij, and Y. A. Guryan (1979, December). Soft gamma-ray bursts from the source B1900+14. *Soviet Astronomy Letters 5*, 641–643.

Mazets, E. P., S. V. Golentskii, V. N. Ilinskii, R. L. Aptekar, and I. A. Guryan (1979, December). Observations of a flaring X-ray pulsar in Dorado. *Nature 282*, 587–589.

Melrose, D. (2004). Pulse Emission Mechanisms. In F. Camilo and B. M. Gaensler (Eds.), *Young Neutron Stars and Their Environments*, Volume 218 of *IAU Symposium*, pp. 349.

Melrose, D. B. (1978, October). Amplified linear acceleration emission applied to pulsars. *ApJ 225*, 557–573.

Melrose, D. B. (1995, June). The Models for Radio Emission from Pulsars - the Outstanding Issues. *Journal of Astrophysics and Astronomy 16*, 137.

Meltzer, D. W. and K. S. Thorne (1966, August). Normal Modes of Radial Pulsation of Stars at the End Point of Thermonuclear Evolution. *ApJ 145*, 514.

Mendoza V., E. E. (1968, March). Infrared Excesses in T Tauri Stars and Related Objects. *ApJ 151*, 977.

Mereghetti, S. (2008, July). The strongest cosmic magnets: soft gamma-ray repeaters and anomalous X-ray pulsars. *A&A Rev. 15*, 225–287.

Mereghetti, S. (2013, December). Pulsars and Magnetars. *Brazilian Journal of Physics 43*, 356–368.

Mereghetti, S., P. Esposito, A. Tiengo, S. Zane, R. Turolla, L. Stella, G. L. Israel, D. Götz, and M. Feroci (2006, December). The First XMM-Newton Observations of the Soft Gamma-Ray Repeater SGR 1900+14. *ApJ 653*, 1423–1428.

Mereghetti, S., D. Götz, A. von Kienlin, A. Rau, G. Lichti, G. Weidenspointner, and P. Jean (2005, May). The First Giant Flare from SGR 1806-20: Observations Using the Anticoincidence Shield of the Spectrometer on INTEGRAL. *ApJ 624*, L105–L108.

Mereghetti, S., G. L. Israel, and L. Stella (1998, May). New limits on the orbital parameters of 1E 1048.1-5937 and 1E 2259+586 from RXTE observations. *MNRAS 296*, 689–692.

Mereghetti, S. and L. Stella (1995, March). The very low mass X-ray binary pulsars: A new class of sources? *ApJ 442*, L17–L20.

Mestel, L. and S. Shibata (1994, December). The Axisymmetric Pulsar Magnetosphere - a New Model. *MNRAS 271*, 621.

Michel, F. C. (1969, November). Relativistic Stellar-Wind Torques. *ApJ 158*, 727.

Michel, F. C. (1973a, February). Rotating Magnetosphere: a Simple Relativistic Model. *ApJ 180*, 207–226.

Michel, F. C. (1973b, March). Rotating Magnetospheres: an Exact 3-D Solution. *ApJ 180*, L133.

Michel, F. C. (1982, January). Theory of pulsar magnetospheres. *Reviews of Modern Physics 54*, 1–66.

Michel, F. C. (2005, October). Winds from Pulsars. In S. Torres-Peimbert and G. MacAlpine (Eds.), *Revista Mexicana de Astronomia y Astrofisica Conference Series*, Volume 23 of *Revista Mexicana de Astronomia y Astrofisica, vol. 27*, pp. 27–34.

Michel, F. C. and H. Li (1999, September). Electrodynamics of neutron stars. *Phys. Rep. 318*, 227–297.

Michel, F. C. and I. A. Smith (2001, March). Axisymmetric Rotator Models as Pulsars: Abject Failure. In J. Cantó and L. F. Rodríguez (Eds.), *Revista Mexicana de Astronomia y Astrofisica Conference Series*, Volume 10 of *Revista Mexicana de Astronomia y Astrofisica, vol. 27*, pp. 168–175.

Mochkovitch, R. and M. Livio (1989, January). The coalescence of white dwarfs and type I supernovae. *A&A 209*, 111–118.

Monaghan, J. J. (1966). The structure of rapidly rotating white dwarfs. *MNRAS 132*, 305.

Morii, M., N. Kawai, J. Kataoka, Y. Yatsu, N. Kobayashi, and H. Terada (2005). Near-infrared, optical, and X-ray observations of the anomalous X-ray pulsar 4U 0142 + 61. *Advances in Space Research 35*, 1177–1180.

Morii, M., N. Kobayashi, N. Kawai, H. Terada, Y. T. Tanaka, S. Kitamoto, and N. Shibazaki (2009, February). Search for Near-Infrared Pulsation of the Anomalous X-Ray Pulsar 4U 0142+61. *PASJ 61*, 51–56.

Morini, M., N. R. Robba, A. Smith, and M. van der Klis (1988, October). EXOSAT observations of the supernova remnant G109.1-1.0 and the X-ray pulsar 1E 2259+586. *ApJ 333*, 777–787.

Napiwotzki, R. (2009, June). The galactic population of white dwarfs. In *Journal of Physics Conference Series*, Volume 172 of *Journal of Physics Conference Series*, pp. 012004.

Ng, C.-Y. and V. M. Kaspi (2011, September). High Magnetic Field Rotation-powered Pulsars. In E. Göğüş, T. Belloni, and Ü. Ertan (Eds.), *American Institute of Physics Conference Series*, Volume 1379 of *American Institute of Physics Conference Series*, pp. 60–69.

Nityananda, R. and S. Konar (2014, May). Strong constraints on magnetized white dwarfs surpassing the Chandrasekhar mass limit. *Phys. Rev. D 89*(10), 103017.

Nityananda, R. and S. Konar (2015, January). Comment on "Strongly magnetized cold degenerate electron gas: Mass-radius relation of the magnetized white dwarf". *Phys. Rev. D 91*(2), 028301.

Nordhaus, J., S. Wellons, D. S. Spiegel, B. D. Metzger, and E. G. Blackman (2011, February). Formation of high-field magnetic white dwarfs from common envelopes. *Proceedings of the National Academy of Science 108*, 3135–3140.

Olausen, S. A. and V. M. Kaspi (2014, May). The McGill Magnetar Catalog. *ApJS 212*, 6.

Oppenheimer, J. R. and G. M. Volkoff (1939, February). On Massive Neutron Cores. *Physical Review 55*, 374–381.

Ostriker, J. (1968, March). Possible Model for a Rapidly Pulsating Radio Source. *Nature 217*, 1227–1228.

Ostriker, J. P. and P. Bodenheimer (1968, March). Rapidly Rotating Stars. II. Massive White Dwarfs. *ApJ 151*, 1089.

Ostriker, J. P. and F. D. A. Hartwick (1968, September). Rapidly Rotating Stars.IV. Magnetic White Dwarfs. *ApJ 153*, 797.

Ostriker, J. P. and J. L. Tassoul (1969, March). On the Oscillations and Stability of Rotating Stellar Models. II. Rapidly Rotating White Dwarfs. *ApJ 155*, 987.

Pacini, F. (1967, November). Energy Emission from a Neutron Star. *Nature 216*, 567–568.

Pacini, F. (1968, July). Rotating Neutron Stars, Pulsars and Supernova Remnants. *Nature 219*, 145–146.

Paczynski, B. (1985). Evolution of cataclysmic binaries. In D. Q. Lamb and J. Patterson (Eds.), *Cataclysmic Variables and Low-Mass X-ray Binaries*, Volume 113 of *Astrophysics and Space Science Library*, pp. 1–12.

Paczynski, B. (1990, December). X-ray pulsar 1E 2259 + 586 - A merged white dwarf with a 7 second rotation period? *ApJ 365*, L9–L12.

Palmer, D. M., S. Barthelmy, N. Gehrels, R. M. Kippen, T. Cayton, C. Kouveliotou, D. Eichler, R. A. M. J. Wijers, P. M. Woods, J. Granot, Y. E. Lyubarsky, E. Ramirez-Ruiz, L. Barbier, M. Chester, J. Cummings, E. E. Fenimore, M. H. Finger, B. M. Gaensler, D. Hullinger, H. Krimm, C. B. Markwardt, J. A. Nousek, A. Parsons, S. Patel, T. Sakamoto, G. Sato, M. Suzuki, and J. Tueller (2005, April). A giant γ-ray flare from the magnetar SGR 1806 - 20. *Nature 434*, 1107–1109.

Parsons, S. G., T. R. Marsh, B. T. Gänsicke, M. R. Schreiber, M. C. P. Bours, V. S. Dhillon, and S. P. Littlefair (2013, November). A magnetic white dwarf in a detached eclipsing binary. *MNRAS 436*, 241–252.

Patterson, J. (1979, December). Rapid oscillations in cataclysmic variables. III - an oblique rotator in an AE Aquarii. *ApJ 234*, 978–992.

Patterson, J. (1994, March). The DQ Herculis stars. *PASP 106*, 209–238.

Patterson, J. and J. E. Steiner (1983, January). H2215-086 -King of the DQ Herculis stars. *ApJ 264*, L61–L64.

Pérez Martínez, A., H. Pérez Rojas, and H. J. Mosquera Cuesta (2003, July). Magnetic collapse of a neutron gas: Can magnetars indeed be formed? *European Physical Journal C 29*, 111–123.

Pérez Martínez, A., H. Pérez Rojas, and H. J. Mosquera Cuesta (2008). Anisotropic Pressures in Very Dense Magnetized Matter. *International Journal of Modern Physics D 17*, 2107–2123.

Perna, R. and J. A. Pons (2011, February). A Unified Model of the Magnetar and Radio Pulsar Bursting Phenomenology. *ApJ 727*, L51.

Pétri, J. (2013, August). General-relativistic electromagnetic fields around a slowly rotating neutron star: stationary vacuum solutions. *MNRAS 433*, 986–1014.

Pétri, J. (2015, June). Multipolar electromagnetic fields around neutron stars: exact vacuum solutions and related properties. *MNRAS 450*, 714–742.

Pétri, J. (2016, December). Radiation from an off-centred rotating dipole in vacuum. *MNRAS 463*, 1240–1268.

Pines, D., J. Shaham, and M. Ruderman (1972, June). Corequakes and the Vela Pulsar. *Nature Physical Science 237*, 83–96.

Pons, J. A., J. A. Miralles, and U. Geppert (2009, March). Magneto-thermal evolution of neutron stars. *A&A 496*, 207–216.

Pons, J. A. and N. Rea (2012, May). Modeling Magnetar Outbursts: Flux Enhancements and the Connection with Short Bursts and Glitches. *ApJ 750*, L6.

Possenti, A., R. Cerutti, M. Colpi, and S. Mereghetti (2002, June). Re-examining the X-ray versus spin-down luminosity correlation of rotation powered pulsars. *A&A 387*, 993–1002.

Potekhin, A. Y. and G. Chabrier (2000, December). Equation of state of fully ionized electron-ion plasmas. II. Extension to relativistic densities and to the solid phase. *Phys. Rev. E 62*, 8554–8563.

Potter, A. T. and C. A. Tout (2010, February). Magnetic field evolution of white dwarfs in strongly interacting binary star systems. *MNRAS 402*, 1072–1080.

Provencal, J. L., H. L. Shipman, E. Høg, and P. Thejll (1998, February). Testing the White Dwarf Mass-Radius Relation with HIPPARCOS. *ApJ 494*, 759–767.

Rea, N., P. Esposito, R. Turolla, G. L. Israel, S. Zane, L. Stella, S. Mereghetti, A. Tiengo, D. Götz, E. Göğüş, and C. Kouveliotou (2010, November). A Low-Magnetic-Field Soft Gamma Repeater. *Science 330*, 944.

Rea, N., G. L. Israel, P. Esposito, J. A. Pons, A. Camero-Arranz, R. P. Mignani, R. Turolla, S. Zane, M. Burgay, A. Possenti, S. Campana, T. Enoto, N. Gehrels, E. Göğüş, D. Götz, C. Kouveliotou, K. Makishima, S. Mereghetti, S. R. Oates, D. M. Palmer, R. Perna, L. Stella, and A. Tiengo (2012, July). A New Low Magnetic Field Magnetar: The 2011 Outburst of Swift J1822.3-1606. *ApJ 754*, 27.

Rea, N., G. L. Israel, J. A. Pons, R. Turolla, D. Viganò, S. Zane, P. Esposito, R. Perna, A. Papitto, G. Terreran, A. Tiengo, D. Salvetti, J. M. Girart, A. Palau, A. Possenti, M. Burgay, E. Göğüş, G. A. Caliandro, C. Kouveliotou, D. Götz, R. P. Mignani, E. Ratti, and L. Stella (2013, June). The Outburst Decay of the Low Magnetic Field Magnetar SGR 0418+5729. *ApJ 770*, 65.

Rebassa-Mansergas, A., C. Agurto-Gangas, M. R. Schreiber, B. T. Gänsicke, and D. Koester (2013, August). White dwarf main-sequence binaries from SDSS DR 8: unveiling the cool white dwarf population. *MNRAS 433*, 3398–3410.

Revnivtsev, M., S. Sazonov, R. Krivonos, H. Ritter, and R. Sunyaev (2008, October). Properties of the Galactic population of cataclysmic variables in hard X-rays. *A&A 489*, 1121–1127.

Rezzolla, L. and B. J. Ahmedov (2004, August). Electromagnetic fields in the exterior of an oscillating relativistic star - I. General expressions and application to a rotating magnetic dipole. *MNRAS 352*, 1161–1179.

Rezzolla, L., B. J. Ahmedov, and J. C. Miller (2001, April). General relativistic electromagnetic fields of a slowly rotating magnetized neutron star - I. Formulation of the equations. *MNRAS 322*, 723–740.

Rezzolla, L., B. J. Ahmedov, and J. C. Miller (2003, January). Erratum: General relativistic electromagnetic fields of a slowly rotating magnetized neutron star - I. Formulation of the equations. *MNRAS 338*, 816–816.

Roesner, W., G. Wunner, H. Herold, and H. Ruder (1984, January). Hydrogen atoms in arbitrary magnetic fields. I - Energy levels and wavefunctions. *Journal of Physics B Atomic Molecular Physics 17*, 29–52.

Rotondo, M., J. A. Rueda, R. Ruffini, and S.-S. Xue (2011a, October). Relativistic Feynman-Metropolis-Teller theory for white dwarfs in general relativity. *Phys. Rev. D 84*(8), 084007.

Rotondo, M., J. A. Rueda, R. Ruffini, and S.-S. Xue (2011b, April). Relativistic Thomas-Fermi treatment of compressed atoms and compressed nuclear matter cores of stellar dimensions. *Phys. Rev. C 83*(4), 045805.

Rotondo, M., J. A. Rueda, R. Ruffini, and S.-S. Xue (2011c, July). The self-consistent general relativistic solution for a system of degenerate neutrons, protons and electrons in β-equilibrium. *Physics Letters B 701*, 667–671.

Roxburgh, I. W. and B. R. Durney (1966). Structure, Oscillations and Stability of Rotating White Dwarfs. *ZAp 64*, 504.

Ruder, H., G. Wunner, H. Herold, and F. Geyer (1994). *Atoms in Strong Magnetic Fields. Quantum Mechanical Treatment and Applications in Astrophysics and Quantum Chaos*.

Ruderman, M. (1969, August). Neutron Starquakes and Pulsar Periods. *Nature 223*, 597–598.

Ruderman, M. A. and P. G. Sutherland (1975, February). Theory of pulsars - Polar caps, sparks, and coherent microwave radiation. *ApJ 196*, 51–72.

Rueda, J. A., K. Boshkayev, L. Izzo, R. Ruffini, P. Lorén-Aguilar, B. Külebi, G. Aznar-Siguán, and E. García-Berro (2013, August). A White Dwarf Merger as Progenitor of the Anomalous X-Ray Pulsar 4U 0142+61? *ApJ 772*, L24.

Rueda, J. A. and R. Ruffini (2012, October). On the Induced Gravitational Collapse of a Neutron Star to a Black Hole by a Type Ib/c Supernova. *ApJ 758*, L7.

Rueda, J. A., R. Ruffini, and S.-S. Xue (2011, December). The Klein first integrals in an equilibrium system with electromagnetic, weak, strong and gravitational interactions. *Nuclear Physics A 872*, 286–295.

Ruffini, R. (1973). On the energetics of black holes. In C. Dewitt and B. S. Dewitt (Eds.), *Black Holes (Les Astres Occlus)*, pp. 451–546.

Ruffini, R. (2008, November). The Role of Thomas-Fermi Approach in Neutron Star Matter. In *Path Integrals - New Trends and Perspectives*, pp. 207–218.

Ruffini, R. and L. Stella (1981, July). Some comments on the relativistic Thomas-Fermi model and the Vallarta-Rosen equation. *Physics Letters B 102*, 442–444.

Salpeter, E. E. (1961, November). Energy and Pressure of a Zero-Temperature Plasma. *ApJ 134*, 669.

Salpeter, E. E. and H. M. van Horn (1969, January). Nuclear Reaction Rates at High Densities. *ApJ 155*, 183.

Scalzo, R. A., G. Aldering, P. Antilogus, C. Aragon, S. Bailey, C. Baltay, S. Bongard, C. Buton, M. Childress, N. Chotard, Y. Copin, H. K. Fakhouri, A. Gal-Yam, E. Gangler, S. Hoyer, M. Kasliwal, S. Loken, P. Nugent, R. Pain, E. Pécontal, R. Pereira, S. Perlmutter, D. Rabinowitz, A. Rau, G. Rigaudier, K. Runge, G. Smadja, C. Tao, R. C. Thomas, B. Weaver, and C. Wu (2010, April). Nearby Supernova Factory Observations of SN 2007if: First Total Mass Measurement of a Super-Chandrasekhar-Mass Progenitor. *ApJ 713*, 1073–1094.

Schmidt, G. D., P. Bergeron, J. Liebert, and R. A. Saffer (1992, August). Two ultramassive white dwarfs found among candidates for magnetic fields. *ApJ 394*, 603–608.

Schmidt, G. D., S. C. West, J. Liebert, R. F. Green, and H. S. Stockman (1986, October). The new magnetic white dwarf PG 1031 + 234 - Polarization and field structure at more than 500 milion Gauss. *ApJ 309*, 218–229.

Scholz, P. and V. M. Kaspi (2011, October). The 2009 Outburst of Magnetar 1E 1547-5408: Persistent Radiative and Burst Properties. *ApJ 739*, 94.

Schreier, E., R. Levinson, H. Gursky, E. Kellogg, H. Tananbaum, and R. Giacconi (1972a, May). Errata: Evidence for the Binary Nature of Centaurus X-3 from UHURU X-Ray Observations; and Further Observations of the Pulsating X-Ray Source Cygnus X-1 from UHURU. *ApJ 173*, L151.

Schreier, E., R. Levinson, H. Gursky, E. Kellogg, H. Tananbaum, and R. Giacconi (1972b, March). Evidence for the Binary Nature of Centaurus X-3 from UHURU X-Ray Observations. *ApJ 172*, L79.

Sedrakyan, D. M. and E. V. Chubaryan (1968, December). Internal solution for stationary axially symmetric gravitational fields. *Astrophysics 4*, 227–233.

Shapiro, S. L. and S. A. Teukolsky ((Wiley-VCH, 1986), June). *Black Holes, White Dwarfs and Neutron Stars: The Physics of Compact Objects*.

Shu, F. H., F. C. Adams, and S. Lizano (1987). Star formation in molecular clouds - Observation and theory. *ARA&A 25*, 23–81.

Silverman, J. M., M. Ganeshalingam, W. Li, A. V. Filippenko, A. A. Miller, and D. Poznanski (2011, January). Fourteen months of observations of the possible super-Chandrasekhar mass Type Ia Supernova 2009dc. *MNRAS 410*, 585–611.

Sorkin, R. (1981, October). A Criterion for the Onset of Instability at a Turning Point. *ApJ 249*, 254.

Sorkin, R. D. (1982, June). A Stability Criterion for Many Parameter Equilibrium Families. *ApJ 257*, 847.

Spitkovsky, A. (2006, September). Time-dependent Force-free Pulsar Magnetospheres: Axisymmetric and Oblique Rotators. *ApJ 648*, L51–L54.

Stergioulas, N. (2003, December). Rotating Stars in Relativity. *Living Reviews in Relativity 6*, 3.

Stoner, E. C. (1929). *Philos. Mag. 7*, 63.

Strickland, M., V. Dexheimer, and D. P. Menezes (2012, December). Bulk properties of a Fermi gas in a magnetic field. *Phys. Rev. D 86*(12), 125032.

Sturrock, P. A. (1971, March). A Model of Pulsars. *ApJ 164*, 529.

Sugahara, Y. and H. Toki (1994, October). Relativistic mean-field theory for unstable nuclei with non-linear σ and ω terms. *Nuclear Physics A 579*, 557–572.

Swedlund, J. B., J. C. Kemp, and R. D. Wolstencroft (1974, October). DQ Herculis : Periodic Circular Polarization Synchronous with the Rapid Light Variations. *ApJ 193*, L11.

Szkody, P., S. F. Anderson, K. Brooks, B. T. Gänsicke, M. Kronberg, T. Riecken, N. P. Ross, G. D. Schmidt, D. P. Schneider, M. A. Agüeros, A. N. Gomez-Moran, G. R. Knapp, M. R. Schreiber, and A. D. Schwope (2011, December). Cataclysmic Variables from the Sloan Digital Sky Survey. VIII. The Final Year (2007-2008). *AJ 142*, 181.

Tananbaum, H., H. Gursky, E. M. Kellogg, R. Levinson, E. Schreier, and R. Giacconi (1972, June). Discovery of a Periodic Pulsating Binary X-Ray Source in Hercules from UHURU. *ApJ 174*, L143.

Tapia, S. (1977, March). Discovery of a magnetic compact star in the AM Herculis/3U 1809+50 system. *ApJ 212*, L125–L129.

Tassoul, J.-L. and J. P. Ostriker (1970, March). Secular Stability of Uniformly Rotating Polytropes. *A&A 4*, 423.

Taubenberger, S., S. Benetti, M. Childress, R. Pakmor, S. Hachinger, P. A. Mazzali, V. Stanishev, N. Elias-Rosa, I. Agnoletto, F. Bufano, M. Ergon, A. Harutyunyan, C. Inserra, E. Kankare, M. Kromer, H. Navasardyan, J. Nicolas, A. Pastorello, E. Prosperi, F. Salgado, J. Sollerman, M. Stritzinger, M. Turatto, S. Valenti, and W. Hillebrandt (2011, April). High luminosity, slow ejecta and persistent carbon lines: SN 2009dc challenges thermonuclear explosion scenarios. *MNRAS 412*, 2735–2762.

Tauris, T. M., V. M. Kaspi, R. P. Breton, A. T. Deller, E. F. Keane, M. Kramer, D. R. Lorimer, M. A. McLaughlin, A. Possenti, P. S. Ray, B. W. Stappers, and P. Weltevrede (2015, April). Understanding the Neutron Star Population with the SKA. *Advancing Astrophysics with the Square Kilometre Array (AASKA14)*, 39.

Terada, Y., T. Hayashi, M. Ishida, K. Mukai, T. Dotani, S. Okada, R. Nakamura, S. Naik, A. Bamba, and K. Makishima (2008, April). Suzaku Discovery of Hard X-Ray Pulsations from a Rotating Magnetized White Dwarf, AEAquarii. *PASJ 60*, 387–397.

Thompson, C. and R. C. Duncan (1995, July). The soft gamma repeaters as very strongly magnetized neutron stars - I. Radiative mechanism for outbursts. *MNRAS 275*, 255–300.

Thompson, C. and R. C. Duncan (1996, December). The Soft Gamma Repeaters as Very Strongly Magnetized Neutron Stars. II. Quiescent Neutrino, X-Ray, and Alfven Wave Emission. *ApJ 473*, 322.

Thompson, C., M. Lyutikov, and S. R. Kulkarni (2002, July). Electrodynamics of Magnetars: Implications for the Persistent X-Ray Emission and Spin-down of the Soft Gamma Repeaters and Anomalous X-Ray Pulsars. *ApJ 574*, 332–355.

Tolman, R. C. (1939, February). Static Solutions of Einstein's Field Equations for Spheres of Fluid. *Physical Review 55*, 364–373.

Tong, H. (2016, January). Pulsar braking: magnetodipole vs. wind. *Science China Physics, Mechanics, and Astronomy 59*(1), 5752.

Toropina, O. D., M. M. Romanova, and R. V. E. Lovelace (2012, February). Bondi-Hoyle accretion on to a magnetized neutron star. *MNRAS 420*, 810–816.

Tout, C. A., D. T. Wickramasinghe, J. Liebert, L. Ferrario, and J. E. Pringle (2008, June). Binary star origin of high field magnetic white dwarfs. *MNRAS 387*, 897–901.

Tremblay, P.-E., P. Bergeron, and A. Gianninas (2011, April). An Improved Spectroscopic Analysis of DA White Dwarfs from the Sloan Digital Sky Survey Data Release 4. *ApJ 730*, 128.

Tremblay, P.-E., H.-G. Ludwig, M. Steffen, and B. Freytag (2013, November). Spectroscopic analysis of DA white dwarfs with 3D model atmospheres. *A&A 559*, A104.

Tsai, Y.-S. (1974, October). Pair production and bremsstrahlung of charged leptons. *Reviews of Modern Physics 46*, 815–851.

Turolla, R. and P. Esposito (2013, August). Low-Magnetic Magnetars. *International Journal of Modern Physics D 22*, 1330024–163.

Turolla, R. and L. Nobili (2013, May). Pulse Profiles from Thermally Emitting Neutron Stars. *ApJ 768*, 147.

Turolla, R., S. Zane, and A. L. Watts (2015, November). Magnetars: the physics behind observations. A review. *Reports on Progress in Physics 78*(11), 116901.

Usov, V. V. (1988, March). Generation of Gamma-Rays by a Rotating Magnetic White Dwarf. *Soviet Astronomy Letters 14*, 258.

Usov, V. V. (1993, June). High-frequency emission of X-ray pulsar 1E 2259+586. *ApJ 410*, 761–763.

Usov, V. V. (1994, June). Glitches in the X-ray pulsar 1E 2259+586. *ApJ 427*, 984–986.

van Paradijs, J., R. E. Taam, and E. P. J. van den Heuvel (1995, July). On the nature of the 'anomalous' 6-s X-ray pulsars. *A&A 299*, L41.

Vauclair, G., H. Schmidt, D. Koester, and N. Allard (1997, September). White dwarfs observed by the HIPPARCOS satellite. *A&A 325*, 1055–1062.

Venter, C. and A. K. Harding (2014, March). High-energy pulsar models: Developments and new questions. *Astronomische Nachrichten 335*, 268–273.

Viganò, D., D. F. Torres, K. Hirotani, and M. E. Pessah (2015, March). An assessment of the pulsar outer gap model - I. Assumptions, uncertainties, and implications on the gap size and the accelerating field. *MNRAS 447*, 2631–2648.

Walker, M. F. (1956, January). A Photometric Investigation of the Short-Period Eclipsing Binary, Nova DQ Herculis (1934). *ApJ 123*, 68.

Warner, B. (1995). The Discovery Of Magnetic Cataclysmic Variable Stars. In D. A. H. Buckley and B. Warner (Eds.), *Magnetic Cataclysmic Variables*, Volume 85 of *Astronomical Society of the Pacific Conference Series*, pp. 3.

Webbink, R. F. (1984, February). Double white dwarfs as progenitors of R Coronae Borealis stars and Type I supernovae. *ApJ 277*, 355–360.

Wheeler, J. A. (1966). Superdense Stars. *ARA&A 4*, 393.

Wickramasinghe, D. T. and L. Ferrario (2000, July). Magnetism in Isolated and Binary White Dwarfs. *PASP 112*, 873–924.

Wickramasinghe, D. T. and L. Ferrario (2005, February). The origin of the magnetic fields in white dwarfs. *MNRAS 356*, 1576–1582.

Wickramasinghe, D. T., G. Schmidt, L. Ferrario, and S. Vennes (2002, May). On the nature of the magnetic DB white dwarfs. *MNRAS 332*, 29–33.

Wilson, C. A., S. Dieters, M. H. Finger, D. M. Scott, and J. van Paradijs (1999, March). Rossi X-Ray Timing Explorer Observations of the Anomalous Pulsar 4U 0142+61. *ApJ 513*, 464–470.

Woods, P. M., V. M. Kaspi, C. Thompson, F. P. Gavriil, H. L. Marshall, D. Chakrabarty, K. Flanagan, J. Heyl, and L. Hernquist (2004, April). Changes in the X-Ray Emission from the Magnetar Candidate 1E 2259+586 during Its 2002 Outburst. *ApJ 605*, 378–399.

Woods, P. M., C. Kouveliotou, F. P. Gavriil, V. M. Kaspi, M. S. E. Roberts, A. Ibrahim, C. B. Markwardt, J. H. Swank, and M. H. Finger (2005, August). X-Ray Bursts from the Transient Magnetar Candidate XTE J1810-197. *ApJ 629*, 985–997.

Woods, P. M. and C. Thompson (2006, April). *Soft gamma repeaters and anomalous X-ray pulsars: magnetar candidates*, pp. 547–586.

Yakovlev, D. G., L. R. Gasques, A. V. Afanasjev, M. Beard, and M. Wiescher (2006, September). Fusion reactions in multicomponent dense matter. *Phys. Rev. C 74*(3), 035803.

Yamanaka, M., K. S. Kawabata, K. Kinugasa, M. Tanaka, A. Imada, K. Maeda, K. Nomoto, A. Arai, S. Chiyonobu, Y. Fukazawa, O. Hashimoto, S. Honda, Y. Ikejiri, R. Itoh, Y. Kamata, N. Kawai, T. Komatsu, K. Konishi, D. Kuroda, H. Miyamoto, S. Miyazaki, O. Nagae, H. Nakaya, T. Ohsugi, T. Omodaka, N. Sakai, M. Sasada, M. Suzuki, H. Taguchi, H. Takahashi, H. Tanaka, M. Uemura, T. Yamashita, K. Yanagisawa, and M. Yoshida (2009, December). Early Phase Observations of Extremely Luminous Type Ia Supernova 2009dc. *ApJ 707*, L118–L122.

York, D. G., J. Adelman, J. E. Anderson, Jr., S. F. Anderson, J. Annis, N. A. Bahcall, J. A. Bakken, R. Barkhouser, S. Bastian, E. Berman, W. N. Boroski, S. Bracker, C. Briegel, J. W. Briggs, J. Brinkmann, R. Brunner, S. Burles, L. Carey, M. A. Carr, F. J. Castander, B. Chen, P. L. Colestock, A. J. Connolly, J. H. Crocker, I. Csabai, P. C. Czarapata, J. E. Davis, M. Doi, T. Dombeck, D. Eisenstein, N. Ellman, B. R. Elms, M. L. Evans, X. Fan, G. R. Federwitz, L. Fiscelli, S. Friedman, J. A. Frieman, M. Fukugita, B. Gillespie, J. E. Gunn, V. K. Gurbani, E. de Haas, M. Haldeman, F. H. Harris, J. Hayes, T. M. Heckman, G. S. Hennessy, R. B. Hindsley, S. Holm, D. J. Holmgren, C.-h. Huang, C. Hull, D. Husby, S.-I. Ichikawa, T. Ichikawa, Ž. Ivezić, S. Kent, R. S. J. Kim, E. Kinney, M. Klaene, A. N. Kleinman, S. Kleinman, G. R. Knapp, J. Korienek, R. G. Kron, P. Z. Kunszt, D. Q. Lamb, B. Lee, R. F. Leger, S. Limmongkol, C. Lindenmeyer, D. C. Long, C. Loomis, J. Loveday, R. Lucinio, R. H. Lupton, B. MacKinnon, E. J. Mannery, P. M. Mantsch, B. Margon, P. McGehee, T. A. McKay, A. Meiksin, A. Merelli, D. G. Monet, J. A. Munn, V. K. Narayanan, T. Nash, E. Neilsen, R. Neswold, H. J. Newberg, R. C. Nichol, T. Nicinski, M. Nonino, N. Okada, S. Okamura, J. P. Ostriker, R. Owen, A. G. Pauls, J. Peoples, R. L. Peterson, D. Petravick, J. R. Pier, A. Pope, R. Pordes, A. Prosapio, R. Rechenmacher, T. R. Quinn, G. T. Richards, M. W. Richmond, C. H. Rivetta, C. M. Rockosi, K. Ruthmansdorfer, D. Sandford, D. J. Schlegel, D. P. Schneider, M. Sekiguchi, G. Sergey, K. Shimasaku, W. A. Siegmund, S. Smee, J. A. Smith, S. Snedden, R. Stone, C. Stoughton, M. A. Strauss, C. Stubbs, M. SubbaRao, A. S. Szalay, I. Szapudi, G. P. Szokoly, A. R. Thakar, C. Tremonti, D. L. Tucker, A. Uomoto, D. Vanden Berk, M. S. Vogeley, P. Waddell, S.-i. Wang, M. Watanabe, D. H. Weinberg, B. Yanny, N. Yasuda, and SDSS Collaboration (2000, September). The Sloan Digital Sky Survey: Technical Summary. *AJ 120*, 1579–1587.

Yusef-Zadeh, F., R. Diesing, M. Wardle, L. O. Sjouwerman, M. Royster, W. D. Cotton, D. Roberts, and C. Heinke (2015, October). Radio Continuum Emission from the Magnetar SGR J1745-2900: Interaction with Gas Orbiting Sgr A*. *ApJ 811*, L35.

Zhang, B. and A. K. Harding (2000, April). Full Polar Cap Cascade Scenario: Gamma-Ray and X-Ray Luminosities from Spin-powered Pulsars. *ApJ 532*, 1150–1171.

Zhang, L. and K. S. Cheng (1997, September). High-Energy Radiation from Rapidly Spinning Pulsars with Thick Outer Gaps. *ApJ 487*, 370–379.

Zhu, W., V. M. Kaspi, R. Dib, P. M. Woods, F. P. Gavriil, and A. M. Archibald (2008, October). The Long-term Radiative Evolution of Anomalous X-Ray Pulsar 1E 2259+586 After its 2002 Outburst. *ApJ 686*, 520–527.

Zhu, W. W., V. M. Kaspi, M. A. McLaughlin, G. G. Pavlov, C.-Y. Ng, R. N. Manchester, B. M. Gaensler, and P. M. Woods (2011, June). Chandra Observations of the High-magnetic-field Radio Pulsar J1718-3718. *ApJ 734*, 44.

Zwicky, F. (1938, November). On Collapsed Neutron Stars. *ApJ 88*, 522–525.